SUMY STATE UNIVERSITY

p-ISSN 2312-2498
e-ISSN 2414-9381

http://jes.sumdu.edu.ua
jes@sumdu.edu.ua

JOURNAL OF ENGINEERING SCIENCES

ЖУРНАЛ ІНЖЕНЕРНИХ НАУК

ЖУРНАЛ ИНЖЕНЕРНЫХ НАУК

Volume 5
Issue 1 (2018)

The Ministry of Education and Science of Ukraine

Міністерство освіти і науки України

Министерство образования и науки Украины

JOURNAL OF ENGINEERING SCIENCES

ЖУРНАЛ ІНЖЕНЕРНИХ НАУК

ЖУРНАЛ ИНЖЕНЕРНЫХ НАУК

Scientific Journal

Науковий журнал

Научный журнал

Volume 5, Issue 1 (2018)

Том 5, № 1 (2018)

Founded in 1994

Заснований у 1994 році

Основан в 1994 году

Sumy State University

Сумський державний університет

Сумский государственный университет

The Journal of Engineering Sciences is an open access scientific journal that covers urgent issues of the up-to-date high-tech production, development of new engineering trends and future technologies. General topics of the journal concerns manufacturing, mechanical and chemical engineering. The main publication language presented for papers is English. The editorial board represented by scientists from different European research institutions allows covering the journal's topics and qualitatively evaluate all the submitted papers. The system of double blinded reviewing process provides a high-quality presentation of papers. The editorial police including the submitting, reviewing, acceptance and publication of the materials are completely transparent.

p-ISSN 2312-2498
e-ISSN 2414-9381

Recommended for publication
by the Academic Council of Sumy State University,
(minutes No. 8 of 21.06.2018)

The Journal is the scientific professional edition of Ukraine in the field of Engineering Sciences (ordered by the Ministry of Education and Science of Ukraine, July 13, 2015, No. 747): http://old.mon.gov.ua/img/zstored/files/747.rar).

The Journal of Engineering Sciences is published with the support of the following partners:
– Faculty of Technical Systems and Energy Efficient Technologies of Sumy State University (Sumy, Ukraine): http://teset.sumdu.edu.ua;
– Faculty of Mechanical Engineering and Management of Poznan University of Technology (Poznan, Poland): https://www.put.poznan.pl;
– Department of Applied Hydro- and Aeromechanics of Sumy State University (Sumy, Ukraine): http://pgm.sumdu.edu.ua.

Editorial Board: 2 Rymskogo-Korsakova St., 40007 Sumy, Ukraine
Contact Phones: +38 (0542) 331024; +38 (099) 3845740
E-mail: jes@sumdu.edu.ua
Web-site: http://jes.sumdu.edu.ua

State registration certificate of the print mass-media No. 20499-10299 ПР.

JOURNAL OF ENGINEERING SCIENCES
ЖУРНАЛ ІНЖЕНЕРНИХ НАУК
ЖУРНАЛ ИНЖЕНЕРНЫХ НАУК

Web site: http://jes.sumdu.edu.ua

Volume 5, Issue 1 (2018)

Crossref
https://search.crossref.org

Directory of Open Access Journals (DOAJ)
https://doaj.org

Index Copernicus International Journals Master List
https://journals.indexcopernicus.com

Google Scholar
https://scholar.google.com

International Institute of Organized Research
http://www.i2or.com

Scientific Indexing Services (SIS)
http://www.sindexs.org

Academic Resource Index (Research Bible)
http://researchbib.com

Directory of Research Journals Indexing (DRJI)
http://www.drji.org

World Cat
http://www.worldcat.org

Eurasian Scientific Journal Indexing (ESJI)
http://esjindex.org

Journal Impact Factor
http://jifactor.org

Impact Factor Services for International Journals (IFSIJ)
http://ifsij.com

Journal Factor
http://www.journalfactor.org

Open Academic Journals Index (OAJI)
http://oaji.net

Academic Keys
http://academickeys.com

International Society for Research Activity (ISRA)
Journal Impact Factor (JIF):
http://www.israjif.org

Advanced Science Index (ASI):
http://journal-index.org

International Scientific Indexing (ISI):
http://isindexing.com

Global Digital Publishing Platform
https://issuu.com

Vernadsky National Library of Ukraine
http://www.nbuv.gov.ua

Electronic Sumy State University Institutional Repository
http://essuir.sumdu.edu.ua

EDITORIAL BOARD

TOPICS

OF THE "JOURNAL OF ENGINEERING SCIENCE":

1. MANUFACTURING ENGINEERING:

- (A) Machines and Tools;
- (B) Technical Regulations and Metrological Support;
- (C) Materials Science.

2. MECHANICAL ENGINEERING:

- (D) Dynamics and Strength of Machines;
- (E) Computational Mechanics.

3. CHEMICAL ENGINEERING:

- (F) Processes in Machines and Devices;
- (G) Energy Efficient Technologies;
- (H) Environmental Protection.

JOURNAL OF ENGINEERING SCIENCES
ЖУРНАЛ ІНЖЕНЕРНИХ НАУК
ЖУРНАЛ ИНЖЕНЕРНЫХ НАУК
Web site: http://jes.sumdu.edu.ua
Volume 5, Issue 1 (2018)

CONTENTS

MANUFACTURING ENGINEERING

Machines and Tools ● ○ ○ ○ ○ ○ ○ ○ **A**

Lishchenko N. V., Larshin V. P.
Profile Gear Grinding Temperature Reduction and Equalization **A 1–A 7**
DOI: **10.21272/jes.2018.5(1).a1**

Pilipenko S. V., Drozhzha P. V., Limonchenko E. A.
Influence of the Wall Thickness Value on the Cross Wall Thickness Deviation
of Tubes Rolled on the Tube Rolling Plant with the Continuous Mill **A 8–A 11**
DOI: **10.21272/jes.2018.5(1).a2**

Sokhan' S. V., Maystrenko A. L., Kulich V. H., Sorochenko V. H.,
Voznyy V. V., Gamaniuk M. P., Zubaniev Ye. M. **A 12–A 20**
DOI: **10.21272/jes.2018.5(1).a3**

Technical Regulations and Metrological Support ○ ● ○ ○ ○ ○ ○ ○ **B**

Kovalev A. I.
How to Assess the Performance Quality of an Enterprise **B 1–B 6**
DOI: **10.21272/jes.2018.5(1).b1**

Materials Science ○ ○ ● ○ ○ ○ ○ ○ **C**

Bilous O. A., Hovorun T. P., Berladir K. V., Vorobiov S. I., Simkulet V. V.
Mathematical Modeling of the Mechanical Characteristic of the Activated
PTFE-Matrix Using the Method of Planning the Experiment **C 1–C 5**
DOI: **10.21272/jes.2018.5(1).c1**

Rud V., Saviuk I., Samchuk L., Povstiana Yu.
Research of Mechanical Properties of Thermite Material on the Basis of Steel Dross **C 6–C 10**
DOI: **10.21272/jes.2018.5(1).c2**

Demchenko M. V., Gaponova O. P., Myslyvchenko O. M., Antoszewski B., Bychenko M. M.
Microstructure and Properties of AlCrFeCoNiCu$_x$ High-Entropy Alloys **C 11–C 15**
DOI: **10.21272/jes.2018.5(1).c3**

Plyatsuk L. D., Tarelnyk V. B., Kundera Cz., Radionov O. V., Gaponova O. P.
Ecologically Safe Process for Sulfo-Aluminizing of Steel Parts **C 16–C 20**
DOI: **10.21272/jes.2018.5(1).c4**

MECHANICAL ENGINEERING

Dynamics and Strength of Machines ○ ○ ○ ● ○ ○ ○ ○ **D**

Nemchynov S. I., Nachovnyi I. I.
Stress-Strain State of the Lower Traverse of the Hydraulic Press **D 1–D 5**
DOI: **10.21272/jes.2018.5(1).d1**

Pavlenko I. V., Simonovskiy V. I., Pitel' J., Demianenko M. M.
Investigation of Non-linear Reactions in Rotors' Bearing Supports
of Turbo-pump Units for Liquid Rocket Engines **D 6–D 14**
DOI: **10.21272/jes.2018.5(1).d2**

Mama B. O., Ike C. C.
Galerkin–Vlasov Method for Deflection Analysis of Isotropic Sandwich Plates under Uniform Load **D 15–D 19**
DOI: **10.21272/jes.2018.5(1).d3**

Computational Mechanics **E**

Pillalamarri L.
UWB Microstrip Line Feeding Planar Modified Circular Antenna **E 1–E 4**
DOI: **10.21272/jes.2018.5(1).e1**

Bondar A. V., Vaneev S. M., Miroshnychenko D. V.
Research of Working Process of the Vortex Expansion Machine with a Side Channel **E 5–E 9**
DOI: **10.21272/jes.2018.5(1).e2**

Djondine P.
Overview of Control Techniques for Multicellular Converter **E 10–E 14**
DOI: **10.21272/jes.2018.5(1).e3**

CHEMICAL ENGINEERING

Processes in Machines and Devices **F**

Azyukovsky A. A., Didevich E. A.
Analysis of the Application of the Galvanic Circuits in Schemes
of the Catodic Protection for Underground Papelines **F 1–F 4**
DOI: **10.21272/jes.2018.5(1).f1**

Varukha D. A., Smirnov V. A., Edl M., Demianenko M. M.,
Yukhymenko M. P., Pavlenko I. V., Liaposhchenko O. O.
Modelling of Separation and Pneumatic Classification Processes
of Aerodisperse Systems in the Shelf Device **F 5– F 9**
DOI: **10.21272/jes.2018.5(1).f2**

Environmental Protection **H**

Kofanova O.
Climate Change Modeling in the Context of Urban Decarbonization Strategy **H 1–H 6**
DOI: **10.21272/jes.2018.5(1).h1**

Plyatsuk L. D., Chernysh Y. Y., Ablieieva I. Y., Kozii I. S. , Balintova, M., Matiash Y. O.
Sulfur Utilization in the Systems of Biological Wastwater Denitrification **H 7–H 15**
DOI: **10.21272/jes.2018.5(1).h2**

Sigal O., Boulanger Q., Vorobiov L., Pavliuk N., Serhiienko R.
Research of Energy Characteristics of Municipal Solid Waste in Cherkasy **H 16–H 22**
DOI: **10.21272/jes.2018.5(1).h3**

Samaulah H., Basir Y., Helmi M., Faturrizky F., Sugawara A.
Efficiency analysis of tracking and stationary solar panel modes against solar radiation **H 23–H 28**
DOI: **10.21272/jes.2018.5(1).h4**


DSMIE 2018
International Conference on
Design, Simulation, Manufacturing:
The Innovation Exchange
June 12-15, 2018 | Sumy, Ukraine
http://dsmie.sumdu.edu.ua
Important Dates
June 12 - Registration & City Tour
June 13 - Keynote Sessions & Exhibition
June 14 - Technical Sessions & Industry Tour
June 15 - Technical Sessions & Awards
Keynote Speeches
• Industry 4.0 – Smart Factory: Challenges and Trends
Olaf Ciszak, Poznan University of Technology, Poland
• Creation of the Intellectual Property Protection System at Universities
Jozef Zajac, Technical University of Kosice, Slovak Republic
• Quo Vadis, Technical Education – Preparation for Professions That Are Not Yet = Education 4.0
Milan Edl, University of West Bohemia, Czech Republic
• Smart Education for Smart Enterprises
Slawomir Luscinski, Kielce University of Technology, Poland
• Strategies of Professional Engineering Education for Modern Machine-Building Industry
Dmytro Kryvoruchko, Center for Technological Initiatives, Ukraine
• Muscle-Based Actuators for Pneumatic Manipulators
Jan Pitel, Technical University of Kosice, Slovak Republic
• Design and Study of Conical Pressure-Swirl Atomizers
Marek Ochowiak, Poznan University of Technology, Poland
Visit us
Springer
EasyChair
UNICHECK
NASOSENERGOMASH
ENERGOMASH
AMCBRIDGE
Engineering Software Development Made Easy
PROMOTION AGENCY SUMY
Sumy 3D Tour
Contacts
Sumy State University, 2 Rymskogo-Korsakova St., Sumy, 40007, Ukraine
E-mail: dsmie@teset.sumdu.edu.ua
Tel.: +38-066-488-03-19
Together we can do more for science,
technology, engineering and education
© DSMIE Team

JOURNAL OF ENGINEERING SCIENCES
ЖУРНАЛ ІНЖЕНЕРНИХ НАУК
ЖУРНАЛ ИНЖЕНЕРНЫХ НАУК

Web site: http://jes.sumdu.edu.ua

DOI: 10.21272/jes.2018.5(1).a1 Volume 5, Issue 1 (2018)

UDC 621.923.1

Profile Gear Grinding Temperature Reduction and Equalization

Lishchenko N. V.[1], Larshin V. P.[2]

[1] Odessa National Academy of Food Technologies, 112 Kanatna St., Odessa, 65039, Ukraine;
[2] Odessa National Polytechnic University, 1 Shevchenka Av., Odessa, 65044, Ukraine

Article info:
Paper received: December 29, 2017
The final version of the paper received: February 3, 2018
Paper accepted online: March 5, 2018

***Corresponding Author's Address:**
odeslnv@gmail.com

Abstract. The profile gear grinding modes definition technique is developed to provide the uniform residual temperatures after heating and subsequent cooling which predetermine uniform thermal deformations on periphery of a cogwheel when grinding. The initial basis for this is a possibility to determine the gear grinding temperature both on the heating and cooling stages and, besides, it is may be also a choice of the operation cycle structure with and without the working stroke omission. In the interval of the profile gear grinding modes, two variants of the gear grinding working cycle structure with reciprocating displacement of the grinding wheel are considered using the simulation method with an omission and without one of the working stroke. Certain combinations of mode parameters are found in the range of their possible values at which the combination of heating and cooling leads to the lowest residual surface temperature both during and after working stroke.

Keywords: profile gear grinding, gear grinding temperature, heating stage, cooling stage, cycle structure, working stroke, temperature.

1 Introduction

Typically grinding modes are selected according to reference statistical tables [1]. The choice of them is not substantiated by any criterion, for example, a criterion of the absence of grinding burns, a criterion of the grinding wheel life, a criterion for uniform heating of the machining cogwheel on its periphery, etc.

It is known the method of determining the modes of profile grinding in the three successive stages of this operation according to the system-wide principle of stage theory for any technical process. These stages are rough, semifinish, and finish ones and each of them depends on grinding temperature [2]. A peculiarity of the third grinding stage is the need to equalize the temperature heating along the periphery of a cogwheel. There is a rule that at the finishing stage, the infeed value should be such that it would be possible to grind all the cogwheel teeth without dressing the profile grinding wheel [3]. This is due to the fact that after the dressing, the grinding wheel changes its cutting capacity and the position line of the cutting edge. The infeed value at the finishing stage is reduced as the grinding stock for this stage decreases, and at the last grinding working stroke it is not recommended to apply the infeed values less than 0.010...0.015 mm [2]. However, these data are also not substantiated by any objective criterion and are more likely to be the result of practice.

In the paper [4] the three staged structure of the gear grinding operation is analyzed and consists of rough, semifinish and finish stages. Moreover, modes for each stage are selected based on the parameters of the specific material removal rate in $mm^3/(s \cdot mm)$ and the specific material removal in mm^3/mm. However, these are formal indicators which are not related, for example, to the grinding temperature and the grinding wheel wear.

The purpose of the paper is to improve the method of determining the grinding modes on the last finish (third) stage of the machining cycle by establishing a connection between formal indicators mentioned and the grinding temperature.

2 Research Methodology

2.1 Initial equations

One of the requirements for the finish (third) stage of machining is to ensure a uniform heating of a cogwheel by eliminating the heat accumulation on the periphery of the cogwheel. Thus, the criterion for optimizing the grinding operation at this stage may be the temperature of the grinding as one of the reasons that determine the

cogwheel heat content. The temperature field at the heating stage is described by a mathematical dependence, which is a solution of a one-dimensional differential equation of heat conductivity. To determine the temperature $T_H(x,\tau_H)$ at the heating stage, we can use the equation [5]

$$T_H(x,\tau_H)=\frac{2q}{\lambda}\sqrt{a\tau_H}\ \mathrm{ierfc}\frac{x}{2\sqrt{a\tau_H}}+T_0, \qquad (1)$$

in which by denoting $\frac{x}{2\sqrt{a\tau_H}}=\xi$, we remind the well-known relations

$$\mathrm{ierfc}\,\xi=\left[\frac{1}{\sqrt{\pi}}\exp(-\xi^2)-\xi\,\mathrm{erfc}\,\xi\right];\ \mathrm{erfc}\,\xi=1-\mathrm{erf}\,\xi;$$

$$\mathrm{erf}\,\xi=\frac{2}{\sqrt{\pi}}\int_0^{\xi}\exp(-\varepsilon^2)\mathrm{d}\varepsilon.$$

In the formula (1) q is the heat flux density (W/m^2), a stands for the temperature conductivity (m^2/s), λ for the heat conductivity (W/(m·K)), x for the dimensional coordinate along the depth of the surface layer (m), $\tau_H=2h_H/V_f$ for the maximum dimensional heating time at the heating stage (s), V_f for the velocity of the source in the direction of the z axis (axial feed or velocity of the part, m/s), h_H for the maximum value of the provisional value h $(0\le h\le h_H)$ at the heating stage, that is, the actual half-width of the real heat source (m), T_0 is the initial temperature of the machining workpiece (room temperature, constant value).

The density of the heat flux q is obtained by averaging the instantaneous value of this parameter $q(r_x)$, and taking into account for each point of the involute profile with an instant radius vector [6]

$$q(r_x)=e_c\psi\frac{dQ}{dS_c}=\frac{P}{V_f\,S_{cc}}\psi\frac{V_f\,t_n(r_x)}{\sqrt{Dt_v(r_x)}}, \qquad (2)$$

where e_c and Q are the specific grinding energy and material removal rate (in J/mm^3 and mm^3/s), S_c stands for the contact area (m^2), P for the grinding power (W), S_{cc} for the cross-section area in the grinding wheel movement direction (m^2), ψ for the share of heat into the workpiece, $t_n(r_x)$ and $t_v(r_x)$ are the normal and vertical depths of cutting at an involute profile separate point (m), D is the instant diameter of the grinding wheel in the considered cross-section of its profile (m).

To determine the temperature at the cooling stage, which follows immediately after heating, with the initial conditions obtained during the heating stage, the following equation can be used [5]:

$$T_C(x,t_C)=\int_0^{\infty}\Bigg[\frac{1}{2\sqrt{\pi a t_C}}\left\{\exp\left(-\frac{(x-x')^2}{4at_C}\right)+\exp\left(-\frac{(x+x')^2}{4at_C}\right)\right\}-$$
$$-A\exp\left(at_CA^2+A(x+x')\right)\times\mathrm{erfc}\left(\frac{x+x'}{2\sqrt{at_C}}+A\sqrt{a\cdot t_C}\right)\Bigg]f(x')\,dx'+$$
$$+aA\int_0^{t_C}\Bigg[\frac{\exp\left(-\frac{x^2}{4a(t_C-\tau_C)}\right)}{\sqrt{\pi a(t_C-\tau_C)}}-A\exp\left(aA^2(t_C-\tau_C)+Ax\right)\times$$
$$\times\mathrm{erfc}\left(\frac{x}{2\sqrt{a(t_C-\tau_C)}}+A\sqrt{a(t_C-\tau_C)}\right)\Bigg]\varphi(\tau_C)\,d\tau_C, \qquad (3)$$

in which

$$f(x')=\frac{2q\sqrt{a\tau_H}}{\lambda}\left[\frac{1}{\sqrt{\pi}}\exp\left(-\frac{x'^2}{4a\tau_H}\right)-\frac{x'}{2\sqrt{a\tau_H}}\mathrm{erfc}\left(\frac{x'}{2\sqrt{a\tau_H}}\right)\right]+T_0,$$

where $\tau_H=2h_H/V_f$ stands for the maximum heating time at the heating stage (s), t_C for cooling time (s); $A=\frac{\alpha_h}{\lambda}$ for the reduced heat transfer coefficient, α_h for heat transfer coefficient (W/(m^2·K)), $\varphi(\tau_C)$ for the starting temperature of the lubricoolant (°C), which can vary over the cooling time interval τ_C, and $0\le\tau_C\le t_C$.

2.2 Technique for decision making

Thus, with a known type and a method of supplying the lubricoolant, for controlling the temperature at the cooling time interval it is possible to control the α_h coefficient value (convection coefficient), the magnitude of the output temperature of the lubricoolant $\varphi(\tau_C)$, and the grinding modes, that is, to regulate the vertical cutting depth t_v and the axial feed V_f. Moreover, the value of t_v affects the maximum heating temperature as well as the value of V_f determines the time of heating and cooling, which affects both on the T_H and the achieved temperature level $T_C(x,t)$ at the end of the cooling stage in the "heating-coolin" cycle on each working stroke. Thus, under otherwise identical conditions (cutting speed, grinding wheel characteristics, lubricoolant kind, etc.), the control and optimization parameters may include elements of cutting modes: t_v and V_f.

The cooling time $0 \le t_C \le \infty$ is counted from the heating interval end. The task is to determine such mode parameters t_v and V_f, under which the heating stage with the surface temperature $T_{\max} = T(0,\tau_H)$ (Figure 1, line 1) will be changed by a cooling stage at which the temperature will change in the required manner (Figure 1, line 2). The control is to choose the grinding modes t_v and V_f which will result in the absence of heat accumulation (Figure 1, line 2): T_{C1}, T_{C2}, T_{C3} and T'_{C1}, T'_{C2}, and T'_{C3} are necessary (completely cooled surface) and actual (not completely cooled surface) surface temperature dependence on time in the first, second and third working passes, respectively.

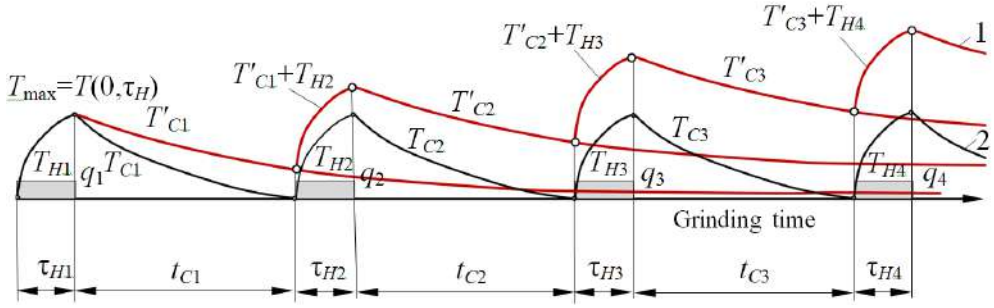

Figure 1– Grinding temperature changing with accumulation heat energy (line 1) and without it (line 2)

With a local increase in the temperature of individual grinded sections of the toothed surface, the temperature field is asymmetric in the symmetric body of the workpiece. This will lead to temperature ununiformed deformations of the heated sections, and, in consequence, to the cogwheel accuracy parameters deviations after the cogwheel cooling.

3 Results

3.1 Gear grinding with and without working stroke omission

There are two structures of the "heating-cooling" cycle: the up–and-down grinding without working stroke omission (Figure 2 a) and the only up grinding with the omission (Figure 2 b). In the cycle structure without working stroke omission the grinding wheel makes a working stroke with the length of $l_1 + B + l_2$ (B is the width of the tooth rim, l_1 and l_2 are the grinding wheel approach and overtravel lengths), i.e. consistently passes the points 1-2-3 (up grinding), which are located in the beginning, middle and end of the length of the tooth rim (Figure 2 a). On the reverse working stroke, the grinding wheel makes reverse displacement (down grinding), i.e. consistently passes the points 3-2-1. In this case, the greatest amount of heating gets the point 3, because at this point, the cooling time is the smallest and is equal to

$$t_1 = \frac{2l_2}{V_f} \qquad (4)$$

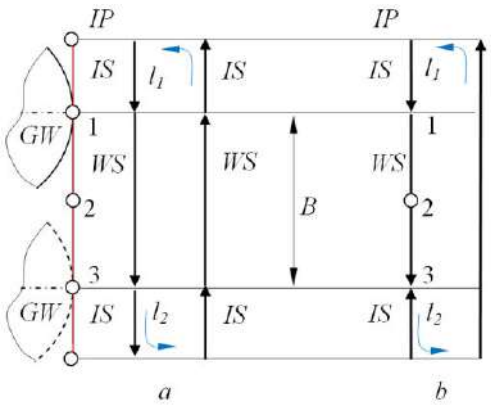

Figure 2 – The grinding cycle structures, in which *GW* is a grinding wheel; IP, IS and WS are the initial position, single and working strokes respectively

When repeating the "heating-cooling" cycle, the point 1 gets the greatest heating amount, because at this point, the cooling time is the smallest and is equal to

$$t_2 = \frac{2l_1}{V_f}. \quad (5)$$

In the structure of the cycle with the working stroke omission, the grinding wheel makes a working stroke $l_1 + B + l_2$ consistently passing the points 1-2-3 (up grinding), which belong to the beginning, middle and end of the tooth rim length (Figure 2 b). Before the reverse stroke the grinding wheel does not move radially to the cutting depth t_v that is this reverse stroke is idle and the grinding wheel makes idle stroke with the length of $l_2 + B + l_1$ (points 3-2-1 without heating) getting to the initial position. When repeating the "heating-cooling" cycle, heating at the up grinding receives the point 1, that is at this point, the cooling time is the smallest and is equal to

$$t_3 = \frac{2l_1 + 2l_2 + 2B}{V_f}. \quad (6)$$

3.2 Reduction and equalization of temperature

Assuming $l_1 = l_2 = l$ for the structure with the working stroke omission we can see that cooling time according to formula (6) increases more than twice because the ratio of t_3 / t_1 is equal to the t_3 / t_2 and is $2(2l + B) / 2l = 2 + B / l$.

Next, we introduce the following symbols for the surface temperature (i.e. x = 0) for heating and cooling: $T_H(0, \tau_H) = T_H$ and $T_C(0, t_C) = T_C$, respectively. For both structures of the cycle the influence of the axial feed V_f and the vertical depth of cutting t_v on the heating time τ_H and the heating temperature T_H by the formula (1) and the cooling temperature T_C by the formula (3) are established with the following initial data: x = 0 (on surface); e_c = 50 J/mm^3; ψ = 0,8; profile angle α = 20° or $\frac{\alpha\pi}{180^o}$ rad; D = 400 mm; a = 5.68·10^{-6} m^2/s; λ = 24 W/(m·K); α_h = 10 000 W/(m^2·K); $A = \frac{\alpha_h}{\lambda}$ = = 416,67 m^{-1}; T_0 = 0 °C; $\varphi(\tau_C)$ = 15 °C; $l_1 = l_2$ = 7.86 mm; B =24 mm. The axial feed V_f varies in the range of 500...7000 mm/min, and the vertical depth of grinding t_v takes the following fixed values: t_v = 0.015 mm (Tables 1, 3) and t_v = 0.074 mm (Tables 2, 4). With increasing V_f for t_v = const (Tables 1, 2), the heating time τ_H decreases and the heating temperature T_H increases. With the increasing t_v at the same values for V_f (pairs of Tables 1, 2, as well as Tables 3, 4), the heating time τ_H and heating temperature T_H increase.

For the cycle with the working stroke omission (Tables 3, 4), the heating time τ_H and the heating temperature T_H did not change compared with the previous structure (without working stroke omission), therefore, τ_H and T_H in Table. 3 and Table 4 are not given. There are both cooling time t_C and cooling temperature T_C changing at t_v = 0.015 mm (Table 3) and t_v = 0.074 mm (Table 4). The reason for the difference between the parameters t_C and T_C in cycles with and without working stroke omission is the only one - the increase in cooling time t_C in the cycle structure with working stroke omission.

Table 1 – Influence the V_f on the τ_H, T_H, t_C, and T_C for the cycle structure without working stroke omission at t_v = 0.015 mm

V_f, mm/min	500	1000	1500	2000	2500	3000	3500
τ_H, s	0.2939	0.1469	0.09798	0.07348	0.05879	0.04899	0.04199
T_H, °C	42.42	59.99	73.47	84.84	94.86	103.91	112.24
t_C, s	1.8868	0.9434	0.6289	0.4717	0.3774	0.3145	0.2695
T_C, °C	11.598	12.002	12.789	13.903	14.906	15.606	16.556
V_f, mm/min	4000	4500	5000	5500	6000	6500	7000
τ_H, s	0.03674	0.03266	0.02939	0.02672	0.02449	0.02261	0.021
T_H, °C	119.986	127.268	134.143	140.696	146.956	152.957	158.731
t_C, s	0.23585	0.20964	0.18868	0.17153	0.15723	0.14514	0.13477
T_C, °C	17.494	18.416	19.317	20.205	21.072	21.922	22.755

Table 2 – Influence of V_f on τ_H, T_H, t_C, T_C for cycle structure without working stroke omission at t_v = 0.074 mm

V_f, mm/min	**500**	**1000**	**1500**	**2000**	**2500**	**3000**	**3500**
τ_H, c	0.65287	0.32644	0.21762	0.16322	0.13057	0.10881	0.09327
T_H, °C	140.428	198.595	243.228	280.856	314.006	343.977	371.537
t_C, c	1.88678	0.94339	0.62893	0.4717	0.37736	0.31446	0.26954
T_C, °C	18.61	26.35	33.541	40.264	46.604	52.618	58.348
V_f, mm/min	**4000**	**4500**	**5000**	**5500**	**6000**	**6500**	**7000**
τ_H, c	0.08161	0.07254	0.06529	0.05935	0.05441	0.05022	0.04663
T_H, °C	397.19	421.284	444.072	465.747	486.456	506.32	525.433
t_C, c	0.23585	0.20964	0.18868	0.17153	0.15723	0.14514	0.13477
T_C, °C	63.832	69.097	74.168	79.065	83.805	88.402	92.869

Table 3 – Influence the V_f on the t_C and T_C for the cycle structure with working stroke omission at t_v = 0.015 mm

V_f, mm/min	500	1000	1500	2000	2500	3000	3500
t_C, c	9.53357	4.76678	3.17786	2.38339	1.90671	1.58893	1.36194
T_C, °C	12.604	11.976	11.657	11.494	11.426	11.42	11.458
V_f, mm/min	4000	4500	5000	5500	6000	6500	7000
t_C, c	1.1917	1.05929	0.95336	0.86669	0.79446	0.73335	0.68097
T_C, °C	11.529	11.624	11.738	11.867	12.008	12.158	12.317

Table 4 – The same as Table 3 at t_v = 0.074 mm

V_f, mm/min	500	1000	1500	2000	2500	3000	3500
t_C, c	9.53357	4.76678	3.17786	2.38339	1.90671	1.58893	1.36194
T_C, °C	13.57	14.342	15.457	16.726	18.078	19.477	20.902
V_f, mm/min	4000	4500	5000	5500	6000	6500	7000
t_C, c	1.1917	1.05929	0.95336	0.86669	0.79446	0.73335	0.68097
T_C, °C	22.339	23.78	25.218	26.651	28.074	29.487	30.889

Let's perform a comparison of the cooling temperatures for two grinding cycle structures at t_v = 0.015 mm (Fig. 3, *a*) and t_v = 0,074 mm (Fig. 3, *b*). There are three ways to achieve the lowest cooling temperature T_C = 11.6°C for t_v = 0,015 mm (Fig. 3, *a*): 1) when grinding without working stroke omission with axial feed V_f = 0.5 m/min (point *A*), 2) when grinding with working stroke omission with axial feed V_f =1.8308 m/min (point *B*, and 3) the latter at V_f = 4226.9 mm/min (point *C*).

There are two ways to achieve the lowest cooling temperature T_C = 18.6 °C for t_v = 0.074 mm (Figure 3 b) when grinding without working stroke omission with axial feed V_f = 0.5 m/min (point *D*; 2) when grinding with working stroke omission with an axial feed V_f = 2.6444 m/min (point *E*).

The time to machine by gear grinding both without and with working stroke omission can be determined by the following formulas, respectively

$$T_M = \left(\frac{B + l_1 + l_2}{V_f} \frac{z_{\max}}{t_v} + \frac{T_{IND}}{60} \right) z ; \qquad (7)$$

$$T_O = \left(\frac{B + l_1 + l_2}{V_f} 2 \frac{z_{\max}}{t_v} + \frac{T_{IND}}{60} \right) z , \qquad (8)$$

where B stands for the width of the tooth rim (B =24 mm), z for the number of cogwheel teeth (z = 40), $l_1 = l_2$ = 7.86 mm, $z_{\max}$ for the grinding stock for machining a cogwheel in the finish (third) stage ($z_{\max}$ = 0,1 mm), T_{IND} for the indexing time (cogwheel angular turning for one tooth, T_{IND} = 4 s).

To ensure the lowest cooling temperature T_C = 11.6 °C, the minimum time to machine is equal to 7.632 min (Table 5) which is obtained in the with working stroke omission cycle structure at t_v = 0.015 mm and V_f = 4226.9 mm / min.

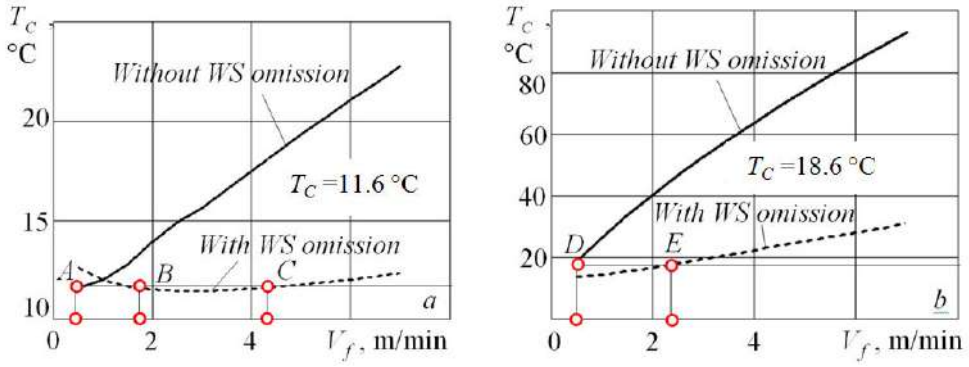

a b

Figure 3 – Cooling temperature T_C vs axial feed V_f for different grinding cycle structures at t_v = 0.015 mm (a) and t_v = 0.074 mm (b)

Table 5 – Determining the time to machine in gear grinding

Grinding cycle structure of the	Without working stroke omission	With working stroke omission	
The lowest cooling temperature T_C = 11.6 ° C at t_v = 0.015 mm			
Grinding conditions	V_f =500 mm/min (point *A*)	V_f =1830.8 mm/min (point *B*)	V_f = 4226.9 mm/min (point *C*)
Time to machine, min	23.852	14.238	7.632
The lowest cooling temperature T_C = 18.6 °C at t_v = 0.074 mm			
Grinding conditions	V_f =500 mm/min (point *D*)	V_f = 2644.9 mm/min (point *E*)	
Time to machine, min	6.961	4.29	

To provide the cooling temperature T_C = 18.6 °C (more than 11.6 °C), the minimum time to machine T_M = 4.29 min (Table 5) is obtained in the cycle structure with working stroke omission at t_v = 0.074 mm and V_f = 2644.9 mm/min. From these five variants (points *A*, *B*, *C*, *D*, and *E* in Figure 3) we choose the variant with the minimum value T_C = 11.6 °C (points *A*, *B*, *C*), since the theoretical value is T_C = 0. It can be seen (Table 5) that the minimum time to machine T_M = 7.632 min is obtained in the cycle structure with working stroke omission at t_v = 0.015 mm and V_f = 4226.9 mm/min (T_C = 11.6 °C).

Thus, the study of the gear grinding temperature models (1) and (3) both at the heating (1) and cooling (3) stages allowed to recommend the working stroke omission in the structure of this operation and to assign the appropriate gear grinding modes for the finish (third) gear grinding stage both for t_v = 0.015 mm (points *A*, *B*, *C* in Figure 3) and t_v = 0.074 mm (points *D*, *E*).

4 Conclusions

As the depth of gear grinding t_v increases the maximum cooling temperature T_C increases as well. In the gear grinding cycle structure with working stroke omission cooling time t_C is greater than that without working stroke omission. As the axial feed V_f increases the cooling temperature T_C for the cycle structure with working stroke omission at t_v = 0.015 mm and t_v = 0.074 mm does not practically change, while for the cycle structure without working stroke omission the cooling temperature T_C increases. The smallest cooling temperature T_C is reached at t_v = 0,015 mm, so it is expedient to accept the minimum possible vertical depth of grinding t_v on the finishing (third) gear grinding stage, for example, for the finishing stage we take t_v = 0,015 mm.

Moreover, in this stage, the axial feed V_f is chosen not only from the condition of maximum productivity (maximum V_f), but also from the condition of surface roughness (in the interval of V_f from 1830.8 to 4226.9 mm/min) and the smallest elastic deformation in the gear grinding system.

References

1. Kalashnikov, S. N. et al. (1990). *Proizvodstvo zubchatykh koles: Handbook*. Moscow, Mashinostroyeniye [in Russian].
2. Lishchenko, N. V. (2016). Opredeleniye intensivnosti zuboshlifovaniya na osnove analiticheskogo uravneniya evol'venty. *Suchasni tekhnologii v mashinobuduvanni*, Issue 11 [in Russian].
3. Dekapolitov, M. I. (2011). *Povysheniye effektivnosti profil'nogo zuboshlifovaniya tsilindricheskikh koles putem rascheta parametrov staticheskoy naladki: Ph.D. thesis*. Specialties 05.02.07 – Tekhnologiya i oborudovanie mekhanich. i fiziko-tekhnologicheskoy obrabotki; 05.02.08 – Tekhnologiya mashinostroyeniya. Moscow.
4. Nishimura, Yu., Katsuma, T., Ashizawa, Y., Yanase, Y., Masuo, K. (2008). Gear grinding processing developed for high-precision gear manufacturing. *Mitsubishi Heavy Industries, Ltd. Technical Review*, Vol. 45, No. 3, 33–38.
5. Carslaw, H. S., Jaeger, J. C.(1959). *Conduction of heat in solids (2nd ed.)*. London, Oxford University Press.
6. Larshin, V. P. (1999). Tekhnologiya mnogonitochnogo rez'boshlifovaniya pretsizionnykh khodovykh vintov. *Proceedings of Odessa National Polytechnic University*, Odessa, Issue 2(8), 87–91 [in Russian].

Зниження та вирівнювання температури профільного зубошліфування

Ліщенко Н. В.[1], Ларшин В. П.[2]

[1] Одеська національна академія харчових технологій, вул. Канатна, 112, м. Одеса, 65039, Україна;
[2] Одеський національний політехнічний університет, просп. Шевченка, 1, м. Одеса, 65044, Україна

Анотація. Розроблено методику визначення режимів зубошліфування на третьому завершальному етапі профільного зубошліфування на верстаті з ЧПК, виходячи із забезпечення вирівнювання температури по периферії і найменшого нагрівання зубчастого колеса. Для цього використано формули для визначення температури зубошліфування на етапі нагрівання та охолодження оброблюваної поверхні. На етапі нагріву температурне поле поширюється по глибині поверхневого шару і змінюється в часі. У момент закінчення етапу нагріву, миттєве температурне поле, яке загасає по глибині поверхневого шару, є початковою умовою для визначення температури на етапі охолодження. Тому температура охолоджувальної поверхні залежить не тільки від регульованого часу охолодження, але також від миттєвого розподілу температури в поверхневому шарі, яке враховується як початкова умова при моделюванні на етапі охолодження. Знайдено оптимальні умови охолодження, в тому числі за рахунок пропусків робочих ходів, які реалізовані зубошліфуванням без установки глибини різання.

Ключові слова: профільне зубошліфування, температура зубошліфування, етап нагріву, етап охолодження, структура циклу, пропуск робочого ходу, вирівнювання температури.

JOURNAL OF ENGINEERING SCIENCES
ЖУРНАЛ ІНЖЕНЕРНИХ НАУК
ЖУРНАЛ ИНЖЕНЕРНЫХ НАУК

Web site: http://jes.sumdu.edu.ua

DOI: 10.21272/jes.2018.5(1).a2 Volume 5, Issue 1 (2018)

UDC 621.774

Influence of the Wall Thickness Value on the Cross Wall Thickness Deviation of Tubes Rolled on the Tube Rolling Plant with the Continuous Mill

Pilipenko S. V.*, Drozhzha P. V., Limonchenko E. A.

National Metallurgical Academy of Ukraine, 4 Gagarina Av., Dnipro, 49600, Ukraine

Article info:
Paper received: January 12, 2018
The final version of the paper received: February 12, 2018
Paper accepted online: March 5, 2018

***Corresponding Author's Address:**
44-08@i.ua

Abstract. The high requirements as to accuracy of the wall thickness are due not only to necessity of assuring the reliability and serviceability of equipment, but also to the trend towards the continuous decrease of metal capacity. In this situation assuring observing of the given parameter is the most difficult affair. The cross wall thickness deviation can be presented in the form of two components: eccentric and symmetric deviation. In the given work authors present the research of the influence of the tube wall thickness on the share of eccentric component of the wall thickness deviation of the tubes rolled on the TRP with the continuous mill. Analysis of research results allowed concluding that with increase of the tube wall thickness the share of wall thickness deviation induced with the eccentricity decreases. On the whole, it is to be noted that for the giving plant, characteristically the influence of methods of longitudinal flaring (in continuous mill with mandrel and multistand mills of rolling without mandrel) on the tube accuracy is greater. In two first cases while reducing tubes to the finish dimension, the share of the number of faces, which depends on the summary reduction through the diameter and the value of tension, increases substantially.

Keywords: tube rolling plant with continuous mill, wall thickness, cross wall thickness deviation, eccentric component.

1 Introduction

Accuracy of the tube wall thickness is one of the most important characteristics of the given kind of metal products. The value of this characteristic's scattering is strictly regulated by the up-to-date standards. The high requirements as to precision of the wall thickness are conditioned not only by the necessity of assuring the reliability and efficiency of equipment, but also by the trend of continuous decreasing the metal capacity (content) [2, 3]. In these conditions the most complicated task is to ensure the maintenance of the mentioned parameter of the tube accuracy [1, 2].

2 Literature Review

Precision of finished tubes is a result of shaping (changing the shape) of a tube on all the stages of deforming the latter. In this situation the special attention should be given to the aggregate (mill), where the proper geometrical sign is formed [1]. In the general form the cross wall thickness deviation can be presented as two components [1, 4]: eccentric wall thickness deviation and deviation occasioned by the "cut" of internal and external surfaces. The "eccentricity" of tubes rolled on the TRA with continuous mill averages 55 %; tubes rolled on the TRP with plug automatic mill have the average value of wall thickness deviation within the limits of 26 % [1]. From the practice of the pipe and tube production it is known that for all the tubes, which were not subjected to considerable degree of reducing, independently of method of production, the share of eccentricity makes the greater part in the scattering of the wall thickness in the cross tube section [4].

The wall thickness is formed in the process of piercing and decreases in the course of rolling out (Figures 1, 2) [1, 2], but the main influence on accuracy of the wall is exerted exactly by the process of piercing [1].

As a whole, the relative wall thickness deviation of tubes rolled on TRA with continuous mill decreases with increase of the tube wall thickness [1] (Figure 3).

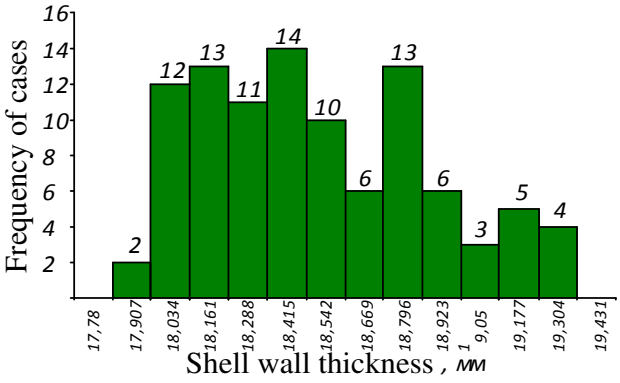

Figure 1 – The statistic distribution of the shell wall thickness [2]

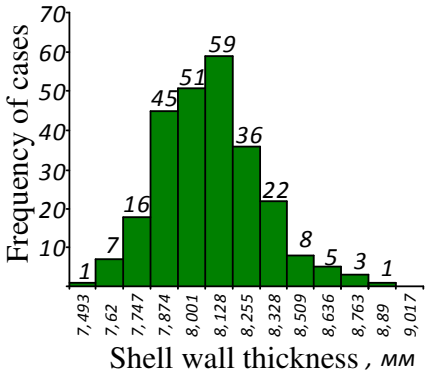

Figure 2 – The statistic distribution of the rough tube wall thickness

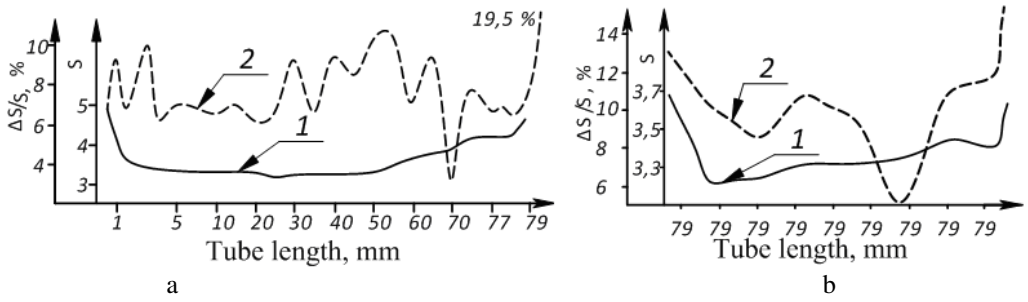

a b

Figure 3 – Change of the average values of the wall thickness (1) and the cross wall thickness deviation (2) along the length of a finished tube with dimensions: 45×3.5 mm (a); 76×3.5 mm (b) [1]

Tubes rolled on the TRA with continuous mill have strongly pronounced bulges on their ends (Figure 4). Wall thickness deviation of a tube on the thickened ends is on the average greater than the deviation in the middle part of a tube.

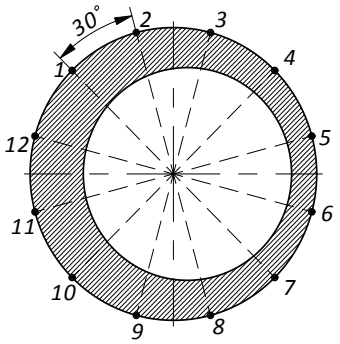

Figure 4 – The scheme of measurement of the wall thickness in the cross section of a tube

Precision of tubes as to wall thickness is an important and difficult to achieve factor of the quality of the given kind of rolled products. It depends on many factors. The degree of importance of majority of these factors is not completely specified. One of the questions, which are not enough taken up – is the investigation of the influence of the wall thickness on the eccentric wall thickness deviation of the cross section of tubes rolled on the TRP with continuous mill, and any investigations taking up this theme are actual.

3 Research Methodology

The following positions of assortment of the TRP with continuous mill have been chosen for investigation of the influence of the wall thickness on the eccentric wall thickness deviation of the cross tube section:

– 73×5.5 mm (D/S = 13.3);
– 32×3 mm (D/S = 10.7);
– 93×13 mm (D/S = 7.2).

After cutting the thickened ends, the pipe sockets have been cut from the tubes, marked and measured in 12 sections (Figure 4). Results of measurements are shown in the Table 1 and the Figure 5. The character of the change of the wall thickness deviation in cross section of the tubes rolled on TRP with continuous mill is shown in the Table 2.

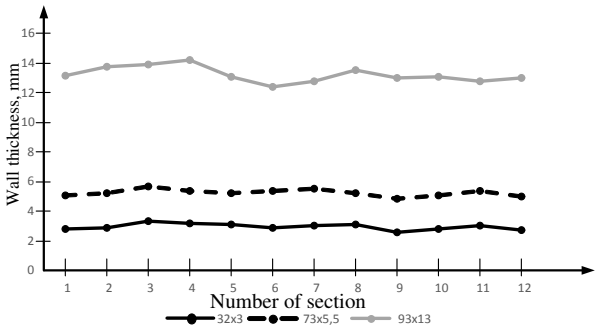

Figure 5 – Change of the wall thickness in the cross section of tubes rolled on the TRP with continuous mill

Table 1 – The change of the wall thickness in the cross section of tubes rolled on the TRP with continuous mill

Dt×St	Number of the point of measurement and value of the wall thickness deviation, mm											
	1	2	3	4	5	6	7	8	9	10	11	12
32×3	2.8	2.9	3.3	3.2	3.1	2.9	3	3.1	2.6	2.8	3	2.7
73×5.	5.1	5.25	5.65	5.4	5.25	5.35	5.55	5.2	4.8	5.1	5.35	5
93×13	13.15	13.75	13.9	14.2	13.1	12.4	12.75	13,55	13	13.1	12.8	13

Table 2 – Change of wall thickness deviation in the cross section of tubes rolled on the TRP with continuous mill

Dt×St	Number of the point of measurement and value of the wall thickness deviation, %											
	1	2	3	4	5	6	7	8	9	10	11	12
32×3	–5.08	–1.69	11.86	8.47	5.08	–1.69	1.69	5.08	–11.86	–5.08	1.69	–8.47
73×5.5	–2.86	0.00	7.62	2.86	0.00	1.90	5.71	–0.95	–8.57	–2.86	1.90	–4.76
93×13	–0.57	3.97	5.10	7.37	–0.95	–6.24	–3.59	2.46	–1.70	–0.95	–3.21	–1.70

As a whole, the cross wall thickness deviation can be presented as two components: eccentric and symmetric wall thickness deviation. To pick out these parts, let us use the approach, set forth in [1].

The main point of the given method consists in the following. On the first stage it is necessary to put in order the experimental data as to measurements of the tube wall thickness in the cross section in the following way. Let us choose the greatest value of the wall thickness in the given cross section and confer the index "1" to it. The rest of values of the given excerpt will be numbered one after another from left to right.

For example, for a tube 73x5.5 mm we have the measurements in the form of a set of the wall thickness values, presented in the table 1. After putting in order the values of wall thickness, the massif will look as following: 5.65; 5.40; 5.25; 5.35; 5.55; 5.2; 4.8; 5.1; 5.35; 5.0; 5.1; 5.25

Further let us determine the average wall thickness of the tube S_{av} in the given cross section, eccentricity e, the part of dispersion σ_e^2, stipulated by eccentric component of the wall thickness deviation, the summary dispersion of the wall thickness σ_Σ^2. Let us find the share (part) a_e, brought into deviation of the tube wall thickness by eccentricity according to the formula:

$$a_э = \frac{\sigma_э^2}{\sigma_\Sigma^2}. \quad (1)$$

Let us calculate the value of the absolute cross wall thickness deviation ΔS_d, supposing that the probability of finding in the given cross section such value of ΔS_φ, which $\Delta S_\varphi > \Delta S_d$ for $P = 0.05$:

$$\Delta S_p = \psi \frac{n}{n-1} \sigma_\Sigma. \quad (2)$$

where n is the number of measurements of the wall thickness in given section; σ_Σ is the meansquare deviation; Ψ is the coefficient binding the share of wall thickness deviation a_e, caused by eccentricity in the total dispersion of the wall thickness:

$$\psi = 2\left(\sqrt{2a_э} + \sqrt{3(1-a_э)} - 0{,}82\sqrt[4]{a_э(1-a_э)}\right) \quad (3)$$

At the discrete measurements of the wall thickness the formula (2) allows calculating with more accuracy the value of the real swing (scattering) of the wall thickness values in the given section, since because of measurements discreteness there is the probability of finding the actual maximum (minimum) between the points of measurement.

Results of experimental data treatment are shown in the Table 3.

Table 3 – Results of treatment of the wall thickness experimental measurements in cross sections of a tube

Dt×St, mm	S_{av}, mm	e, mm	σ_Σ^2, mm^2	Σ ,mm^2	a_e %	ΔS_r, mm	ΔS, mm
32×3	2.92	0.137	0.039	0.009	24.0	0.7	0.72
73×5.5	5.25	0.146	0.050	0.011	21.2	0.085	0.815
93×13	13.2	0.290	0.318	0.042	13.2	2.2	2.03

4 Conclusions

Analysis of data in the Table 3 allows making the following conclusions. The share of the tube wall thickness deviation caused by eccentricity is decreasing with increase of the tube wall thickness. As a whole, it is to note that the characteristic feature for given unit is the greater influence of the process of the lengthwise rolling-off on accuracy of tubes, namely, rolling-off in continuous rolling mill with mandrel and in multistand mills for rolling without mandrel. In the first two cases, while reducing tubes to the final dimension, the share of cutting depending on summary reduction as to diameter and the value of tension, is substantially increased.

References

1. Stoletnij, M. F., Klempert, Ye. D. (1975). *Tochnost' trub*. Moscow, Metallurgiya [in Russian].
2. Vydrin, A. V., Shirokov, V. V. (2014). Teoreticheskiye osnovy povysheniya tochnosti razmerov trub pri prokatke na niepreryvnom stane. *Vestnik Yuzhno-Uralskogo gosudarstvennogo Universiteta, Seriya "Metallurgiya. Sbornik nauchnykh trudov"*, No. 14, 81–86 [in Russian].
3. Khramkov, Ye. V., Shirokov, V. V. (2014). Otsenka vliyaniya razlichnykh faktorov na tochnost' trub / Ye.V/ Khramkov, V.V. Shirokov // Vestnik Yuzhno-Uralskogo gosudarstvennogo Universiteta. Seriya: Metallurgiya. Sbornik nauchnykh trudov N 14. – YuUrGU: Cheliyabinsk, 2014. – S. 76-79 [in Russian].
4. Struin, D. O. (2012). Issledovaniye tochnosti prokata na TPA so stanom PQF. *Innovatsionnye teknologii v metallurgii i mashynostroyenii*. A. F. Golovin Uralskaya nauchno-pedagogicheskaya shkola, pp. 499–501 [in Russian].

Дослідження впливу величини товщини стінки на поперечну різностінність труб, прокатаних на ТПА з безперервним станом

Пилипенко С. В., Дрожа П. В., Лимонченко Е. А.

Національна металургійна академія України, просп. Гагаріна, 4, м. Дніпро, 49600, Україна

Анотація. Високі вимоги до точності товщини стінки обумовлюються не тільки необхідністю забезпечення надійності і працездатності (роботоспроможності) обладнання, але й тенденцією до постійного зниження його металоємності. При цьому забезпечити дотримання даного параметра точності труби найбільш складно. Поперечну різностінність можна представити у вигляді двох складових: ексцентричної та симетричної різностінності. У статті представлено дослідження впливу величини товщини стінки труби на частку ексцентричної складової поперечної різностінності труб, прокатаних на ТПА з безперервним станом. Аналіз результатів досліджень дозволив зробити висновки, що зі збільшенням товщини стінки труби знижується частка різностінності, викликаної ексцентричністю. В цілому, слід зазначити, що для даного агрегату є характерним більший вплив на точність труб способів поздовжньої розкатки: в безперервному оправочному стані і багатоклітьових станах безоправочної прокатки. У перших двох випадках, при редукуванні труб на готовий розмір, істотно зростає частка гранчастості, що залежить від сумарного обтиску по діаметру і величини натягу.

Ключові слова: ТПА з безперервним станом, товщина стінки, поперечна різностінність, екцентрична складова.

JOURNAL OF ENGINEERING SCIENCES
ЖУРНАЛ ІНЖЕНЕРНИХ НАУК
ЖУРНАЛ ИНЖЕНЕРНЫХ НАУК
Web site: http://jes.sumdu.edu.ua
DOI: 10.21272/jes.2018.5(1).a3 Volume 5, Issue 1 (2018)

UDC 621.9.025.77:615.46:616.728

Diamond Grinding the Ceramic Balls from Silicon Carbide

Sokhan' S. V.*, Maystrenko A.L., Kulich V. H., Sorochenko V. H., Voznyy V. V., Gamaniuk M.P., Zubaniev Ye. M.
Bakul Institute for Superhard Materials of NAS of Ukraine, 2 Avtozavodska St., Kyiv, 04074, Ukraine

Article info:
Paper received: November 11, 2017
The final version of the paper received: March 12, 2018
Paper accepted online: March 20, 2018

***Corresponding Author's Address:**
svsokh@ukr.net

Abstract. The influence of the machining regime was experimentally investigated on the output indexes of the diamond grinding the ceramic balls from silicon carbide, such as the rate of the material removal and the rate of changing (decreasing or increasing) the deviation from sphericity of the ball's surface. To distinguish a particle of these indexes as caused by the actual influence of the machining regime was applied a method of graphical approximation of the time-varying ball's diameter and deviation from sphericity. The separated particles of the process indexes can vary both as growing and as decreasing depending on the values of the parameters of the machining regime, such as: the discrete feeding of the diamond wheel to the cutting, the time of grinding between feedings of the wheel and the rotation speed of the table with the balls. For further determining the influence of the machining regime was applied a method of a complete factor-type experiment of type 2^3, in which the factors of the above parameters were specified. As a result, the most effective way to reduce the deviation from the sphericity of the ball's surface is to combine these parameters.

Keywords: ceramic balls from silicon carbide, diamond grinding, rate of the material removal, rate of changing the ball's shape, machining regime, discrete feeding of the diamond wheel to the cutting, time of grinding between feedings of the wheel, rotation speed of the table.

1 Introduction

Many branches of industry exploit a large number of rolling bearings, pumps, hydromotors and other mechanisms, the resource and reliability of which depend on the efficiency and quality of parts such as "ball". Now balls are mainly made of steel and they are relatively quickly failured in conditions of high loads, temperatures, as well as intense abrasive, corrosion, chemical and other types of wear. Replacing steel balls on ceramic in many cases allows you to achieve higher performance and extend the range of functionality of the devices in which they are used. Thus, in hybrid ball bearings combination of rolling ceramic bodies and high quality of surface of steel rings (Figure 1) gives the advantages for longer service life and better performance at high speeds.

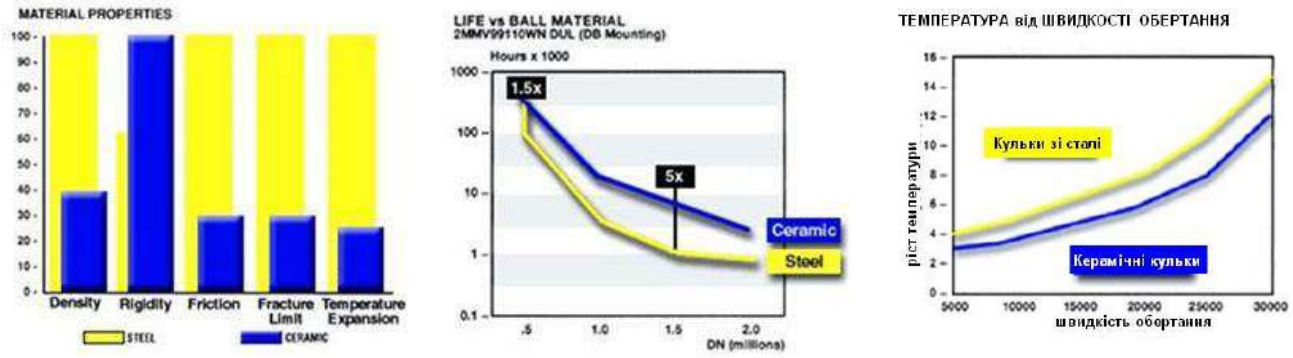

Figure 1 – Comparison of characteristics of hybrid and steel ball bearings [1]

2 Literature Review

In the 1990s, the leading organizations of the National Academy of Sciences of Ukraine contributed to the creation of effective ceramic and composite materials based on boron and silicon carbides, as well as technologies for manufacturing precision products of the "ball" type [2, 3] that work in difficult operating conditions. Firstly, it concerns materials based on boron carbide – it is the third according to the hardness of a material after diamond and cubic boron nitride, and one of the most inert chemical compounds. It has high hardness, durability and unique wear resistance under acting aggressive environments and abrasive wear.

An important incentive for the development of modern technical ceramics is the desire to develop a gas turbine engine with a high efficiency for the aerospace industry. The conditions of the bearings of the main shaft of such engines – the shaft speed more than 30 000 rpm and temperatures above 650 °C. At temperatures above 1 100 °C, only ceramic materials are used because their higher hardness than those of bearing steel or even cobalt alloys and high-speed steels with high content of tungsten.

The most difficult in the manufacture of any ball bearings is the abrasive machining the balls. The operational properties of the bearings depend, first, on the perfomance of their working surfaces, such as the precision of machining, roughness and microstructure. The group abrasive finishing of balls between rotating discs is the most versatile operation of making balls and up to this time attracts the attention of researchers [4–6]. At diamond grinding or finishing ceramic balls are rolled along the tracks of the lower disk without their mixing unlike elevator abrasive machining the steel balls in mass production when their mixing. Becouse of it is limited the number of simultaneously machined ceramic balls by their placement on the tracks of the lower disk and to achive high accuracy the ball's shape is difficult.

3 Research Methodology

3.1 Features of surface layer forming in ceramic products from silicon carbide by diamond grinding

As well as for any brittle nonmetallic material, the diamond grinding of ceramic products, in particular from silicon carbide, is radically different from the abrasive grinding of metals [7–9]. When the diamond grinding brittle nonmetallic materials, there are an elastic-plastic deformation without breaking, as well dispersing the machining allowance at plastic deformation and brittle breaking the material with particle chipping. The probability of one or another mechanism of the destruction of the machining allowance is determined both by the physical and mechanical properties of the material and the load on the diamond grain (depending on the machining regime). A characteristic result of material removing during diamond grinding are lateral breakaways and cluster breaking on the surface layer, which are watched in the form of cells of destruction, which most influence the formation of the surface roughness [10]. In theoretical study of interaction between grains of abrasive powder and machined surface from brittle nonmetallic materials is used the cluster model of formation and removal of slime particles [11, 12].

The nature of the destruction of such brittle nonmetallic material, which is a silicon carbide, depends mainly on the magnitude of the normal force on diamond grains. When the normal force achieves own critical value, which is required for the formation of lateral cracks, the destruction results by scraping. The critical force that forms lateral cracks is determined by the dependence

$$P_{cr} = k_p \cdot \frac{K_{1C}^4}{H_\mu^3},$$

where k_p – constant coefficient; K_{1C} – stress intensity factor of the first type (critical intensity of cracking); H_μ – microhardness [13].

Proceeding from the physical and mechanical properties of the materials under consideration (Table 1), the critical force that forms lateral cracks in the surface layer of the hot-pressed silicon nitride is more than 2.3 times for the reaction-bonded silicon carbide. Therefore, when grinding carbide ceramics, the critical cross-sectional area of the material on the diamond grain [10], which takes place the breakaways, is smaller and, accordingly, several times smaller than for nitride ceramics is required for the cutting depth to appear the breakaways.

On the other hand, the critical size of the median fracture, in which it begins to develop in a steady manner during infusion, is inversely proportional to the square of the material fragility index

$$l_M = \frac{k_M}{\left(H_\mu / K_{1C}\right)^2},$$

where k_M – constant coefficient [13]. Experimentally proved during diamond machining [10] that the magnitude of the maximum half-length of defects in the surface layer of ceramics is linearly dependent on the critical size of the median fracture during the indentation, in which the crack develops. If the the index of fragility of the material is smaller, and consequently, the magnitude of the critical median fracture is greater when indenting, than the higher the value should be expected both the half-length of the maximum crack from the machining, and the depth of the cracked layer. Therefore, based on the data of the Table 1 under the same conditions of grinding, the breakaways on the machined surface of carbide ceramics should be larger, and the depth of the cracked layer – on the contrary, less than that of the surface of the nitride ceramics. At the same time, it should be noted that the comparative analysis taken into account only the physical and mechanical properties of the materials, but not the actual conditions of diamond grinding

(machining regime, etc.), which determine the depth of the cracked layer.

Taking into account the predisposition of the SiC-ceramics to cracking, as well as the peculiarities of the diamond grinding ceramic balls from silicon carbide, the purpose of the work was to determine the influence of the machining regime on the output indixes, such as the rate rate of the material removal and the rate of changing the deviation from sphericity.

Table 1 – Results of treatment of the wall thickness experimental measurements in cross sections of a tube

Indicator	Si_3N_4-ceramics (hot-pressed) [10]	SiC-ceramics (reaction-bonded) [14]
Density, g/sm^3	3.1	3.12
Young's module, GPa	310	413
Microhardness H_μ, GPa	13.9	20
Bending strength $\sigma_з$, MPa	690	370
Index of fragility H_μ/K_{1C}	3.23	4.35
Critical stress intensity factor of the first type K_{1C}, MPa/m$^{0.5}$	4.3	4.6

3.2 Experimental research

Investigation of the influence of the machining regime on the output indixes of diamond grinding ceramic balls from reaction-bonded silicon carbide carried out on a modernized ball-grinding machine VS-D204M (Figure 2) with the technological device for a placement of the balls on its desktop, the scheme of which shown in Fig. 3

As can see from the machining scheme shown in Figure 3, the device separates the kinematic chains on that, which realizes directly shaping, and on that, which realizes portable movements from the chain for the grinding process. Thanks to the device machining balls is carryed out at optimal grinding speeds of 25–30 m/s and the speed of moving balls of 0.15–0.30 m/s. In the experiments, a diamond grinding wheel of 6A2T form was applied with diamonds of grade AS32 with a grain size 250/200 of relative concentration of 100. The number of balls in the batch, which was simultaneously machined, was eight pcs.

The output indixes were the rate of the material removal $v_d = \Delta d / t$ (rate of reducing ball's diameter) and the rate of changing of the ball shape $v_\delta = \Delta\delta / t$ (rate of decrease or increase of deviation from sphericity). There was studied the influence of such regime parameters as discrete feeding of the wheel to the cutting sw, the time of grinding between feedings to and the rotation speed of the table with balls st. The output indixes of machining process were counted after direct measurement on each ball of its diameter and deviation from sphericity before and after each experiment.

Measurement of the diameter of the ball was carried out on a longitudinal vertical type of IZV-2 with division value of measurement scale of 1 μm. The diameter of the ball was measured in 3 mutually perpendicular directions, with the direction chosen arbitrarily. On the basis of measurements, it was calculated the average diameter of each ball and the average diameter of the balls in the batch before and after each experiment.

Figure 2 – The location of ceramic balls in the device on the ball-grinding machine VS-D204M

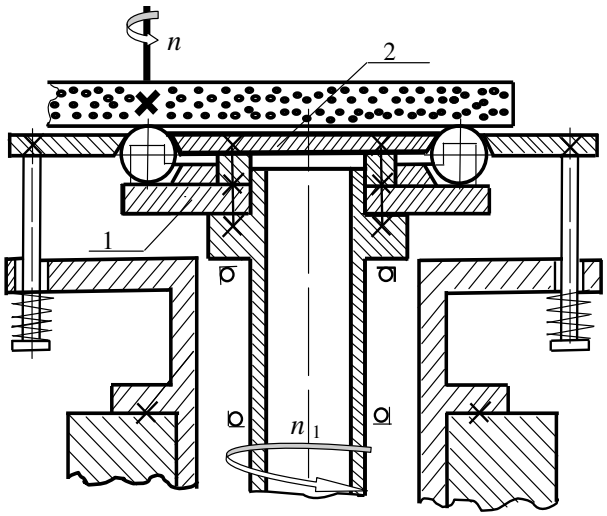

Figure 3 – Scheme of grinding of ceramic balls in a device with kinematically connected upper and lower disks

Measurement of deviation from the sphericity of ball surface was carried out by the indicating gage type MIG-1 with division value of measurement scale of 1 μm. The indicating gage was fixed on a magnetic tripod. The measured ball was located on the base ring with the outer and inner chambers, in order to get as close as possible to the conditions of contact of the ball and the ring around the circle. The base diameter of the ring was chosen as the diameter of the circle inscribed in an equilateral triangle, which in turn is inscribed in a circle with a maximum ball diameter. As a result of measurements when turning the ball on the base ring found the maximum and minimum value of deviation from the sphericity of the ball surface. On the basis of measurements, the average deviation on each ball was calculated as well as the average deviation of the ball surface in the batch before and after each experiment.

Further, the actual influence was separated out of the machining regime in the indicators of diamond grinding of balls (the rate of reducing ball's diameter and the rate of changing ball's shape), which occurs on the background of the general tendency to monotonically nonlinear decline of these indexes from its original value to the level of the minimum possible value for this grinding scheme and this processing time. This tendency is due to our view, firstly, by the gradual transition from the machining of the weakened surface layer as a two-layer combination of relief and cracked layers to the machining of the material itself and the associated increase in the physical and mechanical properties of the material being processed, which leads to a decrease in the circumferential feed of grinding (i.e. speed of run-off on a wheel of removed material) due to the self-regulation of the angular velocity of ball's rolling under the action of friction-coupling and cutting forces. Secondly, this trend is due to the simultaneous monotonous increase in the proportion of the machining time of the main material in the overall time of the experiment.

To separate out the influence of the machining regime, there was used method of graphical approximation using a monotonous continuous time function of the mean values of the ball's diameter d_m and the deviation from the sphericity of the ball's surface δ_m both before and after each experiment. The effect of the treatment mode was considered to be the difference between the mean d_m or δ_m after each experiment and the value of the approximation function at this point of the total processing time. The rate of reducing ball's diameter and the rate of change in the shape of their surface (in general, after approximation and under the action of the machining regime itself) were counted in μm/min after each experiment, taking into account the time of the experiment.

As a method for further determining the influence of machining regime on the indexes of diamond grinding ceramic balls, a complete factor experiment of type 2^3 was chose, since there was no quantitative assessment of the degree of influence of factors. The experiment plan envisaged the variation of all factors on two levels: the discrete feeding of the wheel to the cutting s_w – 50 and 70 μm, time of grinding between feedings to 10 and 20 min, the rotation speed of the table with balls s_t – 35 and 85 rpm. The time for each experiment was 40 minutes. The matrix of experiment planning is given in Table 2. It takes into account the interaction of factors.

Table 2 – Experiment planning matrix type 2^3 in relative values

Exp. no.	x_1	x_2	x_3	$x_1 x_2$	$x_1 x_3$	$x_2 x_3$	$x_1 x_2 x_3$	Alphanumeric characters	y
1	–1	–1	–1	+1	+1	+1	–1	(1)	y_1
2	+1	–1	–1	–1	–1	+1	+1	*a*	y_2
3	–1	+1	–1	–1	+1	–1	+1	*b*	y_3
4	+1	+1	–1	+1	–1	–1	–1	*c*	y_4
5	–1	–1	+1	+1	–1	–1	+1	*ab*	y_5
6	+1	–1	+1	–1	+1	–1	–1	*ac*	y_6
7	–1	+1	+1	–1	–1	+1	–1	*bc*	y_7
8	+1	+1	+1	+1	+1	+1	+1	*abc*	y_8

Based on the results of experiments, linear models of the output variables were constructed, taking into account the interaction of factors in the form

$$y = b_0 + b_1x_1 + \ldots + b_kx_k + b_{k+1}x_1x_2 + \ldots + b_{2k}\,x_{k-1}x_k,$$

in which coefficients of the linear model are calculated by the formulas:

$$b_j = \frac{1}{n}\sum_{i=1}^{n} X_{ji}Y_i,\ j = \overline{0,k};$$

$$b_{j+k} = \frac{1}{n}\sum_{i=1}^{n}[X_{ji}X_{(j+1)i} + X_{ji}X_{(j+2)i}]Y_i,\ j = \overline{1,k}.$$

4 Results

According to the recommendations of statistical data processing [15], in the calculation of the average values of measured parameters – the ball's diameter and the deviation from the sphericity of ball's surface, the results were not found with a confidence probability of 0.95, which are sharply distinguished among others. The validation of samples dispersion according to the Cochran criterion showed that they are homogeneous – in Table 3 the results are given after calculating the samples dispersion in the measurements of 8 balls in each of the 8 experiments, as well as before the start of measurements, and in addition the results of their verification for homogeneity according to the Cochran criteria. If $G \le G_{tabl}$, then the samples dispersions are homogeneous.

Table 3. Samples dispersion in 8 measurements for each of the 8 experiments, and before the start of measurements, their verification for homogeneity according to the Cochran criterion

Experiment number	Dispersion of measurements on 8 balls								Sample's dispersion in the experiment S_i^2	$G = S_{max}^2 / \Sigma S_i^2$	$G_{0,95tabl}$ at k = 8, ν = 1
	1	2	3	4	5	6	7	8			
Measuring the ball's diameter, μm^2											
init.	0.07877	0.01702	0.00977	0.12377	0.00002	0.14102	0.02627	0.00827	0.000058	0.3483	0.6798
1	0.14400	0.02500	0.04900	0.25600	0.19600	0.03600	0.00900	0.02500	0.000106	0.3460	0.6798
2	0.00306	0.03906	0.01406	0.06006	0.03306	0.00006	0.01056	0.08556	0.000035	0.3485	0.6798
3	0.04727	0.17227	0.11827	0.00977	0.22877	0.01502	0.08327	0.35627	0.000147	0.3456	0.6798
4	0.00977	0.08327	0.00127	0.01702	0.00827	0.01702	0.19252	0.02377	0.000050	0.5456	0.6798
5	0.05077	0.00352	0.02377	0.00827	0.05077	0.00077	0.00077	0.00827	0.000021	0.0052	0.6798
6	0.01502	0.11827	0.06202	0.03752	0.12377	0.02627	0.06202	0.06602	0.000073	0.0514	0.6798
7	0.00002	0.02627	0.00002	0.06602	0.00827	0.00977	0.03752	0.39502	0.000078	0.0180	0.6798
8	0.00025	0.04225	0.01225	0.00225	0.05625	0.00025	0.00225	0.00625	0.000017	0.0020	0.6798
Measuring deviation from sphericity, μm^2											
init.	63.57	24.30	58.14	0.23	14.37	3.12	0.14	27.18	27.29	0.3327	0.6798
1	1.00	30.84	61.19	22.02	123.64	0.04	6.03	54.93	42.81	0.4126	0.6798
2	11.50	0.52	3.75	3.28	0.01	16.58	0.35	2.78	5.54	0.4276	0.6798
3	0.01	8.33	1.11	0.80	1.35	0.61	4.39	25.84	6.06	0.6090	0.6798
4	0.12	0.28	2.84	6.85	1.83	22.88	6.52	0.86	6.02	0.5426	0.6798
5	24.96	4.90	2.92	16.38	13.92	0.36	5.93	1.16	10.08	0.3539	0.6798
6	0.76	2.88	0.66	11.58	0.21	10.28	0.01	17.26	62.35	0.3955	0.6798
7	2.84	3.51	0.64	9.07	2.58	6.85	2.38	2.58	4.35	0.2981	0.6798
8	1.41	0.09	1.26	7.66	9.31	1.81	0.55	2.97	3.58	0.3717	0.6798

Since the output variables of the grinding process are estimated values based on each time on the measurement of the geometric indices mentioned in the research methodology, the dispersion of reproduction in each experiment was counted as the average samples dispersion in the current and previous experiments:

$$S_{repr}^2 = \frac{1}{2}(S_i^2 + S_{i-1}^2)$$

and the weighted average variance in the 8 experiments is

$$S_{repr}^2 = \frac{1}{N}\sum_{i=1}^{N} S_{repr\,i}^2$$

at degrees of freedom $f_{repr} = N\,(m-1)$, where N – number of experiments, m – the number of measurements in each experiment.

The dispersion of the reproduction is calculated: for the average diameter of the balls – $6.8452 \cdot 10^{-2}$ and for deviation from sphericity – 12.0663.

To determine the component of ball's diameter and deviation from sphericity whose change does not depend on the influence of the machining regime is used the method of graphical approximation for time changing these indices (Figure 3).

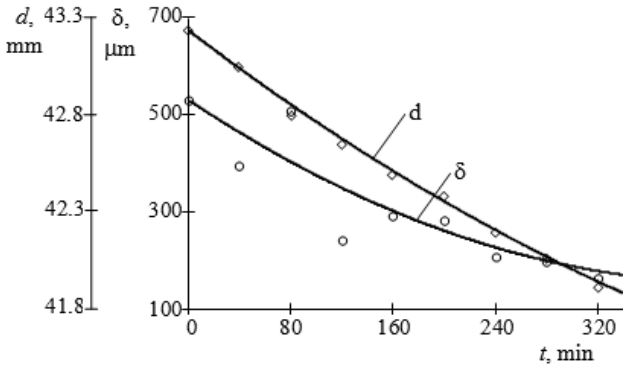

Figure 3 – Dependence of the ball diameter d and the deviation from the sphericity δ from the time of grinding t

In Table 4 the calculated values of the rate of material removal and the rate of changing ball's shape are shown under the action only the machining regime in the 8 experiments.

Based on the results, linear models of the output variables in the normalized form are constructed taking into account the interaction of the factors:

$$v_d = 0.0488 + 0.6426x_1 - 0.2113x_2 + 0.0363x_3 - 0.4129x_1x_2 + 0.0895x_1x_3 + 0.0359x_2x_3 + 0.0105x_1x_2x_3;$$

$$v_\delta = -0.0207 + 1.3241x_1 - 0.6757x_2 - 0.019x_3 + 0.3691x_1x_2 - 1.9998x_1x_3 + 0.7676x_2x_3 - 0.117x_1x_2x_3.$$

Table 4 – Matrix of changing the factors in absolute values, the value of output variables

Exp. no.	Discrete feeding the wheel to the cutting s_w, μm	The time of grinding balls between feedings t_o, min	Rotation speed of the table s_t, rpm	The rate of reducing the ball's diameter v_d, μm/min*			The rate of changing the ball's shape v_δ, μm/min**		
				total	approxi-mated	under effect of machining regime	total	approxi-mated	under effect of machining regime
1	50	10	35	4.7	5.2	–0.5	–3.3	–2.0	–1.3
2	70	10	35	6.2	4.7	1.5	2.8	–1.5	4.3
3	50	20	35	3.8	4.4	–0.6	–6.6	–1.4	–5.2
4	70	20	35	3.8	4.2	–0.4	1.2	–1.2	2.4
5	50	10	85	2.8	3.9	–1.1	–0.2	–1.0	0.8
6	70	10	85	4.8	3.7	1.1	–1.9	–0.9	–1.0
7	50	20	85	3.3	3.4	–0.1	–0.2	–0.7	0.5
8	70	20	85	3.7	3.2	0.5	–0.9	–0.5	–0.4

* the negative value means that the effect of machining regime leads to a decrease in productivity;
** the negative value means that the deviation from sphericity decreases.

The statistical significance of the coefficients of the regression equations was checked by Student's criterion on the basis of the inequality

$$t_j = \frac{|b_j|}{S(b_j)} > t_p(f),$$

in which $S(b_j) = S(\bar{y}) / \sqrt{N}$ – mean square deviation of coefficients, $t_p(f)$ – table value of Student's criterion at $p = 0.95$ for v_d, and at $p = 0.80$ for v_δ at the number of degrees of freedom $f = N(m - 1)$.

If the inequality is fairly then the coefficient differs significantly from zero.

Median deviation of regression coefficients: for medium balls – $3.2704 \cdot 10^{-2}$, for deviation from sphericity – 0.4343.

The result of checking the statistical significance of the coefficients of the regression equations in real values (Table 5): index v_d – 5 statistically significant coefficients (b_1, b_2, b_4, b_5 and b_6) from 7, and index v_δ – 4 coefficients (b_1, b_2, b_5 and b_6).

Table 5 – Calculated and tabular values of Student's criterion from checking the statistical significance of the coefficients of the regression equations

$t_{cj}=\|b_j\|/S(b_j)$							t_{ctabl} for $p = 0.95$ and $f = 56$	t_{ctabl} for $p = 0.80$ and $f = 56$
b_1	b_2	b_3	b_4	b_5	b_6	b_7		
v_d								
19,8	–6,5	1,1	–12,6	2,7	9,4	0,3	2,0031	–
v_δ								
3,0	–1,6	0,0	0,9	-4,6	1,8	–0,3	–	1,2969

To verify the adequacy of the obtained regression equations according to the Fisher criterion, the variance of the adequacy of the calculation results was firstly calculated according to the model's experimental results (Table 6)

$$S_{ad}^2 = \frac{m}{N - l} \sum_{i=1}^{N} (\bar{y}_i - y_j)^2,$$

in which y_i – the result of calculating the value of the model; l – number of significant coefficients of regression equations.

Regression equations are adequate to experimental results if the condition is fulfilled

$$F = \frac{S_{ad}^2}{S_{frepr}^2} \le F_{1-p}(f_{ad}, f_{repr}),$$

in which $F_{1-p}(f_{ad}, f_{repr})$, – tabular value of Fisher's criterion at $p = 0.05$ and numbers of degrees of freedom $f_{ad} = (N - l)$; $f_{repr} = N(m - 1)$.

Since for the obtained regression equations the above condition is satisfied by Fisher's criterion, we conclude that the regression equations are adequate for experimental results.

Table 6 – Calculation of statistical variables for checking the adequacy of regression equations to experimental results

Indicator	v_d	v_δ
Dispersion of reproduction S_{repr}^2	$6.8452 \cdot 10^{-2}$	12.0663
Dispersion of adequacy S_{ad}^2	0.0188	4.950 0
Calculated Fischer's F-criterion $f = S_{ad}^2 / S_{repr}^2$	0.669	0.133
Tabular value of F-criterion at $p = 0{,}05$ and numbers of degrees of freedom $f_{ad} = (N - l)$, $f_{repr} = N(m - 1)$	2.774 ($f_{ad} = 3$, $f_{repr} = 56$)	2.536 $f_{ad} = 4$, $f_{repr} = 56$)

Taking into account the results of the adequacy checking, the models of output variables in the normalized form have been constructed:

$$v_d = 0.0488 + 0.6426x_1 - 0.2113x_2 - 0.4129x_1x_2 + 0.0895x_1x_3 + 0.0359x_2x_3;$$

$$v_\delta = -0.0207 + 1.3241x_1 - 0.6757x_2 - 1.9998x_1x_3 + 0.7676x_2x_3.$$

The same models in real sizes have the form:

$$v_d = 0.04883 + 0.01071s_w - 0.01409t_o - 0.00046s_wt_o + 0.00002s_ws_t + 0.00034t_os_t;$$

$$v_\delta = -0.0207 + 0.0221s_w - 0.045t_o - 0.0006s_ws_t + 0.0009t_os_t.$$

On the basis of the obtained models, graphs of function are constructed $v_d(s_w,t_o)$, $v_d(s_w,s_t)$, $v_d(s_t,t_o)$ and $v_\delta(t_o,s_w)$, $v_\delta(s_t,s_w)$, $v_\delta(s_t,t_o)$ (Figures 4, 5).

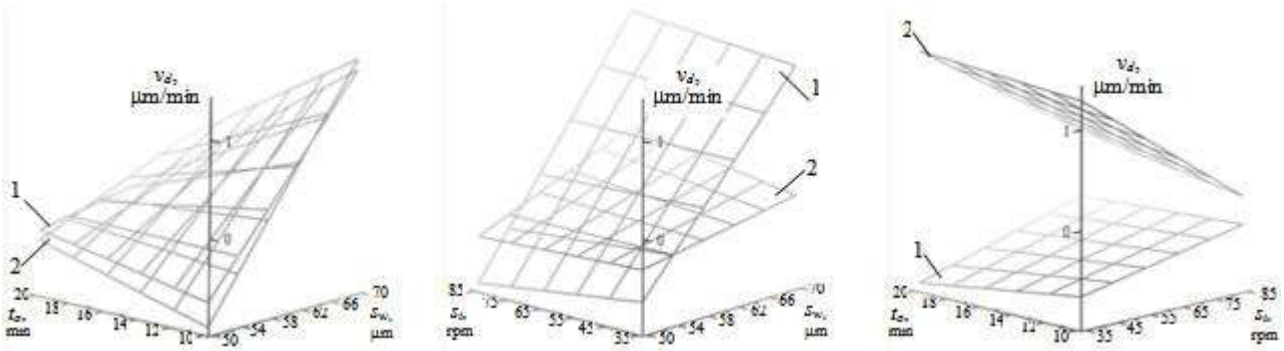

a b c

Figure 4 – Dependencies of the index v_d from the value of feeding the wheel to the cutting s_w and the time of grinding t_o (a) at the rotation speed of the table s_t 35 rpm (1) and 85 rpm (2); from s_w and s_t (b) at t_o 10 min (1) and 20 min (2); from t_o and s_t (c) at s_w 50 (1) and 70 µm (2)

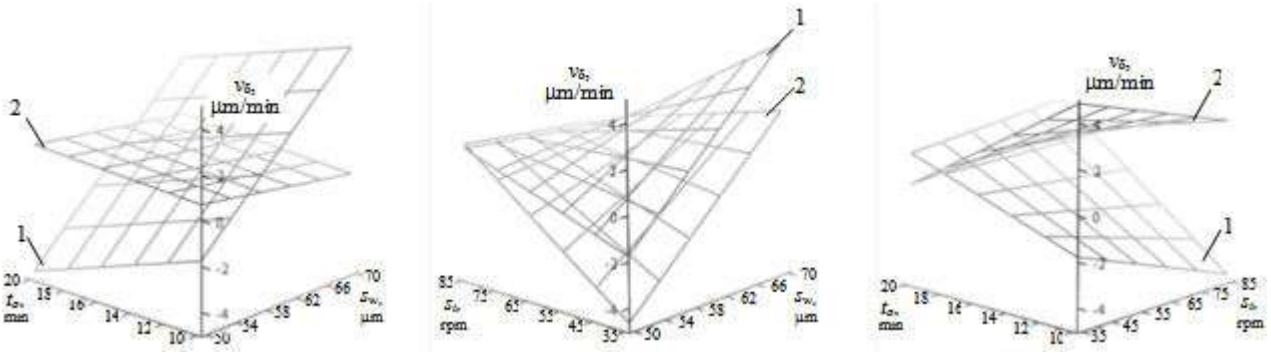

a b c

Figure 5 – Dependencies of the index v_δ from the value of feeding the wheel to the cutting s_w and the time of grinding t_o (a) at the rotation speed of the table s_t 35 rpm (1) and 85 rpm (2); from s_w and s_t (b) at t_o 10 min (1) and 20 min (2); from t_o and s_t (c) at s_w 50 (1) and 70 µm (2)

5 Conclusions

As can be seen from the graphs in Figures 3 and 5, and Table 4, for the diamond grinding ceramic balls the effect of the machining regime on the rate of changing the deviation from sphericity (which estimated by the negative value of the index v_δ) should be considered in two ranges of variance of deviation from sphericity. If the range is above 300 μm then the effect of the machining regime is more significant. If the range is below one the effect is less significant. To reduce the deviation in the first range is possible by the simultaneous decreasing the feeding of the wheel to the cutting s_w up to 50 μm and the rotation speed of the table s_t up to 35 rpm with increasing the time of grinding t_o up to 20 min. This machining regime will ensure changing v_δ in the range from –1.3 to –5.2 μm/min. In the second range, on the contrary, the simultaneous increase of the specified parameters within the studied range will be effective at increasing s_w up to 70 μm and s_t up to 85 rpm and decreasing t_o up to 10 min, that will provide changing v_δ in the range from –0.4 to –1.0 μm/min.

At the same time, the growth of the productivity (which estimated by increasing the index v_d) should be expected at increasing the feeding of the wheel to the cutting s_w within the studied range, so long as the rotation speed of the table s_t and the time of grinding t_o are reduced (Figure 3, 4, and Table 4). Since the strategic goal of the diamond grinding ceramic balls is primarily to achieve the maximum possible rate of decreasing the deviation from the sphericity and only in the second place the acceptable process productivity, the current value of this deviation should be taken into account. Depending on it, it is also necessary to choose the recommendations for choice of the machining regime: more the deviation from sphericity – lower the machining parameters so long as the time of grinding between the feedings increases, and vice versa.

References

1. Hybrid Ball Bearings. Retrieved from: https://www.bearingworks.com/products/hybrid-ball-bearings.php.
2. *Sverhtverdye materialy. Poluchenie e izmerenija. Almazno-abrazivnyy instrument v tekhnolohijah mekhanoobrabotki* (2007). Kyiv, Alkon [in Russian].
3. Pasichnyy, O. O. (2002). *Pidvytshennja efektyvnosti pretsezeonnoji almaznoji obrobky detaley typu „kulia" z konstruktsijnoji keramiky*. Thesis for the Ph.D. degree. Kyiv, Bakul Institute for Superhard Materials of NAS [in Ukrainian].
4. Feng, M., Wu, Y., Yuan, & J., Ping, Z. (2017). Processing of high-precision ceramic balls with a spiral V-groove plate. *Front. Mech. Eng*. 2017, 12 (1), 132–142.
5. Zhou, F., Yuan, J., Lyu, B., et al. (2016). Kinematics and trajectory in processing precision balls with eccentric plate and variable-radius V-groove. *The International Journal of Advanced Manufacturing Technology*, 2016, 84 (9), 2167–2178.
6. Ma, W. (2013). *High efficiency ultra-precision grinding of ceramic balls*. Dissertation for the Doctoral Degree. Saga, Saga University.
7. Filatov, Y. D., Vetrov, A. H., Sidorko, V. I., Filatov, A. Yu., & Kovalev S. V. (2013). Zakonomernosti finishnoy almazno-abrazivnoy obrabotki monokristallicheskoho karbida kremnija. *Superhard Materials*, No 5, pp. 63–71 [in Russian].
8. Filatov, Y. D., Vetrov, A. H., Sidorko, V. I., et al. (2015). Polirovanije elementov optiko-elektronnoy tekhniki iz monokristallicheskoho karbida kremnija. *Superhard Materials*, No 1, pp. 63–71 [in Ruissian].
9. Filatov, Y. D., Filatov, O. Yu., Monteil, G., Heisel, U., & Storchak, M. (2010). Bound-abrasive grinding and polishing of surfaces of optical materials. *Proc. of SPIE*, Vol. 7786, Art. no.778613.
10. Husev, V. V., & Kalafatova, L. N. (2012). *Tekhnolohicheskoje obespechenije kachestva obrabotki izdeliy iz tekhnicheskoy keramiki*. Donetsk, DonNTU [in Russian].
11. Filatov, Y. D., & Rohov, V. V. (1994). Klasternaja model mekhanizma ustalostnoho iznosa SiO_2-sodergatshih materialov pri ikh polirovanii instrumentom so svjazannym polirovalnym poroshkom na osnove dioksida tserija. Chapter 1. *Superhard Materials*, No. 3, pp. 40–43 [in Russian].
12. Filatov, Y. D. (1991). Mekhanizm obrazovanija mikroreljefa poverkhnosti pri obrabotke stekla. *Tam ge*., No. 5, pp. 61–65.
13. Morozov, E. M., Zernin, M. V. (1999). *Kontaktnye zadachi mekhaniki razrushenija*. Moscow, Mashinostroyeniye [in Russian].
14. Kulich, V. H., Kushch, V. I., Tkach, V. N., Maystrenko, A. L. (2009). K voprosu o vozmognostjakh poluchenija vysokoplotnykh keramicheskikh izdeliy na osnove samosvjazannoho karbida kremnija. *Superhard Materials*, No. 1, pp. 18–35 [in Russian].
15. Proverka znachimosti koeffitsientov i adelvatnosti uravnenija regressii, poluchennykh pri obrabotke rezultatov PFE 22 i 23. Retrieved from: https://politeh24.com/4207#more-4207 [in Russian].

Алмазне шліфування керамічних куль з карбіду кремнію

Сохань С. В., Майстренко А.Л., Кулич В. Г., Сороченко В. Г., Возний В. В., Гаманюк М. П., Зубанєв Є. М.

Інститут надтвердих матеріалів ім. В. М. Бакуля НАН України, вул. Автозаводська, 2, м. Київ, 04074, Україна

Анотація. Досліджено експериментально вплив режиму обробки на показники процесу алмазного шліфування керамічних куль з карбіду кремнію: швидкість знімання припуску і швидкість зменшення/збільшення відхилення від сферичності поверхні куль. Запропоновано методику виокремлення з цих показників частки, обумовленої власне впливом режиму обробки. Для цього застосовано метод графічної апроксимації змінювання у часі діаметру кулі і відхилення від сферичності. Встановлено, що виокремлені частки показників процесу можуть змінюватися як у бік зростання, так і бік зниження в залежності від значень параметрів режиму обробки, як-от: дискретної подачі алмазного круга на врізання, частоти подачі круга і швидкості обертання стола з кулями. Як метод подальшого визначення впливу режиму обробки обрано повний факторний експеримент типу 23, в якому факторами були вказані вище параметри режиму обробки. Знайдено найбільш ефективне для зменшення відхилення від сферичності поверхні куль поєднання цих параметрів.

Ключові слова: керамічні кулі з карбіду кремнію, алмазне шліфування, параметри режиму обробки, швидкість знімання припуску і швидкість змінювання форми поверхні куль.

JOURNAL OF ENGINEERING SCIENCES
ЖУРНАЛ ІНЖЕНЕРНИХ НАУК
ЖУРНАЛ ИНЖЕНЕРНЫХ НАУК

Web site: http://jes.sumdu.edu.ua

DOI: 10.21272/jes.2018.5(1).b1 Volume 5, Issue 1 (2018)

UDC 658.5+005.6+006

How to Assess the Performance Quality of an Enterprise

Kovalev A. I.

PJSC "Khmelnytskoblenergo", 11a Khranovskogo St., 29016, Khmelnytskyi, Ukraine

Article info:
Paper received: September 30, 2017
The final version of the paper received: January 14, 2018
Paper accepted online: January 18, 2018

***Corresponding Author's Address:**
polyfitt@gmail.com

Abstract. Proper assessment of enterprise performance quality expands opportunities of those enterprises proven by reputation, and creates favourable environment for investment. However, scientific literature does not present any research of enterprises' performance or functioning quality models from the perspective of all possible results. The article defines, in accordance with the requirements of the international management system standards, functioning efficiency – that is, resources turning into immediate results, immediate results transforming into direct ultimate results; sustained success – direct ultimate results turning into indirect ultimate results. Indirect ultimate results highlight strategic effect of an enterprise's sustained success. Ways of assessing functioning quality are classified, on the basis of which a system of information and analysis for collecting and processing of management information is developed for automation of assessment procedure.

Keywords: efficiency, sustained success, activity, functioning, automation.

1 Introduction

Quality assessment is a special type of the control function aimed at the formation of value judgments about the enterprise as an evaluated object. In accordance with ISO 9000:2015, quality is an independent characteristic of the object's essence for which a level (degree) of the required quality is existed. This level is assessed in relationship to the quality standard. This definition of quality makes it possible to provide a quantity assessment by the degree of compliance.

Quality appears "outside" through its properties. The property is an external demonstration of quality as the inner essence of the object [1]. A characteristic is the distinguishing feature, which can be own or assigned, qualitative or quantitative. The characteristic of quality is own characteristics of the enterprise arising from the requirements. The state of an enterprise is a set of characteristics that it possesses at the operating moment. Each characteristic has its assessment and can be determined.

The determination of quantitative characteristics of the quality of the work of enterprises is metrology, while not joint these characteristics with the justification of management decisions, as is customary in qualimetry. In qualimetry, the property (attribute) is the quality of the evaluation of measured object; value is the quantitative characteristic of a measure. An indicator is the numerical value of a measure by which one can indicate the state, change or development of the enterprise's processes. In the broadest sense of the word, an indicator is the transmitter of information. In the narrow sense, indicators are those characteristics that connect the object and the subject of evaluation [2]. The term "indicator" is also defined as a quantitative characteristic of one or several properties of objects considered under certain parameters [3]. In this case, the terms "indicator" and "parameter" are different. The parameter characterizes the state of an enterprise and its structure, but the indicator characterizes properties. Hence, the parameter is a relatively constant characteristic, which changes only when the enterprise changes itself. Parameters indicate how the enterprise differs from others. Thus, we will consider as indicators variables describing the properties reflecting the target, and parameters – the characteristics of the state, reflecting the quality of the functioning of the enterprise. International process-oriented management standards suggest the following parameters: efficiency, effectiveness, sustained success. Wherein, functioning is the behavior of the enterprise in time, the successive change of its state. At the same time, activity includes a system of processes carried out by an enterprise for the purpose of producing products, providing services or supporting them.

In order to express the state, it is necessary to determine the values accepted by the parameters at the considered moment, namely the values of efficiency, effectiveness, and sustainable success. The nomenclature of indicators evaluated in determining the properties and state of the enterprise should adequately reflect the actual level of parameters. Therefore, the choice of indicators is based on the study and modeling of the properties and condi-

tions of the enterprise. Establishing the range of indicators is not a one-time, even if operation justified by scientific methods, but the process of constant adjustment. It depends on the enterprise development strategy [4].

Requirements of the standard ISO 9001:2015 concern the measurement of processes both for assessing the level of their effectiveness, and for maintaining in the managed state. In the first case, the results of the process are evaluated. In the second one, the indicators of its state at different stages are determined. The system of process quality indicators is divided into two groups. The first includes the implementation of the outputs of the process, and the second one – the characteristics of the dynamics of the process [5]. The first group of indicators fixes where the process comes as a result of control, and the second one – how it gets to the final state. Thus, it is necessary to consider both indicators of quality of activity, and indicators of quality of functioning of the enterprise. The need to assess a sustained success also requires consideration and operationalization of concepts as a final results of the enterprise's activities, as well as the quality of functioning. Operationalization consists in the fact that investigated concepts are determined through the description of special measuring operations.

The purpose of this article is to analyze the models of the quality of activity and the functioning (A&F) of the enterprise under the point of view of all possible outcomes and the development of operational definitions of these results in the context of requirements and recommendations of the standards ISO 9000.

2 Research Methodology

Quality assessment A&F is the formation of value judgments about the enterprise, including an assessment of its properties and states using a set of indicators defined for each of the aspects (directions) of activity, e.g., resources, infrastructure, internal processes, financials, consumers, potential, and development.

The evaluation of the performance of activities is carried out based on direct results as a cost saving in obtaining these results. Evaluation of performance and sustainable success is carried out on the basis of final results (Fig. 1). Immediate results are what we have done, and the outcomes are what happened. Consequently, effectiveness is a characteristic of immediate results, productivity is a characteristic of direct outcomes, sustained success is a characteristic of indirect outcomes. In contrast to the traditional social notion of influence, it established as a strategic effect, correlated with indirect outcomes – quality of operation management, and estimated with the help of assessments of sustainable success in the long term.

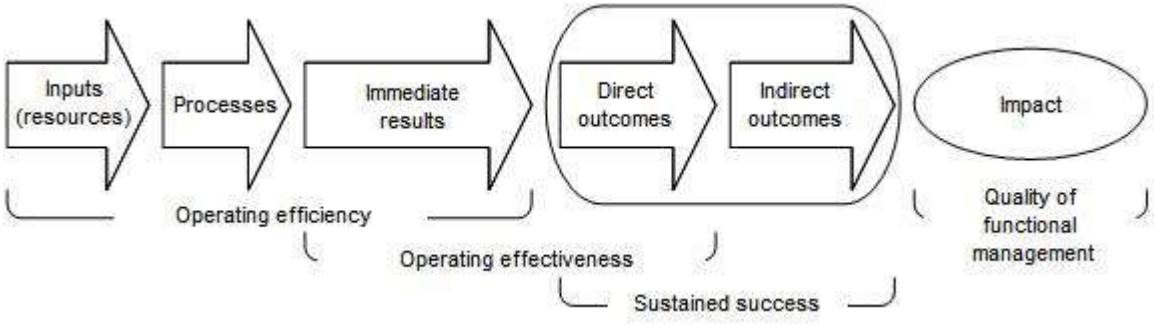

Figure 1 – The relationship between efficiency, effectiveness, sustained success and the quality of management in terms of immediate and final results

Figure 2 shows a diagram describing the company's A&F hierarchy. It includes the company's embedded resources, processes, immediate results (produced goods and services), as well as final results and impact (strategic effect).

Immediate results should be presented in vector form

$$x = \left(x^{(1)},\ x^{(2)},\ldots,\ x^{(n)}\right)^T, \qquad (1)$$

where $x^{(j)}$ – indicators characterizing various properties of the enterprise.

The final results should be presented as a complex indicator. Steady success is as a forecast, through the evaluation of the sequence of complex indicators. The effectiveness of the activity is determined by the evaluation of the resources spent on achieving the multivariate indicator (1). Alternatively, this indicator should contain private resource indicators, for example, as it is provided in the popular balanced scorecard including various aspects of the enterprise, resource and financial [6].

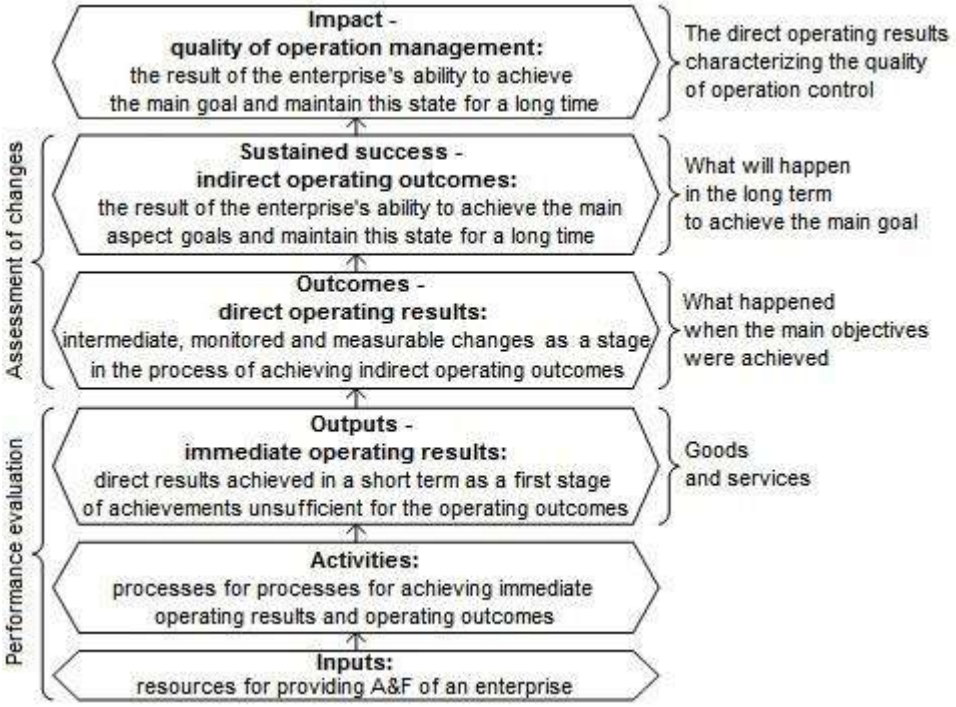

Figure 2 – A flowchart of the hierarchical presentation of the enterprise's operation

To identify possible ways of assessing the quality of A & F, providing for appropriate decision-making procedures, consider the following. For any object of evaluation (the state of the enterprise), the set of its estimates for all indicators is a vector. It contains complete information about the object. If the estimated objects are comparable in the sense of domination, one can specify by binary relations in the space of estimations of indicators that determine the selection rule for each pair of objects of the best:

$$\left(e_r \succ e_k\right) \Leftrightarrow \begin{pmatrix} \forall j = \overline{1,n} : x_r^{(j)} \geq x_k^{(j)}; r,k \in (1,\ldots,m); \\ \exists\, h \in (1,\ldots,n) : x_r^{(h)} > x_k^{(h)} \end{pmatrix}. \quad (2)$$

Substantially, this means that the object e_r no worse than the object e_k on any of the main aspect indicators, and, at least, one of them e_r is better than e_k. Firstly, the evaluated objects will be compared by the indicators of the most important aspect, then – by the indications of the next important aspect, etc.

If the objects of evaluation are incomparable with the private aspect indicators of all aspects of activity, it is advisable to resort to the scalarization of the aspect indicators by building the complex indicators of aspects (CIA). When constructing a CIA, it is advisable to compare by advantage only homogeneous indicators that measure the intensity of properties of the same nature. To do this, the normalizing functions for the transformation $x^{(j)} \Rightarrow y^{(j)} \in [0,1]$ is used

As CIA a weighted sum of indicators is applied, which for *s*-th aspect of *i*-th object of evaluation has the following form:

$$z_i^{(s)} = \sum_{j=1}^{n_s} w_s y_i^{(j)},\ i \in \overline{(1,m)},$$

where n_s – number of indicators of *s*-th aspect; $y_i^{(j)}$ – normalized value of *j*-th indicator for *i*-th object; w_s – weights of partial indicators for *s*-th aspect of activity. The decisive rule has the following form:

$$\left(e_r \succ e_k\right) \Leftrightarrow \begin{pmatrix} \forall s : z_r^{(s)} \geq z_k^{(s)};\ r,k \in \overline{(1,m)}; \\ \exists\ h \in (1,2,\ldots,s) : z_r^{(h)} > z_k^{(h)} \end{pmatrix}. \quad (3)$$

This means that e_r object is no worse than e_k for any of CIA and at least one of CIA e_r is better than e_k.

1. The basis of the application of the method is the assumption of the independence of the influence of the value of each individual indicator $x_i^{(j)}$ or $z_i^{(j)}$ on the estimation of the preference of the object e_i as a whole. In practice, this assumption is often not satisfied. In addition, the objects of estimation may not be comparable in the sense of the componentwise dominance of CIA, if each of the objects is preferable to the other for some particular indicator. It is possible to clarify the problem, to attract some additional assumptions that determine the method of estimation.

2. Additional assumptions may be related to a kind of binary relation as the lexicographic selection rule. It is used in the case of a ranking CIA according to the ranking of aspects of activity. Then, if the object e_r is preferable to e_k object by CIA of the most important aspect, then, independently of the CIA of other aspects of e_r, e_k is preferable. If the objects are incomparable with CIA of the most important aspect, then they are compared according to CIA of the next most important aspect, and so on.

3. Recognition of the enterprise's state is carried out using the data matrix $Y = \| y_i^{(j)} \|_m^n$.

Two classes of states C_g, $g = \{1, 2\}$ are considered, where C_1 – values of indicators correspond to the annual planning assignments; C_2 – already achieved values of the indicators for the previous year. Distance measure $L_g(y, y_{g*})$ of the vector y to reference vectors y_{g*} of these classes can be taken in the following form:

$$L_g\left(y, y_{g*}\right) = \sum_{s=1}^{N} \sum_{j=1}^{n_s} w_s^2 \left(y^{(j)} - y_{g*}^{(j)}\right)^2, \qquad (4)$$

where N – number of identified aspects of activity.

The decisive rule takes the form:

$$y \in C_g \Leftrightarrow L_g = \min\left(L_g\right), \; g = \{1, 2\}. \qquad (5)$$

4. An integral comparative evaluation characterizes the degree of similarity between two different enterprises. It can be presented by an integral measure – a linear distance δ_{rk} between column vectors $y_r^{(j)}$ and $y_k^{(j)}$ of of the transpose matrix Y^T

$$\delta_{rk} = \sum_{s=1}^{N} \sum_{j=1}^{n_s} w_s^2 \left(y_r^{(j)} - y_k^{(j)}\right)^2, \;\; r, k = \overline{1, m}, \qquad (6)$$

where $y_r^{(j)}$, $y_k^{(j)}$ – values of j-th indicator for r-th and k-th enterprises.

Columns of the matrices Y^T correspond to enterprises, and rows – to theirs indicators. An element δ_{rk} is the measure of the difference between enterprises r and k. The matrix $\Delta = \| \delta_{rk} \|_m^m$ specifies the dual relations "to be predominant" or "equal", or "to be no worse", because its components are measures of the difference between enterprises r and k. Such information is interest when conclusions based on numerical indicators include ranking. Particularly, the purpose of a comparative study of enterprises is ranking by the data combination.

5. in general, calculation of the global quality assessment of enterprise's A&F consists in building the exponents of the scalar function y_i^o in the space of indicators, which relates each object to an estimate of its "generalized quality":

$$y_i{}^o = \sum_{s=1}^{N} \sum_{j=1}^{n_s} w_s^2 \left(y_i{}^{(j)} - y_{\max}^{(j)}\right)^2, \;\; i = \overline{1, m}, \qquad (7)$$

where $y^{(j)}{}_{\max}$ – components of the vector characterizing the enterprise, chosen as a reference for comparison.

For convenience of comparison for various variants of objects, estimation limiting values of indicators $y_{\max}$ should correspond to the initial state – the given (normative) values from the point of view of the long-term strategic objectives of the enterprise. To solve the forecasting problem, it is necessary to check periodically the selected set of indicators. Thus, complex factors $y_i^o(t_0)$, $y_i^o(t_1)$, … are obtained, the forecasting of which changes in sustainable success can be predicted.

To automate the evaluation procedure (including the abovementioned method), a block diagram of the algorithm for the corresponding information and analytical system (IAS) (Fig. 3). The technology of estimation based on the estimation methods given by formulas (2)–(7).

IAS is devoted to improve the efficiency and quality of management decisions by automating the information and analytical activities of the enterprise. The object of automation is the procedure for assessing the quality of enterprise's A&F based on the balanced set of indicators (in terms of activities).

All the AIS data are located in the central repository and contain the following levels: collection and primary data processing; extracting, transforming and loading data; data storage; presentation in data marts; data analysis.

Data marts are organized in the form of multidimensional databases, where reference information is presented by indicators and output – by quality parameters of enterprise's A&F summarizing these indicators. Information in a multidimensional data mart is presented in terms of business in the form most accessible to users, which allows significantly reducing time for obtaining information necessary for decision-making. The use of multidimensional data marts and corresponding program for data analysis allows transforming data into useful information based on which effective decisions are made. The program for data analysis is used to access to information, visualize it, as well for the multivariate analysis, form and compose reports. An input data for the analysis is the preprocessed data from the repository or presented in a data mart.

Part of the quality of enterprise's A&F is the quality of management characterizing some ability of the enterprise. It is one of the types of competitiveness. In terms of process-oriented standards, the quality of management characterizes the steady success of an enterprise.

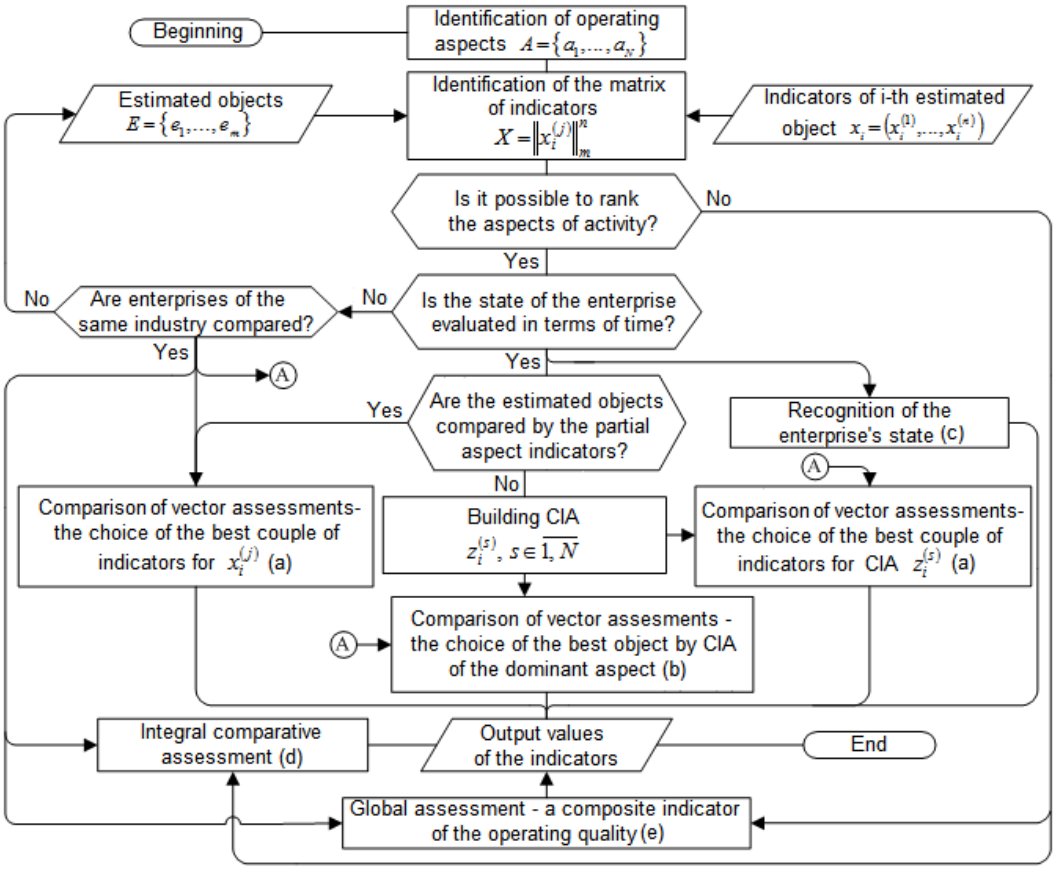

Figure 3 – A flowchart of algorithm of information-analytical system

Management of enterprises is realized by the implementation of interrelated management functions. The quality of management is characterized by a stable interaction of managerial functions, as well as a stable interaction of processes is a characteristic of the quality of operating activities (the transformation of materials and information into a final product and delivery of the product to the consumer). Therefore, management functions should be identified for each enterprise. This fact does not exclude their repeatability, especially in the industry context. At the level of the interrelationships of functions, the differentiation of enterprises should be more significant, because the differentiation is a field of competitive advantages that distinguishes one enterprise from another one. Innovative sustainable relationships of established management functions are the part of intangible assets as an area for creating competitive advantages.

The quality of management is the subject of enterprise strategy, and the criterion of good governance is successful implementation of the strategy. If suppose that an enterprise firstly proposes the quality management functions within the standard ISO 9000: 2015 (quality planning, assurance, control and improvement), then to implement the strategy it can concentrate efforts on detailed quality planning, neglecting, and control: there are goals, tasks, resources. So, the fulfillment of quality requirements is delegated to units. There is another situation where documentation and close monitoring are carried out, particularly statistical control of operating activities. Perhaps, priorities to ensure consumer loyalty, create a brand will be chosen, or the path for resource investments and improvements will be proposed (e.g. new developments and technological innovations). Knowing the capabilities of the enterprise and identified strategies determine the ways to achieve success. If success is achieved, the quality of management is high. If the success is unsufficient, then with the unchanged profile of organizational capabilities and the chosen strategy, the enterprise can change the management functions, their resource supply, introduce new functions, and so on.

So, if control is carried out with the help of a set of interrelated functions, then the functions express an essential determinateness inherent in management, due to which the management is precisely such.. Thus, the quality of management is the degree of correspondence of the inherent characteristics (functions) of management to the established requirements. Particularly, this means that the identification of management functions should be based on the identified requirements of interested parties. The quality of management and the competitive advantage of the enterprise will consist in the extent to which the requirements and needs are investigated, as well as functions are adequately identified and implemented. A certain set of management functions of the enterprise for the market condirions is assessed in their relationships, which allows judging the quality of management as a whole.

Assessment of the quality of management can be approximately realized using the expert assessments based on a number of evaluation categories, if it is possible to correctly select experts and organize an evaluation procedure. The field of managerial quality is dynamic and individual as “know-how”, until it becomes a common

property. Enterprises can find and implement unique functions. How an enterprise works is a consequence of a combination of individual characteristics of its internal and external environments. Consequently, management functions can also be individual.

Finally, the quality of management reflects a stable relationship between the constituent elements of A&F (managerial functions) characterizing the specific management, which allows distinguish management approaches.

3 Conclusions

In this paper, ways for the determination of the enterprise's A&F quality is proposed by the parameters of its condition: efficiency, effectiveness, and sustained success. The traditional presentation of operational results are immediate and final results, as well as the impact. The new approach is in the fact, that efficiency reflects the transition of resources and processes to immediate results, as well as effectiveness reflects the transition of direct results to outcomes, and sustained success reflects the transition of direct outcomes to indirect ones.

In contrast to the presentation of non-productive (non-commercial) impact of the final result (e.g., social), a strategic effect of the sustainable success of the enterprise is established. If a causal relationship is established between the final (remote) results and the effect of sustained success, the outcomes are indirect evidences of it. The trend of a change in sustainable success can be assessed by periodic monitoring of the complex indicator of quality A&F (7) including the identified set of the most informative indicators.

Methods for assessing the quality A&F are defined and corresponding IAS is developed considering the proposed approach, which allows realizing new ways of informatization, and intellectualization of management processes.

The quality of management of functioning is defined as a characteristic of the effectiveness of functioning in the long term. In the standard ISO 9004:2012 it is called as a steady success. This approach is reliable, if it is assumed that enterprises fulfill the adopted restrictions when achieving the goals. However, it is better if the satisfaction of constraints (the achievement of efficiency) is included into the set of vector's indicators (1). If the enterprise uses such indicators (e.g., balanced containing resource (financial) components), the quality A&F (direct results and outcomes) can characterized by joint assessments of efficiency and effectiveness. Additionally, the quality of performance management (indirect outcomes) is assessments of efficiency and effectiveness in a long term: Permanent monitoring of the complex indicator (7) provides a tool for predicting sustainable success.

References

1. Bondarevskiy, A. S. (2008). Axiomatics of informational operations accuracy. Fundamental research, No. 6, 11–25 [in Russian].
2. Guts, A. K., Korobitsin, V. V., Laptev, A. A., Pautova L. A., & Frolova, J. V. (2000). *Mathematical Models of Social Systems*. Omsk State University Publ., Omsk, Russia.
3. Pershikov, V. I., & Savinkov, V. M. (1991). *The explanatory dictionary on informatics*. Finansy i statistika Publ., Moscow, Russia [in Russian].
4. Konyukhov, A. G. (1990). *Metrological support in instrument making. Management aspects*. Izdatel'stvo standartov Publ., Moscow, Russia [in Russian].
5. Kovalev, A. I. (2009). Complex and dynamic processes of management. *Standards and quality*, No. 12, 72–73 [in Russian].
6. Kaplan, R. S., & Norton, D. P. (1996). *The Balanced Scorecard: Translating Strategy into Action*. Harvard Business Press Books, Boston, USA.

Як оцінити якість роботи підприємства

Ковальов О. І.

ПАТ «Хмельницькобленерго», вул. Храновського, 29016, м. Хмельницький, Україна

Анотація. Адекватне оцінювання якості роботи підприємств розширює їх можливості, які підтверджуються репутацією, і створює сприятливі умови для залучення інвестицій. Однак у науковій літературі не представлені дослідження моделей якості діяльності та функціонування підприємств з точки зору всіх можливих результатів. У статті визначено відповідно до вимог міжнародних стандартів на системи управління ефективність діяльності, результативність функціонування, стійкий успіх підприємства і якість управління (стратегічний ефект сталого успіху) згідно логічної послідовності «ресурси – безпосередні результати – прямі і непрямі кінцеві результати». Представлена класифікація способів оцінювання якості діяльності / функціонування, на основі якої розроблена інформаційно-аналітична система збору та обробки управлінської інформації для автоматизації процедури оцінювання.

Ключові слова: ефективність, результативність, стійкий успіх, діяльність, функціонування, автоматизація.

JOURNAL OF ENGINEERING SCIENCES
ЖУРНАЛ ІНЖЕНЕРНИХ НАУК
ЖУРНАЛ ИНЖЕНЕРНЫХ НАУК

Web site: http://jes.sumdu.edu.ua

DOI: 10.21272/jes.2018.5(1).c1 Volume 5, Issue 1 (2018)

UDC 519.242:538.951:539.219.2:678.03

Mathematical Modeling of the Mechanical Characteristic of the Activated PTFE-Matrix Using the Method of Planning the Experiment

Bilous O. A.[1], Hovorun T. P.[1], Berladir K. V.[1*], Vorobiov S. I.[2], Simkulet V. V.[3]

[1] Sumy State University, 2 Rymskogo-Korsakova St., 40007, Sumy, Ukraine;
[2] Institute of Physics, P. J. Šafárik University in Košice, 2 Šrobárova St., 041 54, Košice, Slovakia;
[3] Technical University of Košice, 1 Bayerova St., 080 01, Prešov, Slovakia

Article info:
Paper received: December 20, 2017
The final version of the paper received: April 30, 2018
Paper accepted online: May 5, 2018

***Corresponding Author's Address:**
kr.berladir@pmtkm.sumdu.edu.ua

Abstract. In this paper, the influence of the parameters of the technological process of mechanical activation on the physical characteristics of the polytetrafluoroethylene (PTFE) matrix is investigated. The paper presents a mathematical model of the dependence of breaking strength on the time of activation and rotating speed of working organs of a mill. Mathematical modeling is performed by the method of orthogonal experiment planning. The result of the study was a mathematical relation that explains the connection between the technical characteristics of the process of manufacturing a fluoroplastic composite and the mechanical characteristics of the material.

The statistical analysis of the experimental results is performed and the adequacy of the mathematical relations obtained is estimated. On the basis of the analysis of the obtained data, it can be concluded that the theoretical model obtained is adequate and suitable for performing the corresponding technological calculations. On the basis of the performed calculations, the conclusion is reached on the optimal technological mode of preparing the PTFE-matrix. The analysis shows that theoretical calculations confirm the experimental value of technological indicators under optimal operating conditions of the mill. Thus, the obtained dependence of breaking strength from the technological parameters of the activation process can be embedded in the algorithm for selecting the technological mode that ensures the output of products with specified quality indicators.

Keywords: polytetrafluoroethylene matrix, mechanical activation, mathematical modeling, breaking strength, parameters.

1 Introduction

Modern polymers and composite materials based on them are widely used in engineering as compositions exceeding in some of their characteristics structural steels and alloys [1–4]. A characteristic feature of these materials is the dependence of their mechanical characteristics on the conditions and modes of production of such structures. The question of determining the optimal parameters of the technological process for fabrication of fluoroplastic composites remains a topical issue [5–6].

The basis of any scientific approach for the optimization of technological processes is the application of methods of mathematical modelling with subsequent use of the obtained models for analysis of the influence of the main technological factors and the calculation of the optimal conditions for the performance of the technological process.

2 Literature Review

As shown by the practice of polymer material science [7–8], the physical, mechanical and tribotechnical properties of polymer composite materials (PCM) based on polytetrafluoroethylene (PTFE) are equally dependent on individual modes of technological production operations and on their combination (interaction).

The most acceptable in the case of PCM with a PTFE matrix is the technology of the energy effect on its structure and properties by mechanical activation [8].

A mathematical model of viscoelasticity of polymers was proposed in [9], combining the minimum number of possible parameters and a high degree of reliability in predicting of deformation processes. On the basis of the calculated deformation characteristics of polymers, deformation processes in the material were predicted. A

criterion for the optimality of the choice of such a mathematical model is formulated.

In [10], using the linear differential equations of elastic deformation of a thin-walled cylindrical shell of variable thickness, an elastically deformed state of the fluoroplastic part was investigated. A calculation method for determining the value of the contact loading on the fluoroplastic element was developed. Recommendations to the designer of products from polytetrafluoroethylene at the stage of preliminary design of the unit are offered.

In [11] a simplified approach to the quasilinear viscoelastic modeling of PCM is formulated. It is based on a new principle of inclusion of nonlinearity and requires considerably fewer calculations when used in comparison with existing theories.

At the same time, the question of the influence of the parameters of the technological production process on the mechanical characteristics of the obtained PTFE-composite remains little studied.

The aim of the paper is to study the results of the mechanical activation of PTFE by mathematical modeling and optimization.

3 Research Methodology

Planning the experiment allows you to vary simultaneously all the factors (parameters) of the technological process and obtain quantitative estimates of both the main factors and the effects of interaction between them.

As a research material was chosen polytetrafluoroethylene grade F-4 "O" (GOST 10007-80).

Testing for breaking strength was carried out on the ring samples Ø50×Ø40, height 10 mm, using rigid semi-disks in accordance with GOST 25.603-82 at the tensile machine MP-05-1 at the rate of movement of grippers 10 mm/min and the load of 100 kgf. Density ρ (kg/m^3) of the samples was determined by the method of hydrostatic weighing in accordance with GOST 15139-69.

The influence of the features of the technological regimes of mechanical activation on the properties of the composite material was investigated on a high-speed mill МРП-1М with a maximum loading of 100 g/min. and a power of 1 kW.

To determine the regularities of the results of the technological process, the initial plan of the full factor experiment (FFE) type 2^2 was chosen. Investigation of the dependence of the strength characteristics of the matrix on the parameters of the activation process was performed by the method of orthogonal experimental design [12].

4 Results and Discussion

In studying this issue, as an optimization criterion (response function) was chosen the mechanical characteristic of fluoroplastic material – breaking strength (σ_b, MPa). The dominant factors were:

- X_1 – rotating speed of working organs of a mill (n, min^{-1});
- X_2 – the time of activation (τ, min).

The task was solved with the help of two-factor regression analysis, as a result of which the optimal levels of the main factors and their interactions were determined.

The solution of the overall task of the study was divided into several stages:

- calculating the line average of the response function and the variance of the response at each point in the experiment plan;
- checking the homogeneity of line-by-line variances;
- determination of the coefficients of the mathematical model;
- determination of variance of reproducibility;
- the estimation of the statistical significance of the coefficients of the model;
- analysis of the adequacy of the model and experimental data, forming conclusions about the possibility of applying the developed model;
- determination of optimal parameters optimization of mechanical activation using one of the optimization methods.

For a two-factor experiment, the regression equation was considered as a complete quadratic polynomial of the form:

$$y = b_0x_0 + b_1x + b_2x_2 + b_{12}x_1x_2 + b_{11}x_1^2 + b_{22}x_2^2. \quad (1)$$

where b_i – the coefficient of regression; x_0 – a fictitious variable; y – the optimization parameter.

In order to reduce the number of experiments, a composite (sequential) plan was used [12].

The total number of experiments was calculated by the formula [13]:

$$N = N_0 + 2k + n_0. \quad (2)$$

The length of the "star shoulder" α was determined from the relation:

$$\alpha = \sqrt{\frac{\sqrt{N_0N} - N_0}{2}}. \quad (3)$$

Table 1 shows the parameters of the experiment planning.

Table 1 – Planning an experiment

Parameters of the plan	FFE type 2^2
The number of experiments in the matrix (N_0)	4
The number of star points (2k)	4
Number of zero points (n_0)	1
Star shoulder	1

Factor space region shown in Table 2. The upper and lower levels were established experimentally during preliminary single-factor experiments.

Table 2 – The factor variation matrix

Levels and intervals of variation	Code value	Factors	
		X_1	X_2
Upper level	+1	9000	7
Zero level	0	7000	5
Lower level	-1	5000	3
Variation interval	ε	2000	2

Based on the values of these parameters, the centre of the plan and the variation step were determined. In the dimensionless coordinate system, the upper level was expressed as (+1), the lower level (–1), the coordinates of the centre of the plan were equated to zero.

On the basis of the composed experimental planning matrix, a number of experiments were performed, the results of which made it possible to determine the coefficients of the corresponding dependence. To eliminate errors, randomization of experiments in time was used.

The result of the simulation was the ratio (4) in the coded values of the factors.

$$y = 22{,}943 + 2{,}217X_1 + 2{,}167X_2 - 2{,}175X_1X_2 + \\ + 0{,}8435X_1^2 - 7{,}9065X_2^2 \quad (4)$$

For convenience of practical use of the obtained dependence by means of the encoding formulas by the reverse transition to natural variables, equation (5) is obtained in the natural values of the factors.

$$\sigma_b(n, \tau) = -48{,}348 + 0{,}000875 \cdot n + 24{,}656 \cdot \tau - \\ - 0{,}00054375 \cdot n \cdot \tau + 0{,}0000002109 \cdot n^2 - 1{,}976625 \cdot \tau^2. \quad (5)$$

In work the verification of the results of experiments on homogeneity was carried out, the significance of the model coefficients was investigated, the hypothesis of the adequacy of the model obtained was considered and the model was analyzed for informativeness.

Some statistical results of this work are presented in Table 3.

Table 3 – Results of statistical analysis of the mathematical model

Statistical Analysis Parameters		Symbol	Value
Checking the results of experiments on homogeneity	Dispersion of reproducibility	$S^2_{\{y\}}$	0,4616
	Standard deviation	$S_{\{y\}}$	4,1540
	Number of degrees of freedom for dispersion of reproducibility	f	4,0000
	The experimental value of the G-criterion	G^{exper}	0,2143
	The critical value of the G-criterion	G	0,3518
	Level of significance	α	0,0500
	Homogeneity of data	homogeneous	
Checking the hypothesis of model adequacy	Dispersion of adequacy	S_{ad}^2	1,8216
	The experimental value of the F- criterion	F^{exper}	3,9500
	The critical value of the F-criterion for adequacy	F	4,2800
	Number of degrees of freedom for adequacy	f	6,0000
	Level of significance	α	0,0500
	Adequacy of the model	adequate	

The model has excellent information properties, good computational stability and satisfactory describing properties. The mathematical relation was adopted for use, since it allows us to predict with sufficient accuracy the value of the mechanical characteristic with the corresponding parameters of the technological process.

Fig. 1 shows the response surface and the level lines of dependence of the breaking strength (σ_b, MPa) from rotating speed of working organs of a mill (n, min^{-1}) and the time of activation of PTFE-matrix (τ, min). The dependence (5) was constructed using a graphical editor SIGMAPLOT 11.0.

Using the second-order regression equation allows us to determine the coordinates of the optimum point of the response function. To determine the coordinates of the extremum points, the partial derivatives for each of the values of the factors were found [13].

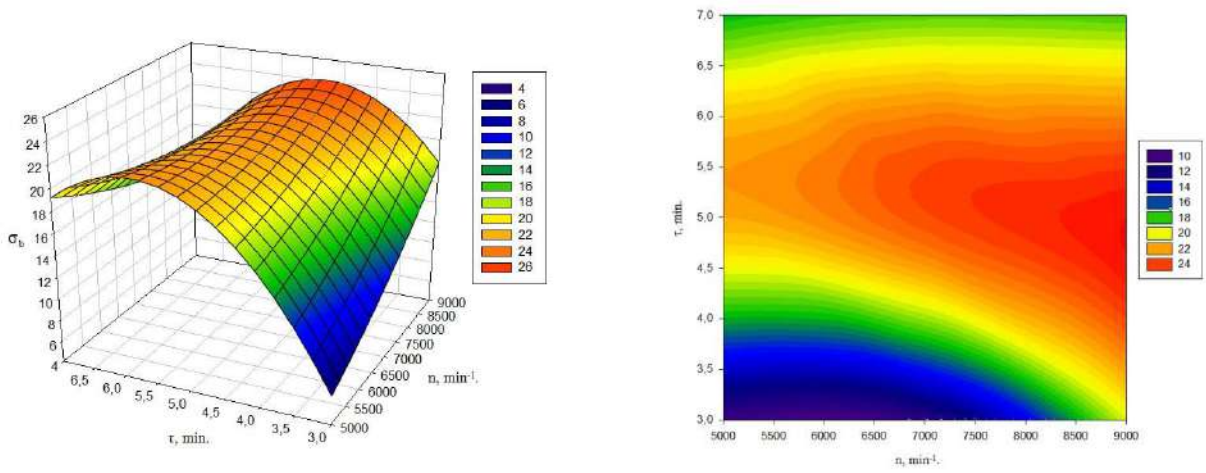

a b

Figure 1 – The response surface (a) and the level lines (b) of dependence of the breaking strength (σ_b, MPa) of PTFE-matrix from rotating speed of working organs of a mill (n, min^{-1}) and the time of activation of PTFE-matrix (τ, min).

We considered a system of equations:

$$\begin{cases} \dfrac{\partial Y(X_1;X_2)}{\partial X_1} = 0, \\ \dfrac{\partial Y(X_1;X_2)}{\partial X_2} = 0. \end{cases} \quad (6)$$

The solutions of the resulting system (6) of equations represent the coordinates of the extremum points of the function being studied for a given area of investigation.

Based on the optimization results, the theoretical value of the maximum breaking strength of the activated PTFE-matrix was calculated (Table 4).

The relative error in determining the breaking strength did not exceed 5 %, which indicates the reliability of the results of mathematical modeling.

Table 4 – Optimal modes of equipment operation during mechanical activation of the PTFE-matrix

Parameter	Model	Experiment
Breaking strength, MPa	26,0035	24,8000
Rotating speed of working organs of a mill (n, min^{-1})	9000	9000
Time of activation (τ, min)	4,999	5,000

5 Conclusions

As a result of the experiment, was obtained a two-factor mathematical model that allows predicting the strength characteristics of the PTFE-matrix and optimally design it depending on the indicators of the technological process.

Thus, the performed researches and the obtained dependences allow theoretically predict the breaking strength of the PTFE-matrix in dependence on the technological characteristics of the mechanical activation (the time of activation and rotating speed of working organs of a mill).

The conducted practical studies show that theoretical calculations confirm the experimental value under optimal operating conditions of a mill.

In addition, the obtained dependence of the value of breaking strength from the technological parameters of the activation process can be embedded in the algorithm for selecting the technological regime that ensures the output of products with given quality indicators, and at the same time achieving an extreme value of a certain efficiency criterion.

References

1. Smith, D. W., Iacono, S. T., & Iyer, S. S. (2014). *Handbook of fluoropolymer science and technology*. Hoboken, Wiley.
2. Negrov, D. A., Putintsev, V. Yu., Peredel'skaya, O. A., Naumova, A. V. (2015). Tekhnologiya izgotovleniya detaley uzlov treniya iz polimernykh kompozitsionnykh materialov. *Bulletin of YuUrGU, series "Mashinostroyeniye"*, Vol. 15, Issue 2, 13–19 [in Russian].
3. Venkateswarlu, G., Sharada, R., & Bhagvanth Rao M. (2014). Polytetrafluoroethylene (PTFE) based composites. *Journal of Chemical and Pharmaceutical Research*, Vol. 6, Issue 10, 508–517.
4. Budnik, O. A., Sviderskii, V. A., Budnik, A. F., Berladir, K. V., Rudenko, P. V. (2016). Composite material for chemical and petrochemical equipment friction assemblies. *Chemical and Petroleum Engineering*, Vol. 52, Issue 1, 63–68, doi: 10.1007/s10556-016-0149-x.
5. Jordan, J. L., Siviour, C. R., Foley, J. R., & Brown, E. N. (2007). Compressive properties of extruded polytetrafluoroethylene. *Polymer*, Vol. 48, Issue 14, 4184–4195, doi: 10.1016/j.polymer.2007.05.038.
6. Struk, V. A., Tsvetnikov, A. K., Antonov, A. S., et al. (2009). Mekhanokhimicheskiye aspekty tekhnologii formirovaniya i primeneniya ftoroplastovykh kompozitov. *Izvestiya NAN Belarusi*, Vol. 3, 28–35 [in Russian].
7. Mohd, F. O., Akil, H. M., & Ahmad, Z. A. (2011). Measurement and prediction of compressive properties of polymers at high strain rate loading. *Mater Des*, Vol. 32, Issue 8–9, 4207–4215.
8. Budnik, O. A., Budnik, A. F., Sviderskiy, V. A., Berladir, K. V., & Rudenko, P. V. (2016). Structural conformation of polytetrafluoroethylene composite material. *Chemistry & Chemical Technology*, Vol. 10, No. 2, 241–246.
9. Bukhkalo, S. I., Ol'khovskaya, O. I., & Borkhovich, A. A. (2008). Otsenka kachestva vtorichnykh polimerov s pomoshch'yu matematicheskoy modeli. *Íntegrovaní tekhnologíÏ ta yenergozberezhennya,* Vol. 2, 51–55 [in Russian].
10. Shevchenko, S. A., Valivakhin, S. O., Hryhor'yev, O. L., & Stepanov, M. S. (2016). Matematychna model′ manzhetnykh ushchil′nen′ iz ftoroplasta dlya ahrehativ pnevmoavtomatyky raketnykh dvyhuniv. *Visnyk NTU «KHPI». Seriya: Matematychne modelyuvannya v tekhnitsi ta tekhnolohiyakh*, Vol. 6, Issue 1178, 124–143 [in Ukrainian].
11. Nekouzadeh, A., Pryse, K. M., Elson, E. L., & Genin, G. M. (2007). A simplified approach to quasi-linear viscoelastic modeling. *Journal of Biomechanics*, Vol. 40, Issue 14, 3070–3078, doi: 10.1016/j.jbiomech.2007.03.019.
12. Dreyper, N., & Smit, G. (2007). *Prikladnoy regressionnyy analiz*. Moscow : Vil'yams [in Russian].
13. Meledina, T. V., & Danina, M. M. (2015). *Metody planirovaniya i obrabotki rezul'tatov nauchnykh issledovaniy*. Saint Petersburg, NIU ITMO [in Russian].

Математичне моделювання механічної характеристики активованої ПТФЕ-матриці на основі методу планування експерименту

Білоус О. А.[1], Говорун Т. П.[1], Берладір Х. В.[1*], Воробйов С. І.[2], Сімкулет В. В.[3]

[1] Сумський державний університет, вул. Римського-Корсакова, 2, 40007, м. Суми, Україна;
[2] Інститут фізики, Університет ім. П. Й. Шафарика у м. Кошице, вул. Шробарова, 2, 041 54, м. Кошице, Словаччина;
[3] Технічний університет м. Кошице, вул. Баєрова, 1, 080 01, м. Прешов, Словаччина

Анотація. Досліджено вплив параметрів технологічного процесу механічної активації на фізичні характеристики політетрафторетиленової (ПТФЕ) матриці.В роботі представлена математична модель залежності міцності при розриві від часу активації та числа обертів робочих органів подрібнювача. Математичне моделювання здійснюється методом ортогонального планування експерименту. Результатом дослідження є математичне співвідношення, яке пояснює зв'язок між технічними характеристиками процесу виготовлення фторопластового композиту та механічними характеристиками матеріалу.

Виконано статистичний аналіз результатів експерименту і проведено оцінку адекватності побудованих математичних співвідношень. На підставі аналізу даних зроблено висновок, що отримана теоретична модель адекватна та придатна для виконання відповідних технологічних розрахунків.На підставі проведених розрахунків зроблено висновок щодо оптимального технологічного режиму підготовки ПТФЕ-матриці. Аналізи показали, що теоретичні розрахунки підтверджують експериментальне значення при оптимальних режимах роботи подрібнювача.Таким чином, отримана залежність міцності при розриві від технологічних параметрів процесу активації може бути закладена в алгоритм вибору технологічного режиму, що забезпечує випуск продукції з заданими якісними показниками.

Ключові слова: політетрафторетиленова матриця, механічна активація, математичне моделювання, міцність при розриві, параметри.

JOURNAL OF ENGINEERING SCIENCES
ЖУРНАЛ ІНЖЕНЕРНИХ НАУК
ЖУРНАЛ ИНЖЕНЕРНЫХ НАУК
Web site: http://jes.sumdu.edu.ua
DOI: 10.21272/jes.2018.5(1).c2 Volume 5, Issue 1 (2018)

UDC 621.619.73

Research of Mechanical Properties of Thermite Material on the Basis of Steel Dross

Rud V., Saviuk I., Samchuk L., Povstyana Y.

Lutsk National Technical University, 75 Lvivska St., 43018, Lutsk, Ukraine

Article info:
Paper received: February 22, 2018
The final version of the paper received: April 1, 2018
Paper accepted online: May 6, 2018

*Corresponding Author's Address:
samchuk204@gmail.com

Abstract. Important direction in the development of technologies for the recycling of wastes of industrial productions is inclination on the use energy saving technologies. The article deals with general aspects of methods of utilization of industrial wastes by methods of powder metallurgy. One of the same methods, which is highly effective and technologically, is the method of utilization of dross by using it as the main component of exothermic mixtures. On the basis of experimental research composition of exothermic charge based on the scale of steel was developed and proposed that can be used for surfacing the details of responsible designation. The choice of main and alloying components of charge was conducted on the analysis of literature data and the calculation of the required chemical characteristics of the material. According to the chemical composition, the termite material can be attributed to qualitative structural steels. Important characteristic of this material is the lack of content of harm fulimpurities, such as sulfur and phosphorus. Research of mechanical properties showed that material has a high resilient deformationon a compression and durability. The analysis of diagram deformation allows to assert that plastic decomposition prevails upon the destruction of the material. The hardness of material at different depths of sampling is different, which indictates the impact of the technological parameters of combustion of exothermic mixtures on the properties of the material. Investigation of impact strength showed that the change in the temperature of the test does not significantly affect its change, which indictates the suitability of the developed termite steel for the surfacing of parts working under reverse friction and shock loads.

Keywords: exothermic mixture, dross, SVS, aluminothermy, material, mechanical description.

1 Introduction

One of important tasks for the further development of Ukrainian industry is the complex use wastes of industrial productions. Wastes of metallurgical and metal-working enterprises of Ukraine are distributed as follows: slags – 57–63; mineral wastes (scrap of refractory materialsand inlet components) – 4–6; scrap metal – 15–17; dust, waste products; dross – 9–13; others – 2–4. A significant amount of waste products in the wastes of metallurgical and metal-working enterprises contains from 45 % to 72 % of iron, 6.0–9.5 % of carbon and 0.5–4 % of zinc [1]. This raw material can be used for an agglomeration and in a converter steel production, manufacturing products on their basis and other. However, 90 % of the wastes after different metallurgical and technological processes together folding in some waste products storage units where they are preserved. The burial and folding of them in the deposits waste products to perform unusual influence on quality of surface and underground waters in general the ecological situation. The methods of powder metallurgy allow the use of such wastes in the technological processes of manufacturing products, which allows them to reduce substantially their cost and non-waste production provides practically.

2 Literature Review

Efficiency of wastes using of metallurgical enterprises, namely domain slags and waste products, in the manufacture of building materials proved in works [2, 3]. However, despite the economic efficiency, such technologies are rarely used in practice. While scrap metal and metals scab are convert practically fully by using them as the basic raw material for the manufacture of products.

A separate point is to allocate dross and sludge, the use of which is insignificant enough due to the high content of impurities such as abrasive, lubricating and cooling liquids. For the use of sludge requires expensive and costly technologies on their renewal [4–6], while a dross, as a rule, only needs to be crushed and sift.

At present existent the file of utilization proposed technologies or processing of dross, as oiled so dry. Most of the proposed technologies are reduced to its briquette

with the further use in agglomeration processes [7,8]. Known methods for using dross for the manufacture of porous products are presented in the works [9, 10]. Such application of dross is conditioned by high maintenance in it iron oxides, that in combination with more easy metals e high content of iron oxides in it, which, in combination with lighter metals are capable of recovery with the release of high temperatures (SVS synthesis).

Application of dross in SVS processes allows one only sintered powder mixtures due to a heat that is distinguished, but also fully to proceed in iron from his oxides, is dross. Efficiency of such technologies is practically and theoretically proven and sometimes applied in industry [11–13]. The dross of steel often serves as the basic component of exothermic mixtures, that used for heating of the gate systems, manufacture of thermite steel, metals welding and component manufacturing by exothermic melting. However, without regard to plenty of researches and theoretical calculations of alumetermic processes with the use dross of steel very small attention is spared to the study of properties the materials obtained. Research of the physical, mechanical and chemical properties of thermite steels and conformities to law of their change will allow to have a close idea about the processes of relation of material at the exothermic burning, to get dependences of mechanical and physical properties on composition, dispersion and technological parameters of burning of charge. Such knowledge will allow forecasting properties of exothermic steel on the stage of development.

The results of researches the temperature indexes burning of exothermic mixtures, given in work [14], allow us to derive the relationship between the specific surface of the pyrophoric powder and the oxides to minimize the activation energy of the SVS reaction. It has been proved that reducing the size of powder contributes to uniformity of reaction. These data are useful in developing the composition of exothermic mixtures. Research of the phase separation of intermetallic of the Fe-Al system obtained in the mode of SVS and its kinetics, described in [15], shows the mechanism of their formation during the rapid heating that occurs in burning exothermic and cooling below the crystallization temperature. During slow heating the formation of intermetallic compounds ofFe_2Al_5 and $FeAl_2$ begins below the melting point of aluminium. When the heating speed is high, intermetallic is formed after the aluminium is cured. These data are key at an idea about the structure and phase formation of thermite metals.

The research aim is determination of the mechanical descriptions of new material which received by metal thermite method.

3 Research Methodology

Exothermic waste products was prepared on the basis of dross steel of 18Ch2N4MA of forging and stamping production of LLC “Kovelsilmash”. The chemical properties of thermite steel directly depends on the composition of the charge. As known [16], the content of aluminium in thermite steel in an amount 0.15–0.20 % leads to deterioration of it plastic and mechanical properties. For saturated and improvement of mechanical properties of thermite steel in composition of exothermic charge enter a ferromanganese and ferrosilicon [17–18]. Introduction to the charge of copper in an amount 3–5 % leads to a uniform passage of the reaction and allows to increase the combustion temperature by 100–150 °C. In addition, copper increases pirofornist charges and assists the best dissociating of liquid metal from a slag [19]. Established that the oxygen balance of 18Ch2N4MA of dross steel forging-stamping production is 22.5–25.0 % O_2, which is lower than that required for stable reaction passage and full blown out of the charge. Introduction to the exothermic charge powder of saltpetre potassium in an amount 7–9 % provides stable combustion due to the uniform distribution of the oxygen balance of the charge. An addition of saltpetre potassium allows bringing down a temperature of ignition of the charge and increase its caloric content.

Therefore, proceeding from the foregoing and using data [20] next composition of exothermic waste products was select (Table 1).

Table 1 – Mass particle of components of exothermic waste products, the masses %:

Dross of steel 18Ch2N4MA	68–72
Aluminium powder PA-3 GOST 6058-73	16–20
Copper powder PMS-1 GOST 4960-75	3–5
Potassium saltpetre GOST 19790-74	7–9
Ferromanganese FMn75A	0.5–0.8
Ferrosilicon FS 45	1.5–2.2

Granulometric composition of the exothermic mixture in mm: iron-aluminum termite; 0.3-0.5 dross; 0.3 powder of aluminum; 0.1 copper powder; 0.4–0,5 powder of potassium saltpetre; 0.1 powder of ferrosilicon and ferromanganese.

As a result of the exothermic reaction a monolithic sample was obtained, the chemical composition of which is given in Table 1.

Correlation of part of metal and slag 63:37.

Table 1 – The chemical composition of the material obtained

Test	Chemical composition, %						
	C	Si	Cr	Fe	Mo	Mn	Ni
1	0.43	0.21	0.22	98.79	0.07	0.17	0.05
2	0.38	0.2	0.25	98.83	0.05	0.19	0.10

The presence of high content of aluminium is explained by division incomplete of metal and slag at passing of exothermic reaction. Identified vanadium probably formed from iron oxides as it is geochemically close to Fe, Mn, Cr, Al, Ti. The presence of vanadium in the amount of 0.2 % and more increases the stability of steel release.

Researches of the obtained steel strength at compression conducted on a machine MT 120-40. With the aim of reduction of force of friction that may break the uniaxial elastic-deformed state, on the butt-end surfaces of standard inflicted a paraffin layer. A standard was executed in cube form with sizes a (5 ± 0.5) mm. Pressure of tests of 40 MPa. Researches conducted on a monolithic sample (Fig. 1 a) and a sample with defect (Fig. 1 b).

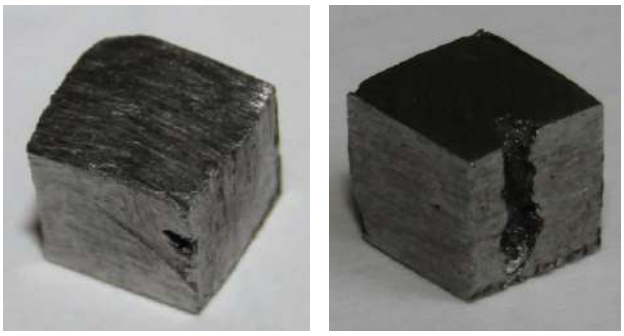

a b

Figure 1 – Samples for strength tests:
a – monolithic sample; b – sample with defect

Depth of pore on sample with defect 0.7–0.9 mm, volume 26 mm^3. The sample with the defect was placed so that the defect axis was parallel to the load axis. The loading speed was determined from the formula [21]:

$$\frac{d\varepsilon}{dt} = (0.01...3), \text{ min}^{-1}. \quad (1)$$

Figure 2 shows that the deformation curve is characteristic for plastic destruction. Section *AB* is the plane of flow. On this area is displacement of atomic layers in relation to each other. On the *BC* section there is strengthening of material by changing the internal structure of the sample, as a result of what a standard shows resistance to deformation. Section *CD* is theplastic deformation. On this section increases the cross-section of the sample. Section *DE* is the discharge curve and shows the zone of elastic deformation of the sample and residual deformation. This deformation curve is characteristic for the dependence of $S_s(\varepsilon_l)$. For such deformation curves intensity of strengthening at insignificant degrees of deformation and then sharply increases [21].

The deformation curve for a defective sample is shown on Figure 3.

As evidently on Figures 2–3, the change in linear deformation for a defect sample is practically no different from the deformation for a monolithic sample. It testifies to strong interatomic connections and low speed of crack propagation.Border of strength material, that was determined by hardness dynamic of TD-42M presents 870–920 MPa.

Hardness measuring conducted on a hardness of HR-150A according to GOST 9013-59. Hardness for a raw sample is given on the HRA scale. As an indenter used a diamond tip with a corner at the top of a 120°, loading 590 N. Measuring of hardness conducted on different depths of the sample.

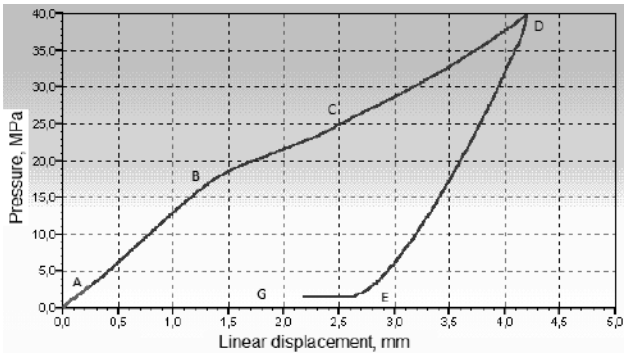

Figure 2 – Dependence of linear deformation on the applied force for a monolithic sample

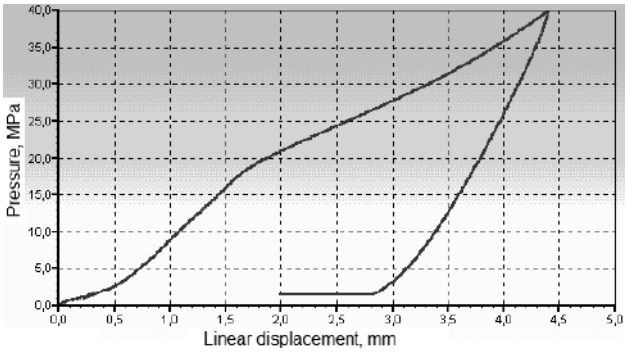

Figure 3 – Dependence of linear deformation on the applied force for a defective sample

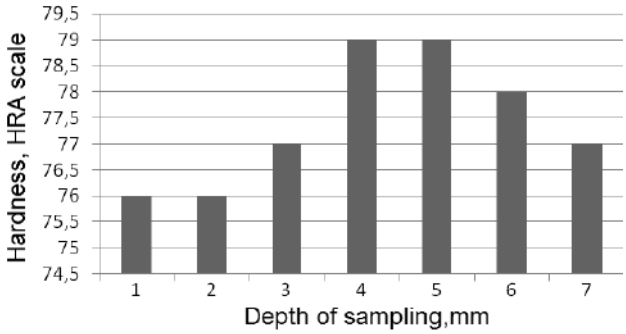

Figure 4 – Hardness of the raw sample depending on sample depth

The change in hardness depending to taking on sample depth is explained change in the chemical composition of the resulting exothermic mixture combustion. The trend of change in hardness suggests the effect of the technological parameters of combustion of exothermic mixtures on the properties of the materials obtained. The change in the granulometric composition of the mixture toward the consolidation of the powders allow increase the hardness. This happened to a lower fill density, which in turn leads to a better passage of gases and, as a consequence, reduces the consolidation of the alloying elements in the upper part of the material.

Important characteristic of the structural strength of materials is the impact strength. It depends both on the

strength and on the plasticity of the material. Research impact strength on the pendulum copier MC-30.

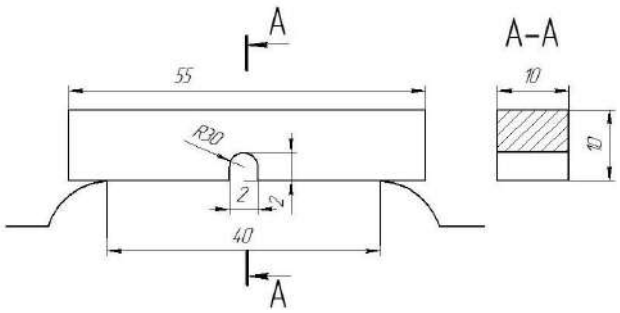

Figure 5 – Design scheme of sample and geometric parameters

For research of impact strength took away sample that no apparent external defects (shells, cracks) and complied with the requirements of GOST 10708-82.

The sample was mounted on the supports of the cow so that the incision was on the opposite side of the impact. Researches conducted at a temperature 60, 40, 20, 0, and –20 °C.

KCU for the raw material at different temperatures is shown on Figure 6.

According to the results of tests samples with U similar incision, the minimum impact strength of the material at a temperature -20 °C, that presents 150 J/cm^2, that is sufficient for materials that work in the conditions of reversible friction and temperatures 40-60 °C.

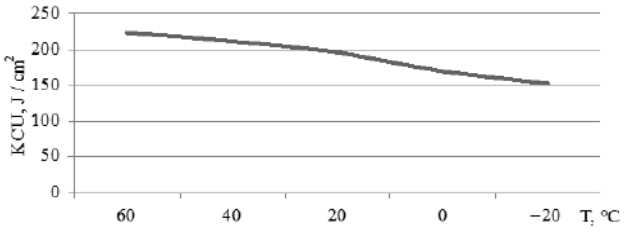

Figure 6 – Impact strength of raw sample

4 Conclusions

The composition of the exothermic charge with the production of steels has been developed. The research results of mechanical properties of steel allow thermite hypothesis about influence of technological parameters of the combustion mixture on the mechanical properties of the material shown by changing the hardness of the sample depending on the depth of sampling. The experimental data obtained show strong interatomic bonds and a low speed of crack propagation. Border of material strength presents 870–920 MPa. Impact strength of raw standard presents 170–220 KCU and is sufficient for material work in the conditions of the dynamic loading and reversible.

References

1. Kripak, S. (2006). *Improvement of technological processes of preparation of metallurgical raw materials for the purpose of utilization of oiled rolling mill*. Abstract of the dissertation for the degree of a candidate of technical sciences, Dnipropetrovsk.
2. Aksenova, L., & Khlebenskykh, L. (2014). Utilization of waste enterprises of ferrous and nonferrous metallurgy in the building industry. *Technical sciences in Russia and abroad, Materials of 3rd International Scientific Conference*, Moscow, pp. 106–108.
3. Valuev, D., & Hyzatulyn, R. (2012). *Technology and processing of metallurgical waste*. Yurginsky Technological Institute. Publishing house of Tomsk Polytechnic University, Tomsk.
4. Rud, V., & Halchuk, T. (2011). Modeling of shredding process of steel powders of BBS 15, obtained from waste from machine-building production in ball mills. *Bulletin of the National Technical University "KhPI", Series"Chemistry, chemical technology and ecology"*, Kharkiv, No. 50, pp. 121–126.
5. Halchuk, T. (2013). The structure and properties of a steel powder BBS 15 is recovered in water. *Scientific notes*, Vol. 41(2), pp. 23–27.
6. Halchuk, T. (2012). Improved technological scheme of processing sludge waste mechanical engineering. *Bulletin of the Khmelnytsky National University*, Vol. 4, pp. 26–30.
7. Mohylatenko, V., Chaikovskyi, O., Khasan, O., Lytvynets, Ye., Sas, A., & Olshevskyi, V. (2011). Use of termite mixture for melting FX025. *Bulletin of the Donbas Machine-Building Academy*, No. 4(25), pp. 122–126.
8. Dobrovolskyi, I., Starykova, N., Volkova, M., & Rymariv, P. (2011). Promising technologies for processing metallurgical scale. Development of the technical heritage. *Polzunovsky Almanac*, No. 2, pp. 137–139.
9. Lebedieva, O., Butyhin, V., & Stepenenko, N. (2008). The use of industrial waste to produce porous composite ceramic materials with high-temperature synthesis in the Fe2O3-Al2O3-Al system. *Polzunovsky almanac*, No. 3, pp. 107–108.
10. Povstiana, Yu., Saviuk, I., Samchuk,L., & Zubovetska, N. (2016). Preparation of porous metalloceramic materials using waste mechanical engineering in the mode of self-propagating high-temperature synthesis. *Journal of Engineering*, Vol. 3, No. 1, pp. 6–12.
11. Stetsenko, V. (2011). Metal thermal processing of shavings of aluminum alloys, scale and blast furnace. *Casting and metallurgy*, No. 3(62), pp. 176–177.
12. Myronenko, O., & Dytynenko, T. (2014). Improvement of the technology of utilization of scale at LLC "Lozovsky Kuznechno-Mechanical Plant". *Physical and computer technologies: Proceedings of the 19th International. Scientific and Practical Conference*, pp. 170–177.

13. Zhyhuts, Yu. (2012). Technology of obtaining termite shipbuilding steels. *Bulletin of the Donbas Machine-Building Academy*, No. 3(28), pp. 283–283.
14. Zhu, C.-G., Wang H.-Z., & Min, L. (2014). Ignition temperatur e of magnesium powder and pyrotechnic composition. *Journal of Energetic Materials*, No. 32, pp. 219–226.
15. Novak, P., Michalcova, A., Marek, I., Mudrova, M., Saksl, K., Bednarcik, J., Zikmund, P., & Vojtech, D. (2013). On the formation of intermetallics in Fe–Al system. *Intermetallics, including complex structural and functional alloys*, Vol. 32, pp. 127–136.
16. Sapchenko, I., Zhylin, S., Komarov, O., & Abashkin, E. (2012). Properties of the weld obtained from the final charge. *Academic notes of Komsomolsk-on-Amur State Technical University*, No. I-1(9), pp. 100–105.
17. Berezhnoi, S., Brindarov, B., & Harbuz, A. (1997). *Termite composition*. Patent of Russia, No. 2134185.
18. Dudenko, P., & Holovyna, N. (1989). *Composition of the thermal mixture*. Patent of the USSR, No. 16111651.
19. Chiharev, V., Zarechenskyi, D., & Belik, A. (2007). Features of melting powdered tapes with exothermic mixtures in the filler. *Automatic welding*, No. 2, pp. 53–55 (2007).
20. Saviuk, I. (2017). Construction of a matrix model for optimizing the charge composition of an exothermic charge. *Scientific notes*, Vol. 60, pp. 206–211.
21. Privalov, N., Shein, A., & Ivashchenko, A. (2014). *Material science. Technological processes*, Volgograd.

Дослідження механічних властивостей термітного матеріалу на основі окалини сталі

Рудь В., Савюк І., Самчук Л., Повстяна Ю.

Луцький національний технічний університет, вул. Львівська, 75, 43018, м. Луцьк, Україна

Анотація. Важливим напрямом у розробці технологій утилізації відходів промислових виробництв є нахил на використання енергозберігаючих технологій. У статті розглядаються загальні аспекти способів утилізації промислових відходів методами порошкової металургії. Одним з таких методів, що є високоефективним та технологічним, є метод утилізації шлаку, який використовується як основна складова екзотермічних сумішей. Вибір основних і легуючих компонентів матеріалу проводився на основі аналізу літературних даних та розрахунку необхідних хімічних характеристик матеріалу. Відповідно до хімічного складу термітний матеріал можна віднести до якісних конструкційних сталей. Важливою характеристикою цього матеріалу є брак вмісту шкідливих домішок, таких як сірка та фосфор. Дослідження механічних властивостей показало, що матеріал має значні пружні деформації при стисканні та довговічність. Аналіз діаграми деформації дозволяє стверджувати, що при руйнуванні матеріалу переважають пластичні деформації. Твердість матеріалу на різних глибинах відбору проб є різною, що обумовлює вплив технологічних параметрів горіння екзотермічних сумішей на властивості матеріалу. Дослідження ударної в'язкості показали, що зміна температури випробувань істотно не впливає на її зміну, що свідчить про придатність розробленої термітної сталі для наплавлення деталей, що працюють за умов реверсивного тертя та ударних навантажень.

Ключові слова: екзотермічна суміш, окалина, СВС, алюмотермія, матеріал, механічні характеристики.

JOURNAL OF ENGINEERING SCIENCES
ЖУРНАЛ ІНЖЕНЕРНИХ НАУК
ЖУРНАЛ ИНЖЕНЕРНЫХ НАУК

Web site: http://jes.sumdu.edu.ua

DOI: 10.21272/jes.2018.5(1).c3 Volume 5, Issue 1 (2018)

UDC 620.178.152:669.265.295

Microstructure and Properties of $AlCrFeCoNiCu_x$ High-Entropy Alloys

Demchenko M. V.[1], Gaponova O. P.[1], Myslyvchenko O. M.[2], Antoszewski B.[3], Bychenko M. M.[1]

[1] Sumy State University, 2 Rymskogo-Korsakova St., 40007 Sumy, Ukraine;
[2] Frantsevich Institute for Problems of Materials Science of the National Academy of Sciences of Ukraine, 3 Krzhizhanovsky St., 03680 Kyiv, Ukraine;
[3] Politechnika Świętokrzyska, al. Tysiąclecia Państwa Polskiego 7, 25-314 Kielce, Poland

Article info:
Paper received: January 17, 2018
The final version of the paper received: May 21, 2018
Paper accepted online: May 22, 2018

***Corresponding Author's Address:**
gaponova@pmtkm.sumdu.edu.ua

Abstract. The peculiarities of the structure formation of alloys of the system $AlCrFeCoNiCu_x$ (where x = 0, 0.5, 1, 2, and 3 moles) were studied. Microstructure of alloys and its phase composition, as the amount of copper increases, undergo significant changes. In all of the investigated concentration interval of change in the content of copper there is a different phase morphology. Confirmed that with increasing of Cu concentration the nature of crystallization of alloys and their phase composition change. Durometric studies of alloys of this system were carried out. Established that an alloy $AlCrFeCoNiCu_{0.5}$ has the highest microhardness 6.1 GPa. Heat resistance tests showed that AlCrFeCoNi and AlCrFeCoNiCu have the highest heat resistance. The connection between the scale composition after the test and the mechanism of oxidation of this alloys revealed. The results of X-ray fluorescence analysis indicate a high content of aluminum in scale. Consequently, the high heat resistance of alloys can be explained by the formation of the Al_2O_3 protective film on the surface.

Keywords: high-entropy alloys, microstructure, microhardness, heat resistance.

1 Introduction

Contemporary development of technology puts forward new requirements for the details of machines and mechanisms operating in extreme conditions. One of the effective methods for improving the physical-mechanical and operational properties of parts is the replacement of traditional structural materials (steels and alloys) with new promising materials. These materials include high-entropy alloys (HEAs). High-entropy alloys are alloys containing in their composition five or more metal elements (usually from five to thirteen) in equimolar or almost equimolar proportions (i. e., the concentration of each element is in the range of 5 to 35 atomic percentages). HEAs are characterized by high entropy of mixing in the initial and liquid (melted) state ($S_{mix} > 1.61R$, where R = 8.314 J/(mol·K) – gas constant). The principal difference between HEAs from traditional alloys containing a solvent and a dissolved substance is the formation of a disordered solid solution in which the atoms of the constituent elements have equal probability to occupy any node of the crystalline lattice. Significant distortion of the crystal lattice arising from the presence of heterogeneous atoms of elements with different electronic structures, sizes and thermodynamic properties affects both the structure and the properties of the resulting alloy. The growth of the number of components of the alloy increases the level of its solid solution hardening. HEAs can be applied in conditions of shock and dynamic loads, friction, elevated temperatures, since disordered solid solutions are more plastic than intermetallics that are formed in high-alloy steels and alloys. From high-entropy alloys can be made both volumetric materials and coatings for application in various spheres.

Over the past few years (mainly in foreign publications), a significant number of articles describing the properties of HEAs [1–4]. In these works the thermodynamics of high-entropy alloys is described, their microstructures are modeled, and methods of obtaining are offered. During the study of HEAs, it was found that they have high mechanical properties, such as high hardness, wear resistance, high temperature strength, corrosion resistance, ductility at low temperatures, and superplastic properties [5]. However, some properties of HEAs are not studied enough.

For HEAs of the AlCrFeCoNiCu system already been investigated the influence of Fe on the microstructure and mechanical properties [6], features of structure formation [7]. In [8] the properties of $AlCrFeCoNiCu_{0.5}$ alloy coatings deposited on the silicon plate by radiofrequency sputtering were considered. However, in general, the properties of AlCrFeCoNiCu system alloys remain insufficiently investigated.

The purpose of this work was to study the structure of high-entropy alloys of the $AlCrFeCoNiCu_x$ system and the relationship between their chemical composition and physical and mechanical properties.

2 Research Methodology

The investigated samples of alloys of the $AlCrFeCoNiCu_x$ system were made by the method of argon-arc melting in the furnace MIFI-9-3. As charge materials used: Cr – hydrogen refined in the form of bits; Ni – cathode in the form of plates 10 mm thick; Co – pressed granules; Cu – vacuum-fused in the form of granules; Fe – carbonyl in the form of granules. Cr, Co, Ni, Cu had a purity of not less than 99.95 % wt, Fe – not less than 99.8 % wt. Melting occurred with a tungsten non-consumable electrode, on a copper water-cooled subunit. After completion of the smelting, the chemical composition was controlled by the loss of mass in the smelt, which in most cases was small and did not exceed 0.3 % wt.

The study of microstructure was carried out on a metallographic microscope MIM-7 at different magnifications on etched materialographic specimen. Dyrometric studies were performed on the microhardness tester PMT-3 in at least 10–15 fields of view at a load of 0.49–0.98 N. As an indenter, a diamond pyramid with a square base and a two-cornered apex with an apex of 136° was used. Measurement accuracy of microhardness ±250 MPa.

The heat resistance test was carried out using a weight method for increasing the mass of samples after exposure to the furnace for 100 hours at a temperature of 1000 °C. Samples for determining the heat resistance of investigated alloys of the same size were carved from cast billets by the method of spark cutting. The surface of the samples was sanded with fine sandpaper and degreased before the test. Before the test, the samples were dried and weighed on analytical weights to within ± 0.1 mg. Also, their surface area was measured. After that, samples in separate crucibles of aluminum oxide were placed in an electric furnace. The furnace was heated to a temperature of 1000 °C, the exposure was 100 hours. Samples were weighed after every 3-7 hours of the test. The chemical composition of the scale was determined by the desktop energy-dispersive X-ray fluorescence spectrometer ElvaX Light SDD.

3 Results and discussions

Fig. 1 shows the microstructures of the $AlCrFeCoNiCu_x$ alloys obtained with an optical microscope. Microstructure of alloys and its phase composition, as the amount of copper increases, undergo significant changes. In all of the investigated concentration interval of change in the content of copper there is a different phase morphology.

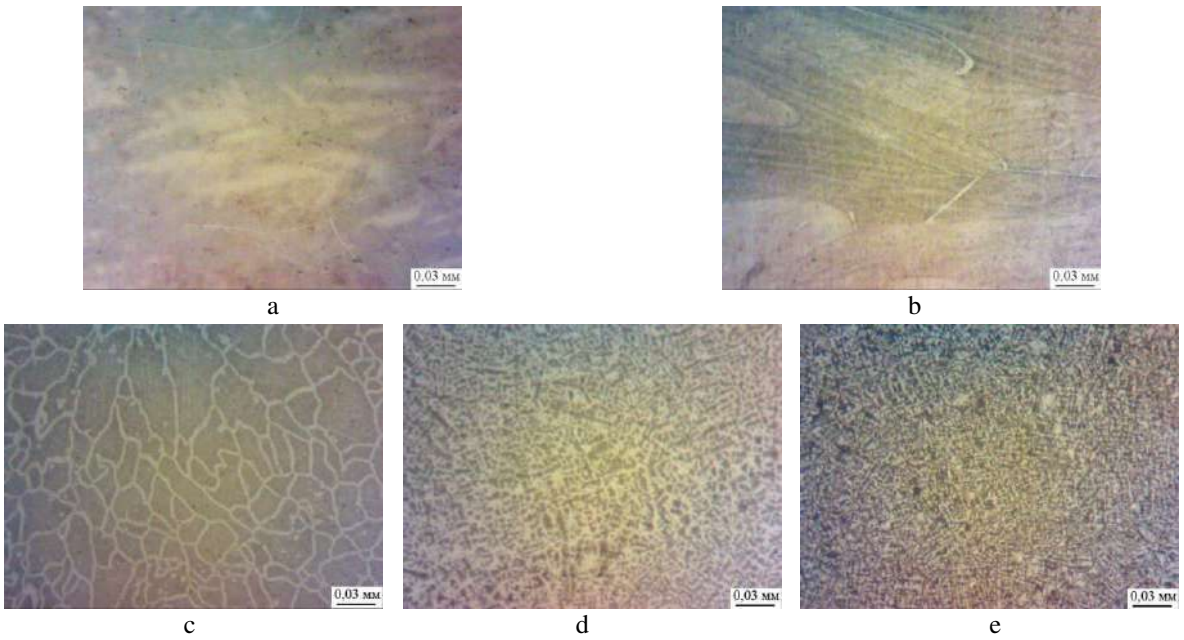

a b c d e

Figure 1 – Microstructures of $AlCrFeCoNiCu_x$ cast high-entropy alloys in a light microscope: $x = 0$ (a); $x = 0.5$ (b); $x = 1$ (c); $x = 2$ (d); x = 3 (e)

The microstructural analysis of the AlCrFeCoNi alloy showed (Fig. 1 a) that the microstructure is homogeneous with a structure consisting of equilibrium grains. Their average grain size is 320 μm.

The microstructures of alloys in which x = 0.5 and 1 mol Cu are added have a similar structure, except that they have the grain boundaries of the light phase layer (Fig. 1 b–c). In [7] argues that the dark phase has a BCC structure, and the light phase has a FCC structure. In addition, with an increase of Cu content from 0 to 1 mole, the grains are refined: its size is 150 μm for the $AlCrFeCoNiCu_{0.5}$ alloy, and 30–40 μm for the AlCrFeCoNiCu alloy.

When adding 2 moles of copper (Fig. 1 d), there is a dendritic nature of crystallization. As shown in [7], dendrite is associated with a solid solution based on the phase with the bcc structure, and the interdendrite area is a solid solution based on the phase with the fcc structure.

When copper content x = 3 mole, the nature of crystallization does not change.

Consequently, the content of Cu greatly affects the structure and phase composition of alloys of the $AlCrFeCoNiCu_x$ system. With the increase in the concentration of copper, the nature of crystallization changes, in addition, according to earlier studies, the phase composition also changes.

Dyrometric analysis showed that the highest microhardness (6.1 GPa) has an AlCrFeCoNiCu0.5 alloy (Fig. 2). In other alloys, the microhardness is proportional to the volume fraction of a solid solution based on the phase with the bcc structure, which in turn is inversely proportional to the amount of copper in the alloy. The high microhardness of the $AlCrFeCoNiCu_{0.5}$ alloy can be explained by the presence of fine-grained structure, since copper in an amount equal to half of the aviation volume is a good modifier of the second kind, which, according to the law of Hall-Petch, leads to strengthening. The mechanism of reducing the size of the grain is as follows: copper or its compounds adsorbed on the surface of growing crystals and inhibit their growth. This leads to an increase in the amount of supercooled melt before the crystallization front and creates favorable conditions for the emergence of new centers of nucleation of crystals, which leads to grain refinement.

As you know, some HEAs have a high corrosion resistance and heat resistance. The author of [9] explains the behaviour of the aggressive medium at elevated temperature by the structure of HEAs, which consists of a homogeneous solid solution. The authors of [10] believe that the increased values of heat resistance are characteristic of HEAs based on refractory metals. In this regard, the task of studying the heat resistance of alloys of the AlCrFeCoNiCu system and the influence of Cu on the parameters of heat resistance is relevant.

The heat resistance tests conducted in an air atmosphere at a temperature of 1 000 °C for 100 hours showed (Fig. 3) that the investigated alloys are characterized by high heat resistance (Δg – mass loss per unit of surface area of tested samples, mg/cm^2). Fig. 3 shows that AlCrFeCoNi and AlCrFeCoNiCu have the highest heat resistance, the heat resistance of $AlCrFeCoNiCu_2$ alloy is slightly lower, and the highest mass loss per unit of surface area (and therefore the lowest heat resistance) have $AlCrFeCoNiCu_3$ alloy.

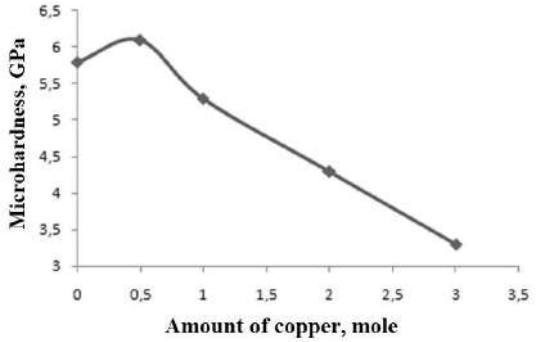

Figure 2 - Concentration dependence of microhardness for alloys of the $AlCrFeCoNiCu_x$ system

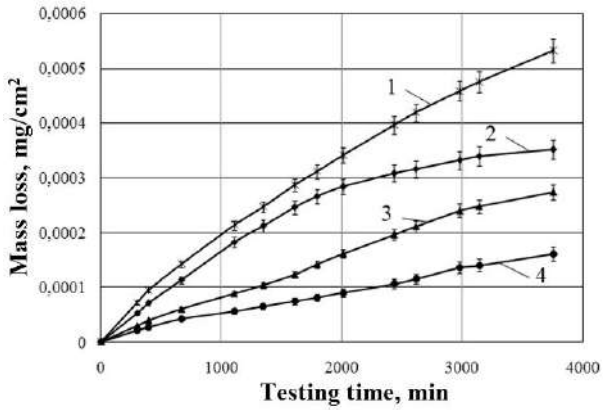

Figure 3 – Curves of $AlCrFeCoNiCu_x$ system alloys during the heat resistance tests (air, 1 000 °C, 100 hours):
1 – $AlCrFeCoNiCu_3$; 2 – $AlCrFeCoNiCu_2$; 3 – AlCrFeCoNi;
4 – AlCrFeCoNiCu

In [11] it was suggested that the mechanism of oxidation of this HEAs can be described on the basis of the Higgins-Pettit's theory of Ni-Cr-Al alloys oxidation. This is an empirical theory that divides Ni-Cr-Al alloys into 3 groups, based on the scheme of their oxidation [12]. Group I corresponds to dilute alloys in which Cr and Al concentrations are too low to establish continuous Cr_2O_3 or Al_2O_3 scales. Instead, the external scales consist of NiO plus $Ni_2Cr_2O_4$ and $Ni_2Al_2O_4$ spinel phases coupled with internal oxidation of Al. Group II corresponds to alloys with large enough Cr concentrations, but relatively low Al concentrations, that results in selective oxidation of Cr, which forms external Cr_2O_3 scale. The formation of internal Al_2O_3 subscale proceeds as a result of internal oxidation. Group III corresponds to alloys containing large enough Al concentration to promote the selective oxidation of Al, that results in formation of external Al_2O_3 scale.

The results of X-ray fluorescence analysis (Table 1) showed a high Al content in scale as compared to an unoxidized alloy, which confirms the above-mentioned assumptions. This fact confirms Al diffusion on the surface of the alloy during oxidation and, accordingly, the formation of an Al_2O_3 oxide film. Thus, the $AlCrFeCoNiCu_x$ system HEAs are characterized by high heat resistance due to the relatively high content of Al in oxide. AlCrFeCoNi and AlCrFeCoNiCu alloys have the highest thermal resistance, and when the copper content is high, the hardness of the alloys is deteriorating. Previously it was shown [7] that copper at concentrations more than half the equio-atom leads to the digestion, the formation of several FCC phases instead of one initial BCC of a solid solution. It is obvious that such an effect of Cu on the microstructure and phase composition worsens the characteristics of heat resistance at its high content due to the fact that the Cu enriched interdendritic area is fusible.

Table 1 – Results of the spectral analysis of scale after the heat resistance test

Atomic number	Element	Series	Intensity	Concentration, % wt
Alloy AlCrFeCoNi				
13	Al	K	56124	16.4093 ± 0.1305
24	Cr	K	323339	29.2553 ± 0.1020
26	Fe	K	188479	21.1143 ± 0.0970
27	Co	K	228360	20.3330 ± 0.1021
28	Ni	K	142385	12.8881 ± 0.0860
29	Cu	K	0	< 0.0343
Alloy AlCrFeCoNiCu				
13	Al	K	210233	31.8171 ± 0.1130
24	Cr	K	175297	16.5350 ± 0.0819
26	Fe	K	163873	14.0406 ± 0.0720
27	Co	K	233312	15.8340 ± 0.0797
28	Ni	K	137857	9.9116 ± 0.0696
29	Cu	K	176183	11.8617 ± 0.0640
Alloy $AlCrFeCoNiCu_2$				
13	Al	K	232208	33.0242 ± 0.1124
24	Cr	K	121213	13.1214 ± 0.0788
26	Fe	K	140157	12.2647 ± 0.0698
27	Co	K	184363	12.7072 ± 0.0757
28	Ni	K	116441	8.9282 ± 0.0678
29	Cu	K	282603	19.9544 ± 0.0800
Alloy $AlCrFeCoNiCu_3$				
13	Al	K	257037	32.7679 ± 0.1070
24	Cr	K	96288	11.2138 ± 0.0754
26	Fe	K	114405	9.8994 ± 0.0637
27	Co	K	154714	10.5938 ± 0.0710
28	Ni	K	121810	9.4739 ± 0.0682
29	Cu	K	367425	26.0512 ± 0.0883

4 Conclusions

The influence of copper concentration on the phase composition and structure of alloys of the $AlCrFeCoNiCu_x$ system has been investigated. Confirmed that with increasing of Cu concentration the nature of crystallization of alloys and their phase composition change.

Durometric studies have shown that the highest microhardness (6.1 GPa) of alloys of the $AlCrFeCoNiCu_x$ system has an $AlCrFeCoNiCu_{0.5}$ alloy, which is due to the presence of fine-grained structure. With an increase in the concentration of Cu, the microhardness of alloys is reduced.

Experimentally determined the heat resistance of the $AlCrFeCoNiCu_x$ system HEAs, revealed a connection between their composition, structure and heat resistance. AlCrFeCoNi and AlCrFeCoNiCu alloys have the highest heat resistance. The high content of Cu in alloys contributes to the formation of several FCC phases instead of one initial solid solution with BCC structure. In addition, the Cu enriched interdendritic area is fusible, which worsens the heat resistance of investigated alloys.

The mechanism of oxidation of alloys of the investigated system at elevated temperature was found. The results of X-ray fluorescence analysis indicate a high content of aluminum in scale. Consequently, the high heat resistance of alloys can be explained by the formation of a Al_2O_3 protective film on the surface.

References

1. Zhang, Y., Yang, X., & Liaw, P. K. (2012). Alloy Design and Properties Optimization of High-Entropy Alloys. *Journal of the Minerals Metals & Materials Society,* Vol. 64, Issue 7, 830–838.
2. Yeh, J. W. (2013). Alloy Design Strategies and Future Trends in High-Entropy Alloys. *Journal of the Minerals Metals & Materials Society*, Vol. 65, Issue 12, 1759–1771.
3. Zhang, L. S., Ma, G. L., Fu, L. C., & Tian, J. Y. (2013). Recent Progress in High-Entropy Alloys. *Advanced Materials Research,* Vol. 227, 631–632.
4. Zhang, Y., Zuo, T. T., Tang, Z., Gao, M. C., Dahmen, K. A., Liaw, P. K., & Lu, Z. P. (2014). Microstructures and properties of high-entropy alloys. *Progress in Materials Science,* Vol. 61, 1–93.
5. Pogrebnyak, A. D., Bagdasaryan, A. A., Yakushchenko, I. V., & Beresnev, V. M. (2014). Struktura i svoystva vysokoentropiynykh splavov i nitridnykh pokrytiy na ikh osnove. *Uspekhi khimii*, No. 83 (11), 1027–1061 [in Russian].
6. Karpets, V., Mislivchenko, A. N., Makarenko, A. S., Krapivka, N. A., & Gorban', V. F. (2014). Mikrostruktura i fiziko-mekhanicheskiye svoystva visokoyentropiynogo splava $AlCrCoNiCuFe_x$. *Fizika i khimiya tverdogo tela*, Vol. 15, No. 3, 661-6656 [in Russian].
7. Karpets, M. V., Mislivchenko, A. N., Makarenko, A. S., Krapivka, N. A., Gorban' , V. F., & Samelyuk, A. V. (2014). Vlastyvosti bahatokomponentnoho vysokoentropiynoho splavu AlCrFeCoNi lehovannoho middyu. *Problemy tertya ta znoshuvannya*, No. 2, 103–1117 [in Ukrainian].
8. Huang, Y. S., Chen, L., & Liu, H. W. (2007). Microstructure, hardness, resistivity and thermal stability of sputtered oxide films of $AlCoCrCu_{0.5}NiFe$ high-entropy alloy. *Materials Science and Engineering: A,* No. 457(1-2), 77–83.
9. Tong, C.-J., Chen, Y.-L., Yeh, J.-W., Lin, S.-J., Chen, S.-K., Shun, T.-T., Tsau, C.-H., Chang, S.-Y. (2005). Microstructure characterization of $Al_xCoCrCuFeNi$ high-entropy alloy system with multiprincipal elements. *Metallurgical and Materials Transactions A,* Vol. 36, Issue 4, 881–893.
10. Senkov, O. N., Wilks, G. B., Scott, J. M., & Miracle, D. B. (2011). Mechanical properties of $Nb_{25}Mo_{25}Ta_{25}W_{25}$ and $V_{20}Nb_{20}Mo_{20}Ta_{20}W_{20}$ refractory high entropy alloys. *Intermetallics,* Vol. 19, 698–706.
11. Butler, T. M., Alfano, J. P., Martens, R. L., & Weaver, M.L. (2015). High temperature oxidation behavior of Al-Co-Cr-Ni-(Fe or Si) multicomponent high-entropy alloys. *Journal of the Minerals Metals & Materials Society,* Vol. 16, 246–259.
12. Giggins, C. S., Pettit, F. S. (1971). Oxidation of Ni-Cr-Al alloys between 1 000 °C and 1 200 °C. *Journal of the Electrochemical Society*, Vol. 118, 1782–1790.

Дослідження структури та властивостей високоентропійних сплавів системи $AlCrFeCoNiCu_x$

Демченко М. В.[1], Гапонова О. П.[1], Мисливченко О. М.[2], Антошевскі Б.[3], Биченко М. М.[1]

[1] Сумський державний університет, вул. Римського-Корсакова, 2, 40007, м. Суми, 40007, Україна;
[2] Інститут проблем матеріалознавства ім. І. М. Францевича НАН України, вул. Кржижановського, 3, 03680, м. Київ, Україна;
[3] Технологічний університет м. Кельце, ал. Тисячоліття Польщі, 7, 25-314, м. Кельце, Польща

Анотація. Досліджені особливості структуроутворення сплавів системи $AlCrFeCoNiCu_x$ (де x = 0; 0,5; 1; 2 і 3 моль). Як і фазовий склад, мікроструктури сплавів по мірі збільшення кількості міді зазнають істотних змін. В усьому досліджуваному концентраційному інтервалі зміни вмісту міді спостерігається різна морфологія фаз. Підтверджено, що при збільшенні концентрації міді змінюються характер кристалізації сплавів даної системи. Проведені дюрометричні дослідження сплавів даної системи. Встановлено, що найвищу мікротвердість 6,1 ГПа має сплав $AlCrFeCoNiCu_{0,5}$. Випробування на жаростійкість показали, що найвищу жаростійкість мають сплави AlCrFeCoNi та AlCrFeCoNiCu. Виявлено зв'язок між складом окалини після випробувань і механізмом окислення даних ВЕСів. Результати рентгенофлуорисцентного аналізу свідчать про високий вміст алюмінію в окалині. Отже високу жаростійкість сплавів можна пояснити утворенням на поверхні захисної плівки Al_2O_3.

Ключові слова: високоентропійний сплав, мікроструктура, мікротвердість, жаростійкість.

JOURNAL OF ENGINEERING SCIENCES
ЖУРНАЛ ІНЖЕНЕРНИХ НАУК
ЖУРНАЛ ИНЖЕНЕРНЫХ НАУК

Web site: http://jes.sumdu.edu.ua

DOI: 10.21272/jes.2018.5(1).c4 Volume 5, Issue 1 (2018)

UDC 621.9.048.669.268

Ecologically Safe Process for Sulfo-Aluminizing Steel Parts

Plyatsuk L. D.[1], Tarelnyk V. B.[2], Kundera Cz.[3], Radionov O. V.[4], Gaponova O. P.[1]

[1] Sumy State University, 2 Rymskogo-Korsakova St., 40007 Sumy, Ukraine;
[2] Sumy National Agricultural University, 160 Gerasyma Kondratieva St., 40021 Sumy, Ukraine;
[3] Politechnika Świętokrzyska, 7 Tysiąclecia Państwa Polskiego Av., 25-314 Kielce, Poland;
[4] "Ferrogidrodinamika" Ltd., 45/5 Bolshaya Morskaya St., 54030 Mykolaiv, Ukraine

Article info:
Paper received: March 3, 2018
The final version of the paper received: May 28, 2018
Paper accepted online: May 29, 2018

***Corresponding Author's Address:**
tarelnik@i.ua

Abstract. The present technical solution refers to the field of electrophysical and electrochemical processing of parts, in particular, to the electroerosion alloying (EEA) of the surfaces of steel parts with aluminum (aluminizing) and sulfur (sulfidizing), and it can be used to treat the surfaces of heat-treated steel parts in order to increase their hardness, wear resistance, to prevent frictional seizure and improve the resistance to atmospheric corrosion. When aluminizing steel parts with the use of the method of electroerosion alloying (EEA) by aluminum electrode at discharge energy W_p = 0.52–6.8 J and productivity of 1.0–3.0 cm^2 / min, before the EEA process by an aluminum electrode, to the surface of the part to be aluminized, there is applied a consistency substance containing sulfur and aluminum powder, and thereafter, not having waited for drying of the consistency substance, the process of aluminizing by the EEL method with an aluminum electrode is carried out, and the consistency substance should have the aluminum powder content of not more than 56 %. There have been carried out metallographic and durametric analyses of the features of the surface layers made of carbon steels after simultaneous aluminizing and sulfidizing them by the EEA method. It is shown that the structure of the layer consists of three portions, namely, a "white" layer, a diffusion zone and a base metal. Such qualitative surface layer parameters as thickness, "white" layer and transition zone microhardness values, and also roughness increase with increasing discharge energy. The "white" layer continuity for all the investigated discharge energies of W_p = 0.52, 2.60 and 6.80 J is 100 %.

Keywords: electroerosion alloying, ecological compatibility, surface layer, aluminizing, sulfidizing, microstructure, microhardness.

1 Introduction

To date, chemical and thermal process (CTP) is one of the most effective methods for strengthening surfaces of parts to improve their durability. The main types of the CTP processes are: carburization, nitration, aluminizing, sulfidizing, cyanidation and others, which consist in simultaneously saturating a surface layer, respectively, with carbon, nitrogen, aluminum, sulfur, carbon and nitrogen, etc.

Despite the fact that the CTP technology is one of the main processes aimed at improving quality of surface layers of machine parts, it also has a number of significant drawbacks as follows: volumetric heating of a part, which results in changing its structure and initial geometric parameters (metal deformation and warps); bulky and expensive processing equipment; long duration of the process and the need in using of energy-intensive equipment, etc.

In addition, certain CTP operations are dangerous for the environment. For example, the main disadvantage of a cyanidation process is toxicity of cyanide salts and, in this regard, there is a need in special measures to provide labor protection.

In recent years, to improve the quality of machine parts surface layers, the method of electroerosion alloying (EEA), that is, the process of transferring material to a product surface by means of spark electric discharge has become increasingly important. It is characterized by the following specific features being attractive for technologists, namely: environmental safety, local action, low energy consumption, lack of volumetric material heating, strong bonding of applied material to substrate, ease of automation, and possibility of combining operations.

In the course of the EEA process, while using different electrode materials and the environment, it is quite possible to implement the technologies being alternative to the CTP ones, but of significantly lower cost. Thus, on applying graphite electrode and saturating a surface of a part with carbon, it is possible to carry out the process of carburization; using the EEA method in nitrogen medium makes it possible to perform the nitriding process, and others.

Thus, there is a very topical problem of developing energy-efficient, energy-saving and environmentally friendly technologies to form surface layers of parts, which technologies being alternative to the CTP ones, sufficiently retaining the advantages of the CTP technologies and having no their disadvantages.

2 Literature Review

There is known a sulfidizing method for enriching surface layers of items with sulfur, which represents a thermo chemical process for processing items made of iron-based alloys. The effect of sulfidizing consists in creating a film of sulfides on a part surface. Sulfides increase the surface activity of metals and alloys and also provide wetting with surfactants and improve resistance to frictional seizure. The sulphide film, which has less strength than the base metal, is easily broken down at friction and separated from the base without plastic deformation, preventing the friction surfaces from frictional seizure. The film of iron sulphide (FeS) increases the wear resistance of rubbing surfaces and improves their running-in ability. The ferrosulfide coating has rather high porosity and absorbs a large amount of lubricant, providing the material with self-lubricating properties [1].

There is known a method for aluminizing surfaces of parts [2], which includes the procedures of applying an aluminum layer to a steel surface (usually by spraying), coating and annealing thereof. Spraying aluminum particles should be large, which fact accelerates the process of aluminum diffusion penetration into surface layer of metal in the course of annealing. The coating layer is continuously applied to the surface in two to three passes, and in doing so, the process should strictly follow the condition of thermal diffusion treatment to preserve the coating layer.

Having been aluminized and applied with a coating, the obtained surface layer of the part is saturated with the use of the thermal diffusion process, that is, it is annealed. The initial temperature is of 600 to 650 °C, followed by rapid heating up to of 900 to 950 °C with the hold time of 2.5 to 3.5 hours, and thereafter the part is slowly cooled together with the furnace to the temperature of 500 to 550 °C, and then it is cooled in the open air. The thickness of the coating applied with the use of molten aluminum depends on the temperature of the part operation. Thus, for the operating temperature of 700 to 800 °C the coating thickness is of 0.2 to 0.3 mm, and for the operating temperature of 900 to 1 000 °C it is of 0.5 to 0.7 mm. Having been metalized with aluminum, the part is covered with 10 to 20 % aluminum chloride solution, and then it is coated with liquid glass, sprinkled with quartz sand, and dried at the temperature of 100 °C. The dried part is newly coated with liquid glass and dried again. At the temperature of 600 to 700 °C, the part is loaded into the furnace and heated up to the temperature of 1 200 to 1 250 °C with the hold time of 14 to 40 minutes, after that it is slowly cooled first in the oven to 800 °C and then in the open air.

Along with the above said positive results, the technology described has a number of drawbacks. Those are the followings: high cost and labor intensity of the process, the need in control at all the technology stages, inevitability of heating the entire part, and accordingly, the presence of structural changes in the metal, deformations and warps, the process duration is more than 8 hours, high power consumption, negative impact on the environment, etc.

In accordance with publication [3], using the method for providing electrospark depositions of titanium on aluminum and aluminum on titanium, there have been created coatings containing the intermetallics of Ti-Al. While applying the methods of electron microscopy, X-ray diffraction and micro-X-ray spectroscopy, there were analyzed the structure and composition of the coatings obtained. It has been found out that, regardless of the duration and frequency of the discharge pulses, the surface layer formed in argon basically contains α-$TiAl_3$ intermetallic. The phases of γ-TiAl and α_2 -Ti_3Al can be obtained by depositing aluminum on titanium followed by depositing a second layer of titanium. At creating electrospark coatings in the open air, there are additionally formed alumina and titanium nitride. This technology is also performed in a protective environment, for example, argon, and it can be used only for parts made of titanium.

The closest to the proposed method is a method for electroerosion alloying (EEA) by an aluminum electrode of steel parts at the discharge energy of W_p = 0.52 to 6.8 J and productivity of 1.0 to 3.0 cm^2 / min. The method provides for the formation of a so-called “white” (aluminized) layer, respectively, of 70 to 130 μm thick having microhardness of 5 000 to 7 500 MPa, roughness (Ra) of 6 to 9 μm and continuity of 95 to 100 % [4].

It should be noted that with this treatment method, the maximum thickness values of the aluminized layers were obtained at the highest discharge energy of W_p = 6.8 J, and they were equal to 70 and 130 μm, respectively, on the substrates made of 20 steel and 40 steel. Such thickness values are not always sufficient to protect steel part surfaces, which are exposed to high temperatures, against destructions thereof. In addition, with a dry (non-lubricated) contact of a part surface aluminized in such a way, there is a possibility of occurrence of frictional seizure, jamming, micro-welding and rupturing individual areas of the surface.

There is known a method for sulfo-carburizing surfaces of steel parts with applying a process of electroerosion alloying by graphite electrode, wherein a consistency sulfur-containing substance has been applied to the steel surface just before alloying with a graphite electrode [5]. The main disadvantage of this sulfo-carburizing process is the lack of possibility of protecting the part from oxidation at high temperatures (700 to 900 °C and higher), as well as from atmospheric corrosion and seawater.

Thus, the aim of the work is to create a process for aluminizing steel parts with the use of the method for electroerosion alloying by an aluminum electrode, which is devoid of the above mentioned drawbacks and which provides an increase in the hardness and wear resistance of parts preventing friction seizure and improving the resistance to atmospheric corrosion.

3 Research Methodology

To determine the effect of the EEA equipment energy parameters on the quality parameters of the coatings, there were made the specimens of 20 steel and 40 steel having a size of 15x15x8 mm, where on a consistency substance was applied in the form of a sulfuric ointment with sulfur content of 33.3 %. Before applying, the aluminum powder of the mark of PAD-0 (GOST 5494-95) had been added into the sulfuric ointment. The maximum amount of the powder was 56%. Further increasing the amount of the powder resulted in decreasing its adhesion to the surface to be aluminized. After that, without waiting for drying the consistency substance, there was produced the EEA method by an aluminum electrode on the unit of "Elitron-52A" model with the use of various operating modes. Moreover, each EEL mode had its own value of discharge energy and productivity, that is, the area of the formed coating per unit of time (Table 1).

Table 1 – EEA productivity dependence on discharge energy

Discharge energy W_p, J	0.52	1.3	2.6	4.6	6.8
Productivity, cm^2 / min	1.0–1.3	1.3–1.5	1.5–2.0	2.0–2.5	2.5–3.0

It should be noted that decreasing the EEA method productivity results in decreasing the qualitative parameters of the surface layer (the appearance of burns, and the most importantly, the destruction of the formed layer), which event especially occurs on 'harder' modes at discharge energy W_p > 1 J. Increase in the productivity results in decrease in the continuity of a coating. As a tool electrode, there was used a ∅ 4 rod with length of 45 mm made of aluminum wire of SvA99 GOST 7871-75 mark.

The metallographic analysis of the coatings was carried out using an optical microscope of МИМ-7 (MIM-7) model, the durametric studies were carried out with the use of the instrument of ПМТ-3 (PMT-3) model.

The surface roughness after EEA method was determined with the use of the profilograph-profilometer of 203 model of the Калибр (Caliber) plant production by taking off and processing the profilograms.

To study the sulfur distribution over the depth of the layer, a local micro-X-ray spectral analysis was performed, based on recording the characteristic X-ray radiation excited by the electron beam of the chemical elements, which were present in the microvolume. For this purpose, there was used an electron microscope equipped with an X-ray spectral micro-analyzer, ISIS 300 Oxford instruments.

4 Results and discussions

Fig. 1 shows the microstructure of the surface layer formed on the specimen made of 20 steel coated with a consistency substance containing sulfur in the amount of 33.3 % and aluminum powder in the amount of 56 % while performing the EEA process by an aluminum electrode at the discharge energy value of W_p = 6.8 J (a), as well as the microhardness distribution while deepening from the surface (b).

The characteristic feature of the structure is a massive "white" layer, the thickness values of which in some portions are of 160 to 200 μm (Fig. 1 a). The microhardness on the surface is about 5 000 MPa. While deepening, the microhardness gradually decreases and at the depth of 170 μm it transfers into the microhardness of the substrate (1 700 MPa).

Figure 2 represents the profilograms of a portion of the 20 steel specimen surface sulfo-aluminized with the use of the EEA method performed by an aluminum electrode at the discharge energy of W_p = 6.8 J.

In Table 2, there are shown the qualitative parameters of the surface layers of 20 steel and 40 steel at performing the sulfo-aluminizing process using the EEA method at the discharge energy values of 0.52, 2.60, and 6.80 J.

The presence of sulfur in the consistency substance contributes to the sulfidizing process. In Table 3, there is shown the sulfur content while deepening from the surface in the course of sulfo-aluminizing 20 steel with the use of the EEA method at the discharge energy of 6.80 J.

Thus, as a result of investigation of the surface layer of the specimen made of 20 steel after sulfo-aluminizing thereof, it has been found out the coating continuity makes up 100 %, the layer thickness is up to 200 μm, and the microhardness is up to 5 000 MPa.

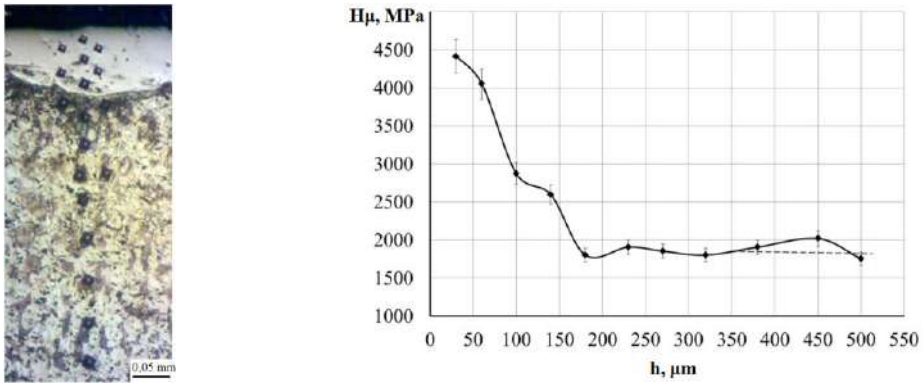

a b

Figure 1 – Microstructure (a) and microhardness distribution in the surface layer (b)

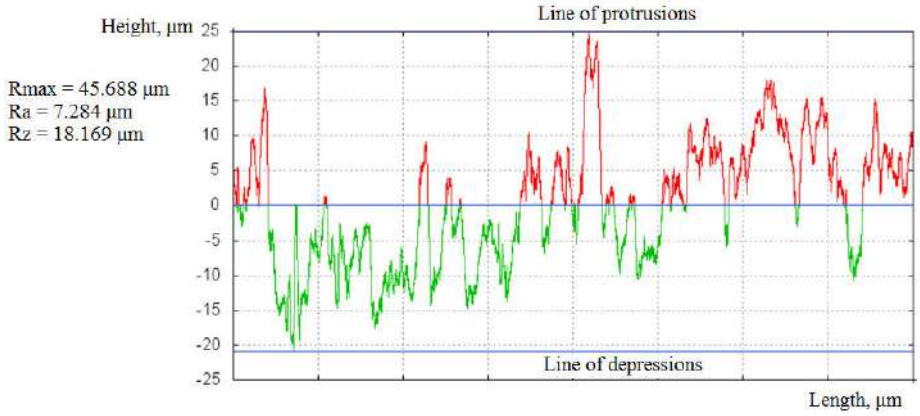

Figure 2 – Profilogram of the surface layer of the specimen made of 20 steel

Table 2 – Qualitative parameters of the surface layers of 20 steel and 40 steel at sulfo-aluminizing them using the EEA method

Discharge energy, J	Thickness of white layer, μm	Micrihardness of white layer, MPa	Roughness, μm			Continuity of white layer, %
			Ra	Rz	R_{max}	
20 Steel						
0.52	50–60	3 500 ± 70	1.9	2.9	8.3	100
2.60	110–130	4 200 ± 70	3.7	9.7	25.2	100
6.80	up to 200	5 000 ± 50	7.3	18.2	45.7	100
40 Steel						
0.52	70–100	3 850 ± 50	1.7	3.2	8.2	100
2.60	140–160	4 700 ± 50	2.9	3.2	11.5	100
6.80	up to 240	5 400 ± 70	6.1	13.3	38.0	100

Table 3 – Sulfur content while deepening from the surface in the course of sulfo-aluminizing 20 steel with the use of the EEA method at the discharge energy of 6.80 J

Depth of measurement, μm	20	40	60	80	100	120	140	160	180	200
Presence of sulfur, %	0.21	0.17	0.12	0.10	0.08	0.07	0.06	0.04	0.03	0.03

5 Conclusions

The possibility of applying an environmentally friendly process of sulfo-aluminizing surface layers of machine parts by the method of electroerosion alloying has been considered. Metallographic and durametric analyses of the features of the surface layers of carbon steels after simultaneously aluminizing and sulfidizing by the EEA method have been carried out. It is shown that the structure of the layer consists of three portions, namely, a "white" layer, a diffusion zone and a base metal. With increasing the discharge energy values, such qualitative parameters of the surface layer as thickness, microhardness of the "white" layer and the transition zone, as well as roughness increase. The continuity of the "white" layer

for all the investigated energies W_p = 0.52; 2.60, and 6.80 J is 100 %.

The presence of sulfur in the consistency substance facilitates the sulfidizing process. While sulfidizing 20 steel by the EEL method at the discharge energy of 6.80 J, the sulfur content decreases with deepening from the surface, and at the depth of 180 μm, it corresponds to its amount in the base.

The comparative analysis of the substrate effect on the qualitative parameters of the surface layer in the course of the sulfo-aluminizing process by the EEL method has exposed that in the event of 20 steel being replaced by 40 steel, the thickness of the "white" layer and the transition zone increases, i.e. there is increased the depth of the increased hardness zone, as well as the magnitude of its microhardness, while the surface roughness varies insignificantly.

For practical purposes, it is possible to recommend the sulfo-aluminizing process by the EEA method on the modes of discharge energy within W_p = 2.6 to 6.8 J and productivity of 2.0 to 3.0 cm^2 / min, which provide for the formation of the "white" layer thickness of 110 to 240 μm, the microhardness values of 4200 to 5 400 MPa, the roughness (Ra) values of 3.7 to 7.3 μm and the continuity of 100 %.

References

1. Zozulya, V. D., Shvedkov, Ye. L., Rovinskiy, D. Ya., & Braun, E. D. (1990). *Slovar-spravochnik po treniyu, iznosu i smazke detaley mashin*. Kyiv, Naukova dumka [in Russian].
2. Yelizavetin, M. A., & Satel', E. A. (1969). *Tekhnologicheskiye sposoby povysheniya dolgovechnosti mashin*. Moscow, Mashinostroyeniye [in Russian].
3. Pyachin, S. A., Burkov, A. A., & Komarova V. S. (2013). Formirovaniye i issledovaniye elektroiskrovykh pokrytiy na osnove alyuminidov titana. *Poverkhnost'. Rentgenovskiye, Sinkhrotronnyye i Neytronnyye Issledovaniya*, No 6, 16–24 [in Russian].
4. Tarelnyk, V. B., Martsynkovskyy, V. S., Bilous, A. V., Gaponova, O. P., Konoplianchenko, Ie. V., Antoszewski, B., Kundera, Cz., & Zhukov, O. M. (2017). *Sposib obrobky poverkhon' stalevykh detaley*. Certificate of the authorship, Ukraine, No. 119316 U, C 23 C 10/48 (2006.01) B23H 9/00, No. u201701845 [in Ukrainian].
5. Tarelnyk, V. B., Martsynkovskyy, V. S., Bilous, A. V., Gaponova, O. P., Konoplianchenko, Ie. V., Antoszewski, B., Kundera, Cz., Zhukov, O. M. (2017). *Sposib sul'fotsementatsiyi stalevykh detaley*. Certificate of the authorship, Ukraine, No. 119318 U, B 23 H 1/00 B 23 H 9/00 C 23 C 8/60 (2006.01), No. u201701847 [in Ukrainian].

Екологічно безпечний спосіб сульфоалітування сталевих деталей

Пляцук Л. Д.[1], Тарельник В. Б.[2], Кундера Ч.[3], Радіонов О. В.[4], Гапонова О. П.[1]

[1] Сумський державний університет, вул. Римського-Корсакова, 2, 40007, м. Суми, Україна;
[2] Сумський національний аграрний університет, 40021 Суми, вул. Герасима Кондратьєва, 160, Україна;
[3] Технологічний університет м. Кельце, ал. Тисячоліття Польщі, 7, 25-314, м. Кельце, Польща;
[4] ТОВ «НПЗП « Феррогдродинаміка», вул. Велика Морська, 45/5, м. Миколаїв, 54030, Україна

Анотація: Подане технічне рішення відноситься до галузі електрофізичної та електрохімічної обробки, зокрема, до електроерозійного легування (ЕЕЛ) поверхонь сталевих деталей алюмінієм (алітування) і сіркою (сульфідування) і може бути застосовано для обробки поверхонь термооброблених сталевих деталей, з метою підвищення їх твердості, зносостійкості, запобігання схоплюванню при терті і для поліпшення опору до атмосферної корозії. При алітуванні електроерозійним легуванням алюмінієвим електродом сталевих деталей з енергією розряду W_p = 0,52–6,8 Дж і продуктивністю 1,0–3,0 $см^2$ / хв перед ЕЕЛ алюмінієвим електродом на поверхню деталі, що підлягає алітуванню, наносять консистентну речовина, що містить сірку і алюмінієву пудру, після чого, не чекаючи висихання консистентної речовини, проводять процес алітування методом ЕЕЛ алюмінієвим електродом, причому, застосовують консистентну речовину з вмістом алюмінієвої пудри не більше 56 %. Проведено металографічний і дюрометричний аналіз особливостей поверхневих шарів вуглецевих сталей після одночасного алітування і сульфідування методом ЕЕЛ. Показано, що структура шару складається з трьох ділянок: «білого» шару, дифузійної зони й основного металу. Зі збільшенням енергії розряду зростають такі якісні параметри поверхневого шару, як товщина, мікротвердість «білого» шару і перехідної зони, шорсткість. Суцільність «білого» шару при всіх досліджених енергіях розряду W_p = 0,52; 2,60 і 6,80 Дж становить 100 %.

Ключові слова: електроерозійне легування, екологічність, поверхневий шар, алітування, сульфідування, мікроструктура, мікротвердість

JOURNAL OF ENGINEERING SCIENCES
ЖУРНАЛ ІНЖЕНЕРНИХ НАУК
ЖУРНАЛ ИНЖЕНЕРНЫХ НАУК

Web site: http://jes.sumdu.edu.ua

DOI: 10.21272/jes.2018.5(1).d1 Volume 5, Issue 1 (2018)

UDC 539.3: 621.226

Stress-Strain State of the Lower Traverse of the Hydraulic Press

Nemchynov S. I.*, Nachovnyi I. I.

State Higher Educational Institution "Ukrainian State University of Chemical Technology", 8 Gagarina Av., 49005, Dnipro, Ukraine

Article info:
Paper received: October 24, 2017
The final version of the paper received: December 4, 2017
Paper accepted online: January 9, 2018

***Corresponding Author's Address:**
sinonis@ukr.net

Abstract. In the present article the stress-strain state of the lower traverse of the central ejector of the hydraulic press for manufacturing large-sized plastic products has been investigated by using finite element analysis. It has been established that the stress-strain state of the traverse is characterized by a general and local uneven distribution of stresses and deformations; normal stresses in the cross section, passing through the plane of symmetry of the traverse, change linearly. Various changes of the equivalent stresses along the height on the inner surfaces of the central and lateral cylinders have been established. The zones of the traverse that are experiencing the highest values of normal and tangential stresses and strains have been identified. The research allowed to change the geometry of the traverse with a slight change in the stress and strain and therefore to reduce the weight of the traverse. This investigation and its results will have practical application in the design of new hydraulic presses as well as in improvement of existing hydraulic presses and are also the basis for further research.

Keywords: finite element method, geometry, stress, strain, displacement.

1 Introduction

Heavy-duty column hydraulic presses are widely used in many industries. The elements of the column frame, i.e. columns and traverses, are subject to high specific loads in the process of operation; therefore, their reliability determines the reliable performance of the press. The basic parts of a column hydraulic press make approximately 80 % of its weight and cost [1]; traverses and tables are the most massive and costly of these. In the operation of hydraulic presses, a significant number of traverse failures is caused by fatigue, since cracks start developing in the high-stress areas. Therefore, the study of stress-strain state (SSS) and search for improving the form of the traverse are very important at the design stage and involve not only technical, but also economic aspects.

To calculate hydraulic press traverses, various simplified methods based on rod models were used over a long period of time.

With the advances in computer technology, numerical methods have been increasingly applied for the calculation of basic parts of hydraulic presses; among the methods, an important place is taken by the finite element method (FEM). Today, the software packages for finite-element analysis, such as ANSYS, NASTRAN, SOLIDWORKS, ABAQUS, LIRA, SCAD, are used as a tool of numerical studies. Recently, free and open-source finite-element analysis applications, such as CalculiX, Elmer and Code_Aster, have been widely used. The above methods, unlike traditional ones that were based on the postulates of the strength of materials and theory of elasticity, allow a thorough study of a general SSS and of a distribution of local stresses in formulating two-dimensional and three-dimensional problems. In many cases, this enables to dispense with experimental studies, although the latter retain their importance as a means of verifying the results of the SSS.

2 Literature Review

For today, there is some experience of designing traverses for hydraulic presses, but in most cases they have been calculated approximately, which can be explained by difficulties describing the stress-strain state and by structural features.

The analysis of publications shows that to determine the SSS of the hydraulic press basic elements, the authors use either methods based on the strength of materials [2], or FEM for the stress state only. For example, according

to the existing methods of calculating the strength, the spatial structure of the traverse is replaced by two beams at the wide and narrow sides, and the cylinder force is applied to the centers of gravity of the reference semi-rings. This technique is simplistic and does not take into account the features of the traverse geometry, which is rather complicated. The technique does not provide a sufficiently complete picture of the SSS and, as a consequence, does not allow for recommendations on improving the traverse design.

In [3, 4], the frame of the P7640A hydraulic press was calculated using FEM in the ANSYS. Proceeding from the stress-strain analysis, the authors proposed a rational, from their point of view, form of the frame. However, the above studies have not proved that the proposed geometry of the frame ensures its strength and stiffness and can be considered optimal. No publications are available on a systematic study of the traverse strain state.

In [5] and [1] it has been established that the major cause of damage and fractures in the cross-members of heavy-duty presses is the emergence and propagation of fatigue cracks that appear in zones with high levels of stress, i.e. on the contours of technological and structural openings in the internal ribs, outer walls and plates under tension.

In [6], the major directions of retaining and improving the technological capabilities of heavy-duty hydraulic presses are outlined.

In the last decade, the scientific journals of the near and far abroad have published a sharply increased number of studies, which use various software packages of finite-element analysis to analyze the SSS of the frames of hydraulic and mechanical presses. On the basis of the SSS obtained, the authors optimized the geometry of the frames under study. Thus, in [7, 8], the ANSYS software was used to analyze the SSS of the frames of 0.2 MN and 8 MN hydraulic presses. The results of the study allowed changing the geometry of the frames with 50 % and 23 % decrease in their weights, respectively.

The results of calculating the stresses using the classical method of the strength of materials and the finite-element method (FEM) were presented in [9] for a mechanical press frame. It was revealed that the values of stresses obtained by the classical method are higher than the values of stresses determined using FEM. In [9] it was also noted that the classical method may be used for verification.

The performed analysis showed that:

- most of the studies deal with the calculations of heavy-duty hydraulic presses, while methods of calculating presses used in the chemical industry are practically unavailable;
- the data obtained in the studies are sometimes contradictory, and indicate the influence of one or another factor on the performance of the traverse;
- using FEM, which is currently the standard for calculating strength and stiffness, allows analyzing the SSS of any construction from a single position.

3 Research Methodology

The purpose of the work is a stress-strain analysis of the lower traverse of the central ejector of a hydraulic press with a nominal pressing force of 20 MN intended for the manufacture of large-sized plastic products, and justifying the proposed improvements in the traverse geometry.

The traverse of a hydraulic press, whose geometric model is presented in Figure 1, is subject to a uniformly distributed load. It is necessary to analyze its stress-strain state.

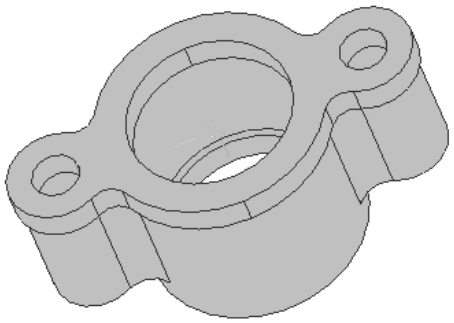

Figure 1 – The geometric model of the hydraulic press traverse

The hydraulic press traverse is a spatial construction of a complex configuration; therefore, analytical methods of calculation are practically unacceptable. The reliable results can only be obtained by numerical methods implemented on a computer. Therefore, to solve this three-dimensional problem of the theory of elasticity, we apply FEM, which in our time is obviously the world standard for calculations of strength, stiffness and other parameters of structures.

FEM allows obtaining a system of algebraic equations

$$[k]\cdot\{u\}=\{R\}, \tag{1}$$

where $[k]$ is the stiffness matrix of the finite-element model, $\{u\}$ is the nodal displacement vector, $\{R\}$ is vector of nodal forces.

Having solved the system (1), we find the displacement u_i, and following that we find stress σ_{ij} and strain ε_{ij} using the strain-displacement relations (Cauchy) and stress-strain relations (Hooke's law).

The application of FEM involves the simulation of the geometry of a construction and its meshing into finite elements, the formation of a global stiffness matrix and solving large systems of linear equations ($5\cdot10^3$ – $5\cdot10^5$). The above problems have prompted the authors to apply the SALOME-MECA platform-based, open-source Code_Aster application as a tool of numerical simulation. Code_Aster software allowed analyzing the SSS of the traverse, taking into account the features and modes of operation.

4 Results

The study is devoted to a numerical calculation of the SSS of the lower traverse of the hydraulic press central ejector. The overall dimensions of the traverse were 1 440 mm × 800 mm × 650 mm. The mass of the traverse was 747 kg.

Prior to the simulation of a finite element model, a solid-state spatial model of the traverse (Figure 1) was created based on the working drawings. The model was made using the KOMPAS-3D system for three-dimensional modeling, which allows to effectively create models of complex forms. Taking into account the plane of symmetry (the form of the traverse, established boundary conditions, and applied loads); the stress-strain analysis was performed on half of the model.

The obtained half of the solid-state model was then transferred to the SALOME-MECA platform-based open source Code_Aster, which was used to set the boundary conditions, the load and the area where the load was applied, and to create a mesh of the finite-element model.

The boundary conditions were set so as to exclude the displacements of the traverse as an absolutely rigid body. According to the working conditions, the load on the lower traverse of the central ejector was assumed to be equal to the nominal ejection force of 3.24 MN. Figure 2 shows the calculation scheme and indicates the loads and boundary conditions.

Three-dimensional finite elements with a maximum size of 0.035 m were used for the discretization of the traverse as a spatial body. As a result of the discretization, a mesh of 9 881 tetrahedra and 19 241 nodes was obtained. The finite-element model of the traverse is shown in Figure 2 b.

The material selected was 35 *L* steel with a Young's modulus $E = 2 \cdot 10^5$ MPa, Poisson's ratio $\nu = 0.32$, yield strength $\sigma_y = 248$ MPa, strength limit $\sigma_{str} = 482$ MPa.

As a result of the static calculation, the following parameters of the traverse SSS were obtained: stresses and strains along the corresponding axes; principal stresses and corresponding strains; equivalent stresses σ_{eq} calculated by Guber-Mises energy theory of strength; total displacements; displacements along corresponding axes; factors of safety.

Given that cracks originate on high-stress surfaces, the changes in normal, tangential and equivalent stresses were studied on the internal surfaces of the central and lateral cylinders in sections I and II (Figure 3 a).

The performed calculations show that the stress-strain state of the traverse is characterized by general and local uneven distribution of stresses and displacements (Figure 3).

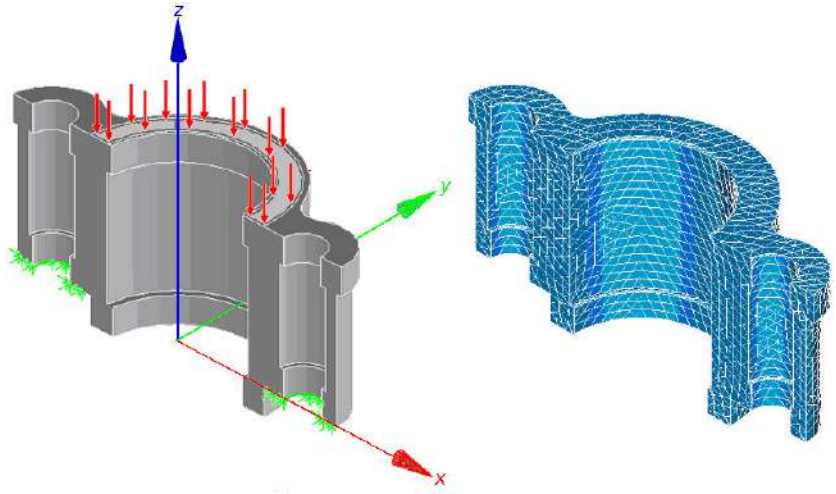

a b

Figure 2 – Calculation scheme (a) and finite element model (b) of the traverse

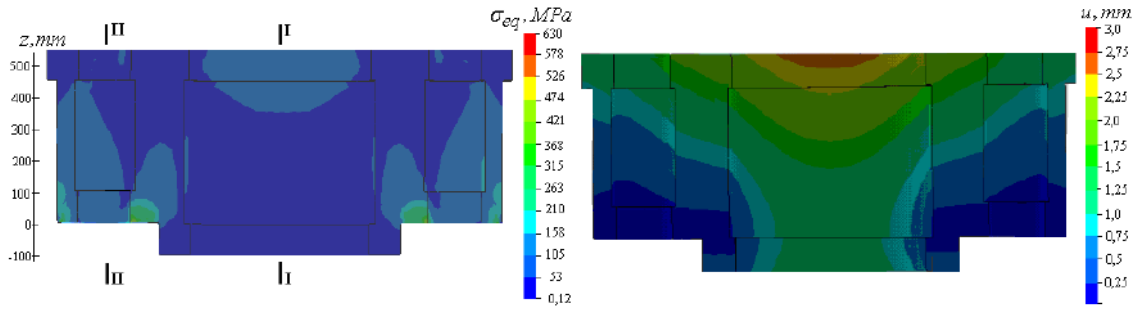

a b

Figure 3 – Isosurfaces of equivalent stresses σ_{eq} (a) and total displacements u (b)

Areas of maximum stress levels were located maximum equivalent stresses calculated by the Guber-Mises theory were observed at the points of load application, on the supporting surfaces, and in the areas of abrupt changes in geometry (Figure 3 a). The maximum equivalent stresses occurring at the points of load application are equal to 132 MPa, and at some points of the supporting surfaces they even exceed σ_y. Maximum total displacements are observed at the points of applying loads, while minimum displacements occur on the supports (Figure 3 b).

It should be noted that the equivalent stresses on the internal surfaces of the central and lateral cylinders also change significantly with the height, but the nature of their changes differs. The equivalent stresses increase with the height on the internal surface of the central cylinder in section I, while on the internal surface of the lateral cylinder in section II, they show a decrease with the height (Figure 4 a). The displacements increase in both cases (Figure 4 b).

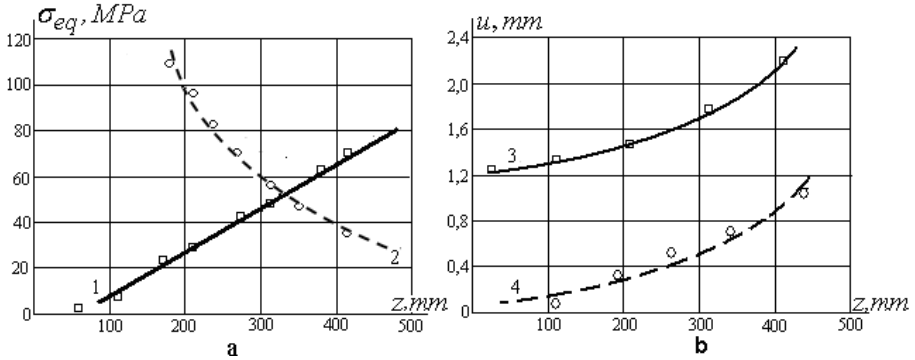

Figure 4 – Dependences of equivalent stresses and displacements on z-coordinate for the interior surfaces of the traverse cylindrical parts: a – dependence of equivalent stresses σ_{eq} on z-coordinate: 1 – internal surface of the central cylinder (section I); 2 – internal surface of the lateral cylinder (section II); b – dependence of displacements u on z-coordinate: 3 – internal surface of the central cylinder (section I); 4 – internal surface of the lateral cylinder (section II)

Furthermore, the study showed that:

- normal stresses σ_x, σ_y, σ_z on the central cylinder surface in section I change according to the linear law, changing the sign at $z \approx 69.6$ mm. A relationship was found between the normal stresses: $\sigma_x > \sigma_z > \sigma_y$. In this case, the values σ_x and σ_z were an order higher than the σ_y values. Linearity distortions were observed in the zones of an abrupt change in geometry. Thus, the maximum compressive stress σ_x on the upper belt did not exceed 135 MPa, while inside the cylinder it did not exceed 90 MPa (Figure 5).
- the maximum values of tangential stresses on the central cylinder surface did not exceed 1 MPa.

Thus, the study shows that the stresses on the internal surfaces of the traverse cylindrical parts and on the traverse upper belt rim do not exceed stress $[\sigma]$ for the selected material. These findings allow changing the geometry of the traverse so as to reduce its weight. The authors have proposed a traverse with the increased diameters of the internal cylindrical parts and the decreased external dimensions of the traverse upper belt. To assess the strength of the proposed traverse, an analysis of the stress fields, strains and factors of safety n was performed. It was found that the increase in stresses and strains did not exceed 13 %.

The analysis of the n diagram of the proposed traverse (Figure 6) showed that the values of factors of safety ranged from 1.8 to 6.4 (2.0–7.0 in the existing traverse) on the internal surfaces of the small cylinders, and from 3.7 to 27.3 (3.8–27.4 in the existing traverse) on the internal surface of the central cylinder. The feature of the n diagram is an area with overestimated factors of safety on the internal surface of the central cylinder, both for the existing and for the proposed traverse. Here, the values of n exhibit a sharp increase, reaching n = 100 at z = 69.2 mm. It should be noted, that when z ≈ 69.6 mm, the stresses σ_x, σ_y, σ_z are equal to zero, while σ_{eq} values acquire their minimum.

Thus, the study shows that the strength and stiffness of the proposed traverse are ensured. The changes in the geometry allowed reducing the mass of the traverse by almost 13 %.

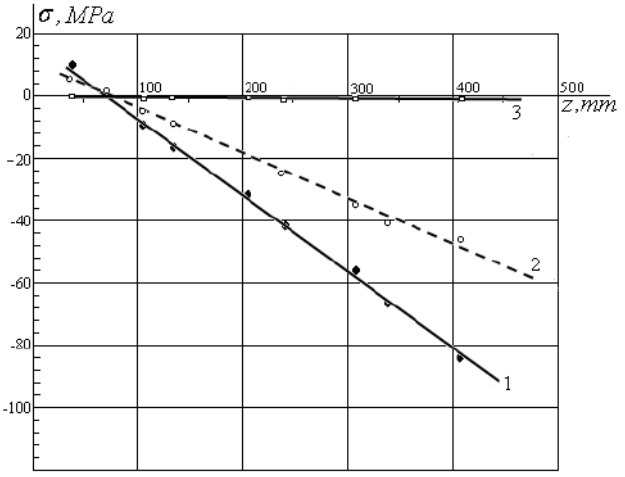

Figure 5 – Dependence of normal stresses on z-coordinate on the internal surface of the central cylinder in section I: 1 – normal stress σ_x; 2 – normal stress σ_z; 3 – normal stress σ_z

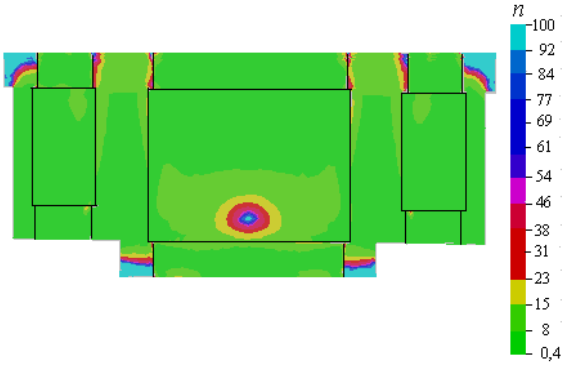

Figure 6 – Factor of Safety diagram of the proposed traverse

5 Conclusions

The SSS of the lower traverse of the hydraulic press, which was obtained by means of finite element modeling, is characterized by general and local uneven stresses and strains. The stress-strain analysis of the traverse revealed the zones of maximum stresses: points of load application, supports and areas of abrupt changes in geometry. It has been found that normal tensions in section I change linearly, and values σ_x and σ_z are an order higher than values σ_y. It has been established that the equivalent stresses increase with height on the internal surface of the central cylinder, and decrease on the internal surface of the lateral cylinder. The study allowed changing the geometry and reducing the weight of the traverse with a slight change in stresses and strains. The findings will have practical application in designing new and improving existing hydraulic presses.

References

1. Surkov, I. A. (2004). Sostoyaniye i perspektivy obespecheniya prochnostnoy nadezhnosti bazovykh detaley moshchnykh gidravlicheskikh pressov. *Blank production in mechanical engineering. Forging-stamping,foundry and other production*, No. 3, 24–28 [in Russian].
2. Zhivov, L. I., Ovchinnikov, A. G., & Skladchikov, E. N. (2006). Kuznechno-shtampovochnoye oborudovaniye. *N. E. Bauman MGTU Publishing House*, Moscow [in Russian].
3. Dashchenko, O. F., Kovalov, V. D., & Lymarenko, O. M. (2012). Rozrakhunok napruzheno-deformovanoho stanu stanyny hidropresa. *Pratsi Odeskoho politekhnichnoho universytetu*, No 2 (39), 39–43 [in Ukrainian].
4. Dashchenko, O. F., & Lymarenko, O. M. (2013). Napruzheno-deformovanyy stan bazovykh detaley hidravlichnykh presiv. *Machine Science*, No 1–2, 33–38 [in Ukrainian].
5. Surkov, A. I. (2013). Vosstanovleniye rabotosposobnosti i preduprezhdeniye razrusheniy poperechin moshchnykh gidravlicheskikh pressov s primeneniyem styazhnykh ustroystv. *Chief mechanical engineer*, No 10, 51–56 [in Russian].
6. Surkov, A. I., Kurovich, A. N., & Surkov, I. A. (2003). Obespecheniye prochnostnoy nadezhnosti bazovykh detaley moshchnykh gidravlicheskikh pressov na stadiyakh proyektirovaniya i ekspluatatsii. *Heavy Engineering*, No. 5, 35–37 [in Russian].
7. Kamate, A. M. (2016). Design, Development and Analysis of a 20 Ton Hydraulic Press. *International Journal of Innovative Technology and Research*, Vol. 4, 2560–2563.
8. Burli, P. S., & Zalake, R. M. (2015). Design optimization of Hydraulic press structure. *International Journal of Latest Trends in Engineering and Technology*, Vol. 5, 118–126.
9. Iancu, C. (2013). Comparision between Analytical Calculus and FEM for a Mechanical Press Bed. *American Journal of Mechanical Engineering*, Vol. 1, 6–13.

Напружено-деформований стан нижньої траверси гідравлічного пресу

Немчинов С. І., Начовний І. І.

Державний вищий навчальний заклад «Український державний хіміко-технологічний університет»,
просп. Гагаріна 8, 49005, м. Дніпро, Україна

Анотація. У статті досліджено напружено-деформований стан нижньої траверси центрального виштовхувача гідравлічного преса для виготовлення великогабаритних виробів з пластмас з використанням програмного комплексу скінчено-елементного аналізу. Встановлено, що напружено-деформований стан траверси характеризується загальним і локальним нерівномірним розподілом напружень і деформацій, нормальні напруження в перерізі, що проходить через площину симетрії траверси, змінюються за лінійним законом. Виявлено різний характер зміни еквівалентних напружень по висоті на внутрішніх поверхнях центрального і бічних циліндрів. Визначено зони траверси, в яких спостерігаються максимальні напруження та деформації. Дослідження дозволило змінити геометрію траверси з незначною зміною напружень та деформацій і зменшити її вагу. Результати досліджень можуть бути застосовані при удосконаленні існуючих і проектуванні нових гідравлічних пресів, а також є основою для подальших досліджень.

Ключові слова: метод скінченних елементів, геометрія, напруження, деформація, переміщення.

JOURNAL OF ENGINEERING SCIENCES
ЖУРНАЛ ІНЖЕНЕРНИХ НАУК
ЖУРНАЛ ИНЖЕНЕРНЫХ НАУК

Web site: http://jes.sumdu.edu.ua

DOI: 10.21272/jes.2018.5(1).d2 Volume 5, Issue 1 (2018)

UDC 534.13:[621.22+621.515.1]

Investigation of Non-linear Reactions in Rotors' Bearing Supports of Turbo-pump Units for Liquid Rocket Engines

Pavlenko I. V.[1*], Simonovskiy V. I.[1], Pitel' J.[2], Demianenko M. M.[1], Verbovyi A. Ye.[1]

[1] Sumy State University, 2 Rymskogo-Korsakova St., Sumy, 40007, Ukraine;
[2] Technical University of Košice, 1 Bayerova St., Prešov, 08001, Slovak Republic

Article info:
Paper received: December 10, 2017
The final version of the paper received: March 11, 2017
Paper accepted online: March 17, 2018

[*]**Corresponding Author's Address:**
i.pavlenko@omdm.sumdu.edu.ua

Abstract. This paper is aimed at refinement of the computational model of the turbopump rotor systems associated taking into consideration the effect of rotation of moving parts and compliance of bearing supports elements. The up-to-date approach for investigation of non-linear reactions in rotor's bearing supports is proposed for turbo-pump units for liquid rocket engines. Five models for modelling contact interaction are investigated, and comparative bearing stiffness characteristics are given. The geometry of the housing and corresponding design scheme are set for each support due to the assembly drawing of the turbopump unit. Rotation of the shaft is taking into account by applying corresponding inertial forces to the inner cage of the bearing. Experimental points of the dependence "load – displacement" as the diagram "$F - v$" are built by the calculated points as an array of numerical simulation data, obtained by the ANSYS software. As a result of numerical simulation, including loading of the bearing support on the scheme "remote force" in a wide range of rotor speeds, the corresponding displacements are determined. The brand-new approach for evaluation of bearing stiffness coefficients is proposed based on the linear regression procedure. As a result, the obtained values of coefficients are summarized and approximated by the quadratic polynomials.

Keywords: Ansys Workbench, axial preloading, centrifugal force, contact interaction, finite element analysis, numerical simulation, remote force, stiffness characteristic.

1 Introduction

Intensification of the development in the field of power engineering occurs by using the modern energy-intensive equipment, an essential role of which is performed by multistage rotor machines. Permanently raising theirs parameters leads to increasingly significant problems of vibration reliability. Furthermore, the problem of investigation of dynamics of flexible rotors is based on determination of the critical frequencies and corresponding mode shapes. This problem is currently actual due to the impossibility of absolutely accurate dynamic rotor balancing [1].

General approaches are used for investigation of the rotor dynamics that are closely intersected with the issues of strength of materials and the theory of elasticity, the theory of linear and nonlinear oscillation of mechanical systems, as well as the problems for the identification of mathematical models of dynamic systems. Most problems can be solved in combination of 2D and 3D formulation by using modern software.

The problem of identification of bearing stiffness characteristics is complicated in the case of new designs with the insufficient experimental data. At the same time, the process of creating reliable mathematical models of the rotor dynamics is usually carried out in a permanent comparison with experimental data by means of the identification of coefficients of mathematical models and structures of design schemes. This process takes place in researching the vibration reliability and rotor balancing for centrifugal pumps and turbochargers [2, 3].

2 Literature Review

Up-to-date approaches for refinement of mathematical models of oscillatory systems according to experimental data is presented in the work [4]. The monograph [5] is aimed at evaluation of coefficients of mathematical models for oscillatory systems, including rotary systems for multistage centrifugal machines. The paper [6] dials with the phenomena of stability loss of rotor rotation at tilting pad bearings.

Modern treatments in the feld of linear and non-linear rotor dynamics is stated in the work [7] with the related practical applications. Estimation of segment bearing stiffness with the balancing procedure for flexible rotors of turbocharge units in the accelerating-balancing stand are presented in the paper [8]. Modern approaches for determination of active magnetic bearings stiffness and damping identification from frequency characteristics of control systems are realized within the work [9].

Application of the finite element analysis for stiffness and critical speed calculation of a magnetic bearing-rotor system for electrical machines is proposed in the work [10]. The problem of stability and vibration analysis of non-linear comprehensive flexible rotor bearing systems is analyzed in the paper [11]. A phenomenon of subharmonic resonance of a symmetric ball bearing-rotor system is investigated in the paper [12]. Approaches for analytical research and numerical simulation for investigation of critical frequencies of a centrifugal compressor rotor taking into account non-linear stiffness characteristics of bearings and seals are proposed in the paper [13].

3 Research Methodology

The ANSYS Workbench software is used for determination of bearing stiffness. The related design scheme is presented in Figure 1.

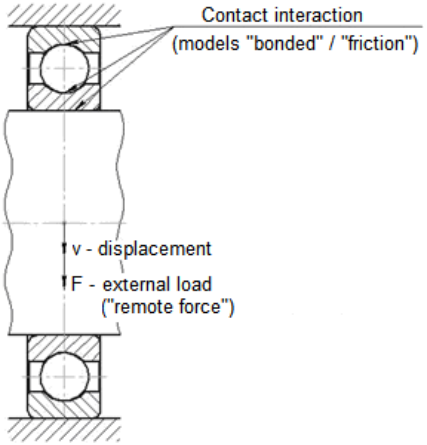

Figure 1 – Design scheme of bearing supports loading and determination of corresponding displacements

In the simulation of contacts by using ANSYS software, one of the most important problems is the selection of reliable model of interaction between elements of the contact pairs "target – contact". There are five models of contact interaction, the comparative characteristics of which are given in Table 1.

Further calculations are provided for each of the selected contact type:

– "bonded" – from the group of linear contacts;

– "frictional" – from the group of nonlinear contacts.

These models allow determining the maximum possible range of variation for the stiffness of bearing supports.

Table 1 – Comparative table of the main characteristics of models for the contact interaction between the surfaces of mating parts

Contact model	Contact type	Number of iterations	Normal behavior	Tangent behavior
Bonded	Linear	One	Not allowed	Not allowed
No separation				Allowed
Rough	Nonlinear	Several	Allowed	Not allowed
Frictionless				Allowed
Frictional				Allowed

"Bonded" is the contact model, in which the target and contact surfaces of the matched bodies are connected to each other, and the contact area does not change under the action of the applied loads. The sliding between faces and edges, as well as their separation is not allowed.

"Frictional" is the contact model that takes into account the sliding of the surfaces "target" and "contact" relative to each other. In this case, the contact area changes, if the module of the tangential force takes the limiting value.

4 Results

4.1 Basic approach

As a result of numerical simulation (loading of the bearing support according to the scheme "remote force") for discrete values of the force F in a range from zero to the maximum load capacity, the corresponding displacements are determined (Figures 2, 3).

The calculated points allow determining an array of data by means of a numerical simulation, on which the points of the "load – displacement" diagram "$F - v$" are built (Table 2, Figure 4).

The obtained data are interpolated by the corresponding curves $F = F(v)$. In this case, the stiffness of the bearing supports for linear models is determined as the tangent of the initial slope angle α of the diagram "$F - v$":

$$c = tg\,\alpha = \left(\frac{\partial F}{\partial v}\right)_0. \quad (1)$$

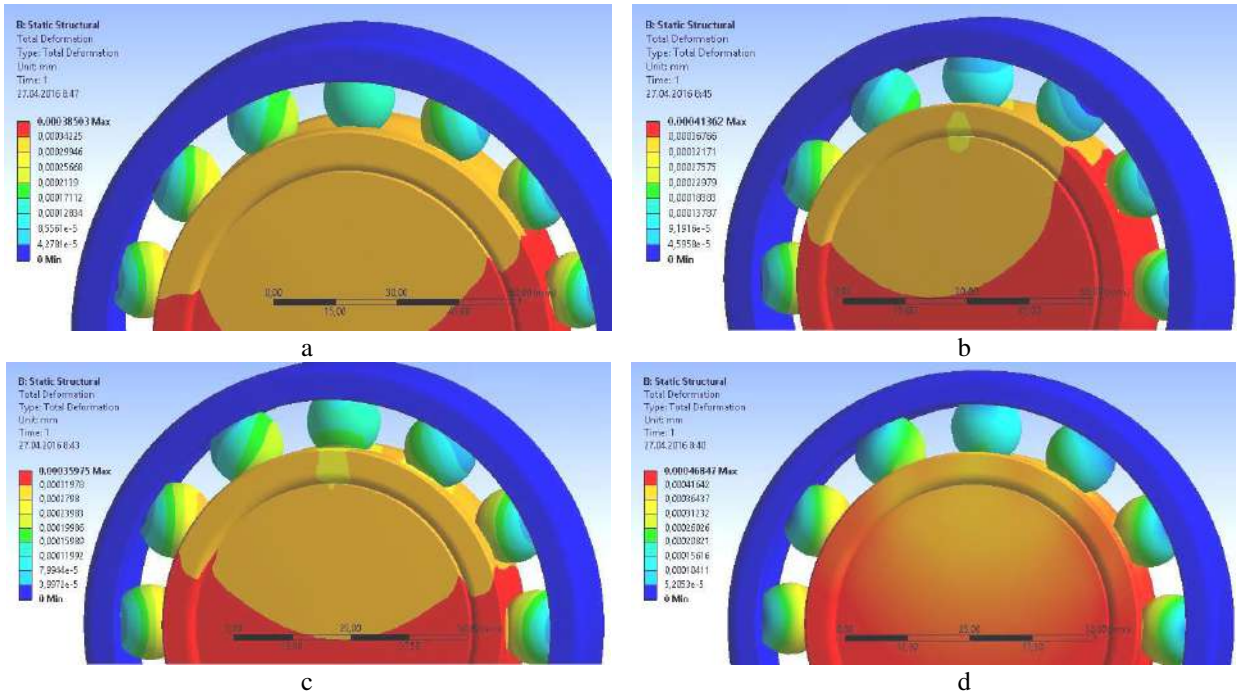

a b c d

Figure 2 – Determination of the bearing stiffness for the model "bonded" of the contact interaction between the rolling elements with cages of bearings 45-216 (a), 45-276214 (b), 46-276212 (c) and 36-211 (d)

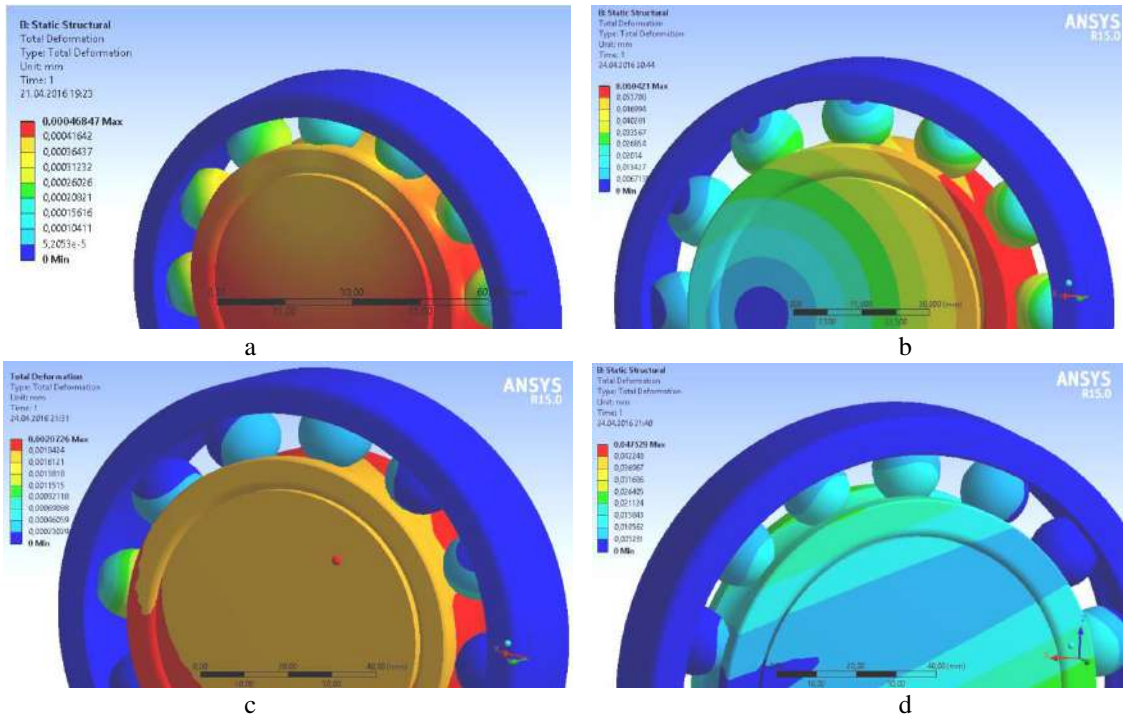

a b c d

Figure 3 – Determination of the bearing stiffness for the model "frictional" of the contact interaction between the rolling elements with cages of bearings 45-216 (a), 45-276214 (b), 46-276212 (c) and 36-211 (d)

Table 2 – Results of numerical simulation
for determining diagram "$F - v$"

Bearing	Load, N	Displacement, m	
		"frictional"	"bonded"
45-216	$1 \cdot 10^3$	$3.03 \cdot 10^{-6}$	$3.43 \cdot 10^{-7}$
	$1 \cdot 10^4$	$2.12 \cdot 10^{-5}$	$3.43 \cdot 10^{-6}$
	$7 \cdot 10^4$	$1.12 \cdot 10^{-4}$	$2.40 \cdot 10^{-5}$
45-276214	$1 \cdot 10^3$	$4.76 \cdot 10^{-6}$	$3.62 \cdot 10^{-7}$
	$1 \cdot 10^4$	$1.96 \cdot 10^{-5}$	$3.62 \cdot 10^{-6}$
	$6 \cdot 10^4$	$1.0 \cdot 10^{-4}$	$2.17 \cdot 10^{-5}$
46-276212	$1 \cdot 10^3$	$7.69 \cdot 10^{-6}$	$3.16 \cdot 10^{-7}$
	$1 \cdot 10^4$	$2.43 \cdot 10^{-5}$	$3.16 \cdot 10^{-6}$
	$5 \cdot 10^4$	$8.82 \cdot 10^{-5}$	$1.56 \cdot 10^{-5}$
36-211	$1 \cdot 10^3$	$3.85 \cdot 10^{-6}$	$4.18 \cdot 10^{-7}$
	$1 \cdot 10^4$	$3.90 \cdot 10^{-5}$	$4.18 \cdot 10^{-6}$
	$4{,}5 \cdot 10^4$	$1.26 \cdot 10^{-4}$	$1.88 \cdot 10^{-5}$

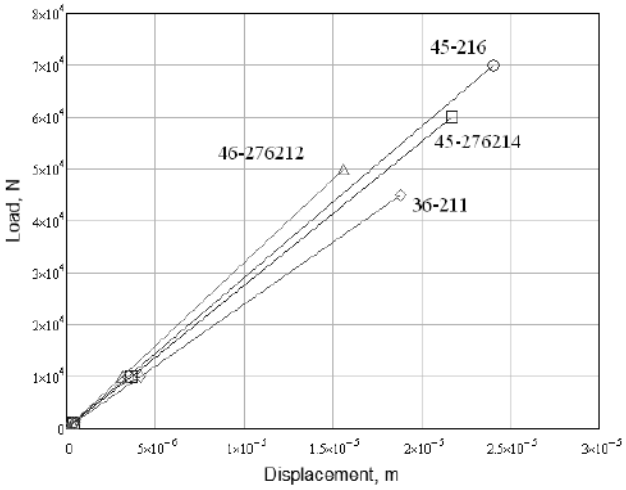

Figure 4 – Diagram "$F - v$" for the model "bonded"

The stiffness coefficients for bearings calculated by the abovementioned procedure, are summarized in Table 3.

Table 3 – Stiffness coefficients for bearing supports

Bearing	Stiffness coefficient, 10^8 N/m	
	"frictional"	"bonded"
45-216	3.3	29.2
45-276214	2.1	27.6
46-276212	1.3	31.7
36-211	2.6	23.9

4.2 Refinement of the numerical model

This part is aimed at refinement of the computational model of the turbopump rotor systems associated taking into consideration the effect of rotation of moving parts and compliance of bearing supports elements. The first factor causes an increasing quadratic dependence of the bearing stiffness on the rotor speed, and consequently, shift of the spectrum of critical frequencies to the right. This circumstance increases the detuning from the resosanse mode. The second factor decreases the bearing stiffness and critical frequencies.

The clarification of the stiffness parameters of the supporting units is carried out by combination of two computational means. Firstly, the loading patterns of supporting units using ANSYS software (three-dimensional finite element models) are considered due to a significant computational time.

ANSYS software is used for determination the bearing stiffness with considering rotation of the rotor and compliance of housing elements. The related design scheme is presented on Figure 5.

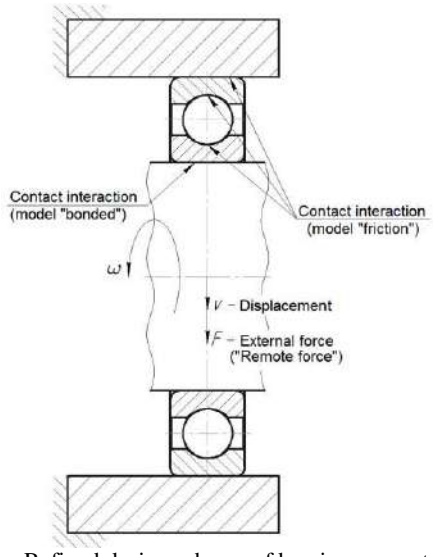

Figure 5 – Refined design scheme of bearing supports loading

The geometry of the housing and corresponding design scheme are set for each support due to the assembly drawing of the turbopump unit. The rotation is taking into account by applying corresponding inertial forces to the rotating (inner) cage of the bearing.

Modelling of contacts by using ANSYS software is performed according to Table 4.

Table 4 – Models of contact interaction between surfaces

Mating surfaces		Contact model
Shaft	Inner cage	"bonded"
Inner cage	Rolling elements	"frictional"
Rolling elements	Outer cage	
Outer cage	Housing	

As a result of numerical simulation (loading of the bearing support on the scheme "remote force" $F = 1 \cdot 10^3$ N for the following values of operating rotor speed: 0, 10 500, 18 750, and 21 150 rpm), the corresponding displacements are determined (Figures 6–9).

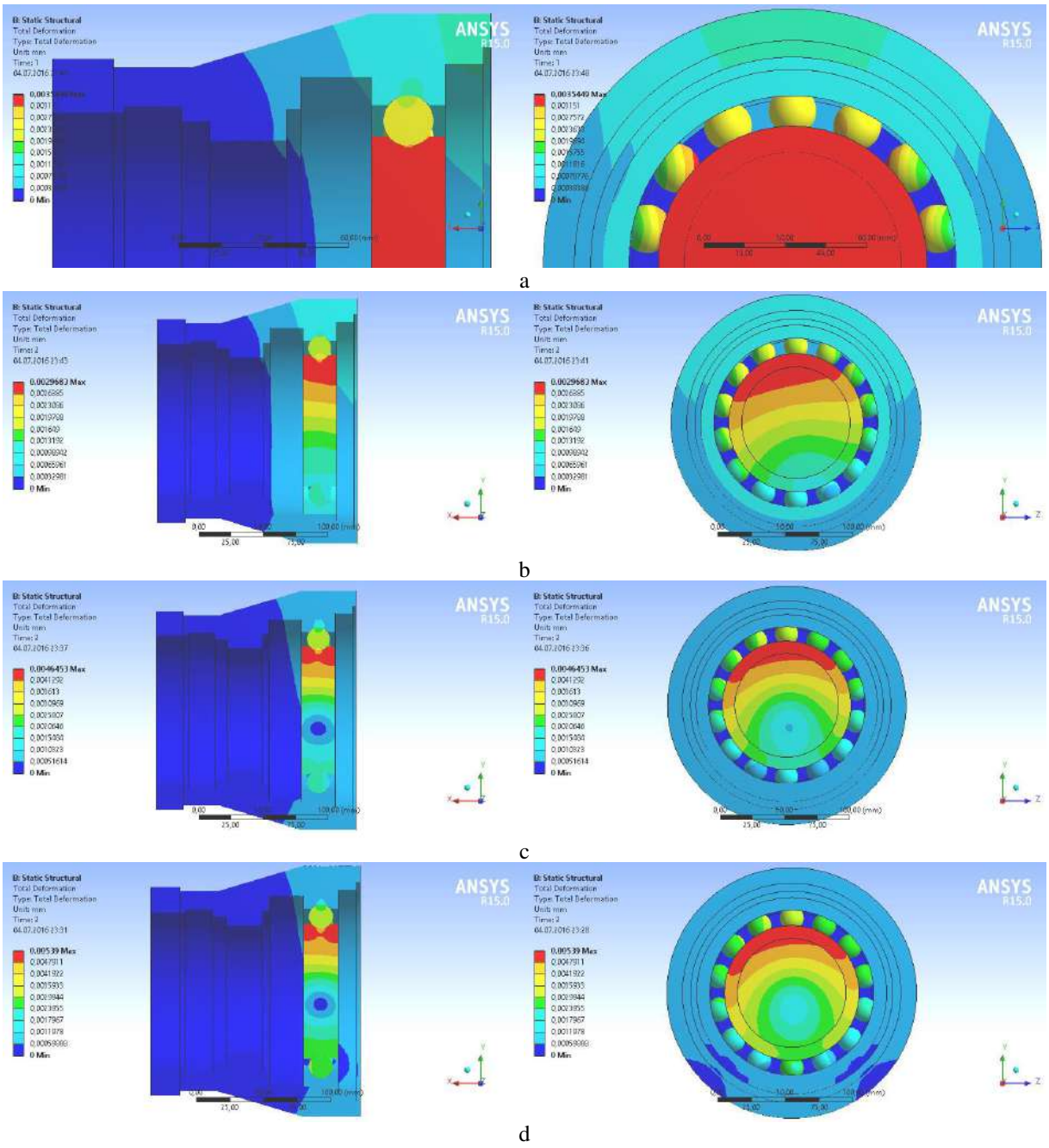

Figure 6 – Bearing stiffness for the support 45-216: 0 rpm (a), 10500 rpm (b), 18750 rpm (c), 21150 rpm (d)

In this case, determined bearing stiffness coefficients are summarized in Table 5.

Table 5 – Bearing stiffness of the supports

Bearing	Stiffness coefficient, 10^8 N/m, for the operating frequency, rad/s			
	0	1100	1963	2215
45-216	2.9	5.3	7.3	8.3
45-276214	2.4	2.9	4.4	4.5
46-276212	2.2	2.4	3.4	4.4
36-211	1.1	1.1	1.2	1.3

The analytical dependence for creating the mathematical models of free and forced oscillations of the turbopump rotor is proposed taking into account the rotation:

$$c = c_0 + \alpha\omega^2, \qquad (2)$$

where c – stiffness coefficient of the bearing support; ω – rotor speed, rad/s; c_0 – stiffness coefficient in case of $\omega = 0$; α – additional coefficient, N·s^2/m.

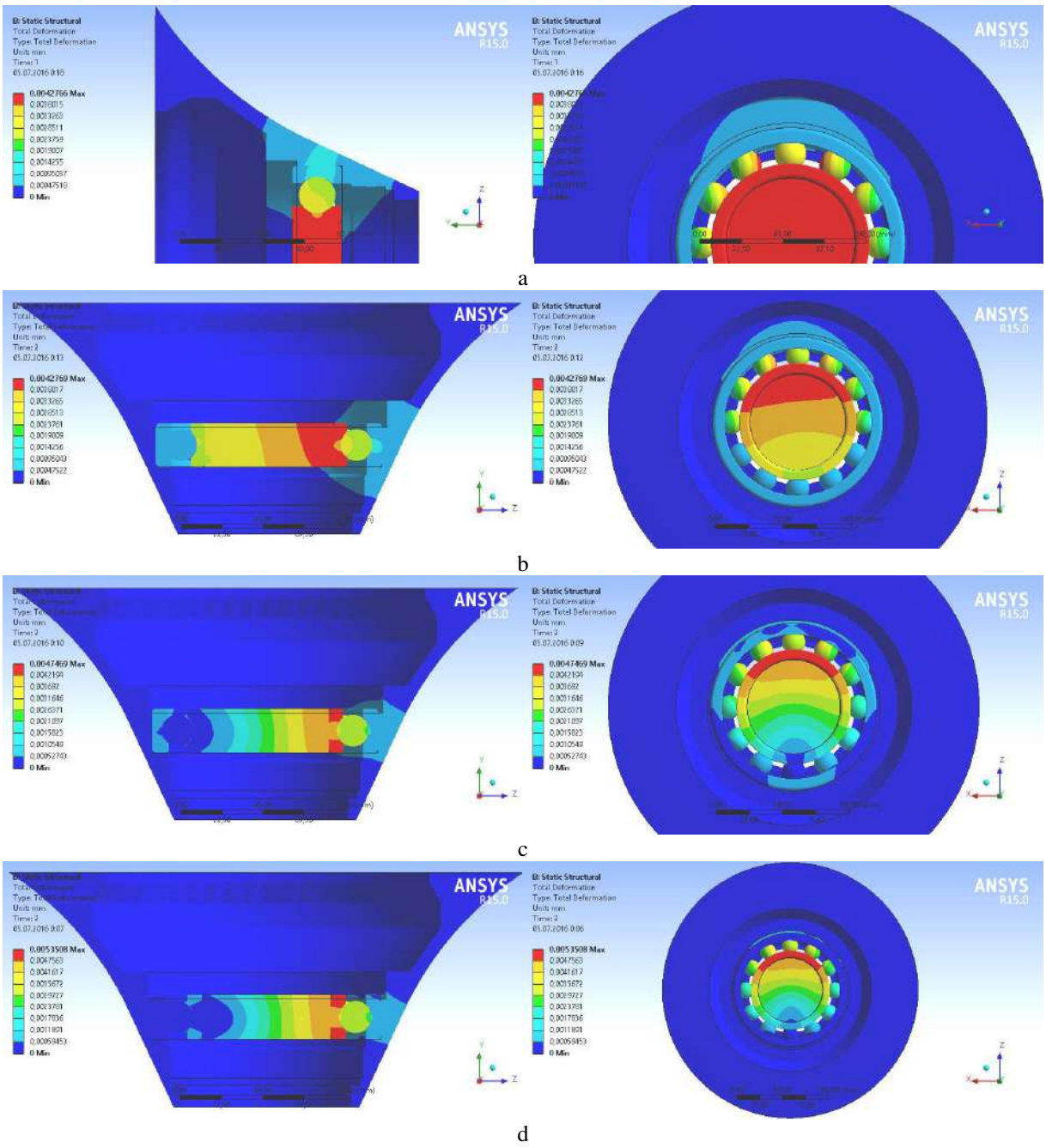

Figure 7 – Bearing stiffness for the support 45-276214: 0 rpm (a), 10500 rpm (b), 18750 rpm (c), 21150 rpm (d)

The evaluation of the coefficient α of the formula (2) is carried out by the linear regression procedure according to the following formula:

$$\alpha = \frac{\sum_{k=1}^{3}(c_k - c_0)\omega_k^2}{\sum_{k=1}^{3}\omega_k^4}, \quad (3)$$

where c_k – bearing stiffness, determined as a result of the numerical simulation for the rotor speed ω_k (Table 5); k – number of the experimental point.

Finally, the obtained values of coefficients α are summarized in Table 6, and approximating curves (2) are also shown on Figure 10.

Table 6 – Bearing stiffness parameters

Bearing	Coefficients	
	c_0, N/m	α, N·s^2/m
45-216	2.9	116.3
45-276214	2.4	46.6
46-276212	2.2	38.3
36-211	1.1	4.1

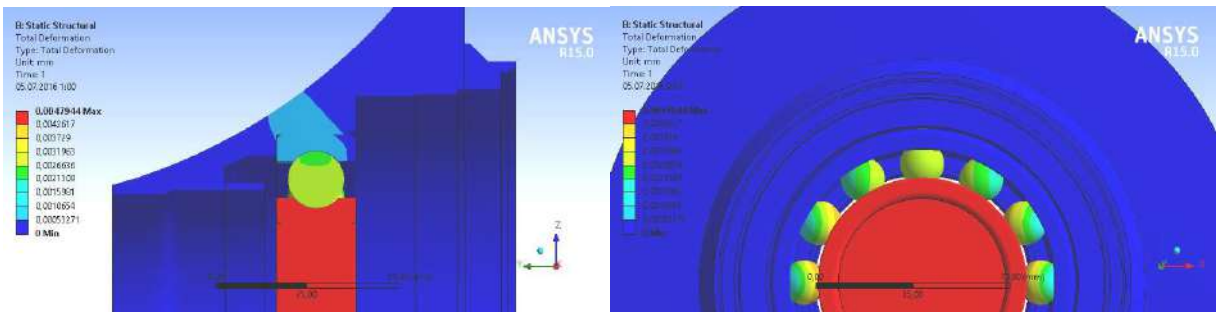

a

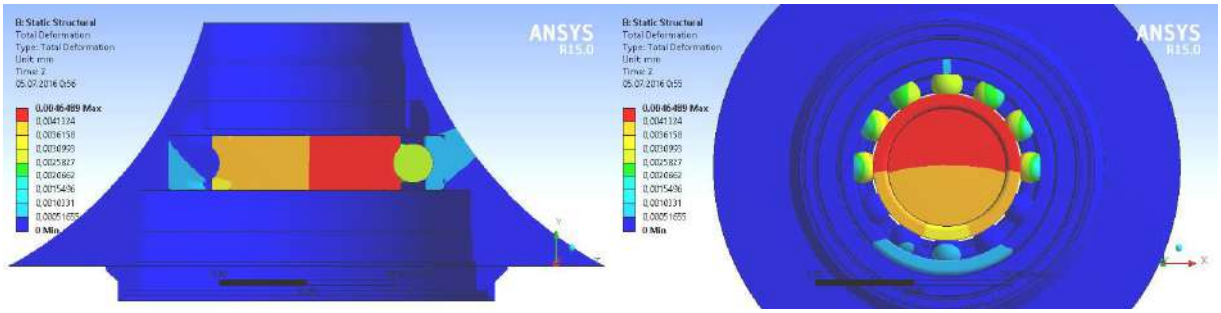

b

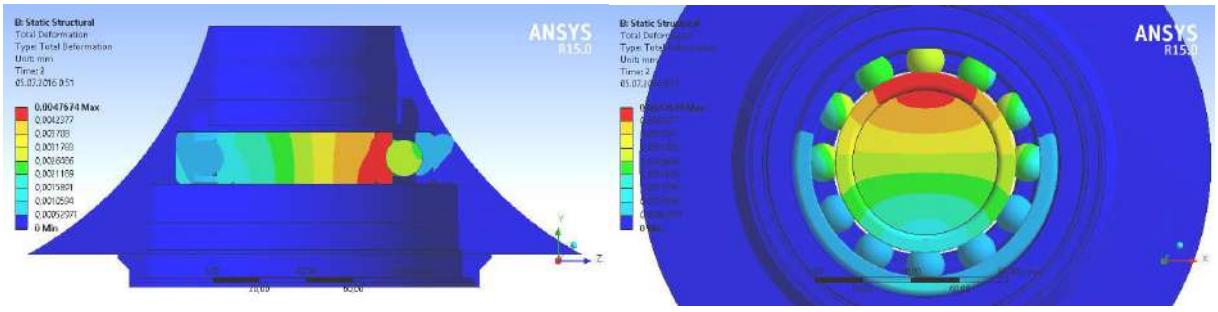

c

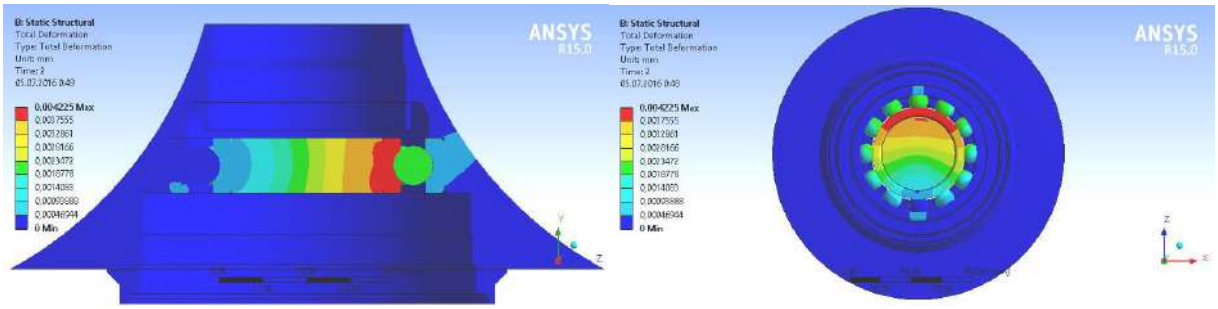

d

Figure 8 – Bearing stiffness for the support 46-276212: 0 rpm (a), 10500 rpm (b), 18750 rpm (c), 21150 rpm (d)

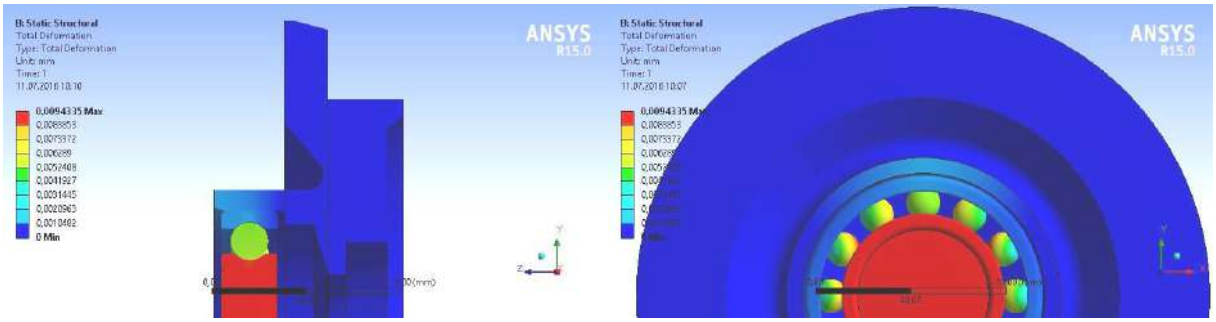

a

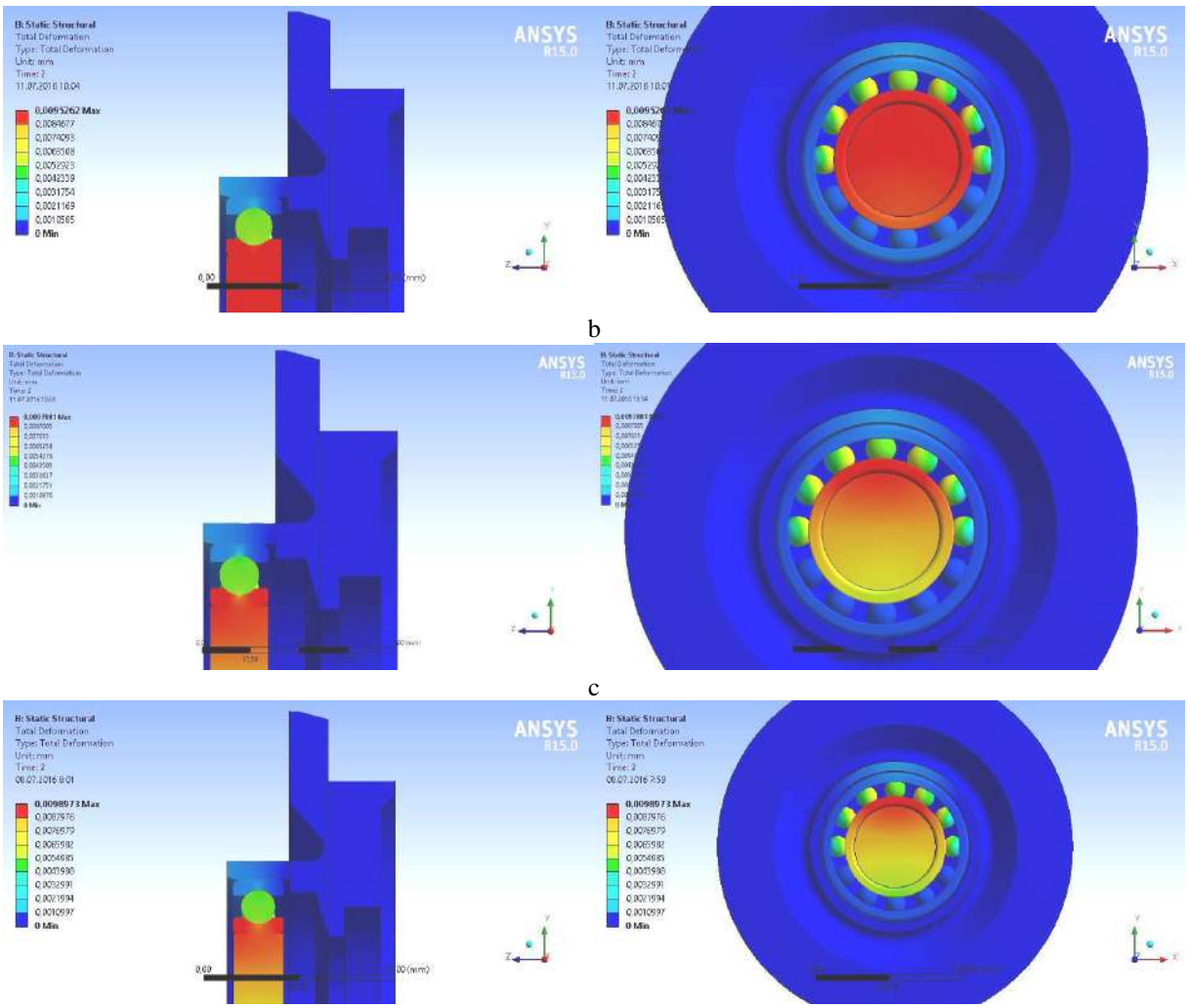

Figure 9 – Bearing stiffness for the support 36-211: 0 rpm (a), 10500 rpm (b), 18750 rpm (c), 21150 rpm (d)

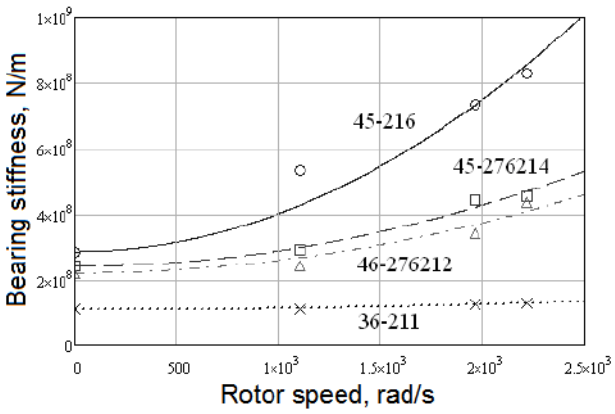

Figure 10 – Dependence of the bearing stiffness on the rotor speed

5 Conclusions

In this paper the methodology of determination of the bearing stiffness is proposed based on using different models of contact interaction between the mating surfaces of bearing parts. An appropriate methodology for refinement of the computational model is proposed taking into account the effect of rotation of moving parts and compliance of bearing supports elements.

The clarification of the stiffness parameters of the supporting units is carried out by combination of several computational means.

Further research should be aimed at obtaining spectrums of critical frequencies and related mode shapes for the rotor systems in abovementioned bearing supports.

6 Acknowledgements

The main part of the achieved results were obtained within the research project “Rotordynamic Research for the Turbopumps of the Liquid Rocket Engines” (Reg. no. 51.24-01.15.SP).

References

1. Pavlenko, I., Simonovskiy, V., Pitel', J., & Demianenko, M. (2018). *Dynamic analysis of centrifugal machines rotors with combined using 3D and 2D finite element models*. Lüdenscheid, RAM-VERLAG.
2. Vance, J., Zeidan, F., & Murphy, B. (2010). *Machinery vibration and rotordynamics*. New York, John Wiley & Sons Inc.
3. Simonovskiy, V. I. (2006). *Rotor dynamics for centrifugal machines*. Sumy, Sumy State University.
4. Simonovskiy, V. I. (2010). *Refinement of mathematical models of oscillatory systems according to experimental data*. Sumy, Sumy State University [in Ukrainian].
5. Simonovskiy, V. I. (2015). *Evaluation of coefficients of mathematical models for oscillatory systems*. Saarbrücken, LAP LAMBERT Academic Publishing [in Russian].
6. Gadyaka, V. G., Leikych, D. V., & Simonovskiy, V. I. (2011). Phenomena of stability loss of rotor rotation at tilting pad bearings. *13th International Scientific and Engineering Conference "Hermetic, Vibration Reliability and Ecological Safety of Pump and Compressor Machinery (HERVICON-2011)"*, Vol. 39, 244–253.
7. Ishida, Y., & Yamamoto, T. (2012). *Linear and nonlinear rotordynamnics. A modern treatment with applications*. Verlag, Willey-VCH.
8. Gadyaka, V. G., & Simonovskiy, V. I. (2005). Estimation of segment bearing stiffness while balancing flexible rotors for turbocharge units in the accelerating-balancing stand. *Bulletin of Sumy National Agrarian University, Series "Mechanization and Automation of Industrial Processes*, No. 11, 145–150.
9. Jin, C., Xu, Y., Zhou, J., et al. (2016). *Active magnetic bearings stiffness and damping identification from frequency characteristics of control systems*. Cairo, Hindawi Publishing Corporation.
10. Wang, T., Wang, F., Bai H., et al. (2008). *Stiffness and critical speed calculation of magnetic bearing-rotor system based on FEA*. Electrical machines and systems, IEEE Xplore.
11. Villa, C., Sinou, J., & Thouverez, F. (2008). Stability and vibration analysis of a complex flexible rotor bearing system. *Communications in Nonlinear Science and Numerical Simulation*, Vol. 13(4), 804–821.
12. Bai, C., Zhang, H., & Xu, Q. (2013). Subharmonic resonance of a symmetric ball bearing-rotor system. *International Journal of Non-Linear Mechanics*, Vol. 50, 1–10.
13. Pavlenko, I. V., Simonovskiy, V. I., Pitel, J., et al. (2017). Investigation of critical frequencies of the centrifugal compressor rotor with taking into account stiffness of bearings and seals. *Journal of Engineering Sciences*, Vol. 4, Issue 1, pp. C1–C6.

Дослідження нелінійних реакцій підшипникових опор роторів турбонасосних агрегатів рідинних ракетних двигунів

Павленко І. В.[1*], Симоновський В. І.[1], Пітель Я.[2], Дем'яненко М. М.[1], Вербовий А. Є.[1]

[1] Сумський державний університет, вул. Римського-Корсакова, 2, м. Суми, 40007, Україна;
[2] Технічний університет м. Кошице, вул. Баєрова, 1, м. Прешов, 08001, Словаччина

Анотація. Стаття присвячена уточненню числової моделі дослідження роторних систем турбонасосних агрегатів рідинних ракетних двигунів, що базується на урахуванні обертання валопроводу та податливості елементів підшипникових опор. Запропоновано сучасний підхід до дослідження нелінійних реакцій у підшипникових опорах роторів турбонасосних агрегатів рідинних ракетних двигунів. Досліджено п'ять моделей контактної взаємодії та представлено відповідні порівняльні характеристики жорсткостей підшипникових опор. Врахована геометрія корпуса та відповідна складена відповідна конструкційна схема для кожної опори, що базується на складальному кресленні турбонасосного агрегату. Урахування обертання вала здійснено шляхом прикладання сил інерції до внутрішньої обойми підшипника. Побудовано експериментальні точки залежності «навантаження – переміщення» діаграми "$F - v$" за допомогою розрахованих даних як масиву результатів моделювання, отриманих із застосуванням програмного комплексу ANSYS. У результаті числового моделювання, у тому числі навантаження опорного підшипника за схемою «віддалена сила» в широкому діапазоні частот обертання ротора, визначені відповідні радіальні переміщення. Запропоновано новий підхід до оцінки коефіцієнтів жорсткості підшипників на основі процедури лінійної регресії. У результаті отримані значення коефіцієнтів, що апроксимуються поліномами другої степені.

Ключові слова: Ansys Workbench, попереднє осьове навантаження, відцентрова сила, контактна взаємодія, скінченноелементний аналіз, числове моделювання, віддалена сила, характеристики жорсткості.

JOURNAL OF ENGINEERING SCIENCES
ЖУРНАЛ ІНЖЕНЕРНИХ НАУК
ЖУРНАЛ ИНЖЕНЕРНЫХ НАУК

Web site: http://jes.sumdu.edu.ua

DOI: 10.21272/jes.2018.5(1).d3 Volume 5, Issue 1 (2018)

UDC 519.63:539.3

Galerkin–Vlasov Method for Deflection Analysis of Isotropic Sandwich Plates under Uniform Load

Mama B.O.[1], Ike C. C.[2*]

[1] University of Nigeria, Nsukka, 410101 Enugu State, Nigeria;
[2] Enugu State University of Science and Technology, P.M.B. 01660, Enugu, Nigeria

Article info:
Paper received: January 27, 2018
The final version of the paper received: March 27, 2018
Paper accepted online: May 3, 2018

[*]**Corresponding Author's Address:**
charles.ike@esut.edu.ng

Abstract. In this work, the Galerkin–Vlasov method was used to solve the governing partial differential equation of equilibrium for isotropic sandwich plates with simply supported edges ($x = \pm a$, $y = \pm b$) and under uniform load on the plate domain $(-a \le x \le a, -b \le y \le b)$. Vlasov procedure was adopted in choosing the displacement shape functions as orthogonal eigen functions of dynamic Euler Bernoulli beams with equivalent spans, simple supports and loading as the plate. The resulting Galerkin-Vlasov equation was solved to obtain the unknown generalised shape function. It was found that the deflections obtained were exact solutions to the problem of bending isotropic sandwich plates. The deflection was found to be made up of two components: flexural deformation and shear deformation.

Keywords: isotropic sandwich plate; Galerkin–Vlasov method; governing differential equation of equilibrium; orthogonal eigen functions; generalized displacements parameters.

1 Introduction

The idea of sandwich construction in the use of composite structures has become very popular due to the development of man-made cellular materials as core materials. Sandwich structures are composite structures made up of a pair of thin stiff, strong skins (called faces, facings or covers) a thick light weight core to separate the skins and carry loads from one skin to the other and an adhesive attachment capable of transmitting shear and axial loads to and from the core (Petras, 1998). Figures 1–2 show typical cross-sectional view and three dimensional view of a sandwich plate. Sandwich plates are plates made of three layers, the top and bottom layers (called facings) are usually thin and are made from high strength material while the thick middle layer (called core) is made from a relatively light and low strength material (Magnucka–Blandzi and Wittenborg, 2013). The motivation for use of sandwich plate as a structural material is two fold. First, in plate bending theory, the maximum normal stresses occur at the top and bottom surfaces. Hence it is sensible using high strength materials at the top and bottom and low and light weight materials in the middle. Second, the bending resistance for a plate is proportional to the value of the thickness. Thus, increasing the thickness by adding a core in the middle increases the flexural resistance. (Kormaniková and Mamuzic, 2011).

Due to the thick core, the use of the Kirchhoff (classical) plate theory results in an underestimation of the deflections since it does not account for the affect of the transverse shear deformation. The simplest shear deformable plate theories that takes cognizance of the transverse shear deformation effect are the Reissner and the Mindlin first order shear deformation plate theories.

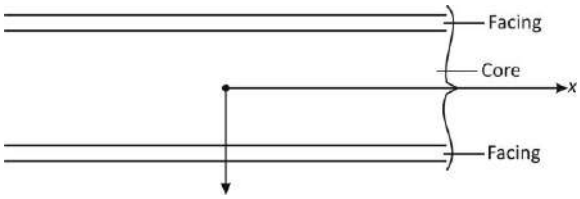

Figure 1 – Typical cross-sections of a sandwich plate

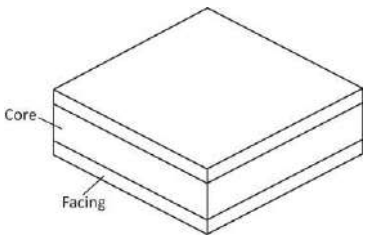

Figure 2 – 3D view of isotropic sandwich plate

The maximum shear stress generally occurs in the middle of the sandwich plate, requiring a core to resist the shear.

The most commonly used sandwich plate theory is linear, and is an extension of the first order shear deformation plate theory. Linear sandwich plate theory is of vital importance in the analysis and design of sandwich panels which are frequently encountered in building construction, vehicle construction, airplane construction and refrigeration systems. (Liaw Boen Dar, 1965, Balken et al 2010). Some advantages of sandwich plates are (Allen, 1969; Vinson, 2001; Raville, 1955):

– sandwich plates have composite cross-sections with a considerably higher shear strength to weight ratio than the equivalent non composite plate. The composite plate also has a higher tensile strength to weight ratio;

– the high stiffness of the face sheet results in high bending strength to weight ratio for the composite plate.

The advantages in weight and bending stiffness make sandwich plates attractive in many applications.

Sandwich plates have found widespread application in the aircraft industry for both civil and military aircrafts, in the structure of missiles and satellites. Magnueka – Blandzi and Wittenbeek (2013) formulated equations for the mathematical model of a sandwich circular plate consisting of two facings and a core with variable mechanical properties. They derived their equation using the principle of total potential energy. Wang (1995) derived the governing equilibrium equations for sandwich plates on the basis of the Reissner–Mindlin shear deformation plate theory, and presented exact relationships between the deflections of isotropic sandwich plates and their corresponding Kirchhoff plates.

Kormenikova and Manuzic (2011) used the shear deformation plate laminate theory for sandwich plates by neglecting the membrane and bending deformations in the core and the shear deformation in the findings.

2 Research Methodology

2.1 Theoretical framework

The governing differential equation of equilibrium of rectangular sandwich plates can be obtained by ignoring the non linear terms in the Reissner's plate equation, (Liaw Boen Dar, 1968) thus,

$$D\nabla^2\nabla^2 w = p(x,y) - \frac{D}{D_s}\nabla^2 p(x,y), \quad (1)$$

where

$$D_s = hG_c; \quad (2)$$

$$D = \frac{Eh^3}{12(1-\mu^2)}; \quad (3)$$

$$\nabla^2 = \frac{\partial^2}{\partial x^2} + \frac{\partial^2}{\partial y^2}; \quad (4)$$

$$\nabla^4 = \nabla^2\nabla^2 = \frac{\partial^4}{\partial x^4} + 2\frac{\partial^4}{\partial x^2\partial y^2} + \frac{\partial^4}{\partial y^4}; \quad (5)$$

$w(x, y)$ is the transverse displacement; p is the distributed transverse load; D_s is the shear modulus; D is the flexural modulus.

Equation (1) can be expressed as:

$$\nabla^4 w(x,y) = \frac{p(x,y)}{D} - \frac{1}{D_s}\nabla^2 p(x,y); \quad (6)$$

$$\left(\frac{\partial^4 w(x,y)}{\partial x^4} + 2\frac{\partial^4 (w(x,y)}{\partial x^2\partial y^2} + \frac{\partial^4 w(x,y)}{\partial y^4}\right) = \frac{p(x,y)}{D} - \frac{1}{D_s}\nabla^2 p(x,y). \quad (7)$$

2.2 Methodology

The rectangular sandwich plate ($2a \times 2b$) shown in Figure 3 and subject to uniform transverse load p_0 on the entire domain was considered. The region of Cartesian coordinates was taken at the plate centre due to symmetry of the plate and the load.

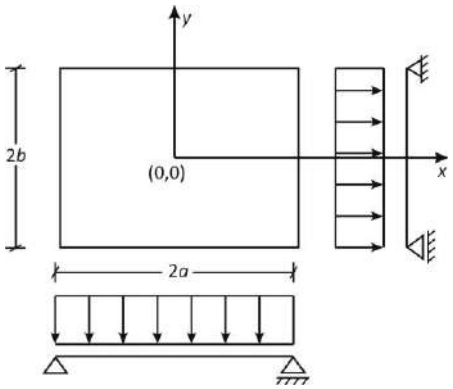

Figure 3 – Simply supported rectangular sandwich plate under uniformly distributed load

By the Galerkin–Vlasov variational method, $w(x, y)$ and $p(x, y)$ were considered as linear combinations of orthogonal eigen functions of vibrating simply supported Euler beams of spans $2a$ and $2b$ with simple supports at $x = -a$; $x = a$; $y = -b$; $y = b$. The boundary conditions for the simply supported sandwich plates are:

$$w(x = \pm a, y) = 0; \quad (8)$$

$$w_{xx}(x = \pm a, y) = \frac{\partial^2 w}{\partial x^2}(x = \pm a, y) = 0; \quad (9)$$

$$w(x,\ y = \pm b) = 0; \quad (10)$$

$$w_{yy}(x,\ y = \pm b) = \frac{\partial^2 w}{\partial y^2}(x,\ y = \pm b) = 0. \quad (11)$$

By the Vlasov method, suitable shape functions chosen as the eigen functions of vibrating Euler-Bernoulli beams are found by applying Equations (8)–(11) on

$$w(x) = c_1 \sin \alpha_1 x + c_2 \cos \beta_1 x\,; \tag{12}$$

and

$$w(y) = c_3 \sin \alpha_2 y + c_4 \cos \beta_2 y\,, \tag{13}$$

where c_1, c_2, c_3 and c_4 are constants and α_i and β_i are to be determined, $i = \{1; 2\}$.

Hence,

$$F_m(x) = \cos\frac{m\pi x}{2a},\ m = \{1, 3, 5, 7\}; \tag{14}$$

$$G_n(y) = \cos\frac{n\pi y}{2b},\ n = \{1, 3, 5, 7\}. \tag{15}$$

Following Kantorovich technique, $w(x, y)$ and $p(x, y)$ are considered as variable separable functions

$$w(x, y) = \sum_m^\infty \sum_n^\infty w_{mn} F_m(x) G_n(y)\,; \tag{16}$$

$$p(x, y) = \sum_m^\infty \sum_n^\infty p_{mn} F_m(x) G_n(y)\,. \tag{17}$$

The Galerkin – Vlasov variational integral becomes:

$$\int_{-b}^{b}\int_{-a}^{a}\left\{\left(\frac{\partial^4}{\partial x^4} + 2\frac{\partial^4}{\partial x^2 \partial y^2} + \frac{\partial^4}{\partial y^4}\right)\sum_m^\infty \sum_n^\infty w_{mn} F_m(x) G_n(y) - \frac{1}{D}\sum_m^\infty \sum_n^\infty p_{mn} F_m(x) G_n(y) + \frac{1}{D_s}\left(\frac{\partial^2}{\partial x^2} + \frac{\partial^2}{\partial y^2}\right)\sum_m^\infty \sum_n^\infty p_{mn} F_{mn} G_n\right\} F_i(x) G_j(y)\, dxdy = 0 \tag{18}$$

Simplifying,

$$\sum_m^\infty \sum_n^\infty w_{mn} \int_{-b}^{b}\int_{-a}^{a}\left(\frac{\partial^4}{\partial x^4} + 2\frac{\partial^4}{\partial x^2 \partial y^2} + \frac{\partial^4}{\partial y^4}\right) F_m(y) G_n(y) F_i(x) G_j(y)\, dxxy = \sum_m^\infty \sum_n^\infty \frac{p_{mn}}{D}\int_{-b}^{b}\int_{-a}^{a} F_m(x) \times G_n(y) F_i(x) G_j(y)\, dxdy - \sum_m^\infty \sum_n^\infty \frac{p_{mn}}{D_s}\int_{-b}^{b}\int_{-a}^{a}\left(\frac{\partial^2}{\partial x^2} + \frac{\partial^2}{\partial y^2}\right) F_m(x) G_n(y) F_i(x) G_j(y)\, dxdy \tag{19}$$

Simplification yields for particular integer values of m and n,

$$w_{mn}\int_{-b}^{b}\int_{-a}^{a}(F_m^{iv}(x) G_n(y) F_i(x) G_j(y) + 2F_m''(x) G_n(y) F_i(x) G_j(y) + F_m(x) G_n^{iv}(y) F_i(x) G_j(y))dxdy = p_{mn}\int_{-b}^{b}\int_{-a}^{a} F_m(x) G_n(j) F_i(x) G_j(y) dxdy - \frac{p_{mn}}{D_s}\int_{-b}^{b}\int_{-a}^{a}(F_m''(x) G_n(y) G_i(x) G_j(y) + F_m(x) G_n''(y) F_i(x) G_j(y))\, dxdy\,. \tag{20}$$

The orthogonality properties of the integrals of the eigen functions $F_m(x)$ and $G_n(y)$ lead to the simplification of the Galerkin – Vlasov variational integral to obtain:

$$w_{mn}\int_{-b}^{b}\int_{-a}^{a}(F_m^{iv}(x) F_m(x) G_n^2(y) + 2F_m''(x) F_m(x) G_n''(y) G_n(y) + F_m^2(x) G_n^{iv}(y) G_n(y))dxdy = \frac{p_{mn}}{D}\int_{-b}^{n}\int_{-a}^{a} F_m^2(x) G_n^2(y)\, dxdy - \frac{p_{mn}}{D_s}\int_{-b}^{b}\int_{-a}^{a}(F_m''(x) F_m(x) G_n^2(y) + F_m^2(x) G_n''(y) G_n(y))dxdy \tag{21}$$

Let

$$\int_{-b}^{b}\int_{-a}^{a} F_m^{iv}(x) F_m(x) G_n^2(y)\, dxdy = I_1; \tag{22}$$

$$\int_{-b}^{b}\int_{-a}^{a} F_m''(x) F_m(x) G_n''(y) G_n(y)\, dxdy = I_2\,; \tag{23}$$

$$\int_{-b}^{b}\int_{-a}^{a} F_m^2(x) G_n^{iv}(y) G_n(y)\, dxdy = I_3\,; \tag{24}$$

$$\int_{-b}^{b}\int_{-a}^{a} F_m^2(x) G_n^2(y)\, dxdy = I_4\,; \tag{25}$$

$$\int_{-b}^{b}\int_{-a}^{a} F_m''(x) F_m(x) G_n^2(y)\, dxdy = I_5\,; \tag{26}$$

$$\int_{-b}^{b}\int_{-a}^{a} F_m^2(x) G_n''(y) G_n(y)\, dxdy = I_6\,. \tag{27}$$

Then

$$w_{mn}(I_1 + 2I_2 + I_3) = \frac{p_{mn}}{D} I_4 - \frac{p_{mn}}{D_s}(I_5 + I_6)\,; \tag{28}$$

$$w_{mn} = \frac{\frac{p_{mn}}{D} I_4}{(I_1 + 2I_2 + I_3)} - \frac{\frac{p_{mn}}{D_s}(I_5 + I_6)}{(I_1 + 2I_2 + I_3)}\,; \tag{29}$$

$$w_{mn} = w_{mn}^{(f)} + w_{mn}^{(s)} = \frac{p_{mn}}{D}\left(\frac{I_4}{I_1 + 2I_2 + I_3}\right) - \frac{p_{mn}}{D_s}\left(\frac{I_5 + I_6}{I_1 + 2I_2 + I_3}\right). \tag{30}$$

Using the Wolfram Mathematica integration software,

$$I_1 = \frac{m^4\pi^4}{16a^4} ab = \left(\frac{m\pi}{2a}\right)^4 ab\,; \tag{31}$$

$$I_2 = -\left(\frac{m\pi}{2a}\right)^2 a - \left(\frac{n\pi}{2b}\right)^2 b = \frac{n^2 m^2 \pi^4}{16a^2 b^2} ab\,; \tag{32}$$

$$I_3 = \frac{n^4\pi^4}{16b^4} ba\,; \tag{33}$$

$$I_4 = ab\,; \tag{34}$$

$$I_5 = -ba\frac{m^2\pi^2}{4a^2}\,; \tag{35}$$

$$I_6 = -ba\frac{n^2\pi^2}{4b^2}\,. \tag{36}$$

For uniformly distributed transverse load of intensity p_0 over the entire plate domain,

$$p_{mn} = \frac{16 p_0}{mn\pi^2}(-1)^{\left(\frac{m+n-2}{2}\right)}. \tag{37}$$

Using the integrals, and Equation (37), we obtain

$$w^f = \sum_m^\infty \sum_n^\infty \frac{256 p_0 (-1)^{(m+n-2)/2}}{D\pi^6 \left(mn \left(\frac{m^2}{a^2} + \frac{n^2}{b^2} \right)^2 \right)} \cos\frac{m\pi x}{2a} \cos\frac{n\pi y}{2b}; \quad (38)$$

$$w^s(x,y) = \sum_m^\infty \sum_n^\infty \frac{64 p_0 (-1)^{(m+n-2)/2}}{D_s\pi^4 \left(mn \left(\frac{m^2}{a^2} + \frac{n^2}{b^2} \right) \right)} \cos\frac{m\pi x}{2a} \cos\frac{n\pi y}{2b}. \quad (39)$$

2.3 Maximum deflection

The maximum deflection occurs at the plate centre, and the components are given by:

$$w_{\max}^{(f)} = \sum_m^\infty \sum_n^\infty \frac{256 p_0 (-1)^{(m+n-2)/2}}{D\pi^6 \left(mn \left(\frac{m^2}{a^2} + \frac{n^2}{b^2} \right)^2 \right)} = \frac{256 p_0}{D\pi^6} \sum_m^\infty \sum_n^\infty \frac{(-1)^{(m+n-2)/2}}{mn \left(\frac{m^2}{a^2} + \frac{n^2}{b^2} \right)^2} \quad (40)$$

$$w_{\max}^{(s)} = \frac{64 p_0}{D_s\pi^4} \sum_m^\infty \sum_n^\infty \frac{(-1)^{(m+n-2)/2}}{mn \left(\frac{m^2}{a^2} + \frac{n^2}{b^2} \right)}. \quad (41)$$

The values of maximum deflection for the flexural and shear components are calculated for various values of aspect ratio, and presented in Table 1 for various ratios of D/D_s. The convergence properties of the deflation functions Equations (37)–(38) are illustrated by considering the m, n terms in the series of maximum deflection for the case of square plates (b/a = 1) and shown in Table 2.

Table 1 – Maximum deflection coefficients for the centre of uniformly loaded sandwich plates ($2a \times 2b$) with simply supported edges ($x = \pm a$; $y = \pm b$)

b/a	$w_{\max}^{(f)}\left(\times\frac{p_0 a^4}{D}\right)$	$w_{\max}^{(s)}\left(\times\frac{p_0 a^2}{D_s}\right)$	$\frac{D_s a^2}{D} = 1$; $w_{\max}^{s}\left(\times\frac{p_0 a^4}{D}\right)$	$\frac{D_s a^2}{D} = 10$ $w_{\max}^{s}\left(\times\frac{p_0 a^4}{D}\right)$	$\frac{D_s a^2}{D} = 20$ $w_{\max}^{s}\left(\times\frac{p_0 a^4}{D}\right)$	$\frac{D_s a^2}{D} = 50$ $w_{\max}^{(s)}\left(\times\frac{p_0 a^4}{D}\right)$
1.0	$6.496\cdot10^{-2}$	$28.48\cdot10^{-2}$	$28.48\cdot10^{-2}$	$2.848\cdot10^{-2}$	$1.424\cdot10^{-2}$	$0.5696\cdot10^{-2}$
1.2	$9.024\cdot10^{-2}$	$34.72\cdot10^{-2}$	$34.720\cdot10^{-2}$	$3.4720\cdot10^{-2}$	$1.7360\cdot10^{-2}$	$0.69440\cdot10^{-2}$
1.4	$11.280\cdot10^{-2}$	$38.68\cdot10^{-2}$	$38.68\cdot10^{-2}$	$3.868\cdot10^{-2}$	$1.934\cdot10^{-2}$	$0.7736\cdot10^{-2}$
1.6	$13.280\cdot10^{-2}$	$41.68\cdot10^{-2}$	$41.68\cdot10^{-2}$	$4.168\cdot10^{-2}$	$2.084\cdot10^{-2}$	$0.8336\cdot10^{-2}$
1.8	$14.896\cdot10^{-2}$	$43.92\cdot10^{-2}$	$43.92\cdot10^{-2}$	$4.392\cdot10^{-2}$	$2.196\cdot10^{-2}$	$0.8784\cdot10^{-2}$
2.0	$16.208\cdot10^{-2}$	$45.56\cdot10^{-2}$	$45.56\cdot10^{-2}$	$4.556\cdot10^{-2}$	$2.278\cdot10^{-2}$	$0.9112\cdot10^{-2}$
3.0	$19.568\cdot10^{-2}$	$49.08\cdot10^{-2}$	$49.08\cdot10^{-2}$	$4.9080\cdot10^{-2}$	$2.454\cdot10^{-2}$	$0.9816\cdot10^{-2}$
4.0	$20.512\cdot10^{-2}$	$49.80\cdot10^{-2}$	$49.80\cdot10^{-2}$	$4.980\cdot10^{-2}$	$2.49\cdot10^{-2}$	$0.9960\cdot10^{-2}$
5.0	$20.752\cdot10^{-2}$	$49.96\cdot10^{-2}$	$49.96\cdot10^{-2}$	$4.996\cdot10^{-2}$	$2.498\cdot10^{-2}$	$0.9992\cdot10^{-2}$
∞	$20.832\cdot10^{-2}$	$50.00\cdot10^{-2}$	$50.00\cdot10^{-2}$	$5.000\cdot10^{-2}$	$2.500\cdot10^{-2}$	$1.0000\cdot10^{-2}$

Table 2 – Convergence characteristics of w^f and w^s for b/a = 1

m	n	$w_{\max}^{f}\left(\times10^{-2}\frac{pa^4}{D}\right)$	$w_{\max}^{s}\left(\times10^{-2}\frac{pa^4}{D_s}\right)$
1	1	6.657	32.851
3	1	6.568	30.661
1	3	6.479	28.470
3	3	6.489	28.876
3	5	6.487	28.748
5	3	6.486	28.619
5	5	6.486	28.671
5	7	6.486	28.646
7	5	6.486	28.620
7	7	6.486	28.634

3 Results and Discussion

The governing partial differential equation of equilibrium of rectangular isotropic sandwich plate with simply supported edges (x = ±a; y = ±b) given by Equation (1) has been solved to obtain the unknown deflections for the case of uniformly distributed load over the entire plate. Vlasov procedure was adopted to choose the shape functions as the orthogonal eigen functions of vibrating Euler Bernoulli beams as Equations (14) and (15). The Galerkin – Vlasov variational integral was obtained as Equation (18). Simplifications by use of the orthogonality of the eigen basis functions and integrations yielded the solution for the unknown generalized displacement coordinates as Equation (30).

It was observed that the solution for displacements showed there are two displacement components; flexural displacements and shear displacements. For uniform loads, the flexural displacements were obtained as Equation (40) and the shear displacements as Equation (41). The series obtained for the displacements were rapidly convergent and the convergent solutions after five (5) terms of the series for different aspect ratios were calculated and presented in Table 1. The table shows that as the ratio Ds/D increases, the contribution of shear deformation to the overall deformation of the sandwich plate reduces.

Table 2 illustrates that the expression for flexural component of deflection converges faster than the expression for the shear component. Convergence to the exact flexural component is achieved for m = n= 5, while that for the shear component is achieved for higher values of m, n. The Galerkin Vlasov solutions obtained in this study were in exact agreement with solutions obtained for simply supported isotropic sandwich plates by Plantema, (1966) who used a Navier series method.

4 Conclusions

The Galerkin–Vlasov method has been successfully used to solve the governing partial differential equations of isotropic sandwich plates with simply supported edges ($x = \pm a$; $y = \pm b$) under uniformly distributed load.

The solution gave exact solution for the deflection as a rapidly converging double trigonometric (cosine) series of infinite terms.

The deflection $w(x, y)$ was found to be made up of a flexural component $w^{(f)}(x, y)$ and a shear component $w^{(s)}_{(x,y)}$.

The contribution of the shear deformation to the total (resultant) deformation reduces as the ratio D_s/D increases.

This paper will hopefully enhance our understanding of the deflection behaviour of simply supported isotropic sandwich plates under uniformly distributed load.

References

1. Allen, H.G. (1969). *Analysis and Design of Structural Sandwich Panels*. Pergamon Press, Oxford.
2. Balken, D., Azar, O., Turkmen, H. S., & Mecitoglu, Z. (2010). Transient response of a laminated sandwich plate with viscoelastic core subjected to air blast: Theory and experiment Structures under shock and impact. *XI 113 WIT Transactions on The Built Environment*, Vol. 113, doi.10.2495/sui00101.
3. Magnucka, E., et al. (2013). Approximate solutions of equilibrium equations of sandwich circular plate. *AIP Conference Proceedings*, Vol. 1558, Issue 1(2352), doi: 10.1063/1.48260 13.
4. Kinh, H. H. (1972). *Analysis of Three Dimensional Orthotropic Sandwich Plate Structures by Finite Element Method*. Ph.D. thesis, University Montreal.
5. Kormaniková, E., & Mamuzić, I. (2011). *Shear Deformation Laminate theory used for sandwiches*. Metabk, 50(3), pp. 193–196.
6. Boen, L.-D. (1965). *Theory of Bending of Multilayer Sandwich Plates*. Ph.D. thesis, Oklahoma State University.
7. Plantema, F. J. (1966). *Sandwich Construction (The Bending and Buckling of Sandwich Beams, Plates and Shells)*. John Wiley & Sons, New York.
8. Achilles, P. (1998). *Design of sandwich structures*. Ph.D. thesis, Cambridge University.
9. Raville, M. E. (1955). *Deflection and Stresses in a Uniformly loaded, Simply Supported Rectangular Sandwich Plate*. FPL Report.
10. Vinson, J. R. (2001). Sandwich Structures. *Applied Mechanics Reviews*, No. 54(3), pp. 201–214.
11. Wang, C. M. (1995). Deflection of sandwich plates in terms of corresponding Kirchhoff plate solutions. *Archive of Applied Mechanics*, Vol. 65, Issue 6, 408–414.

Метод Гальоркіна–Власова для аналізу напружено-деформованого стану рівномірно навантаженої ізотропної шаруватої пластини

Мама Б. О.[1], Іке Ч. Ч.[2*]

[1] Нігерійський університет, м. Нсукка, 410101, Штат Енугу, Нігерія;
[2] Державний університет науки і технології м. Енугу , П.М.Б. 01660, м. Енугу, Нігерія

Анотація. У роботі застосовано метод Гальоркіна–Власова для розв'язання диференціальних рівнянь рівноваги ізотропних шаруватих пластин з рівномірно навантаженими шарнірно опертими краями ($x = \pm a$; $y = \pm b$). Обрана процедура Власова для визначення функцій форми як ортогональних власних функцій за моделлю Ейлера–Бернуллі для випадку шарнірних опор і рівномірного навантаження. Результуюче рівняння Гальоркіна–Власова розв'язане з метою визначення невідомої функції узагальненої форми. Встановлено, що отримані переміщення є точними рішеннями задачі про вигин ізотропних шаруватих пластин. Виявлено, що переміщення складаються з двох компонентів: згинальної деформації та деформації зсуву.

Ключові слова: ізотропна шарувата пластина; метод Гальоркіна–Власова; рівняння рівноваги; ортогональні власні функції; узагальнені параметри.

JOURNAL OF ENGINEERING SCIENCES
ЖУРНАЛ ІНЖЕНЕРНИХ НАУК
ЖУРНАЛ ИНЖЕНЕРНЫХ НАУК

Web site: http://jes.sumdu.edu.ua

DOI: 10.21272/jes.2018.5(1).e1 Volume 5, Issue 1 (2018)

UDC 621.396.67

UWB Microstrip Line Feeding Planar Modified Circular Antenna

Pillalamarri L.

Department of Electronics and Communication Engineering, Radio Frequency and Microwave Laboratory, IIT Hyderabad, Telanagana-State, India

Article info:
Paper received: July 5, 2017
The final version of the paper received: December 12, 2017
Paper accepted online: February 28, 2018

Corresponding Author's Address:
laxmanpillalamarri85@gmail.com

Abstract. In this paper we have investigated compact printed semicircular disc monopole antenna, which is basically printed microstrip antenna with etched ground plane for UWB applications. In particular we have simulated very compact semicircular disc monopole antennas for UWB communication. Simple rectangular microstrip line is used for feeding the printed monopole antenna and its frequency bandwidth under –10 dB return loss is ranging from 3 GHz to 11.6 GHz. This compact printed monopole antenna works well for the whole UWB frequency band 3.1–10.6 GHz.

Keywords: UWB, semicircular printed monopole antenna, microstrip line.

1 Introduction

Ultra-Wideband (UWB) commonly refers to signal or system that either has a large relative bandwidth (BW) or a large absolute bandwidth [1–4]. Such a large BW offers specific advantages with respect to signal robustness, information content and/or implementation simplicity. But such systems have some fundamental differences from the conventional narrowband systems. The Federal communications Commission (FCC) has designated the 3.1 to 10.6 GHz band with Effective Isotropic Radiated Power (EIRP) below –40dbm/kHz for UWB Communications.

2 Literature Review

Some UWB antennas are much more complex than other existing single band, dual band and multi-band antennas [5, 6]. Most of the UWB monopole antennas are investigated till today is non-planar as in [7, 8] and due to its protruded structure they cannot be integrated with integrated circuits and they are fragile. Few researchers have also studied printed monopole Antennas

In this paper, we will investigate UWB antenna, which is basically a printed microstrip antenna with etched ground plane. First we will investigate in depth the semicircular disk printed monopole antenna for UWB applications. For getting compactness, we have etched the half of the part of circular patch without disturbing the bandwidth as well as antenna parameter. We have used conventional rectangular microstrip lines as feed lines for printed UWB antennas which are properly matched to the antenna impedance. In future we will also investigate other broadband matching techniques to further improve the UWB performance of the printed monopole antennas [9–11]. CAD-FEKO simulation software has been employed for obtaining the simulation results.

3 Research Methodology

This modified UWB monopole antenna is designed directly from the circular disc UWB-Monopole antenna with some modifications in the patch shape as shown in Figure 1. We have used the same FR4 substrate with 4.4 relative permittivity and 1.6 mm thickness. The real part of antenna impedance is exactly 50 Ω at 8.5 GHz and 10.8 GHz when the imaginary part of antenna impedance cross zero. The final optimal dimensions of the UWB-monopole antenna are:

– dimensions of patch: radius r = 12 mm; metal thickness 0.035 mm;

– dimensions of substrate: W_1 = 34 mm; L_1 = 50 mm;

– dimensions of ground: W_2 = 34 mm; L_2 = 26 mm;

– microstrip line: W_3 = 2.6 mm; L_3 = 27.5 mm, where g is a gap between the ground plane and patch.

After doing an extensive simulation study, we have fixed the dimensions of UWB monopole antenna and the value of g as 1 mm. The antenna impedance, f_{low}, f_{high} and radiation efficiency are tabulated in Table 1. Note that proposed semicircular disc Monopole antenna is more

compact and high efficient antenna for UWB applications. It has maximum directivity at –26° and 180° at 3 GHz and at the frequency 10.6 GHz, it has been tilted to 10° and –26.4° as frequency increases it is slightly titled with 5° to 10°. The H-plane radiation pattern on the other hand is purely omni-directional pattern throughout the band of frequencies.

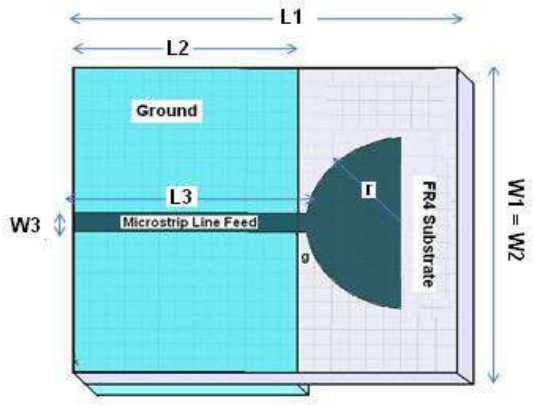

Figure 1 – Geometry of Circular UWB Antenna

4 Results

The simulated 3D radiation patterns of the proposed antenna at 3.1, 5, 8, 9, 10.6 and 11.2 GHz are shown in Figures 2–4. The radiation pattern looks like a doughnut, similar to that of a dipole pattern, at the first resonant frequency, i. e. 3 GHz. At the second resonant frequency i.e. at 5 GHz and the third resonance frequency, i. e. at 8 GHz the radiation pattern is somewhat like pinched doughnut (i.e. omni directional). As the frequency moves toward the upper end of the bandwidth the radiation pattern is some what slightly distorted as it reaches higher frequencies (i. e.10.6 GHz and 11.2 GHz.).

The transition of the radiation patterns from a simple doughnut at the lower frequencies to the slowly distorted radiation patterns at the higher resonances indicates that this antenna must have gone through major changes in its behavior but it had omni directionality, this was possible because of the partial ground plane i.e. ‘g’ the gap between the ground plane and the patch which was a major factor for perfect impedance matching of the antenna, due to the proper impedance matching the antenna has very less reflections. As the impedance matching was good the radiation power and radiation intensity were very high.

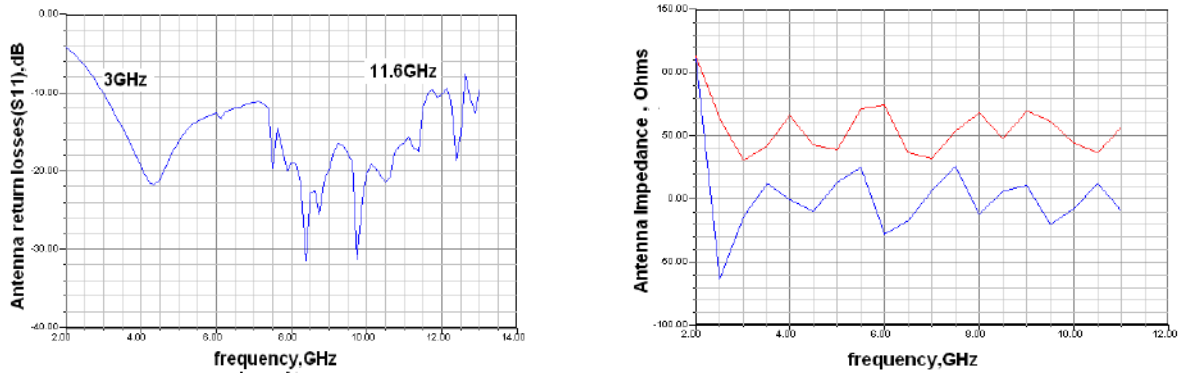

a b

Figure 2 – Return losses (a) and antenna impedance (b)

Table 1 – Parameters of the Circular Disc UWB monopole Antenna

g, mm	F_{low}, GHz	F_{high}, GHz	Antenna Impedance, Ω	P_{acc}, W	P_{rad}, W	Max U, W/Sr	Peak Gain	η, %
0.8	3.2	11.5	50	0.98	0.88	0.13	1.69	89.6
1	3	11.6	50	0.97	0.87	0.13	1.64	89.3

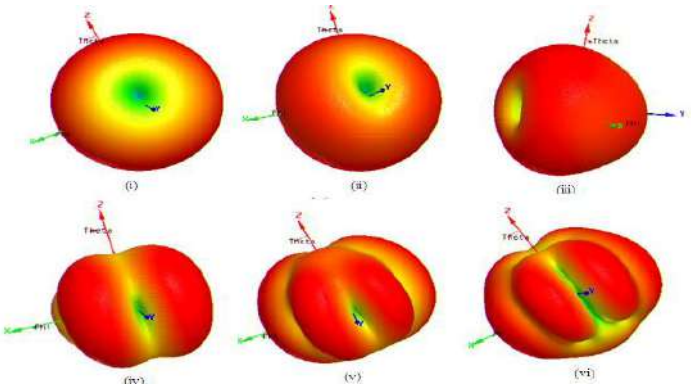

Figure 3 – 3D Radiation Plots

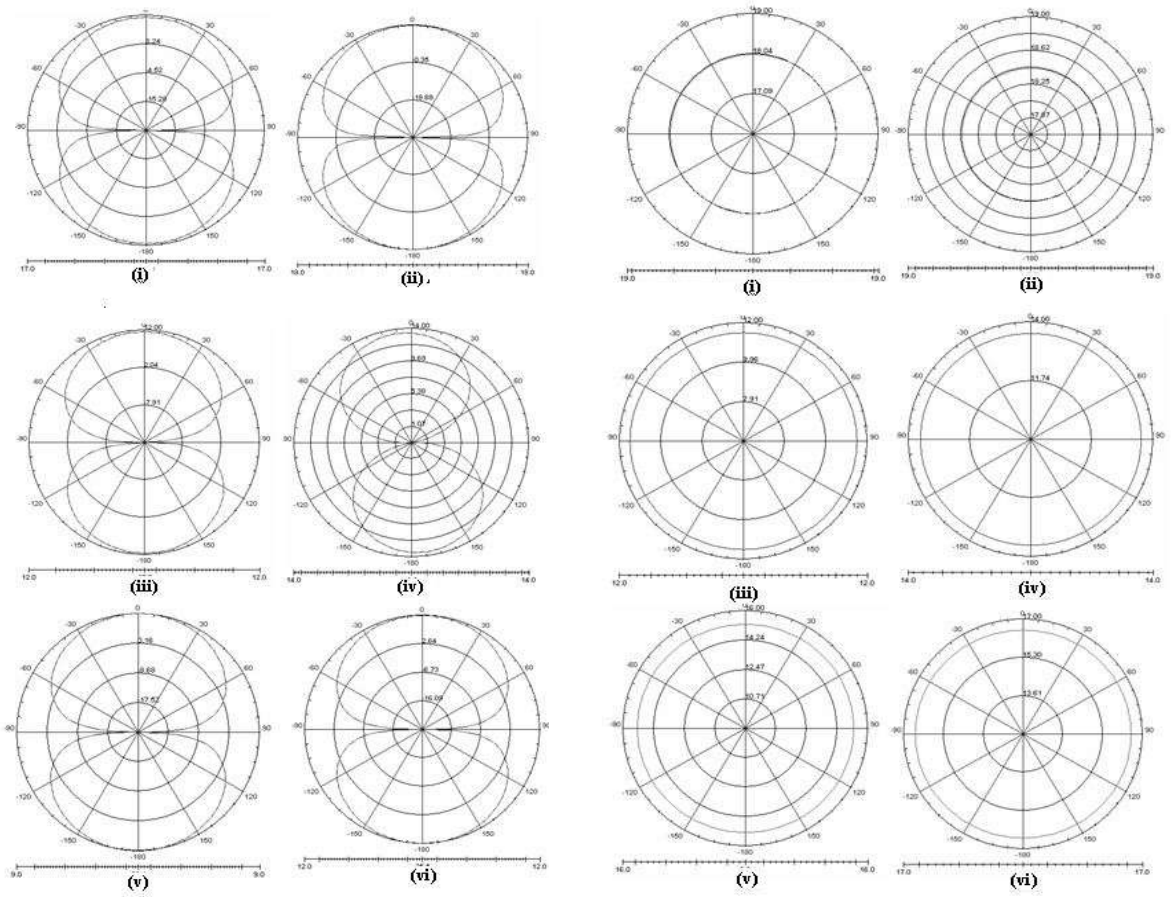

a b

Figure 4 – E-plane (a) and H-plane (b) radiation patterns

5 Conclusions

In this paper, the printed semicircular disc UWB monopole antenna with huge bandwidth has been investigated, which is basically the printed microstrip antenna with the etched ground plane. Printed UWB monopole antennas are less fragile, planar and can be integrated with the integrated circuits unlike monopole antennas which have non-planar or protruded structures above the ground plane. In particular, we have simulated very compact UWB monopole antenna and it has higher efficiency. The E-plane radiation the printed monopole antenna is in the form of 8 shapes and it is slightly tilted at higher frequencies. The H-plane radiation pattern has omni-directional patterns throughout the frequencies of the BW. It has been observed that such monopole antennas are suitable for UWB operations.

References

1. Schantz, H. (2005). *The Art and Science of Ultra wideband Antennas*. Artech House Inc.
2. Aiello, G. R., & Rogerson, G. D. (2007). Ultra-wideband Wireless Systems. *IEEE Microwave Magazine*, pp. 36–47.
3. Allen, B., Dohler, M., Okon, E. E., et al. (2007). *Ultra-Wideband Antennas and Propagation for Communications. Radar and Imaging*. John Wiley & Sons Inc.
4. Pozar, D. M. (2005). *Microwave Engineering*. John Wiley & Sons Inc.
5. Pillalamarri, R., & Kshetrimayum, R. S. (2007). Printed UWB Circular and Modified Circular Disc Monopole Antennas. Accepted for *IEEE Applied Electromagnetics Conference*, Kolkatta, India.
6. Kshetrimayum, R. S., & Pillalamarri, R. (2009). UWB printed monopole antenna with a notch frequency for coexistence with IEEE 802.1a WLAN devices. *Proceedings of 5th National Conference on Communications (NCC)*.

7. Pillalamarri, R., & Kshetrimayum, R. S. (2007). Single Printed Monopole Antenna and Notched Antenna with Triangular Tapered Feed Lines for Triband and Penta band Applications. *Proceedings of IEEE Indicon*, Bangalore.
8. Pillalamarri, R., & Kshetrimayum, R. S. (2007). Accurate Determination of Antenna Impedance of Microstrip Line-Fed Patch Antennas. *Proceedings of IEEE Indicon 2007*, Bangalore.
9. Liang, J., Chiau, C., Chen, X., & Yu, J. (2004). Study of a circular disc monopole antennas for ultra wideband applications. *International Symposium on Antennas and Propagation*.
10. Agrawall, N. P., Kumar, G., & Ray, K. P. (1998). Wide-Band Planar Monopole Antennas. *IEEE Transactions on Antennas and Propagation*, Vol. 46, No. 2, 294–295.
11. Hammoud, M., Poey, P., & Colombel, F. (1993). Matching the Input Impedance of a Broadband Disc Monopole. *Ellectronics Letters*, Vol. 29, No. 4, 406–407.
12. CAD-FEKO Suite 4.2. *Feko Corporation*, South Africa.

Модифікована плоска кругова UWB-антена

Піллаламаррі, Л.

Відділ електроніки та зв'язку, Лабораторія радіочастот і мікрохвиль, м. Хайдарабад, Індія

Анотація. У роботі досліджено компактну друковану напівкруглу дискову антену, що є UWB-антеною із заземленням. Зокрема, змодельовано дуже компактні антени з напівкруглими дисками для UWB-зв'язку. Проста прямокутна мікрополосковая лінія використовується для живлення антени з частотною пропускною смугою –10 дБ із втратами від 3 ГГц до 11.6 ГГц. Ця модифікована антена добре працює для всього діапазону UWB-частот 3.1–10.6 GHz.

Ключові слова: UWB, модифікована антена, мікрополосковая лінія.

JOURNAL OF ENGINEERING SCIENCES
ЖУРНАЛ ІНЖЕНЕРНИХ НАУК
ЖУРНАЛ ИНЖЕНЕРНЫХ НАУК
Web site: http://jes.sumdu.edu.ua
DOI: 10.21272/jes.2018.5(1).e2 Volume 5, Issue 1 (2018)

UDC 621.438.9

Research of Working Process of Vortex Expansion Machine with Side Channel

Bondar A. V.*, Vaneev S. M.

[1] Sumy State University, 2 Rymskogo-Korsakova St., 40007, Sumy, Ukraine

Article info:
Paper received: November 10, 2017
The final version of the paper received: April 16, 2018
Paper accepted online: April 20, 2018

***Corresponding Author's Address:**
artembondar89@gmail.com

Abstract. At gas distribution stations, a large amount of energy of compressed gases is lost. In such cases, the useful power is obtained with the aid of a turboexpander. The problem is that there is a great need for turboexpanders with a capacity of up to 500–700 kW. For these capacities, the turboexpander with the use of classical turbines turns out to be high-speed, complex, expensive, with a payback period that is more than two years. The solution of this problem is seen in the creation of turboexpander installations based on vortex machines.

A promising type of vortex expansion machines are side channel machines. Results of studies of vortex hydraulic turbines with side channel showed high values of the efficiency.

The goal of this research is study of the working process of vortex expansion machine with side channel by performing a computational experiment in the ANSYS CFX software package.

The results of the research showed that the efficiency of vortex expansion machine with side channel is greater than in vortex expansion machine with peripheral channel (real experiment).

Keywords: vortex expansion machine, efficiency, turboexpander, computational experiment, ANSYS CFX, working process.

1 Introduction

At gas distribution stations necessarily installed throttle devices, in which a large amount of energy of compressed gases is lost. As a rule, in such cases, the useful power is obtained with the help of a turboexpander.

The problem is that there is a big need for turbo expander with a capacity of 500–700 kW. For these capacities turboexpander with classical turbines turns out to be high-speed, complex, and expensive, with a payback period of more than two years. Key of solving this problem is turboexpander based on vortex machines.

However, it is advisable to use machines of this type not only in turboexpander units. The vortex expansion machines have the potential to be used in various pneumatic devices.

2 Literature Review

Literary analysis showed that knows three main types of vortex expansion machines: with peripheral channel, with side channel and with peripheral-side channel. flowing parts of vortex expansion machines can be single-channel, dual-channel and multichannel.

For compressed fluids, the most studied are vortex expansion machines with peripheral channel [1–3, 6]. Vortex expansion machines with side channel are practically unexplored.

For incompressible fluids known researches of vortex hydraulic turbines with side channel [5, 6]. In particular, known the results of experimental tests of vortex machines what working on water. Tests were conducted for the following types of flowing part:

– with side round channel (open and closed types);
– with side rectangular channel of closed type;
– with external peripheral channel.

According to the results of the tests:

– efficiency of vortex machine with side round channel of the closed type with the optimal mode is 54 %;
– with a coefficient of fastness n_s = 4, the power of vortex machine with side round channel of a closed type is 7 times greater than the power of an axial partial turbine with the same dimensions and rotational speed;
– efficiency of vortex machine with a rectangular channel is smaller than with a round;
– efficiency of the stage with external peripheral channel in the optimal mode is 13 %.

Thus, in these researches [4] declares the advantage of vortex machines with side channel over machines with external peripheral channel, what working on water.

Also known researches of vortex machines what working on gas.

According to researches of vortex machine with internal peripheral channel [1], the application of this type of flowing part can increase the efficiency of the machine by 25–30 %.

Vortex machine with external peripheral channel is considered the most technologically and constructively simple. The application of the nozzle in the design of the turbine and the optimization of flowing part allowed to arrange the flow of gas at the inlet section and along the length of flowing part, and to increase the efficiency of the turbine from 10 % to 30–35 % [2, 3].

Considering the possibility of a significant increase in the efficiency of vortex machine with peripheral channel, and high values of the efficiency of vortex hydraulic turbines with side channel, it seems advisable to study vortex expansion machines with side channel what working on water.

3 Research Methodology

3.1 Incoming data

The goal of this research is study of the working process of vortex expansion machine with side channel due a computational experiment. Virtual model (Fig. 1) of vortex expansion machine with side channel based on an experimental model of a vortex pneumatic expansion machine with external peripheral channel [2].

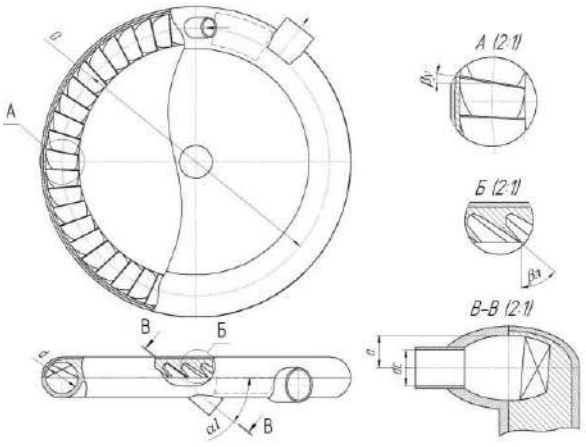

Figure 1 – Constructive scheme of the virtual model

The main geometric parameters of the virtual model were taken from [2], as parameters of modes with a high level of efficiency. Geometric parameters and input data for calculation are presented in Table 1 and Table 2, respectively.

Table 1 – Geometric parameters of the virtual model

Name	Value
Average diameter of the impeller, D	180 mm
Diameter of meridional intersection of flow section, d	22 mm
Angle of blades (the angle between the edge of the shoulder blade and the axis perpendicular to the axis of rotation of impeller) β_y	10°
Angle of inclination of blades (angle between axis of blades and direction, reverse direction of circumferential speed of impeller), β_l	50°
Number of blades, z	48
Angle of gas flow from nozzle to edge of impeller, α_1	40°
Diameter of outlet of nozzle, d_s	12 mm
The value of displacement of the axis of nozzle along the width of side channel, a	11 mm

Table 2 – Incoming data

Parameter	Test mode						
	1	2	3	4	5	6	7
Total inlet pressure $P_1 \cdot 10^{-5}$, Pa	1.53	1.87	2.16	2.58	3.25	3.87	3.60
Pressure reduction, Π_T	1.46	1.74	1.93	2.19	2.49	2.73	2.53
Total inlet temperature T_1*, K	298						
Rotational speed, rpm	4000		5000				6000
Working fluid	Viscous air						

3.2 Methodology

Research methodology was taken from [4]. A computational experiment was carried out in the ANSYS CFX software. Verification of the results of a computational experiment in ANSYS CFX with the results of a physical experiment for a vortex expansion machine with external peripheral channel was performed [4]. Verification showed the possibility of using ANSYS CFX for the study of vortex expansion machines.

The calculation process consists of five main stages:

1. Creation of a geometric model (CAD-model).

2. Creation of a virtual model of expansion machine based on a geometric model in a grid generator ANSYS Meshing (number of elements more than 1.5 million).

3. Creation of a virtual model from a grid by imposing settlement conditions. The simulation of turbulent effects was carried out using the SST model. As input data for calculations were taken: total inlet pressure, total inlet temperature and static outlet pressure. The working fluid

is a viscous compressed air. Roofing of the walls of the flow part – 6.3 μm.

4. Search for solutions. At this stage, the search for such parameter values in each calculation element is performed so that the entire calculated zone has the maximum correct equation of flows. A solution is considered to be found when the value of the mean-square residual does not exceed 10^{-4}, as well as no significant fluctuations in the values of the output parameters (torque, mass flow, outlet temperature).

5. Analysis of results of calculation. The calculation of necessary parameters (efficiency, torque, flow, power, temperature, pressure) is organized. Also, we obtain the flow visualization and the distribution of parameters along length of flowing part. The model takes into account the effect of flow in the gap between the cutter and impeller.

Assumption: gaps between housing and impeller is not modeled; no heat exchange with the environment; flow parameters are considered to be evenly distributed over the inlet cross section.

Efficiency during computational experiment is determined by the formula:

$$\eta = \frac{M_Z \cdot \omega}{h_s \cdot m}, \tag{1}$$

M_z – torque on the shaft of expansion machine, N·m;
ω – angular rotational speed of the impeller, rad/s;
m – mass flow, kg/s;
h_s – specific isenthropic difference of enthalpy, J/kg.

Specific isentropic difference of enthalpy is determined by the formula:

$$h_s = \frac{k}{k-1} \cdot T_1^* \cdot R \cdot \left(1 - \left(\frac{1}{\Pi_T} \right)^{\frac{k-1}{k}} \right), \tag{2}$$

k – isentrope index of the working fluid;
R – specific gas constant, J/(kg·K);
T_1* – total inlet temperature, K;
Π_T – pressure reduction.

Values h_s and ω are determined by the input data, and values M_z and m are obtained as a result of computational experiments.

4 Results and Discussion

At the first stage, computational experiment was conducted in steady-state mode, on the second - in transient mode.

Table 3 – Results of computational experiment

Mode	Steady-state mode			
	Mass flow, kg/s	Torque, N·m	Power, kW	Efficiency
1	0.022	0.580	0.24	0.366
2	0.028	1.024	0.43	0.347
3	0.036	1.256	0.66	0.357
4	0.043	1.700	0.89	0.345
5	0.055	2.325	1.22	0.323
6	0.067	3.008	1.58	0.315
7	0.066	2.480	1.56	0.338

Table 4 – Results of real experiment [2]

Mode	Real experiment			
	Mass flow, kg/s	Torque, N·m	Power, kW	Efficiency
1	0.023	0.525	0.22	0.315
2	0.030	1.002	0.42	0.32
3	0.039	1.164	0.61	0.305
4	0.049	1.698	0.89	0.305
5	0.063	2.405	1.26	0.29
6	0.104	4.313	2.26	0.29
7	0.074	2.309	1.45	0.28

As we see, the value of the efficiency of vortex expansion machine with side channel (computational experiment) is higher than efficiency of vortex expansion machine with peripheral channel (real experiment) in all modes. Such results show that vortex expansion machine with side channel is a promising type of such machines.

The data of visualization of flow and distribution of total temperature along the length of flowing part of vortex expansion machine were analysed (Fig. 2–4).

The values of total temperature were taken on a plane between rotor and stator on the average diameter of impeller. Figure 2 shows that on the segment 0°–150° total temperature is not changing, and on the segment 150°–330° change in total temperature is much higher. Consequently, the main energy transfer from flow to impeller of vortex expansion machine with side channel occurs on the segment 150°–330° unlike the vortex expansion machine with the peripheral channel [4].

Figures 3–4 present visualization of flows of two modes with different efficiency. As seen, better organized longitudinal-vortex movement along the length of flowing part has more efficiently working process of the vortex expansion machine.

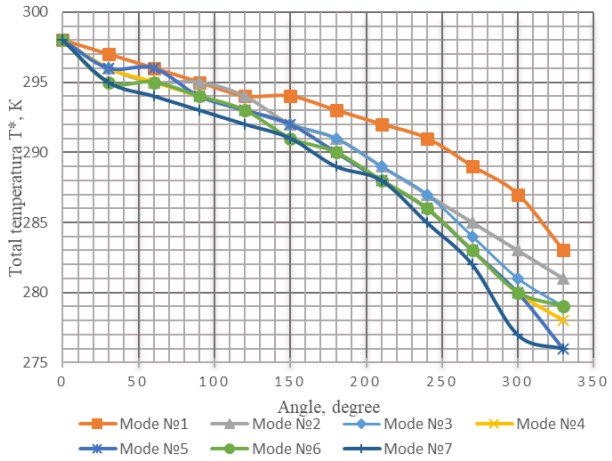

Figure 2 – Distribution of total temperature along the length of flowing part

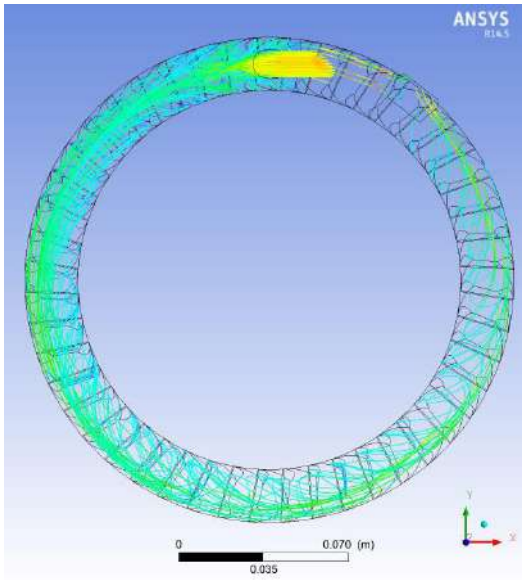

Figure 3 – Visualization of flow of gas in flowing part (mode 1; efficiency 0.366)

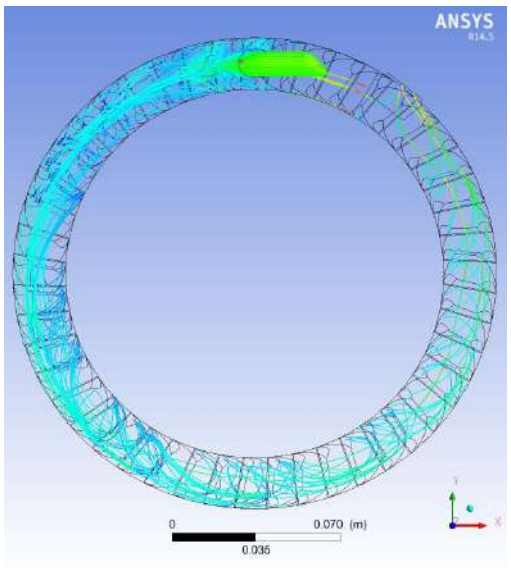

Figure 4 – Visualization of flow of gas in flowing part (mode 6; efficiency 0.315)

5 Conclusions

Experiment in steady-state mode in all modes had high values of absolute residuals. However, all of them are localized in the area of the shut-off, what indicates the complex and uncertain nature of flow in this area of flowing part.

Experiment in transient mode failed, solutions were not found on all modes. Experiment in transient mode in essence should be the most accurate and closest to the real work process. In addition, the results of the experiment in steady-state mode are input data for the experiment in transient mode. Failure to obtain a solution in a transient mode indicates that results of experiment in steady-state mode need to be confirmed by a real experiment.

References

1. Sergeev, V. N. (1986). *Development vortex actuator with an internal peripheral channel and research of the effect of gas-dynamic and geometric parameters of its effectiveness*. Dissertation Candidate of Engineering Sciences, Moscow.
2. Vaneev, S. M. (1986). *Development and research vortex pneumo drive with an external peripheral channel and nozzle device*. Dissertation Candidate of Engineering Sciences, Moscow.
3. Staroverov, K. V. (1990). *Improvement and research of vortex machine with a peripheral channel in pneumo drive mode*. Dissertation Candidate of Engineering Sciences, Moscow.
4. Vaneev, S. M., & Miroshnichenko, D. V. (2015). Research vortex expansion machine with external peripheral channel using virtual test rig. *Journal of Engineering Sciences*, Vol. 2, Issue 2, pp. B10–B12.
5. Cheban, V. G. (2003). *The small-sized rotational turbine as a driving of hydrodynamic purifier of thick liquids*. Dissertation Candidate of Engineering Sciences, Sumy State University, Sumy.
6. Baybakov, O. V. (1981). *Vortex hydraulic machines*. Moscow, Machinery.

Дослідження робочого процесу вихрової розширювальної машини з бічним каналом

Бондар А. В.[*], Ванєєв С. М.

[1] Сумський державний університет, вул. Римського-Корсакова, 2, 40007, м. Суми, Україна

Анотація. На газорозподільних станціях втрачається велика кількість енергії стислих газів. В таких випадках корисну потужність отримують за допомогою турбодетандера. Проблема полягає в тому що, є велика потреба в турбодетандерах потужністю до 500-700 кВт. Для цих потужностей турбодетандер при використанні класичних турбін виходить високообертовим, складним, дорогим, з терміном окупності, який становить більше двох років. Вирішення цієї проблеми вбачається у створенні турбодетандерних установок на основі вихрових машин.

Перспективним типом вихрових розширювальних машин є машини з бічним каналом, так як відомі дослідження, результати яких показали високі значення ККД вихрових гідравлічних турбін з бічним каналом.

Метою даної статті є дослідження робочого процесу вихрової розширювальної машини з бічним каналом шляхом проведення числового експерименту в програмному комплексі ANSYS CFX.

Результати досліджень показали, що значення ККД вихрової розширювальної машини з бічним каналом більше ніж у вихрової розширювальної машини з периферійним каналом (реальний експеримент).

Ключові слова: вихрова розширювальна машина, коефіцієнт корисної дії, турбодетандер, числовий експеримент, ANSYS CFX, робочий процес.

JOURNAL OF ENGINEERING SCIENCES
ЖУРНАЛ ІНЖЕНЕРНИХ НАУК
ЖУРНАЛ ИНЖЕНЕРНЫХ НАУК
Web site: http://jes.sumdu.edu.ua
DOI: 10.21272/jes.2018.5(1).e3 Volume 5, Issue 1 (2018)

UDC 621.314

Overview of Control Techniques for Multicellular Converter

P. Djondiné

The University of Ngaoundéré, Faculty of Science, Department of Physics, B.P. 454, Ngaoundéré, Cameroon

Article info:
Paper received: February 21, 2018
The final version of the paper received: April 30, 2018
Paper accepted online: May 5, 2018

*Corresponding Author's Address:
pdjondine@yahoo.fr

Abstract. The structure multicellular converters, which appeared at the beginning of the 1990s, makes it possible to share the constraints in tension and it also improves the harmonic contents of the wave forms. To benefit as well as possible from the large potential of the multicellular structure, an appropriate distribution of the voltages crossing each cell is needed. These converters are drastically used in industry as well as in research. One of the main limitations of these converters is unregulated supply of voltage and current. To overcome these problems there are various control techniques used in combination with these converters. In this review we summarized few of these control techniques. Some well known control techniques are PID, sliding mode control and Petri nets control. We have also paid attention on the advantages and disadvantages of these techniques with basic operating principle.

Keywords: multicellular converter, PID, sliding mode, Petri Nets control.

1 Introduction

Power electronics knew important technological developments thanks to the improvements of semiconductors, power components and systems of energy conversion. Among these systems, multicellular converters, which are built upon a series-association of elementary commutation cells, are more and more used in industrial applications. Indeed, they are characterized by their modularity and high efficiency. However, the major drawback of this kind of converter is their control complexity. This structure, which appeared at the end of the 20th century [6], makes it possible to share the constraints in tension and it also improves the harmonic contents of the wave forms [4].

Moreover, modeling is a very important step for control laws and observers synthesis. In literature, several approaches have been considered to develop methods of control and observation of the multicell converter. Initially, models have been developed to describe their instantaneous [5], harmonic [6] or averaging [1] behaviors. These various models were used for the development of control laws in open-loop [10].

This control is very simple, to ensure the functioning of the converter with pulses delayed by 1/3 to the period relative to each other. But it can do more to ensure the stability of tension capacitors. It will be necessary to use a closed loop control that take into account the evolution of the capacitor voltages and can meet the requirement to control and maintain voltage levels defined [2]. In the other hand, the following model must be adequately simple to allow real time control but enough precise to achieve the desired behavior. Because it's based on continuous variables and discrete variables, Multicell converter modeling is claimed to be difficult [7, 8]. According to previous studies, three types of models could be found.

The average model consists of calculating average value of all variables during one sampling period. Nevertheless, this model cannot represent the capacitors terminal voltage natural balancing. The harmonic model consists of the calculation of the voltage harmonic phases and amplitudes by considering the charging current in steady-state operation. The instantaneous model deals with time-evolution of all variables including the switch states (discrete location). This model is hard to use as controllers and observers design is impossible since the converter is not a continuous system but the mixture of continuous and discrete systems [2, 3].

For a better exploitation of controller possibilities, hybrid modeling allows multicell converters using analysis and synthesis powerful tools [9].

Aim of this paper is to have an overview of all the control techniques used to facilitate the performance of various kinds of multicellular converters. We will briefly discuss the basic concept, advantages and disadvantage of each control technique throughout this review.

2 Research Methodology

2.1 PID control

The main objective of the PID control law is to regulate the output current and all voltages across the flying capacitors.

PID control is one of the oldest and classical control technique used for DC-DC converters. It uses one of its families of controllers including P, PD, PI and PID controllers (Figure 1). These different combinations will gives us various ways to regulate dc power supply in these converters. Due to the various advantages of PID it is widely used for industrial applications in the area of power electronics. One of the main causes for the use of this classical technique still in industrial applications is easy implementation of tuning method like Ziegler-Nichols tuning procedure by which we can easily optimize proportional, integral and derivative term of this control method needed to achieve a desired closed-loop performance. A proportional integral derivation controller is a generic control loop feedback mechanism widely used in industrial control system as well as in research. This approach is often viewed as simple, reliable, and easy to implement.

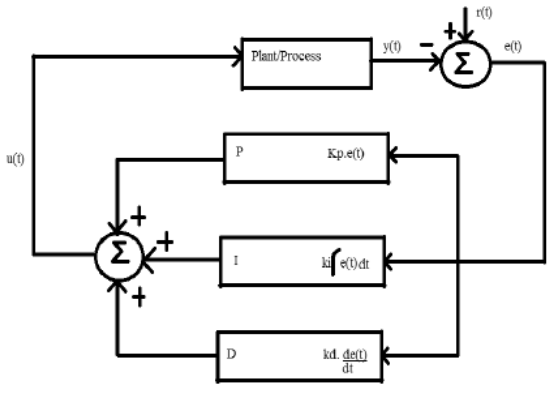

Figure 1 – Block diagram of PID controller

Some important advantages and disadvantages of PID control technique are:

Advantages of PID controllers:

– they are easy and simple to implement;

– easy to understand;

– reliable for linear systems.

Disadvantages of PID controllers:

– they do not reliable and satisfactorily in case of nonlinear systems;

– it shows longer rise time when overshoot in output voltage decreases;

– they suffer from dynamic response and produces overshoot affecting the output voltage regulation of converter.

Applied to a two cells converter [11], it results that the capacitor voltages and the output current reach the desired reference values without static errors (Figure 2). To test the robustness of the control the authors consider the variation of the input voltage and the load resistance. From these variations, we can deduce that the PID control law is suitable for the studied converter. Moreover, it rejects external perturbations and some controlled system parameters variations. Thus, we can confirm that the PID control applied to a multicellular converter is robust for the considered load variation.

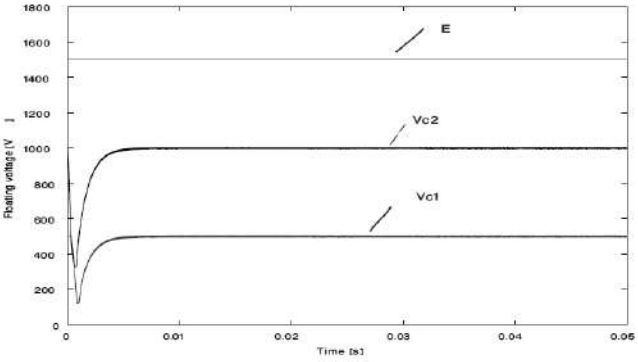

Figure 2 – Floating voltage V_{C1}, V_{C2} and E evolutions

2.2 Sliding Mode Control

SM controller is a type of non-linear controller. It is employed and adopted for controlling variable structured systems. It is very easy to implement as compared to other types of nonlinear and classical controllers. Two important steps in SM control is to design a sliding surface in state space and then prepared a control law to direct the system state trajectory starting from any arbitrary initial state to reach the sliding surface in finite time, and at the end it should arrive to a point where the system equilibrium state exists that is in the origin point of the phase plane. There are three important factors responsible for the stability of SM controllers, existence, stability, and hitting condition. Sliding Mode control principle is graphically represented in Figure 3.

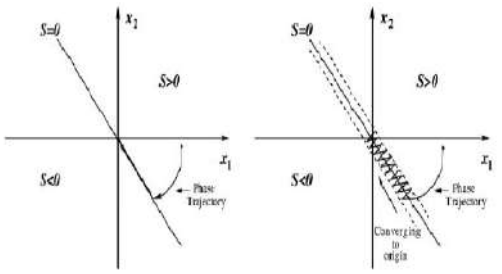

Figure 3 – Graphical representation of SM control

The sliding line divides the phase plane into two main regions shown in the figure. Each region is represent by a switching state and when the trajectory comes at the system equilibrium point, in this case the system is considered as stable system. A unique feature of an ideal sliding mode control technique is that it operates at infinite switching frequency. But practical SM controllers are operated at finite switching frequencies only which represent a quasi-sliding mode.

Advantages of SM controllers:

– they show good stability for large line and load variations;

– high robustness;

– fast dynamic response;

– simple and easy implementation.

Disadvantages of SM controllers:

– SM controlled converters suffers from switching frequency variation;

– these controllers are not available in integrated-circuit (IC) forms for their power electronic applications;

– there is no systematic procedure available for the design of sliding mode controllers.

Sliding mode control become more and more attractive to control for multi-cell converter. Applied to a two cells converter connected to a nonlinear load, the control keeps the load current constant at the desired I_{ref} value and the floating voltages change with the variation of the input voltage [12] (Figure 4). The control aims to insure the convergence of switching surfaces S_i to zero, to allow the reaching of the state variables to their references.

In [13] the robustness of the SMC was tested with a load resistance variation of 50 %. In this paper, the performances of the sliding mode control for load variation are satisfactory.

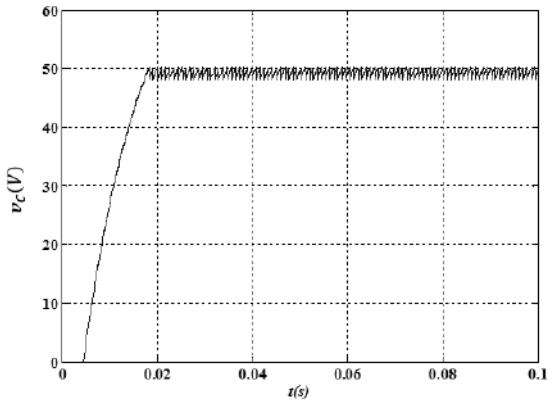

Figure 4 – Floating voltage V_C evolutions obtained by application of the sliding mode control

2.3 Petri nets control

The method applied to a two cells converter connected to a nonlinear load is illustrated in Figure 5

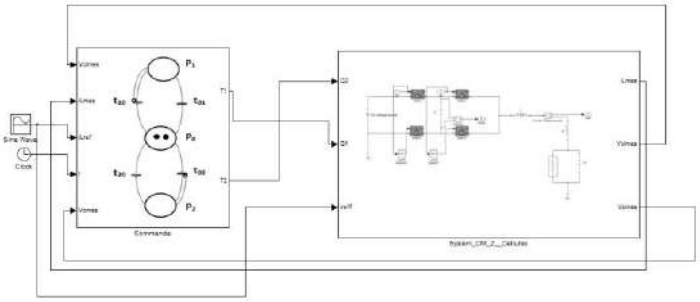

Figure 5 – Global structure of the Petri net control

The control consists of two parts, a continuous and a discrete. The first is based on a classical PI control loop for regulating the output voltage. This loop has as input the error $E_1 = v_{Cref} - v_C$ and i_{Lref} as output a current. The second control loop is done by a Petri net whose mission is the current regulation I_s to value i_{Lref} calculated by the PI. The current regulation is followed by a voltage balancing to ensure a better distribution of the latter in each cell. This algorithm is developed in order to control the system, in case it has an imbalance in the voltage of cells. The transition from one place to another is dependent on the voltage state, current i_{Lref} and chopper configurations. The closure of the switch of the cell (Celli) depends on the validation of the transition t_{i0} and the elapsed delay d_i.

This delay models the time allowed between two successive commutations, it is based on the technology used for making the switch. For our work we took the same delay ie $d = d_1 = d_2$. In the Petri the role of two arcs inhibitors, is to prevent the presence of more than one, token in places P_1 and P_2.

The imbalance of the cells voltage is one of the major problems of this type of converter, the de-balancing causes a failure of the voltage source if the string current exceeds the current permitted entry. Pollution of the power system harmonics reactions is one of the other consequences of this problem; we will show in the simulation result the contribution of this approach. In [14], the simulation results show the convergence of the current branch to a neighborhood of the value of the nominal operating current response times over (Figure 6). The evolution of the input current exhibited a remarkable performance of Petri nets control on pollution network lover converter input to the conventional control. Applied to a two cells converter associated to a nonlinear load, the floating capacitor voltage and the output current reach the desired reference values (Figures 6–7)

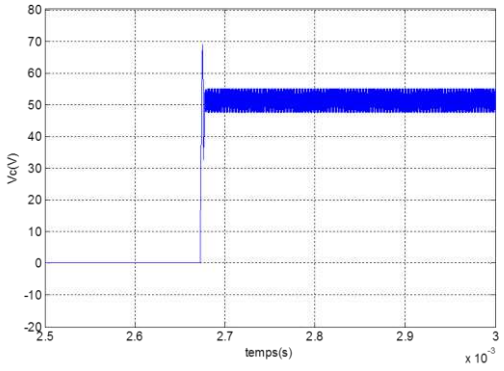

Figure 6 – Floating voltage v_C evolutions obtained by application of the Petri nets control

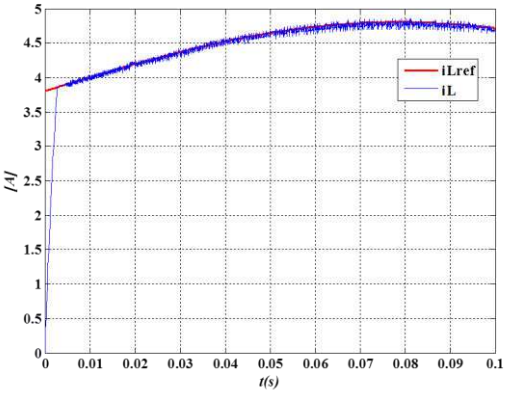

Figure 7 – Current load i_L evolutions obtained by application of the Petri nets control

3 Conclusions

In this review we provided an overview of control techniques used for multicellular converters. We briefly explained the basic concepts of each control techniques. We highlighted the advantages and disadvantages of each technique. We can conclude that each control techniques have their own limitations and drawback. It depends on our need that what kind of control technique is needed for particular purpose. There is still scope for the development of more reliable and efficient control technique.

References

1. Sadigh, A. K., Hosseini, S. H., & Gharehpetian, G. B. (2010). Double flying capacitor multicell converter based on modified phase-shifted pulsewidth modulation. *IEEE Transactions on Power Electronics,* Vol. 259, Issue 6, 1517–1526.
2. Ghanes, M., Bejarano, F., & Barbot, J.P. (2009). On sliding mode and adaptive observers design for multicell converter. *in Proceedings of the 2009 IEEE ACC,* 2134–2139.
3. Lienhardt, A. M., Gateau, G., & Meynard, T. (2007). Digital sliding-mode observer implementation using FPGA. *IEEE Trans. Industrial Electronics,* Vol. 54, Issue 4, 1865–1875.
4. Ajami, A., & Armaghan, M. (2010). Vector control of induction motor drive based on mixed multi-cell cascaded inverter. *International Review on Modelling and Simulations,* Vol. 3, Issue 5, 767–774.
5. Ladoux, P., Machmoum, M., & Batard, C. (2009). Harmonic currents compensation for 1.5 kV DC railway substations. *International Review of Electrical Engineering,* Vol. 4, Issue, 380–391.
6. Stala, R., Pirog, S., Mondzik, A., Baszynski, M., Penczek, A., Czekonski, J., & Gasiorek, S. (2009). Results of investigation of multicell converters with balancing circuit, *IEEE Trans. Industrial Electronics,* Vol. 56, Issue 7, 2620–2628.
7. Patino, D., Riedinger, P. & Iung, C. (2008). Predictive control approach for multicellular converters, *in Proceedings of the 2008 IEEE IECON,* 3309–3314.

8. Meynard, T. A., Foch, H., Thomas, P., Courault, J., Jakob, R. & Nahrstaedt, M. (2002). Multicell converters: basic concepts and industry applications, *IEEE Trans. Industrial Electronics,* Vol. 49, Issue 5, 955–964.
9. Gateau, G., Fadel, M., Maussion, P., Bensaid, R. & Meynard, T. A. (2002). Multicell converters: active control and observation of flying-Capacitor voltages, *IEEE Trans. Industrial Electronics,* Vol. 49, Issue 5, 998–1008.
10. Ghanes M., & Barbot J. P., (2009). On sliding mode and adaptive observers design for multicell converter, *IEEE American Control Conference, St Louis, Missouri, USA*.
11. Ben Said, S., Ben Saad, K., & Benrejeb, M. (2014). On two control strategies for multicellular converters, *International journal of control, energy and electrical engineering (CEEE)* Vol. 1, 37–42.
12. Djondiné, P., Barbot, J.-P., & Ghanes, M. (2018). Comparison of Sliding Mode and Petri Nets Control for Multicellular Chopper, *International Journal of Nonlinear Science*, Vol. 25, Issue 2, 67–75.
13. Ben Said, S., Ben Saad, K., & Benrejeb, M. (2013). Sliding mode control for a multicell converters, *International Conference on Control, Engineering and Information Technology (CEIT'13), Proceedings Engineering & Technology*, Vol. 2, 39–44.
14. Amghar, B., Darcherif, M., Barbot, J.-P., & Gauthier, P. (2012). Modeling and control of parallel multicell chopper using Petri nets, *8th Power Plant and Power System Control Symposium – PPPSC*.

Огляд методів контролю багатокоміркового перетворювача

Ф. Джондіне

Університет м. Нгаундере, B.P. 454, м. Нгаундере, Камерун

Анотація. Конструкція багатокоміркового перетворювача, що з'явилася на початку 1990-х років, дає змогу розподілити обмеження напруги, а також покращує гармонічний вміст хвиль. Для максимально ефективного використання потенціалу багатоклітинної структури, необхідно забезпечити відповідний розподіл напруги для кожної комірки. Такі перетворювачі широко використовуються у промисловості й наукових дослідженнях. Одним із основних їх є нерегульоване постачання напруги та струму. Для подолання цих проблем існують різні методи керування, які використовуються для цих перетворювачів. У цій статті коротко описані деякі з цих методів керування. Деякі добре відомі методи керування – це застосування ПІД-регулятора, режиму ковзання, та управління мережами Петрі. Особлива увага приділена перевагам і недолікам цих методів із основним принципом роботи.

Ключові слова: багатоклітинний перетворювач, ПІД-регулятор, режим ковзання, управління мережею Петрі.

JOURNAL OF ENGINEERING SCIENCES
ЖУРНАЛ ІНЖЕНЕРНИХ НАУК
ЖУРНАЛ ИНЖЕНЕРНЫХ НАУК

Web site: http://jes.sumdu.edu.ua

DOI: 10.21272/jes.2018.5(1).f1 Volume 5, Issue 1 (2018)

UDC652.1:586.24

Analysis of the Application of the Galvanic Circuits in Schemes of the Catodic Protection for Underground Papelines

Azyukovsky A. A., Didevich E. A.*

State Higher Educational Institution "National Mining University", 19 Dmytra Yavornytskoho Av., 49600, Dnipro, Ukraine

Article info:
Paper received: October 26, 2017
The final version of the paper received: January 4, 2018
Paper accepted online: February 24, 2018

***Corresponding Author's Address:**
evgeniya.didevich@gmail.com

Abstract. The possibility of using anode earthing in an assembly with a container is considered. Ensuring the integrity of the pipeline is a topical issue in connection with the environmental and economic consequences. The process of pipeline protection is accompanied by the removal of metal particles, at the electronic level. When creating a potential difference, the current will shift from the anode to the cathode. In the process of this shift electrons from the anode earthing switch are moved to the pipeline under the influence of an electromagnetic field. It thereby destroying the anode and expanding the metal elements under protection. Description of galvanic capacitive solution for cathodic protection stations is executed. To exclude the effect of the electrochemical protection on the cathode and, thus, improve the protection of the pipeline.

Keywords: cathodic protection station, underground metal pipeline, electrochemical corrosion.

1 Introduction

Ensuring the integrity of the pipeline is a topical issue in connection with the environmental and economic consequences. Currently, one of the effective methods of protection is the use of cathodic protection stations (HVAC). The article considers the possibility of using anode earthing in the assembly with the container. It contains a titanium dioxide magnesium anode, mounted inside a galvanized tube and filled with coke oven.

The urgency of considering the use of the anode in the assembly, in increasing the term of its operation, as well as improving agro-ecological indicators.

Consider using anode earthing plug in a container assembly. It contains a titanium dioxide magnesium anode, mounted inside a galvanized tube and filled with coke oven, which will increase the life of the anode earthing, as well as improve the agro-ecological parameters. Perform a description of the electrical system anode-ground-object that is protected. Consider the process that generates protective capability.

2 Materials and Methods

The basis of the work of electrochemical protection is the process of suppressing the influence of anode currents cathode due to the work of an external source. When the current flowing on an object that is protected more than a drain, an anodizing process occurs.

Anodizing allows you to create a thin, oxide film on the surface of the metal that acts as a protective layer. The method is based on the physical properties of the current of the galvanic pair.

When a difference in potentials between the metals is created and the current from the tread flies to the protected object, in our case the pipeline. This process is also accompanied by the removal of metal particles, at the electronic level. When creating a potential difference, the current will shift from the anode to the cathode. In the process of this shift electrons from the anode earthing switch are moved to the pipeline under the influence of an electromagnetic field. It thereby destroying the anode and expanding the metal elements under protection.

Anodic earthing doped metal (conductor) provided with a large number of free carriers (electrons) to generate electric current (Figure 1). The flow of current occurs due to the motion of electrons from the anode, which is an anode earthing, under the influence of the electromagnetic field on the cathode, in the case considered pipeline [1].

The result of cathodic protection is the excessive formation of ions of hydroxide, that is, the oxidation of the environment occurs. As a result, a violation of the balance of salts in the soil, which leads to the formation of salt deposits on the surface of the pipeline.

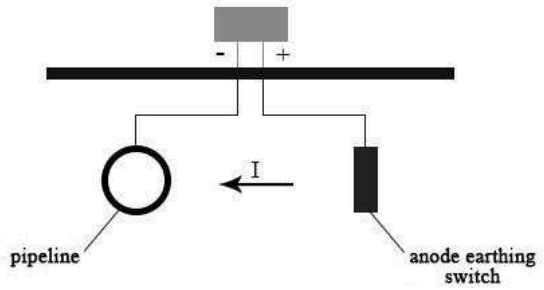

Figure 1 – The classical scheme of cathodic protection

3 Results and Discussion

These factors change the processes of electrochemical protection on the cathode. Complicating the cathode reaction in a double electric layer, due to diffusion problems with the transfer of oxygen. Similarly, a decrease in polarization current or an increase in polarization resistance, due to the growth of the layer of sediments near the protective pipeline [2].

At atomic level, metal is a crystalline lattice, with atoms. Which consist of electrons, negatively charged particles, and positively charged nuclei. Electrons that move freely and are not bound to the atom are valence electrons. Which and determine the behavior of the substance during the chemical process. The places where the electrons are absent are weak. If an ion with a missing electron will interact with the water molecule, the water molecule will be able to suppress this ion. Such a process will take place under the action of electrostatic force of gravity. In addition to the water molecule, which tries to suppress the ion of the ferrum, it acts on the free metal electrons that are attracted to the ion of the metal to free electrons. Free electrons return ions. When the process of dragging the ions comes to equilibrium on the boundary of the metal medium, an exchange current is formed and a double electric layer is formed. In this process, besides water, is still affected by oxygen, which attracts electrons, thus breaking the balance. Oxygen, taking electrons, creates a new negatively charged particle outside the metal. After removing the electron, oxygen contributes to the destruction of the metal [2]:

$$4Fe + 6H_2O + 3O_2 \rightarrow 4Fe(OH)_3. \quad (1)$$

In the case of cathode protection, we obtain an anode medium-cathode chain. Which is characterized by current, voltage and resistance. This can be expressed as follows:

$$I = (\varphi_{ок} - \varphi_{оа}) / Z, \quad (2)$$

where I – current circuit anode-medium-cathode; Z – resistance of the circuit anode-medium-cathode; $\varphi_{ok} - \varphi_{oa}$ – potentials between the anode and the cathode.

$$Z = \sqrt{R^2 + \frac{1}{\omega^2 C^2}}. \quad (3)$$

The resistance in the circuit anode medium cathode will have both an active and a reactive component. The resistance depends on the environment, which means that it is variable and as a result the protection current will not be constant.

The deflection current on the pipeline oxidizes the medium, and leads to the formation of salts around the pipeline. Thus, changing the chemical composition of the soil. Which entails a change in the resistance of the medium and the currents of protection.

The result of cathodic protection is excessive formation of ions of hydroxide OH^-, that is, the oxidation of the environment occurs. As a result, a violation of the balance of salts in the soil, which leads to the formation of salt layer on the surface of the pipeline. These factors change the processes of electrochemical protection on the cathode. Complicating the cathode reaction in a double electric layer, due to diffusion problems with the transfer of oxygen. Similarly, a decrease in the polarization current or an increase in the polarization resistance, due to the growth of the precipitation layer near the protective pipeline [2].

The result of cathodic protection is the excessive formation of ions of hydroxide, that is, the oxidation of the environment occurs. Soil oxidation affects yields, as well as one of the factors influencing the occurrence of diseases in plants. Just an insignificant acidification of the environment, a decrease pH per unit, causing a decrease in the potential of the metal on 0.06 V.

The layer of precipitation near the protective pipeline is the salt. Which leads to deterioration of agro-ecological indicators.

At the moment, a method has been developed that allows the galvanic solution to be maintained without destroying the anode earthing.

In this method, the object consists of a container. It contains a titanium-dioxide magnesium anode, mounted inside a galvanized tube and filled with coke oven.

Anode earthing is protected from the environment, removal of electrons in the soil from its surface does not occur. To anode earthing lead « + » power and an electric field is created around it. What attracts electrons from the environment, that is, the soil. Thus, creating a directed motion of electrons in the medium and the flow of electric current into the pipeline. In this way, the cathodic protection of the pipeline with galvanic decoupling is created. The scheme is shown in Figure 2.

Consider the work of a bipolar and field transistor. In Figure 3, an example of the field and in Figure 3 b, a bipolar transistor is shown.

In a field transistor, it is generally assumed that electrons move from source to drain, and controls the current voltage applied to the p-region, the gate [2].

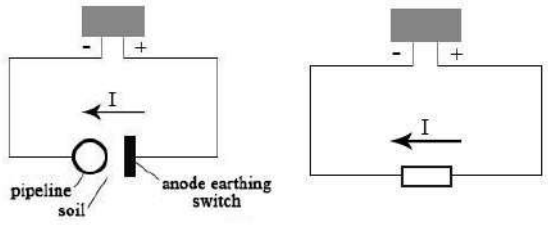

a b

Figure 2 – Cathodic protection of the pipeline with galvanic decoupling

The bipolar transistor of Figure 3b consists of two p-n transitions formed by a layer of semiconductors with impurities. The transition of the collector-base in the bipolar transistor with the common emitter is shifted in the opposite direction, resulting in a potential barrier preventing the main carriers from moving when the key is unlocked and power is not supplied to the base. From emitter to collector, which create current. When the power is fed to the base, the base-emitter transition becomes displaced in the forward direction.

As a result, the electrons from the emitter through diffusion pass through the base to the collector. Non-basic carriers from the base moving to the collector create a collector current in the transistor.

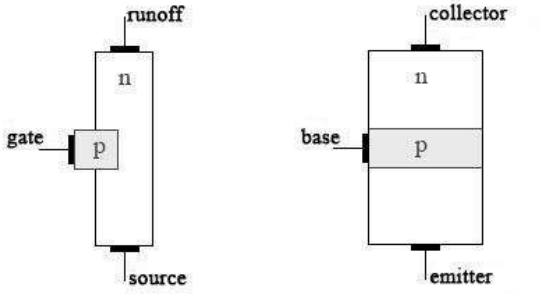

a b

Figure 3 – Field and bipolar transistor: a – schematic representation of the design of the field-type transistor with the n-type channel; b – a schematic representation of the construction of a bipolar p-n-p transistor

With the displaced forward direction of transition, the base-emitter flows through the circle emitter-collector [2]. In the field transistor Figure 4 with p-n transition, the current depends on the size of the depleted layer, near the gate. The shutter is doped to a large extent, compared to the n channel.

Typically, n-type areas are located on both sides of the p-type bar, Fig.5, in which case the conducting channel will be between the two depleted layers. By applying the voltage to the gate, a magnetic field will be formed around it. What kind of electrons will be attracted to the region under the dielectric, after which a channel is formed between the leak and the drain, which will move the electrons. As a result, there will be an electric current [2].

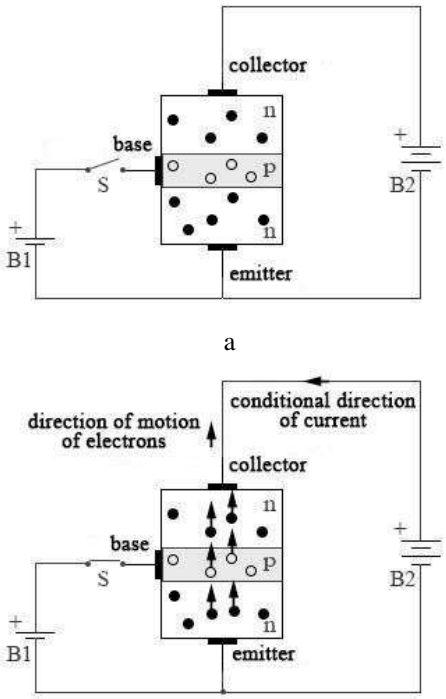

Fig.4 Schematic image of the operation of the bipolar transistor: a – without the base current; b – with the base current

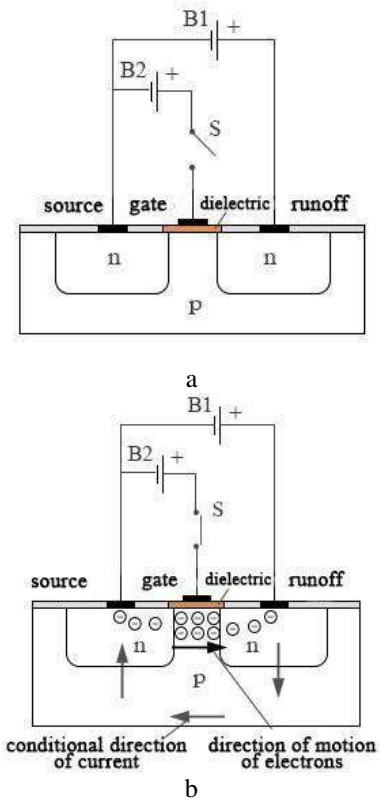

Figure 5 – Schematic image of the field transistor operation: a – without the current; b – with the current

Similarly, one can consider the electrical system of the anode-ground-protected object. Consider the process in which the protective potential is formed.

Important for electrical engineering is the phenomenon in which, the flow of electric current through conductors leads to the emergence in the surrounding space of the magnetic field. Having two conductors with charges $+q$ and $-q$, and driving them in motion with the help of EMF, we get the electric current in the conductor [3].

A magnetic field is formed around such a conductor. Which affects the moving charges, having magnetic moment and polarity, located in the environment between the pipeline and the anode. The magnetic field arranges the orientation of the molecules from the plus to the minus, thereby creating a directed motion.

The medium between the anode and the pipeline is a dielectric. Which when moving to an electric field is able to change its properties. The dielectric molecule consists of different charges of $+q$ and $-q$. In what the -q rotates around + q and their rotation centers converge. When the molecule is affected by an external field, the orbit of the electron is deformed, their centers cease to coincide. The molecule begins to behave like an electric dipole [4].

To protect the pipeline from the steel without a protective coating from corrosion, a certain current density is required. In a sterile neutral state, the current density is in a range of 4.3–16.1 mA/m^2; well aerated neutral soil 21.5–32.5 mA/m^2; dry, well aerated soil 5.4–16.1 mA/m^2; wet soil 16.9–64.6 mA/m^2; sour soil 53.8–161.4 mA/m^2; a soil that supports the activity of sulfate-reducing bacteria 451.9 mA/m^2.

For a pipeline with a protective coating in the soil, the required current is un a range of 0.01–0.2 mA/m^2. As the coating is destroyed, the current density needs to be increased [5].

4 Conclusions

The description of galvanically capacitive solution for cathodic protection stations is executed. This method allows to prevent damage to the balance of salts in the soil. The considered method allows prolonging the life of the anode earthing switch. The creation of a protective current under the influence of the magnetic field, which is the EMF, affects the electrons in the soil. Electrons, which are the charge carriers under the action of EMF, form a directed motion, thereby creating a current of protection. This method also allows improving agro-ecological parameters.

References

1. Johns, M. H. (2006). *Electronics – Practical course*. Moscow, Technosphere [in Russian].
2. Tkachenko, V. N. (2004). *Elektrokhimicheskaya zashchita truboprovodnykh setey*. Moscow, Stroyizdat [in Russian].
3. Bessonov, L. A. (1996). *Teoreticheskiye osnovy elektrotekhniki*. Moscow, Higher School [in Russian].
4. Baskakov, S. I. (1973). *Osnovy elektrodinamiki*. Moscow, Soviet Radio, 1973 [in Russian].
5. Chemistry and chemical technology: Handbook. Retrieved from http://chem21.info/page/238210172011081120132078224074009228204058029200 [in Russian].
6. Strizhevskiy, I. V., Dmitriyev, V. I. (1967). *Teoriya i raschet vliyaniya elektrifitsirovannoy zheleznoy dorogi na podzemnyye metallicheskiye sooruzheniya*. Moscow, Mashinostroyeniye [in Russian].

Аналіз застосування гальванічної розв'язки в схемах катодного захисту підземного трубопроводу

Азюковський А. А., Дідевич Е. А.

Державний вищий учбовий заклад «Національний гірничий університет»,
просп. Дмитра Яворницького, 19, 49600, м. Дніпро, Україна

Анотація. У статті розглянуті можливість використання анодного заземлювача в збірці з контейнером. Забезпечення цілісності трубопроводу, є актуальним питанням у зв'язку з екологічними і економічними наслідками. Процес захисту трубопроводу супроводжується виносом частинок металу, на електронному рівні. При створенні різниці потенціалів, струм буде зміщуватися від анода до катода. У процесі даного зсуву електрони з анодного заземлювача переміщаються до трубопроводу під впливом електромагнітного поля. Тим самим руйнуючи анод і виносячи елементи металу з, що знаходиться під захистом. Виконано опис гальванічної ємнісний розв'язки для станцій катодного захисту. Що б виключити результат впливу процесу електрохімічного захисту на катоді. Тим самим поліпшити захист трубопроводу.

Ключові слова: станція катодного захисту, підземний металевий трубопровід, електрохімічна корозія.

JOURNAL OF ENGINEERING SCIENCES
ЖУРНАЛ ІНЖЕНЕРНИХ НАУК
ЖУРНАЛ ИНЖЕНЕРНЫХ НАУК
Web site: http://jes.sumdu.edu.ua
DOI: 10.21272/jes.2018.5(1).f2 Volume 5, Issue 1 (2018)

UDC 66.074.2

Modelling of Separation and Pneumatic Classification Processes of Airodisperse Systems in the Shelf Device

Varukha D. A.[1], Smirnov V. A.[1], Edl M.[2], Demianenko M. M.[1], Yukhymenko M. P.[1], Pavlenko I. V.[1], Liaposhchenko O. O.[1]

[1] Sumy State University, 2 Rymskogo-Korsakova St., 40007, Sumy, Ukraine;
[2] University of West Bohemia, 22 Univerzitni St., 306 14 Pilsen, Czech Republic

Article info:
Paper received: February 8, 2017
The final version of the paper received: May 24, 2017
Paper accepted online: May 26, 2017

*Corresponding Author's Address:
o.liaposhchenko@pohnp.sumdu.edu.ua

Abstract. The following paper considers the process of classification of polydisperse free-flowing material according to granulometric composition using a gravitational air classificator. There were considered the problems of the purity of separation of polydisperse bulk materials and methods for increasing the degree of separation of particles. There were presented and analyzed obtained the results of the comparison, the data of experimental research and computer simulation of two-phase hydrodynamics flow by CFD methods. The versatility of this complex allowed carrying out simulation of the process using various parameters. As a result, were obtained optimal operating parameters, which were experimentally verified. Based on the obtained data as a result of numerical modelling, the possibility of increasing gas flow influence to the polydispersed material were found, as well as organization along the walls of coarse fraction downward flow by dint of the optimizing the devise design (specifically through the organization of additional inlets for airflow) were obtained.

Keywords: pneumatic classification, grading, bulk material, polydisperse material, two-phase flow, degree of separation.

1 Introduction

In the chemical, mining, building and other industries, the feed stock or finished products are the dispersed materials, the high requirements for fractional composition of which are set. The quality of products obtained as dry chemical, coarse material or granules essentially depends on their homogeneity. The separation of a polydisperse material into narrow fractions with a given grain composition is provided by carrying out the technological process of gravitational pneumatic classification. Fractionation of granular materials is used to remove finely dispersed fractions and to obtain dust-free products, as well as to remove coarse fractions and to obtain a finely dispersed product, and to separate the particulate material from the desired fraction by the particle boundary size, or to separate more than two fractions from the polydisperse material with a predetermined grain size composition. This method is widely used in producing mineral fertilizers, electrode, food, grain processing and other industries.

2 Literature Review

Pneumatic classification is based on the difference in the velocities of the flittering of particles of different fractions in the air stream, as a result of which the initial material is divided into fractions according to the set of the following mechanical properties of particles: size, shape, surface roughness and density, and the possibility to obtain products in dry form reduces the energy capacity of the technological processes that are conducted. The change in the shape of the device's working volume increases the quality of separation, the hydraulic resistance decreases, and consequently the specific productivity and efficiency of the pneumatic classification process increases [1]. It was also found that the continuous supply of material to the device reduces the efficiency of the classification process, at which point the flow is raised by the jet of air will not dissipate. Therefore, clusters of fractions are created, which include both coarse and fine fractions that increases the energy intensity of the installation due to the formation of a sufficient lift [2]. For the rational use of the working space and more effective means and methods of influencing the flow of bulk material, a hardware model has been developed that provides a significant improvement of the separation quality [3]. A high degree of separation in the process of classifying dispersed materials affects not only the consumption rates of raw materials and their quality. However, it determines the own efficiency and the efficiency of other machines

and devices in the technological scheme, which ultimately affects the technical and economic indicators of the production in a whole. Processing phosphorites in the production of phosphoric mineral fertilizers, and raw materials with coarser particles (more than 0.2-0.3 mm) requires longer time for acid decomposition, but with smaller (less than 0.05-0.06 mm) leads to intense dusting in the places of overload. Therefore, such technologies require an additional stage of separation, which are realized in one volume of the device for the pneumatic classification [4]. It has been experimentally determined the optimal design of the bulk material feeding unit in a conical pneumatic classification. The obtained results show the need to install an inclined perforated plate at an angle 30º to the vertical opposite the inlet nozzle of the original mixture, that allows increasing the velocity of the air carrier and reducing the hydraulic resistance. This allowed stabilizing the process of classification, reducing the time to enter the operating mode, and increasing the purity of the bottom product [5]. As a result of carrying out mathematical modelling of the classification process, the calculated dependencies connecting the distribution curve and the dispersed composition of the fission products with the design and regime parameters of the apparatus were obtained. Classifier's operating results and characteristics of the dispersed composition were calculated based on the calculated values of the functions [6]. Finally, due to the need of increasing requirements to the quality of products and saving of raw materials, the development of new principles for organizing the process of gravitational pneumatic classification and developing its theoretical foundations and instrumentation are the topical issue.

3 Research Methodology

3.1 Procedure of laboratory experiment

At the unit (Fig. 1), a series of experiments was carried out using a two-component mixture of fractions -0.315 + 0.2 mm and –0.63 + 0.4 mm.

The initial mixture of bulk material in the amount 0.03 kg/s from the batch hopper 3 and transferred by the belt doser 4 to the lower section of the pneumatic classificator 2. Airflow enters the lower section of the device at a velocity 2.6 m/s, which flow rate is measured by the fill valve 6. Separation airflow is generated using the gas pump 8 by air-sweeping through the device. During the separation process, the fraction is caught by the airflow and settled on them while flowing over inclined shelves.

Further, the dust-air flow enters cyclone 1, where the purified air is discharged into the atmosphere, and the fine particles are trapped and released into the fine fraction collecting hopper 7.

The coarse fraction comes in the lower section of the device to the collecting hopper for the heavy fraction 5. After the separation process, the selected samples are classified into fractions using a set of scalpers. The obtained fractions are weighed. Thus, the degree of mixture separation into fractions is determined.

The photo of the experimental unit is given below.

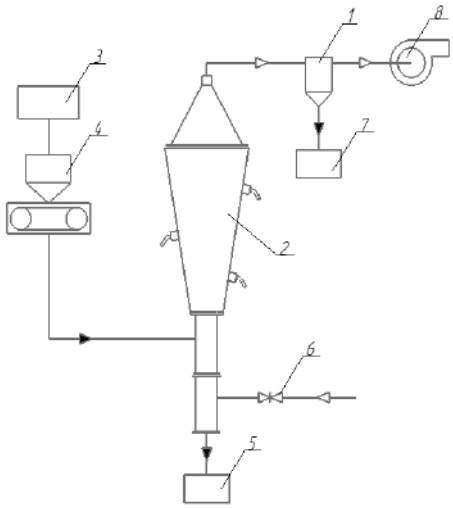

Figure 1 — Technological scheme of the pneumatic classification unit

Figure 2 — Assembled representation of the laboratory unit for pneumatic classification [7]

The results of the experiments are shown in Fig. 3.

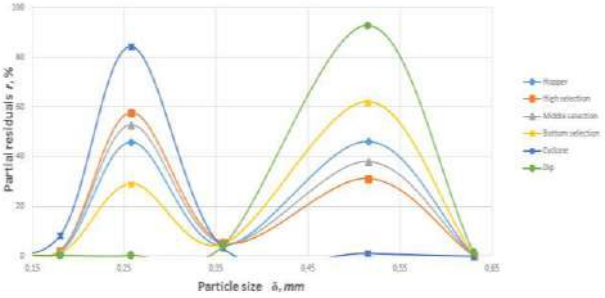

Figure 3 – Sieving curves of initial mixture particles, its entertainment, dip, and material from intermediate selections

3.2 Conducting a computer modelling

The computer modelling of the classification process was used to compare data that were got during the experiment, as well as calculated sizes, construction design of the pneumatic classificator's flow part and sufficient quality of bulk separation in accordance with requirements of the technological regulations with the help of universal software complex ANSYS Workbench.

The calculation of airflow hydrodynamics and determination of the optimum process parameters are conducted with the help of universal software complex ANSYS Workbench and its module "Fluent Flow". All the calculations are based on the finite volume method. In the general case, the equation of motion of polydisperse particles is considered due to the following forces: hydrodynamic resistance from the side of the carrier gas flow, gravity, particles collision with the device's walls and contact elements, particles hitting with each other, particles rotation and their interaction with the gas flow.

The structure of the device's flow affects the dispersed fraction distribution process. The efficiency of the shelf pneumatic classificator is substantially determined by the flow field of the gas stream, which vice versa affects the concentration of the solid phase in the two-phase flow. Considering the character of gas flow is important for establishing the regularities of its interaction with the solid phase that determines the motion speed and particle residence time in the device's operating volume [8].

The computer-aided design system SolidWorks 2017, which tools allowed simulating vessel's flow part is used for building the computer model. The obtained device's geometry applies to ANSYS "Design Modeler" that is set as geometry editor for existing CAD models, as well as for their preliminary processing. ANSYS "Meshing" provides the flexible design of the computational grid that allows generating a qualitative grid with respect to the device's geometry using the three-dimensional tetrahedral, hexahedral and pyramidal elements (Fig. 4). For further simulation process the, Fluent preprocessor is applied for setting the process parameters. The "Pressure-based" solver method is chosen that allows using the Navier-Stokes algorithm based on a pressure parameter. The "Transient" time dependence is set that indicates the non-stationary process running. The calculation process is conducted using the k-ε turbulence model. The k-ε RNG model improves accuracy for whirling flows because it relies on the whirl effect on the turbulence and is more accurate and reliable for a wider class of flows than the standard model. The function "Standard Wall Functions" determines the wall processing that is applied for airflow turbulence simulation. To calculate the flow of dispersed particles in the device's volume, the "Discrete Phase Model" is used. This approach allows setting parameters related to the calculation of the particles discrete phase. The determination of the particle sorting percentage with density 2600 kg/m^3 is carried out in the established channel of particle diameter 0.200-0.315 mm and 0.40-0.63 mm at the air rate 2.6 m/s. The boundary conditions at the input (Inlet 1) for the polydisperse phase discharge 0.03 kg/s; at the inlet (Inlet 2) by the airflow velocity 2.6 m/s (Fig. 3) are set.

The calculation of the process based on the pressure is carried out using the ANSYS "Fluent". The pressure equation is derived from the continuity equation and conservation of momentum. As far as the control equations are not linear and related to each other, the process of solution involves iterations, where the whole set of control equations is solved multiply until the solution converges.

The ANSYS "CFD-Post" allows obtaining the values of the main parameters (gas velocity, solid particles, hydraulic resistance and distribution of the solid phase in the vessel's volume).

Sizing	
Size Function	Curvature
Relevance Center	Coarse
Max Face Size	3,e-003 m
Mesh Defeaturing	Yes
Defeature Size	Default (1,5e-005 m)
Transition	Slow
Growth Rate	Default (1,20)
Span Angle Center	Fine
Min Size	Default (3,e-005 m)
Max Tet Size	Default (6,e-003 m)
Curvature Normal Angle	Default (18,0 œ)
Bounding Box Diagonal	1,73210 m
Minimum Edge Length	2,e-003 m
Quality	
Target Skewness	Default (0.900000)
Smoothing	Medium
Mesh Metric	Skewness
Min	1,3057e-010
Max	0,95538
Average	0,33389
Standard Deviation	0,1964

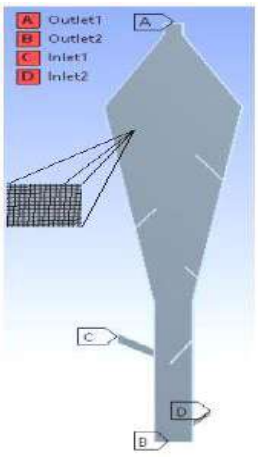

Figure 4 – The main parameters of the computational grid and boundary conditions of the computational model: A – outlet of the finely dispersed phase to the carryover; B – outlet of the coarse phase to the trough; C – inlet of the polydisperse material for separation; D – inlet of the airstream

4 Results and Discussion

The pressure distribution (Fig. 6) and velocity fields (Fig. 5) were obtained as a result of computer modelling of classification process. These results made possible the determination of the device operation hydrodynamic features and their effect to the classification process efficiency. Confirmed optimum shape of the flow part contributes to the formation of stable vortices in the volume of the apparatus (Fig. 5). After carrying out experimental estimation the positive influence effect of the perforated contact elements to the air flow structure and the allocation of solid particles in the volume of devise were confirmed. The volume concentrations of the particles on the contact elements, as well as outgoing particles into the entrainment and dip were calculated during the simulation. The possibility of separating polydisperse materials in the volume of one device without the usage of sequentially located devices was confirmed comparing obtained and experimental data.

The air flow velocity field in the flow part of device was determined (Fig. 7). This approach allowed specifying operating, technological and design parameters for the classification process of polydispersed materials. This approach ensures an efficiency of the process and high-degree of separation in the shelf device.

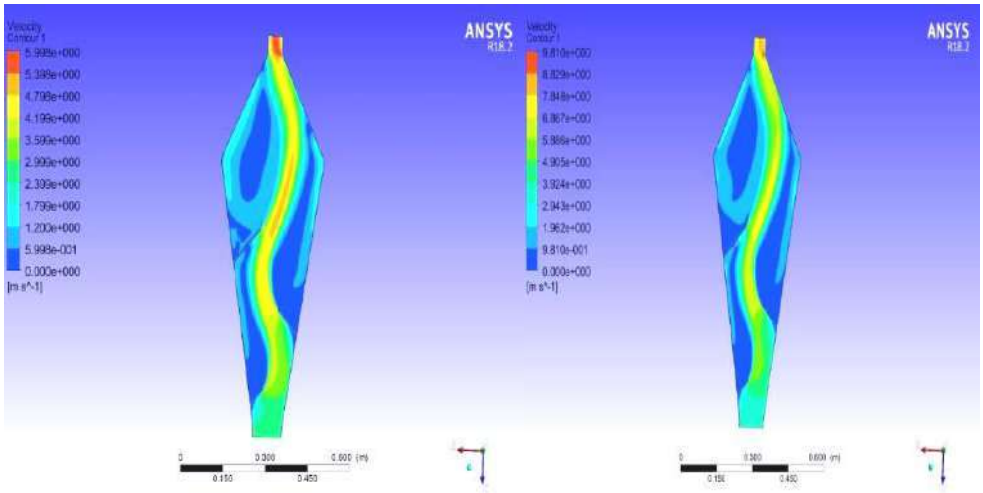

a b

Figure 5 – Contours of air flow velocity for particles d = -0.315 + 0.2 mm, V = 2,6 m/s (a), and d = –0.63 + 0.4 mm, V = 3.784 m/s (b)

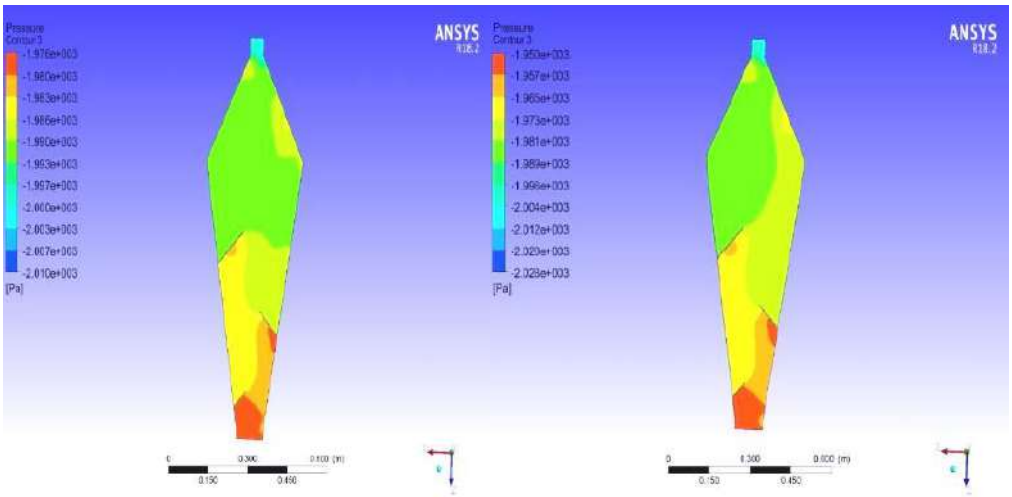

a b

Figure 6 – Contours of internal pressure for particles d = -0.315 + 0.2 mm, V = 2,6 m/s (a), and d = –0.63 + 0.4 mm, V = 3.784 m/s (b)

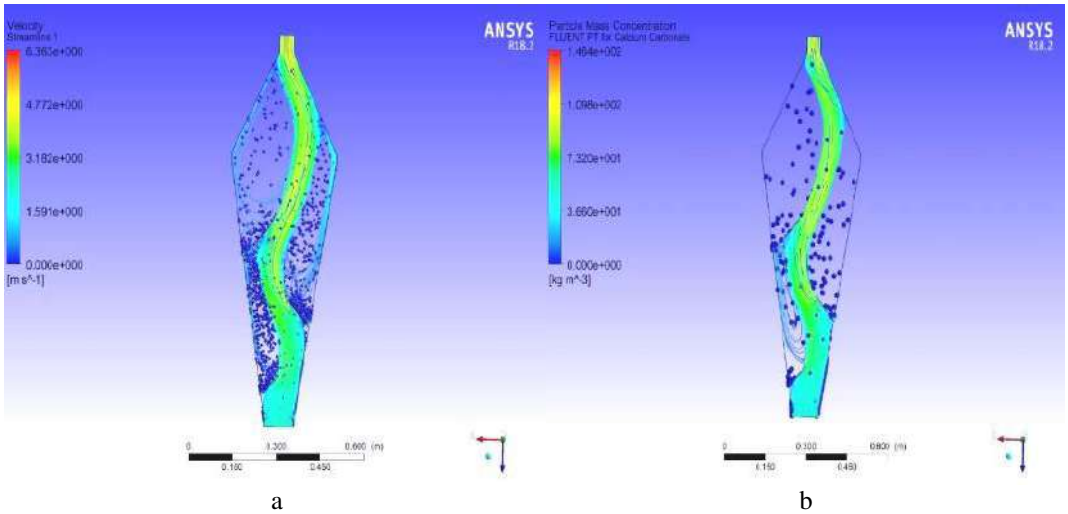

a b

Figure 7 – Air flow velocity streamlines for particles d = -0.315 + 0.2 mm, V = 2.6 m/s (a), and d = –0.63 + 0.4 mm, V = 3.784 m/s (b)

5 Conclusions

Based on the obtained data as a result of numerical modelling, the possibility of increasing gas flow influence to the polydispersed material were found, as well as organization along the walls of coarse fraction downward flow by dint of the optimizing the devise design (specifically through the organization of additional inlets for airflow) were obtained. The future research will be aimed at using CFD simulation methods for testing the achieved results by the creation of a computational model with new design features.

6 Acknowledgements

The main part of the presented research was obtained at the Faculty of Technical Systems and Energy Efficient Technologies of Sumy State University (Sumy, Ukraine) within the project "Development and implementation of energy efficient modular separation devices for oil and gas purification equipment" (No. 0117U003931) ordered by the Ministry of Education and Science Ukraine.

Numerical simulations were provided by the Department of Power System Engineering at the Faculty of Mechanical Engineering, University of West Bohemia (Pilsen, Czech Republic) within the scholarship programme "Numerical simulation of dynamic processes of vibration-inertial separation of gas-liquid flows in dynamic separation devices".

References

1. Smirnov, V. A., & Yukhimenko, N. P. (2013). Multi-product pneumatic classification of granular materials. *Proceedings SWorld*, Volume 11, Issue 2, P. 102.
2. Yoshida, H., Fukui, K., Yoshida, K., & Shinoda, E. (2001). Particle separation by Iinoya's type gas cyclone. Powder Technology, Vol. 118, pp. 16–23.
3. Peukert, W., & Wadenpohl, C. (2001). Industrial separation of fine particles with difficult dust properties. Powder Technology, Vol. 118, Issues 1–2, 136–148.
4. Tsuji, H., Makino, H., & Yoshida, H. (2001). Classification and collection of fine particles by means of backward sampling. Powder Technology, Vol. 118, Issues 1–2, 45–52.
5. Suzuki, M., Sato, H., Hasegawa, M., & Hirota, H. (2001). Effect of size distribution on tapping properties of fine powder. *Powder Technology*, Vol. 118, Issues 1–2, 53–57.
6. Sibanda, V., Greenwood, R. W., & Seville, J. P. K. (2001). Particle separation from gases using cross-flow filtration. *Powder Technology*, Vol. 118, Issues 1–2, 193–202.
7. Yukhimenko, M., & Litvinenko, A. (2016). Pneumatic classification of the granular materials in the "Rhombic" apparatus. *Journal of Manufacturing and Industrial Engineering*, Vol. 2, 1–3.
8. Ambrós, W. M., Cazacliu, B. G., & Sampaio, C. H. (2016). Wall effects on particle separation in air jigs. *Powder Technology*, Vol. 301, 369–378.

Моделювання процесів сепарації та пневмокласифікації аеродисперсних систем у поличковому апараті

Варуха Д. А.,[1], Смирнов В. А.[1], Едл М.[2], Дем'яненко М. М.[1],
Юхименко М. П.[1], Павленко І. В.[1], Ляпощенко О. О.[1]

[1] Сумський державний університет, вул. Римського-Корсакова, 2, 40007, м. Суми, Україна;
[2] Західноческький університет, вул. Університетська, 22, 306 14, м. Пльзень, Чехія

Анотація. У представленій роботі розглядається процес класифікації полідисперсного сипучого матеріалу за заданим гранулометричним складом із використанням гравітаційного пневмокласифікатора. Розглядались проблеми якості поділу полідисперсних сипучих матеріалів і способи підвищення ступеня поділу частинок. Представлені і проаналізовані отримані у результаті порівняння дані експериментального дослідження та комп'ютерного моделювання гідродинаміки двофазного потоку CFD-методами. Універсальність даного комплексу дозволила здійснити моделювання процесу з використанням варіювання параметрів. У результаті отримані оптимальні робочі параметри, які були експериментально апробовані. На підставі отриманих даних у результаті чисельного моделювання виявлена можливість збільшення впливу потоку газу на полідисперсний матеріал, а також його розподіл уздовж стінок потоку вниз по грубій фракції за рахунок оптимізації розробленої конструкції, зокрема через наявність додаткових впускних отворів для повітряного потоку.

Ключові слова: пневмокласифікація, гранулометричний склад, сипучий матеріал, полідисперсний матеріал, двофазний потік, ступінь поділу.

JOURNAL OF ENGINEERING SCIENCES
ЖУРНАЛ ІНЖЕНЕРНИХ НАУК
ЖУРНАЛ ИНЖЕНЕРНЫХ НАУК
Web site: http://jes.sumdu.edu.ua
Volume 5, Issue 1 (2018)

JOURNAL OF ENGINEERING SCIENCES
ЖУРНАЛ ІНЖЕНЕРНИХ НАУК
ЖУРНАЛ ИНЖЕНЕРНЫХ НАУК
Web site: http://jes.sumdu.edu.ua
DOI: 10.21272/jes.2018.5(1).h1 Volume 5, Issue 1 (2018)

UDC 502/504

Climate Change Modeling in the Context of Urban Decarbonization Strategy

Kofanova O.

National Technical University of Ukraine "Igor Sikorsky Kyiv Polytechnic Institute", 37 Peremohy Av., 03056, Kyiv, Ukraine

Article info:
Paper received: January 16, 2018
The final version of the paper received: February 7, 2018
Paper accepted online: February 23, 2018

*Corresponding Author's Address:
alexina555@gmail.com

Abstract. The anthropogenic influence on the Earth's climate is growing and the risks of the irreversible impacts on ecosystems also increase. This paper is focused on the long-term prediction of the climate change in Kyiv region and decarbonization strategy development. The bcc-csm1-1 and IPSL-CM5A AR 5 climate models were used. It was determined that the average annual temperature in Kyiv region under the RCP 8.5 high-emission future scenario will increase noticeably (up to 23.8 °C according to the IPSL-CM5A model) while at the RCP 2.6 low-emission future scenario it won't change significantly (maximum value of 11.5 °C according to the IPSL-CM5A model). So, the research recommendations were organized in order to develop decarbonization strategy for Ukraine that will help to reduce emission levels and reach the RCP 2.6 scenario. The practical and scientific value of the work is specified by the fact that obtained results take into account updated information about climate changes and can be used to increase the awareness of citizens about it. The results of the study confirm the existence and danger of the problem of climate change and show how GHG emissions can affect the ecological balance of the urbanized ecosystem. The risks of the certain natural disasters occurrence were also considered. It was found that amplification of the natural hazards is one of the main dangers of the RCP 8.5 scenario for the world, Ukraine and Kyiv region.

Keywords: climate modeling, global warming, decarbonization, climate change, natural hazards.

1 Introduction

In 2014 the Intergovernmental Panel on Climate Change (IPCC) that was created by UNEP and WMO has published the most recent Fifth Assessment Report (AR 5) with the newest information about climate changes and global warming (GW) [1]. The IPCC Synthesis Report confirms that anthropogenic influence on the Earth's climate is growing and the consequences can be observed across all continents and oceans on the planet. So, the risks of the irreversible impacts on ecosystems also increase [2].

Ukrainian industrial and transport complexes consume too much fossil fuel which leads to the significant emissions. According to the State Statistics Service of Ukraine, in 2016 carbon dioxide emissions to the atmosphere from the stationary pollution sources reached 150581.0 thous. t, which is 8.4 % more than in 2015. At the same time, the total amount of all other pollutants and greenhouse gases (GHG) emissions from stationary sources reached 3078.1 thous. t, which is 7.7 % more than in 2015. Pollution from the mobile sources is also considerable – carbon dioxide emissions into the atmosphere in 2015 reached 23139.8 thous. t while emissions of all other pollutants and GHG from mobile sources reached 1663.9 thousand tons [3].

Thus, to prevent climate changes it is important to reduce the usage of fossil fuels. But today they are the key energy source for our country and it is too hard to abandon them instantly. So, it is essential to develop a governmental decarbonization strategy in order to reduce the percentage of fossil fuel usage and, in turn, increase the percentage of alternative energy, such as wind or solar energy, biofuels, etc.

2 Literature Review

Mathematical modeling is widely used in GW and climate change assessment. In particular, in [4] BCC_CSM1.1 climate model was used to make predictions for East Asia under various RCP (Representative Concentration Pathways). In [5] Earth system models were used to assess the sensitivity of surface warming to carbon emissions from fossil fuel; in [6] − global TIMES model was used to estimate the impacts of technology influence on various aspects including CO_2 emissions. In [7] the analysis of the surface temperature modeling data from global climate models, CRU and regional climate model REMO was conducted.

It was found that considered models take into account different sets of factors affecting the climate and in different ways. The choice of the factors depends on the purposes of the model developers. The scale (global or regional) is also an important aspect because it is equally important to describe changes at the planetary level and to provide a clear understanding of the consequences for specific regions. It was also discovered that models have different simulation periods and their predictive capabilities are not limited by surface temperature – the distribution of precipitation, humidity, snow and plant cover, etc. around the world can be also forecasted.

According to [8], in comparison with the previous model generation, IPCC AR 5 climate models have an improved ability to simulate surface temperature and can predict a climate state that significantly differs from the present one. AR 5 models take into account the more rapid warming in the second half of the 20 century and the cooling following large-scale volcanic eruptions. To provide climate information at the smaller scales, regional downscaling methods are used in AR 5 models. Thus, their usage is considered appropriate for the study.

Today the main unsolved problem is climate change itself. And although the creation of new models and the improvement of the existing ones can't solve it, more accurate modeling results provide an opportunity to understand how specific measures will affect the state of the environment. At the same time, the increased accuracy of models increases the probability of making the right and economically reasonable decision during the development and implementation of the decarbonization strategy.

Despite the fact that climate modeling is often discussed in the literature, currently, this issue is not fully covered. First of all, it is more often considered in a global context, while changes of the specific urbanized ecosystems are not taken into account. In addition, with the development of science and new data appearance, new opportunities arise and more factors can be taken into account. Consequently, improved models provide more accurate results.

3 Research Methodology

The paper is focused on the long-term prediction of the climate change in Kyiv region and decarbonization strategy development. To achieve the aim of the research, the following tasks have been set:

– estimate the surface annual mean temperature changes in the world in general by the bcc-csm1-1 AR 5 model;

– by the bcc-csm1-1 and IPSL-CM5A AR 5 climate models predict the average annual temperature changes in Kyiv region for the long-term period;

– analyze possible consequences of the climate change in Kyiv region and Ukraine for the environment, economy and humans;

– consider international experience due to the decarbonization strategy and give recommendations for Ukraine.

The study is based on the most recent and improved IPCC AR 5 climate models. Two key software instruments were used in the investigation – AR 5 Climate Model Mapper (CMM) [9] and Climate Time Series Browser (CTSB) [10] provided by The University of Chicago. AR 5 CMM is a map making online software and analysis system. It is based on the limited set of the AR 5 models output archive and can be used in order to examine predictions about surface and atmospheric temperatures, specific humidity, precipitation, leaf area index, snow cover etc. in the world [9].

In turn, CTSB collects data about monthly mean temperature records from the NOAA National Climatic Data Center from 7169 weather stations around the world (26 stations in Ukraine, one in Kyiv). These data can be compared with the AR 5 climate model results, obtained from computational grids in order to correspond closely to the meteorological stations [10]. So, CTSB gives an opportunity to analyze four climate scenarios:

– "human and natural so far" – models data since 1850 taking into account natural changes such as solar intensity and volcanic eruptions, as well as anthropogenic impact;

– "natural only so far" – considers only non-anthropogenic impacts;

– "low-emission future" – is the RCP 2.6 scenario which pays attention to the existing climate changes without further emissions of GHG;

– "high-emission future" – the RCP 8.5 scenario which examines the situation with high-level emissions [10].

4 Results

At the first stage of the study, the CMM was used. The bcc-csm1-1 AR 5 model was chosen. The modeling results are shown in the Figure 1 for 2 100, 2 200 and 2 300 years. It was found that the surface temperature in most regions of the world will rise significantly leading to the changes in climate. These processes will affect Ukraine.

In the second part of the study bcc-csm1-1 and IPSL-CM5A AR 5 models have been chosen to estimate future climate changes in Kyiv region. These models can make predictions up to the 2299 year for the place of interest and cover two different but overlapping regions on the basis of the Kyiv station (Figure 2). In particular, these models are representative because modeled under the human and natural so far scenario historical data and the real data from the meteorological station are closely related (Figures 3, 4).

As can be seen from the Figure 3, according to the bcc-csm1-1 AR 5 model, at a high-emission future RCP 8.5 scenario, the average annual temperature in the area (1) around Kyiv meteorological station (Figure 2) will rise rapidly from 9.5 °C in 2016 and reach the value of 12.7 °C in 2100, 17.2 °C in 2200 and then reach the maximum value of 19.1 °C in 2259. Then there will be a slight decrease but in general, the temperature will remain at approximately the same level from 2200 to 2299 with the value of 16.9 °C in 2299. But at a low-emission future RCP 2.6 scenario, the temperature in the investigated region won't change significantly from 2016 and will reach the maximum value of 10.5 °C in 2116.

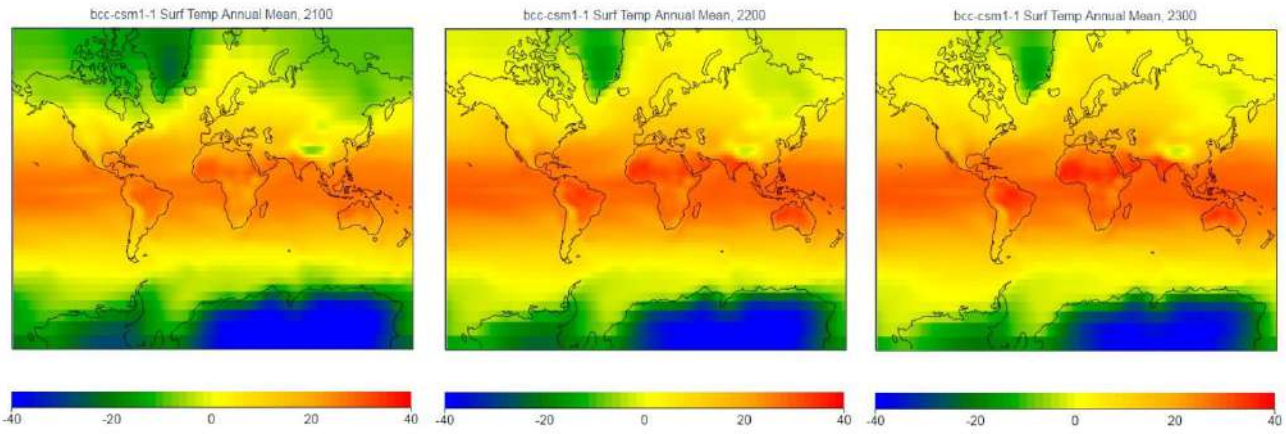

Figure 1 – World maps displaying the surface annual mean temperature in 2100, 2200 and 2300 as a result of the GW and climate changes under the bcc-csm1-1 AR 5 model, obtained by the author on the CMM

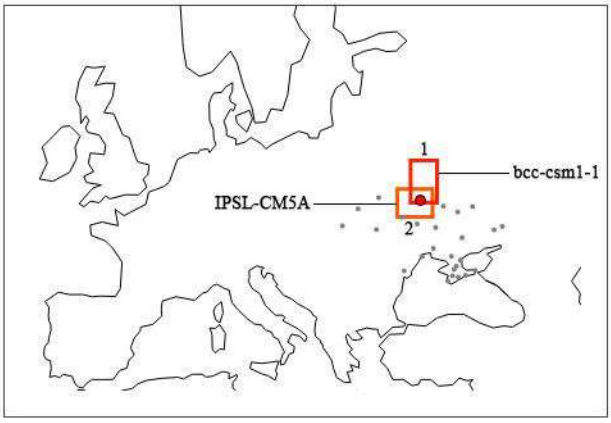

Figure 2 – The map that indicates the areas for which obtained results are representative (by the author on the CTSB)

The modeling results of the average annual temperature in the area (2) (Figure 2) obtained by the IPSL-CM5A model are shown on the Fig. 4. It was found that in the case of the high-emission future RCP 8.5 scenario, the temperature will reach the maximum value of 23.8 °C in 2267 and 2291. In 2100 the predicted temperature will be 13.9 °C, in 2200 it will be 22.1 °C and in 2299 it will be 22.8 °C. But at a low-emission future RCP 2.6 scenario, the temperature in Kyiv region will stay almost the same with a maximum in 2085 (11.5 °C).

So, according to the Figures 3–4, the only way to reach sustainability in Kyiv, Ukraine and other parts of the world is to reduce GHG and pollutant emission levels to reach the low-emission future scenario. And even taking into account the fact that preventing environmental degradation is not the problem that can be solved by a single city or country, all contributions are important. Otherwise, the consequences can lead to a significant aggravation of the ecological crisis.

One of the dangers of the high-emission future scenario is that the temperature isn't going to change in all parts of the world equally. Some places will be affected more than others and it will lead to aggravation of natural disasters such as droughts, floods, fires, and hurricanes. The places that are dry today will become dryer; areas that suffer from disasters now will suffer even more. Dangerous natural phenomena are going to affect areas where they were not seen before. So, the climate will become weirder around the world.

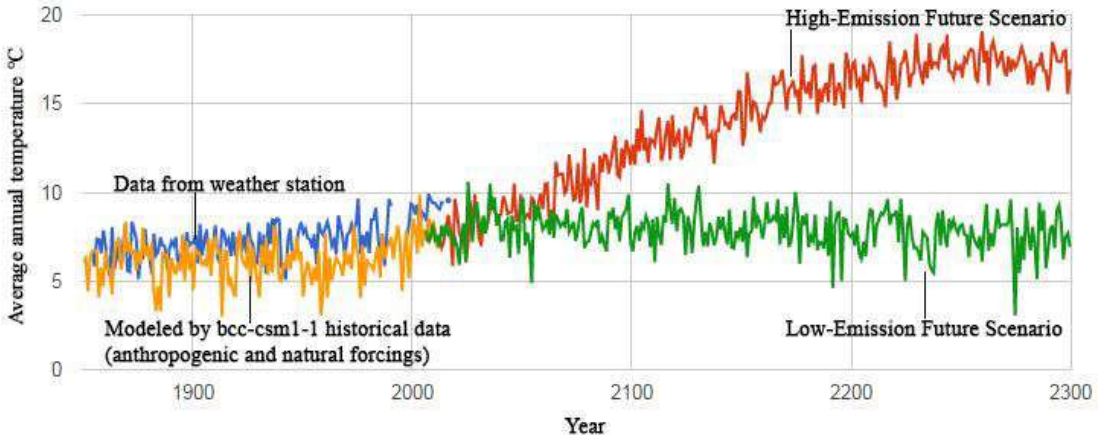

Figure 3 – Average annual temperature modeling results for Kyiv region by the bcc-csm1-1 AR 5 model at RCP 2.6 and RCP 8.5 scenarios, obtained by the author on the CTSB

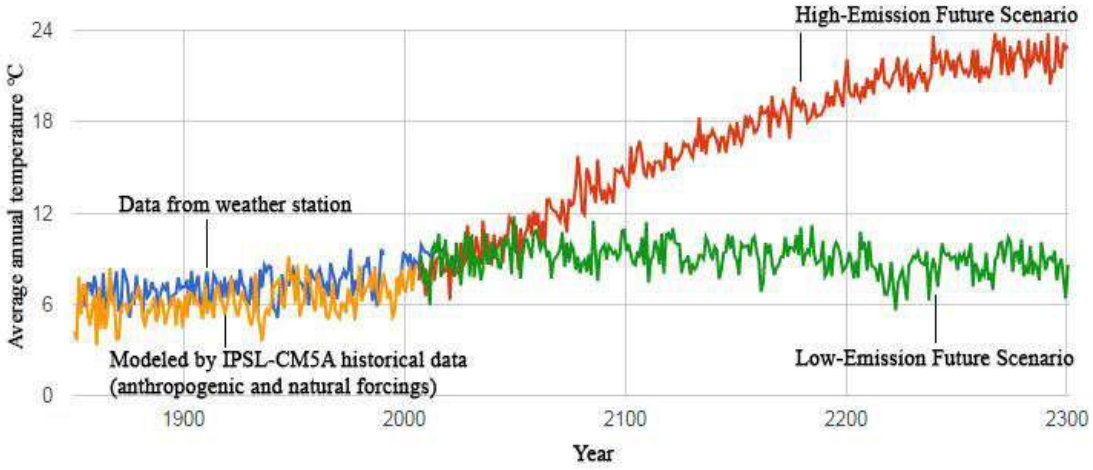

Figure 4 – Average annual temperature modeling results for Kyiv region by the IPSL-CM5A AR 5 model at RCP 2.6 and RCP 8.5 scenarios , obtained by the author on the CTSB

The consequences of such "weirding" have been already observed in 2016 and 2017. For example, according to [11], in 2017 forest fires in Portugal killed 64 people and destroyed nearly 30 000 ha of forest; Hong Kong was hit by a powerful typhoon [12]; Northern Ireland was affected by heavy rains and storms that caused flood [13]; terrible floods were also observed in India, Nepal and Bangladesh [14]; hurricane Harvey hit Texas [15], etc.

According to The State Emergency Service of Ukraine data [16], only on the time interval from 2010 to 2016 (Figure 5) the overall number of natural hazards in Ukraine reached a value of 540 (89 hazards occurred in 2016). According to the platform PreventionWeb [17] managed by the UN Office for Disaster Risk Reduction, the main natural hazards in Ukraine are droughts, extreme temperatures, floods and storms. As can be seen (Fig. 6), floods are the most common disasters in the country (Figure 6 a, in 51.9 % of cases), while extreme temperatures are the main cause of death (Figure 6 b, in 90 % of cases) and droughts are the key reason of the economic issues among all disasters (Figure 6 c, in 50.5 % of cases). PreventionWeb also highlights climate changes and environmental degradation among the main risk drivers.

So, climate changes can do much harm to Kyiv and Ukraine and it is important to implement “decarbonization” lifestyle. Analysis of the literature sources and experience of the international community has shown that green urban initiatives are an important part of the decarbonization strategy and can make Kyiv eco-friendly, healthy and sustainable city. And it was determined that experience of Scandinavian countries can be especially valuable for Ukraine. For example, the "eco-city" green urban initiative in the Western Harbour in Malmö, Sweden, is the evidence of a possibility of the industrial area transformation into the sustainable urban environment. This "eco-city" has a renewable energy system with wind power plant, solar cells, solar collectors on the roofs & walls, as well as a waste treatment system, green roofs and limited car traffic [18].

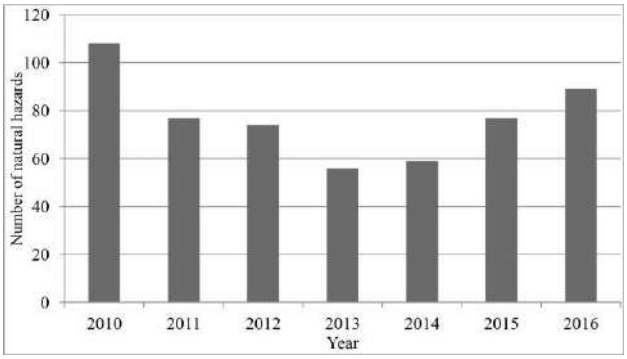

Figure 5 – Number of natural hazards in Ukraine since 2010, created by the author on the bases of the data [16]

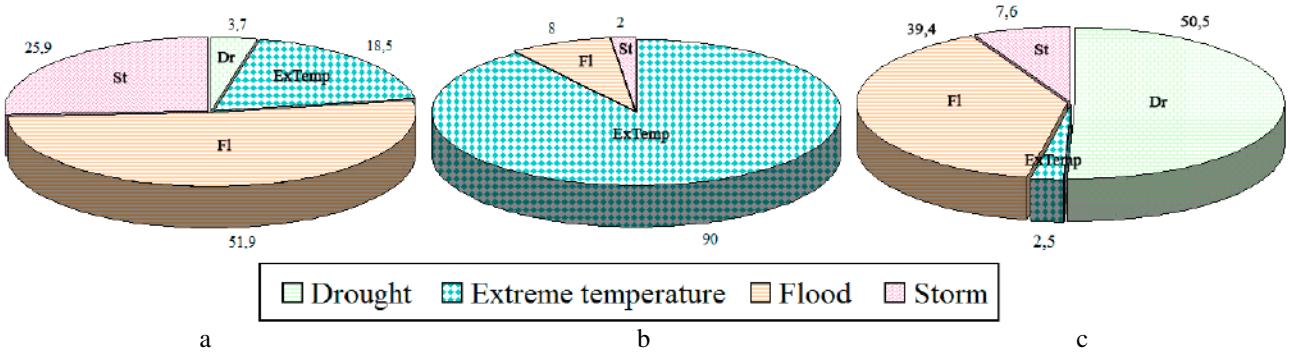

a b c

Figure 6 – Distribution of the main natural hazards in Ukraine (%) by frequency (a), mortality (b) and economic issues (c) [17]

Business and universities also play an important role in the sustainability of the country. For example, in 2016 MIT launched startup accelerator "The Engine" in order to help startups with funding of the projects devoted to such areas as clean energy & water, nuclear power, and climate change. And this accelerator is available not only for the MIT students and graduates [19].

5 Conclusions

By the bcc-csm1-1 AR 5 model, it was found that the surface temperature in most regions of the world will rise significantly leading to the changes in climate and these processes will affect our country too. According to investigated bcc-csm1-1 and IPSL-CM5A models, the average annual temperature in Kyiv region under the RCP 8.5 scenario will increase noticeably while at the RCP 2.6 scenario the temperature won't change significantly and will remain almost stable. Thus, the only way to prevent severe consequences for the environment and society is to develop the decarbonization strategy and reduce GHG and pollutant emission levels.

The practical and scientific value of the work is specified by the fact that obtained results take into account updated information about climate change dynamics and consequences and can be used to increase the awareness of citizens about the importance of this problem. The results of the study, obtained by AR 5 models and statistical analysis methods, confirm the existence and danger of the problem of climate change and can be used for the decarbonization strategy development. The results of the study also show how the increase or decrease in GHG emissions from transport and industry can affect the ecological balance of the urbanized ecosystem.

The risks of natural disasters occurrence were also considered. It was determined that climate "weirding" leading to aggravation of natural hazards is one of the main dangers of the RCP 8.5 scenario. Floods, extreme temperatures and droughts are particularly dangerous for Ukraine. All results of the study were evaluated in the context of the author's experience in the field of environmental safety and physical aspects of natural disasters and substantiate the need for the "decarbonization" lifestyle implementation on the basis of the international experience, as well as the interaction between government, business and universities.

References

1. Fifth Assessment Report (AR 5). *IPCC*. Retrieved from http://www.ipcc.ch/report/ar5/index.shtml.
2. Pachauri, R. K., & Meyer, L. A. (2014). *Climate Change 2014: Synthesis Report. Contribution of Working Groups I, II and III to the 5th Assessment Report of the Intergovernmental Panel on Climate Change*. Geneva, IPCC. Retrieved from http://www.ipcc.ch/pdf/assessment-report/ar5/syr/SYR_AR5_FINAL_full_wcover.pdf.
3. State Statistics Service of Ukraine. Retrieved from http://www.ukrstat.gov.ua.
4. Xin, X., Zhang, L., Zhang, J., Wu, T., & Fang, Y. (2013). Climate Change Projections over East Asia with BCC_CSM1.1 Climate Model under RCP Scenarios. *Journal of the Meteorological Society of Japan*, 91(4), 413–429, doi:10.2151/jmsj.2013-401.
5. Williams, R. G., Roussenov, V., Goodwin, P., Resplandy, L., & Bopp, L. (2017). Sensitivity of Global Warming to Carbon Emissions: Effects of Heat and Carbon Uptake in a Suite of Earth System Models. *Journal of Climate*, 30(23), 9343–9363, doi:10.1175/jcli-d-16-0468.1.
6. Huang, W. L., Chen, W. Y., & Anandarajah, G. (2017). The role of technology diffusion in a decarbonizing world to limit global warming to well below 2 °C: An assessment with application of Global TIMES model. *Applied Energy*, 208, 291–301, doi:10.1016/j.apenergy.2017.10.040.
7. Holiuk, O.V., & Moiseienko, L.V. (2011). Veryfikatsiia danykh pryzemnoi temperatury povitria MZTsAO, CRU ta REMO za 1850–2000 roky. [Verification of the surface air temperature data of the CMIP, CRU and REMO for the period 1850-2000]. *Heohrafiia ta turyzm – Geography and Tourism*, 12, 213–220. Retrieved from http://nbuv.gov.ua/UJRN/gt_2011_12_40 [in Ukrainian].
8. Flato, G., Marotzke, J., Abiodun, B., et al. (2013). Evaluation of Climate Models. Climate Change 2013: The Physical Science Basis. Contribution of Working Group I to the Fifth Assessment Report of the Intergovernmental Panel on Climate Change. *Cambridge University Press*, *Cambridge, New York*, pp. 741–866. Retrieved from http://www.ipcc.ch/pdf/assessment-report/ar5/wg1/WG1AR5_Chapter09_FINAL.pdf.
9. AR 5 Climate Model Mapper. Climate and Carbon Cycle Models. Retrieved from http://climatemodels.uchicago.edu/maps/maps.doc.html.
10. Climate Time Series Browser. Climate and Carbon Cycle Models. Retrieved from http://climatemodels.uchicago.edu/timeseries/timeseries. doc.html.
11. Jones, S. (2017). Portugal forest fires under control after more than 60 deaths. *The Guardian*. Retrieved from https://www.theguardian.com/world/2017/jun/22/portugal-forest-fires-under-control.
12. High waves crash on coastline as Typhoon Hato hits Hong Kong (2017). *The Guardian*. Retrieved from https://www.theguardian.com/world/video/2017/aug/23/high-waves-crash-on-coastline-as-typhoon-hato-hits-hong-kong-video.
13. North of Ireland sees flooding after battering by heavy rain (2017). *The Guardian*. Retrieved from https://www.theguardian.com/uk-news/2017/aug/23/north-of-ireland-battered-by-heavy-weather.

14. Ratcliffe, R. (2017). Floods claim more than 800 lives across India, Nepal and Bangladesh. *The Guardian*. Retrieved from https://www.theguardian.com/global-development/2017/aug/22/floods-across-india-nepal-and-bangladesh-claim-more-than-800-lives-south-asia.
15. Owen, P., Helmore, E., & Dart, T. (2017). Texas hit by Hurricane Harvey: What we know so far. *The Guardian*. Retrieved from https://www.theguardian.com/us-news/2017/aug/26/texas-hurricane-harvey-what-we-know-so-far.
16. The State Emergency Service of Ukraine. Retrieved from http://www.dsns.gov.ua.
17. Ukraine Disaster and Risk Profile (2014). *PreventionWeb*. Retrieved from https://www.preventionweb.net/countries/ukr/data.
18. The Ecological City of Tomorrow in the Western Harbour, Malmö. *Smart City, Sweden*. Retrieved from http://smartcitysweden.com/reference-objects/161/the-ecological-city-of-tomorrow-in-the-western-harbour-malmo.
19. McFarland, M. (2016). MIT launches startup accelerator to tackle the world's biggest challenges. *CNNtech*. Retrieved from http://money.cnn.com/2016/10/26/technology/mit-innovation/index.html?section=money_technology.

Моделювання зміни клімату відповідно до міської стратегії декарбонізації

Кофанова О. В.

Національний технічний університет України «Київський політехнічний інститут імені Ігоря Сікорського», просп. Перемоги, 37, 03056, м. Київ, Україна

Анотація. Антропогенний вплив на клімат Землі постійно зростає, а тому зростають і ризики незворотної деградації екосистем. Статтю присвячено моделюванню довгострокового прогнозування змін клімату та розробці стратегії декарбонізації. Використано кліматичні AR 5 моделі bcc-csm1-1 та IPSL-CM5A. Встановлено, що прогнозована середньорічна температура у Київській області відповідно до сценарію із високими рівнями викидів парникових газів RCP 8.5 значно збільшиться (до 23,8 °С відповідно до моделі IPSL-CM5A) протягом декількох сотень років, тоді як при реалізації сценарію із низькими рівнями викидів RCP 2.6, цей показник не зазнає критичних змін (його максимальне значення сягне 11,5 °С відповідно до моделі IPSL-CM5A). Запропоновано рекомендації щодо розробки стратегії декарбонізації для України, яка надасть можливість зменшити рівні викидів парникових газів та досягти сценарію RCP 2.6. Практична і наукова цінність отриманих результатів визначається тим, що враховується новітня інформація про зміни клімату, яка може бути використана для підвищення обізнаності громадян. Результати дослідження підтверджують небезпеку змін клімату на планеті та показують, яким чином викиди парникових газів можуть вплинути на екологічний баланс високоурбанізованої екосистеми. У статті також розглянуто ризики збільшення кількості стихійних лих у світі, Україні та Київській області, спрогнозованих за умови реалізації сценарію RCP 8.5.

Ключові слова: моделювання клімату, глобальне потепління, декарбонізація, зміни клімату, стихійні лиха.

JOURNAL OF ENGINEERING SCIENCES
ЖУРНАЛ ІНЖЕНЕРНИХ НАУК
ЖУРНАЛ ИНЖЕНЕРНЫХ НАУК

Web site: http://jes.sumdu.edu.ua

DOI: 10.21272/jes.2018.5(1).h2 Volume 5, Issue 1 (2018)

UDC 628.365.3:628.33

Sulfur Utilization in the Systems of Biological Wastwater Denitrification

Plyatsuk L. D.[1], Chernysh Y. Y.[1*], Ablieieva I. Y.[1], Kozii I. S.[1], Balintova, M.[2], Matiash Y. O.[1]

[1] Sumy State University, 2 Rymskogo-Korsakova St., Sumy, 40007, Ukraine;
[2] Technical University of Košice, 1 Letna St., 040 01 Košice, Slovakia

Article info:
Paper received: January 12, 2018
The final version of the paper received: March 1, 2018
Paper accepted online: March 5, 2018

[*]**Corresponding Author's Address:**
e.chernish@ssu.edu.ua

Abstract. This paper focuses on the study of the possibility of using mineral carriers from sulfur (bio-sulfur/elementary sulfur) in anaerobic wastewater treatment systems under autotrophic denitrification conditions. The theoretical aspects of the work are based on the biochemical formalization of the studied processes using the system-ic-synergetic approach for the description of the patterns of autotrophic denitrification microorganisms based on the principles of autocatalysis of natural systems. Special software was used in the work to identify the necessary ecolog-ical and trophic groups of microorganisms and implement the schemes of trophic interactions in association of deni-trification microorganisms. The taxonomic classification was assigned based on the KEGG database (Kyoto Ency-clopedia of Genes and Genomes). Bio-filtration set-up system was formed for carrying out the process wastewater denitrification with using bio-sulfur and gaseous sulfur. The filtration method is used under anaerobic conditions along with immobilization on the carrier based on sulfur autotrophic denitrifying bacterial species such as Thiobacil-lus denitrificans and Thiomicrospira denitrificans. Thus, sulfur conversion leads to the reduction of nitrates to nitrites and, ultimately, the release of molecular nitrogen. The mechanisms of sulfur conversion in natural ecosystems make it possible to conclude its expediency of use it as a sorption sulfur-containing mineral carrier in wastewater purifica-tion systems with further conversion to an organic form (with microbial cell carbonate). The interactions pathways model in the association of heterotrophic and autotrophic denitrification bacteria in the process of wastewater and sewage sludge purification was formed under condition of elementary sulfur presence. Energetic and synthesis reac-tions for an autotrophic denitrification were described. The implementation of wastewater treatment systems with au-totrophic denitrification process use will provide an opportunity to expand the application scope of by-products such as gaseous sulfur and bio-sulfur that currently minimal recycling in traditional industrial processing.

Keywords: denitrification, bio-sulfur, gaseous sulfur, wastewater, mineral carrier.

1 Introduction

Sulfur is one of the main types of chemical raw for materials, which have strategic importance for the coun-try's economy. Due to continuing growth of population and areas under cultivation, it is required an intensifica-tion of agriculture, which significantly depends on the introduction of mineral and organic fertilizers that contain sulfur [1].

Ecological aspects of sulfur application during obtain-ing sulfuric acid is the emission of such harmful sub-stances as acid fog and sulfurous anhydride SO_2. Moreo-ver, in gas sulfur, which is a waste of the process of puri-fication of gases of petroleum processing, non-ferrous metals, associated petroleum and natural gases can con-tain arsenic and other harmful impurities [2], which, with the open method of storing of gas sulfur can migrate to the environment.

The emergence of the problem of elemental sulfur as a large-capacity technogenic formation is connected with the existence of a stable disproportion between the pro-cess of its accumulation in the environment and the con-sumption reduction in traditional areas (sulfuric acid pro-duction, paper-and-pulp industry, etc.). There is an urgent need to diversificate the application of sulfur, particularly the materials production based on its ground in order to apply them in filtration biotechnological waste water treatment systems [3].

Another important mission of the environmental safety is the deprivation of nutrients from wastewater, which after getting into surface water cause significant damage to the ecological system for the region, and this requires an effective discharge treatment from such compounds (nitrogen and phosphorus, in particular).

Nitrates are considered to be the most widespread type of inorganic pollutants that contribute to rapid develop-

ment of blue-green algae and other lower plants with short life cycles for the decomposition course of decaying organic matter of which a large amount of the oxygen dissolved in water is consumed leading to decaying of the dominant groups of aquatic organisms. At the same time, nitrates cause great harm to the human body, generally due to their consecutive transformation into nitrites and nitro compounds which belong to carcinogenic substances. In ground waters, nitrates are accumulated due to transfer sewage disposal chemical and petrochemical factories in them, as well as the fertilizers which are washed away from agricultural fields, drains of cattle farms. Nitrate content may vary depending on chemical and biological composition of soils [4].

Thus, the possibility of a unified approach developing to solve the problem of removing nitrogen compounds from liquid waste and using nonorganic sulfur varieties in biological denitrification systems is of great importance in reducing the environmental footprint in the region. In our opinion, the expansion of biosulfur using as a product of gas flows biodesulfurizationis, which is possible due to its application together with gas sulfur in biofiltration systems for removing nitrates from effluents, which requires further scientific, theoretical and experimental evidence.

2 Literature Review

Among the methods for effluents purification from nitrates, a special niche is occupied by biological methods of denitrification, which are divided into autotrophic and heterotrophic.

Anaerobic activated sludge is used in many studies for restoration of nitrites and nitrates in the process of denitrifying sewage. Denitrifying bacteria are found among representatives of Acrobacterium sp. and others, which, being in anoxic conditions, use oxygen for breathing that contained in nitrites and nitrates instead of dissolved oxygen. Herewith, most of the studies focused on studying and increasing the effectiveness of the use of heterotrophic bacterium-denitrifying agents which represent a group of facultative anaerobes. This is facilitated by the fact that they are present in the sewage in large quantities and can use pollutants as a carbon feed (methanol, ethanol, acetic acid), greatly facilitates the exploitation of structures, as it eliminates the need to grow a special adapted microflora [5].

Downflow denitrification filters operate in a conventional filtration mode and consist of media and support gravel supported by an underdrain. Wastewater enters a downflow filter over weirs along the length of the filter bed on both sides.

Filter effluent is conveyed from the bottom of the filter over a control weir into a clear well. During the process, nitrate is metabolized to nitrogen gas, which becomes embedded in the filter media. Nitrogen-release cycles are needed to remover these nitrogen gas bubbles that accumulate. The piping for the filter influent and backwash is similar to that of conventional filters.

Wastewater enters the filter through the influent pipe and then is transported downward through a supply pipe and distributors (Figure 1). The water moves up through the filter media and filtrate is discharged from the upper portion of the filter.

The preferred media for each filter manufacturer is also presented in Table 1.

Separate-stage denitrification can be carried out either as a suspended or attached growth process, both of which require an external carbon source, such as methanol. Because they require a large area and their own sludge settling and recycling system, separate suspended growth denitrification systems are not very common (Figure 2).

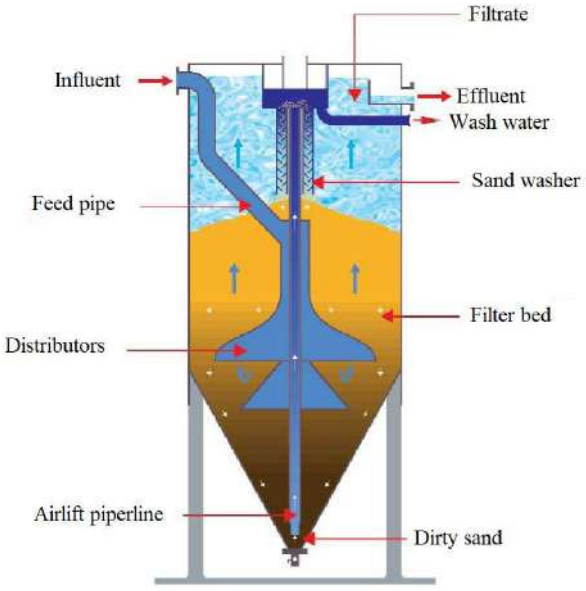

Figure 1 – Astrasand upflow continuous - backwash filter

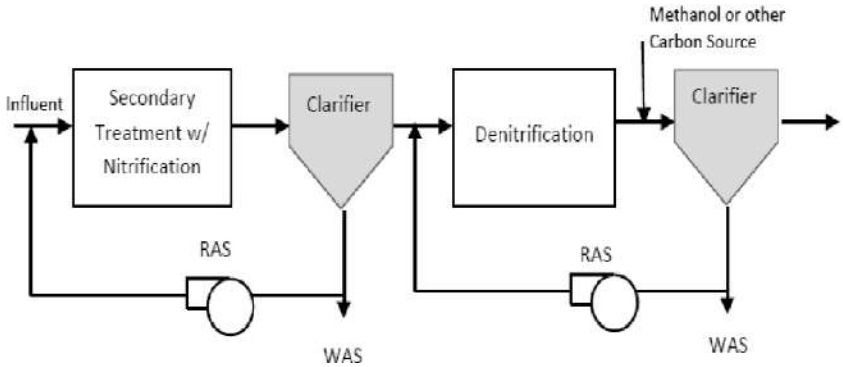

Figure 2 – Separate-stage suspended growth denitrification process

Table 1 – Filtration material in denitrification systems [6]

Manufacturer / filter	Severn Trent Services/ TETRA® Denite®	F. B. Leopold / elimi-Nite	USFilter/Davco	Parkson / DynaSand	Paques and USFilter/ Astrasand
Flow regime	Downflow	Downflow	Downflow	Upflow	Upflow
Media	457 mm (18 in) graded gravel, 1.8 m (6 ft) of 6×9 mesh silica sand, uniformity coefficient 1.35, 0.8 minimum sphericity	381 mm (15 in) graded gravel, 1.8 m (6 ft) of 6×12 mesh sand	2 layers support gravel, 1.8 m (6 ft) of 6×9 mesh sand	1.35 to 1.45 mm subround media or 1.55 to 1.65 mm subangular media with uniformity coefficient of 1.3 to 1.6; 2-m (6.6 ft) bed depth	1.2 to 1.4 mm sand, 2-m (6.6-ft) bed depth

Denitrification filters are popular, because they are an easy retrofit and require less area and sludge handling. The units can simply be added to the end of a secondary treatment process that includes nitrification. Both downflow and upflow filters are in use. Downflow filters require backwashing to remove solids and nitrogen gas trapped in the filter media. Upflow filters skirt this problem by having the filter media continuously removed from the bottom of the unit, cleaned, and recycled to the top of the filter (Figure 3) [7].

The main components of a modern Continuous Activated Sludge Biological Nutrient Removal (BNR) systems are presented in Figure 4.

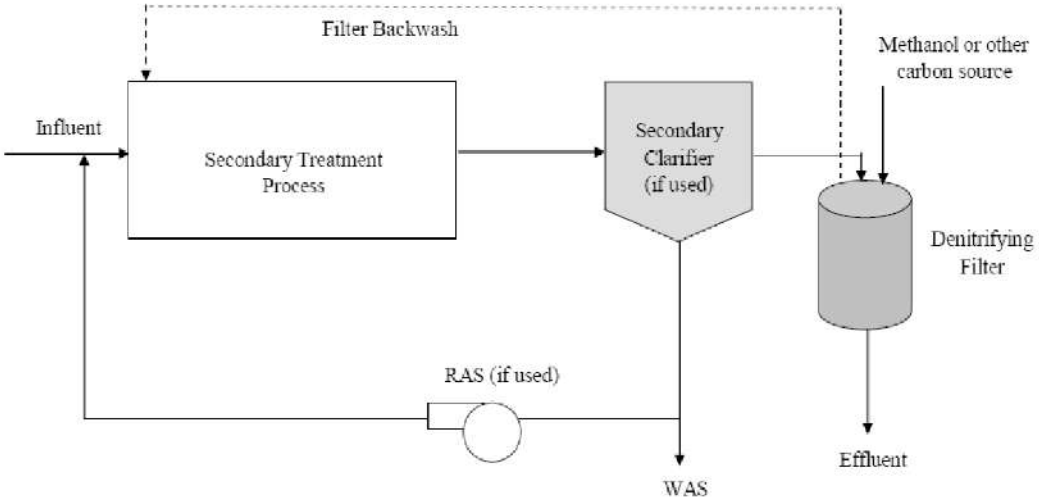

Figure 3 – Separate-stage denitrification filter process

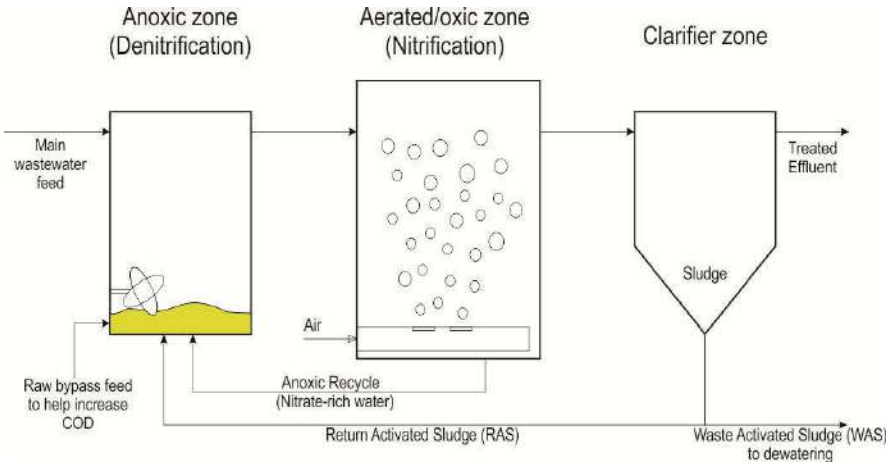

Figure 4 – Continuous Activated Sludge BNR systems

The anoxic (denitrification) basin or zone continually receives several streams including the main feed of ammonia-rich wastewater from the upstream anaerobic pond. This is a large volume stream containing the bulk of the new nitrogen load to the system. Unfortunately, the COD content of this stream is usually insufficient to provide all the COD needed for the denitrifying bacteria so additional COD is added [8].

In autotrophic denitrification, sulfur or hydrogen is used by microorganisms as a source of energy.

The continuously stirred tank reactor (CSTR) that capable of providing an adequate seed source of autotrophic denitrifiers was used in the study [9]. As shown in Figure 5, anaerobic upflow fixed-bed reactor was constructed from 2.5-inch I.D. acrylic tubing with four sampling ports. The empty bed reactor volume is 1.11 liters. The sulfur and limestone grain sizes ranged from 2.38 mm to 4.76 mm. Gas collection and monitoring systems have been included in this design.

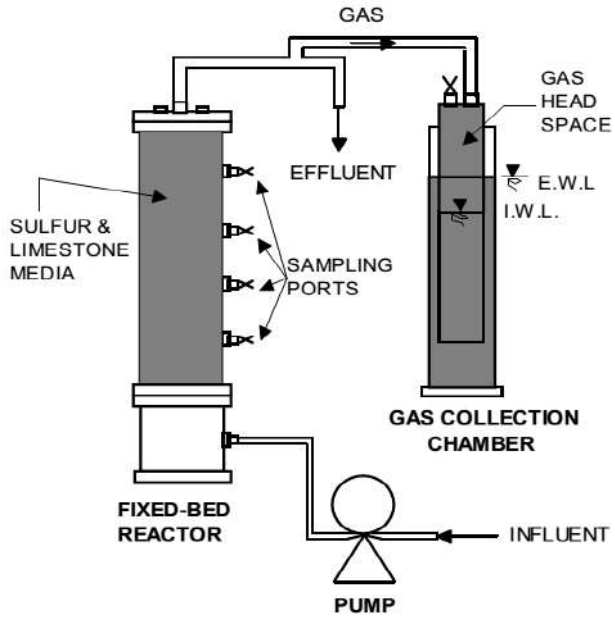

Figure 5 – Upflow fixed-bed column reactor [9]

The feed solution composition for the CSTR: KNO_3, 3.0 g/l; $Na_2S_2O_3 \cdot 5H_2O$, 6.0 g/l; $NaHCO_3$, 1.5 g/l; Na_2HPO_4, 1.5 g/l; KH_2PO_4, 0.3 g/l; $MgSO_4 \cdot 7H_2O$, 0.4 g/l; and 1 ml of stock trace nutrient solution per liter of feed solution [9].

However, these methods need to be improved. These disadvantages are water pollution residual methanol or sulfur, and a large content of microorganisms in the treated water. In addition, this process is characterized by increased sensitivity to temperature conditions, and its rate decreases in cold water, which makes it difficult to use biological denitrification in regions with a cold climate [4].

In [10], methods for the oxidation of ammonium and a hardly available organic matter of wastewater are offered in aerobic-anoxid conditions. To carry out the process of simultaneous autotrophic and heterotrophic denitrification, a batch reactor with a volume of 61 dm^3 was built.

A complete retention of the biomass of the active sludge was carried out in the reactor, the residence time of the liquid was 2,5-5 days, the sludge dose was 1.5–2.5 g/dm^3, the temperature was 20-28 °C, and the pH was 7.5-8.5. The concentrations of ammonium nitrogen and nitrogen nitrite in renovated water were 0.3-8 mg/dm^3 and, accordingly, 0.2-4 mg/dm^3 (Table 2) [10]. The efficiency of nitrogen removal was 91% -80% due to the process of autotrophic denitrification and 11 % due to the heterotrophic denitrification process.

Table 2 – Composition of water received for treatment and after treatment in two successive reactors

Parameter	Crude filtrate	Nitrifiable filtrate	Refined filtrate
$N\text{-}NH_4$, mg/dm^3	250–300	100–120	0.3–8.0
$N\text{-}NO_2$, mg/dm^3	–	130–150	0.2–4.0
$N\text{-}NO_3$, mg/dm^3	–	0.4–3.3	5–10
COD, mg/dm^3	150–190	60–120	60–120

During the experiment it was noted that a significant part of the biomass of the microorganisms in this reactor was secured with the walls of the reactor. The ability of microorganisms for effective adhesion was used to increase the reliability of the reactor by increasing the surface area to which microorganisms could be secured.

A plastic load of polyethylene (AnoxKaldnes K1, 30 % of the volume of the reactor) was placed in the reactor. After a while at the loading has developed the biofilm, in which up to 75 % of the biomass of microorganisms was located. The use of this method led to the stabilization of the quality of water purification in the reactor at the same average (removal of 90–92 % of nitrogen).

However, the biological technologies currently available for nitrate degradation are associated with significant drawbacks including: long start-up times and long recovery times after system upsets; the production of biological solids requiring costly treatment and disposal; low organism densities necessitating large footprints to achieve sufficient treatment capacity.

Thus, an important area of research is the immobilization of active biomass on carriers to reduce their leaching from the bioreactor space and the transfer of the process to a continuous technological regime for treating effluents. As well as the introduction of carrier-feed to stimulate the development of autotrophic groups of microorganisms with the minimization of nutrient removal from the system.

Developing biocomposites for natural, nitrate-degrading organisms that are irreversibly retained within these systems and never leave the biofilter, as they are

protected from washout, overgrowth, toxicity, and abrupt changes in operation.

This paper focuses on the study of the possibility of using mineral carriers from sulfur (bio-sulfur / elementary sulfur) in anaerobic wastewater treatment systems under autotrophic denitrification conditions.

To achieve the aim, the following tasks were set:

– analytical studies of the possibility of bio-sulfur and gaseous sulfur use as mineral carriers for bacteria growth under autotrophic denitrification conditions;

– development bio-filtration set-up system for carrying out the process wastewater denitrification with using bio-sulfur and gaseous sulfur.

3 Research Methodology

During biochemical processing and in the course of Claus's reactions, all hydrogen sulfide, which was a part of gas-liquid mixes, is used to produce sulfur: bio-sulfurs (from bio-desulfurization systems) [11] and the gaseous sulfur resp., which have both similar physical and chemical properties and some differences features. It should be noted that bio-sulfur is more demanded in the use in agriculture as a component of fertilizers and fungicides [12].

The analysis of the composition of gaseous sulfur is presented in Table 3 and its general form is shown in Figure 6. Gaseous sulphur has the same chemical formula as solid or liquid Sulphur, S_8.

Table 3 – The technological parameters of gaseous sulfur [13]

Parameter (minimum value), %	Norm for technical gaseous sulfur
Sulfur mass fraction	99.2
Water mass fraction	1.0
Refuse burnout mass fraction	0.4
Organic substances mass fraction	0.5
Acids mass fraction in conversion to spirit of sulfur	0.02

Figure 6 – Photo of the gaseous sulfur granules (3–6 mm)

The main stages of bio-sulfur production are described in the block diagram in Figure 7 with an indication of its component composition according to [11].

Diffractometric research and raster microanalysis of the bio-sulfur structure were held (conducted) and the fact, that 60 % of it consist of orthomolecules S_8^0, was determined. Besides, sulfur organic inclusion (S_{org}) and particles of components of transformed granules ($CaSO_4$, H_2O, $CaCO_3$, $Ca_3(PO_4)_2$, etc.) were found.

It should be noted that the presence of additional biogenic elements in the biosulfur will allow to reduce or eliminate the necessity of supply of additional nutrients to the system. Also, calcium fluoride may be present in the bio-sulfur in the presence of fluorine in the composition of secondary mineral raw materials (phosphogypsum) for the production of an immobilized carrier for the systems of biochemical purification of waste gases from hydrogen sulphide. Calcium fluoride is a chemically relatively passive compound.

The theoretical foundations of the work are based on the biochemical formalization of the purification processes using the systemic-synergetic approach for the description of the patterns of autotrophic denitrification microorganisms based on the principles of autocatalysis of natural systems.

Culture-identify approach. Special software was used in the work to identify the necessary ecological and trophic groups of microorganisms and implement the schemes of trophic interactions in associations of microorganisms-denitrifiers.

The taxonomic classification of each read was assigned based on the KEGG database (Kyoto Encyclopedia of Genes and Genomes).

KEGG is a database resource for understanding high-level functions and utilities of the biological system, such as the cell, the organism and the ecosystem, from genomic and molecular-level information. It is a computer representation of the biological system, consisting of molecular building blocks of genes and proteins (genomic information) and chemical substances (chemical information) that are integrated with the knowledge on molecular wiring diagrams of interaction, reaction and relation networks (systems information). Denitrification (nitrate => nitrogen) module M00529 was used for modelling of association of main ecological and trophic groups of microorganisms involved in individual stages of this process. This program provides the definition of basic biochemical reactions, involved enzymes and microorganisms that contain the relevant genes.

4 Results

4.1 Analytical studies of the possibility of bio-sulfur and gaseous sulfur use as mineral carriers for bacteria growth under autotrophic denitrification conditions

Autotroph denitrification explains the thermodynamic instability of nitrates in critical areas or the lack of lysed organic connections.

Apart from organic carbon, some of the denitrifying bacteria can use inorganic substances, such as hydrogen and sulfur, manganese and ferrum in the capacity of donor of electrons. Few researches showed the application of this process for removing the nitrate out of fouled waters, and the sulfur-limestone reactor was used for the autotroph denitrification of waste waters.

Hence, in [14, 15] the possibility of usage of the industrial waste of desulfurizing of flue gases for considerable decrease of the volume of dregs over the cleaning of waste waters. Therewith the main groups of eco-trophic microorganisms are distinguished, which interact in bioorganic cycles of transformation of biogenous elements (Figure 8).

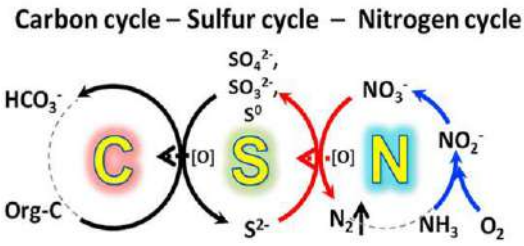

Figure 8 – The scheme of interactions in biochemical cycles between heterotrophic and autotrophic groups of microorganisms used in biological wastewater treatment [15]

The possibility of denitrification in low ratio COD (chemical oxygen demand)/N is demonstrated in the reactor, which establishes the symbiotic balance between the denitrifying sulfur bacteria and sulfate-reduction bacteria [16]. The advantages of autotrophic denitrification include:

– decreasing of the reactor pollution with dead biomass;

– the treated water isn't contaminated with organic carbon.

The implementation of wastewater treatment systems with autotrophic denitrification process use will provide an opportunity to expand the application scope of a number of by-products that currently minimal recycling in traditional industrial processing. For example, the utilization of gaseous sulfur and bio-sulfur.

Figure 9 represents an analysis of the main ecological-trophic groups of microorganisms which take part in autotrophic and heterotrophic denitrification.

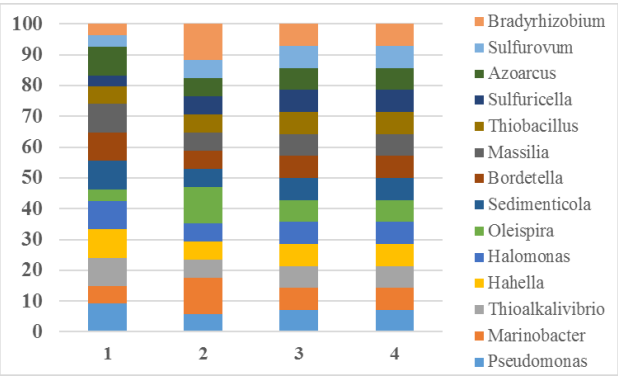

Figure 9 – Taxonomic classification of the microbial composition according to the stages of denitrification: 1 – nitrate to nitrite; 2 – nitrite to nitric oxide; 3 – nitric oxide to nitrous oxide; 4 – nitrous oxide to nitrogen, using KEGG database

The bacterial communities were dominated by Pseudomonas, Bradyrhizobium, followed by Thioalkalivibrio, Thiobacillus, Sulfuricella and Sulfurovum.

Figure 10 presents the data on the metabolic interactions of cooperated communities of microorganisms-denitrifiers in the process of wastewater treatment.

The mechanisms of sulfur conversion in natural ecosystems make it possible to conclude its expediency of use it as a sorption sulfur-containing mineral carrier in wastwater purification systems with further conversion to an organic form (with microbial cell carbonate) (Figure 11).

According to modern conseptualizations, sulfur from surroundings enters the cellular vacuole (filled with voluntarily) of thiobacillus, including T. denitrificans by diffusion and accumulates in it as a reserve material. This sulfur may oxidase as the case should be require. The speed of its oxidation depends on the area of contact of sulfur with bacterial cells. This suggests that there are ferments on the cell area of bacteria that contribute the entry of sulfur into the cell, and under their influence, sulfur is reduced to a sulfide ion, the oxidation of which arises further intracellularly.

Energy and synthesis reactions for an autotrophic denitrification can be written in the form of the following equations.

Energy reaction:

$$2NO_3^- + 5H_2 \rightarrow N_2 + 4H_2O + 2OH^-; \quad (1)$$

$$2NO_3^- + 2H^+ + 5H_2 \rightarrow N_2 + 4H_2O. \quad (2)$$

Synthesis reaction [17]:

$$H_2 + 0.35NO_3^- + 0.35H^+ + 0.052CO_2 \rightarrow$$

$$\rightarrow 0.17\ N_2 + 1.1\ H_2O + 0.010C_5H_7O_2N. \quad (3)$$

The stoichiometric equation for the reduction of nitrate using elemental sulfur proceeds as follows:

$$55S + 20\ CO_2 + 50NO_3^- + 38\ H_2O + 4NH_4^+ \rightarrow$$

$$\rightarrow 4\ C_5H_7O_2N + 25\ N_2 + 55SO_4^{2-} + H. \quad (4)$$

Heterotrophic denitrification bacteria produce electrons and protons necessary for the transformation of nitrate from organic compounds. These substances include carbohydrates, organic alcohols, amino acids and fatty acids. For example, the utilization of acetate, as a source of carbohydrate, occurs as follows [16]:

$$5CH_3COO^- + 8NO_3- + 3H^+ \rightarrow$$

$$\rightarrow 10HCO_3^- + 4N_2(g) + 4H_2O. \quad (5)$$

Therefore, developing the denitrification complex technology using gaseous sulfur and bio-sulfur as immobilized sorbing agent for denitrification bacteria followed to technogenic sulfur utilization and fertilizer production.

Thus, it is essential to carry out experimental researches of efficiency of stock package use based on bio-sulfur and gaseous sulfur in biological filters of denitrification systems.

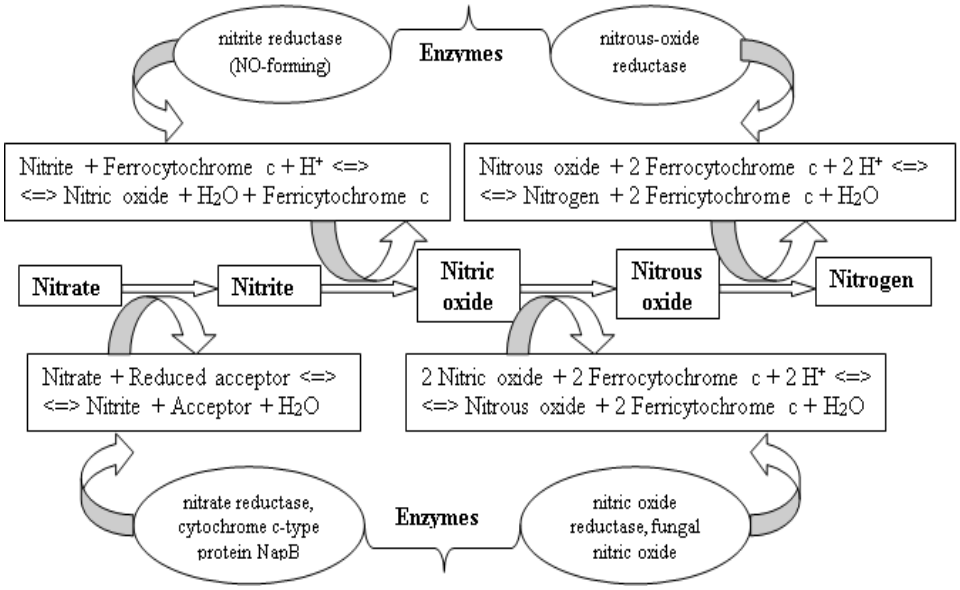

Figure 10 – Block diagram of metabolic processes of interaction in the association of denitrification microorganisms

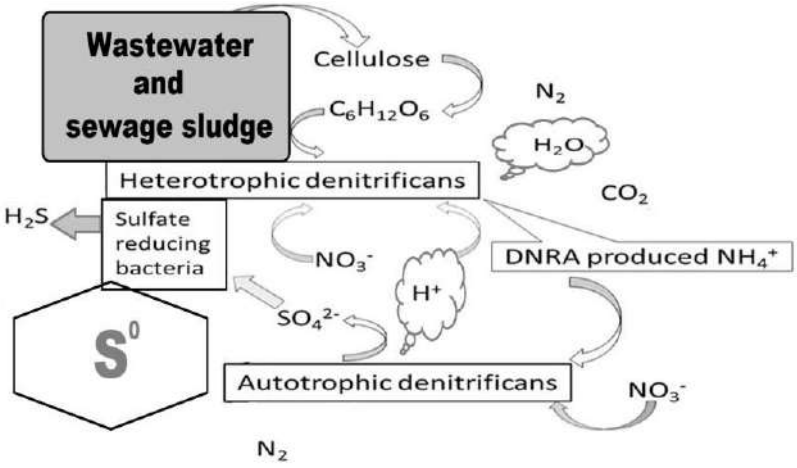

Figure 11 – The flowchart of interactions pathways model in the association of heterotrophic and autotrophic denitrification bacteria in the process of wastewater and sewage sludge purification under condition of elementary sulfur presence

4.2 Bio-filtration set-up system for carrying out the process wastewater denitrification with using bio-sulfur and gaseous sulfur

For pattern drains purification, filtration method is used under anaerobic conditions along with immobilization on the carrier made of autotrophic denitrifying bacterial species such as Thiobacillus denitrificans and Thiomicrospira denitrificans, also usage of phototrophic bacterial species such as Rhodopseudomonas sphaeroides f. denitraficans is possible.

These species will oxidize various kinds of reduced sulfur to sulfate, in this case the nitrate is reduced and oxygen is released for its own metabolism of facultative thiobacteria. Thus, sulfur conversion leads to the reduction of nitrates to nitrites and, ultimately, the release of molecular nitrogen.

Composition of a model contaminated solution: KH_2PO_4, 25 g/dm^3; $MgSO_4 \cdot 7H_2O$, 260 g/dm^3; $KHCO_3$, 753 g/dm^3; $NaNO_2$, 893 g/dm^3; EDTA ($C_{10}H_{16}N_2O_8$), 15 g/dm^3; $FeSO_4$, 5 g/dm^3; $MnCl_2 \cdot 4H_2O$, 0.99 g/dm^3; $ZnSO_4 \cdot 7H_2O$, 0.43 g/dm^3; $CuSO_4 \cdot 2H_2O$, 0.25 g/dm^3.

Figure 12 shows the experimental set-up that is planned to use for wastewater denitrification modelling. The biofilter is a cylindrical container of plexiglass with a volume of 10 dm^3. The reverse flow method is used, in which water is pumped through a hole at the bottom of the filter and ends up, recirculating the water flow through the pump. Also, the gas phase is recycled with the possibility of its recycling into the system to intensify purification process.

In this case, for the implementation of the experiment, the ratio of the main components of the mixture of the filtration material to fill the biofilter is suggested: 2/3 granular sulfur and 1/3 granules (diameter 10 mm) from the calcium-containing material for increasing the pH of the purified water.

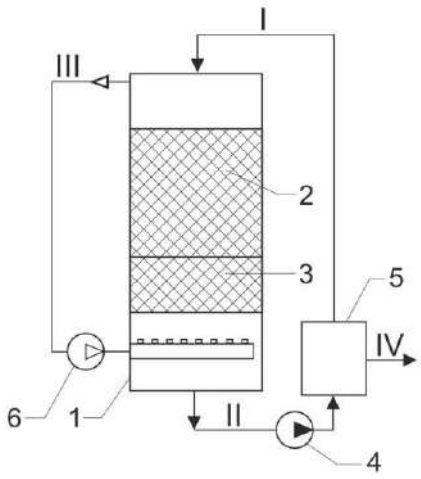

Figure 12 – The bio-filtration set-up system:
1 – biofilter body; 2 – sulfur carrier; 3 – granules of calcium-containing material; 4 – pump; 5 – capacity for selection of model flow; 6 – pump; I – input stream for cleaning; II – output flow for recycling; III – cycle of the gas phase; IV – purified stream

In this case, for the implementation of the experiment, the ratio of the main components of the mixture of the filtration material to fill the biofilter is suggested: 2/3 granular sulfur and 1/3 granules (diameter 10 mm) from the calcium-containing material for increasing the pH of the purified water.

Intensive internal circulation stimulates the growth of the necessary ecological-trophic groups of bacteria, the descending flow of model effluents passes through a layer of granular sulfur and during the bioconversion sulfuric elements of T. denitrificans are used in order to reduce the nitrate to molecular nitrogen. In the process of biochemical conversion, the acid-base balance of the system changes to the acidic side, so a calcium-containing drainage material is loaded in the lower part of the biofilter to buffer the flow of water.

The qualitative character of sulfur use is enlargement of pore spaces inside sulfur-containing granules in the process of sulfur consumption by microorganisms. In 2–3 days after immobilization and beginning of biological filter exploitation, during working presence of essential ecologically-trophic groups of bacteria is exhibited, when gas bubbles begin to form in time intervals between batching of granulated sulfur. It is expected, that in 12–14 days, the durable biofilm with well-developed bacterial intercellular matrix, which covers the whole bulk of sulfur filter medium, is to function. For this purpose, continuous monitoring of the nitrate level in ppm or mg/dm^3 in simulated runoffs before and after purification in the biological filter is conducted.

5 Conclusions

The mechanisms of sulfur conversion in natural ecosystems make it possible to conclude its expediency of use it as a sorption sulfur-containing mineral carrier in wastewater purification systems with further conversion to an organic form (with microbial cell carbonate). The interactions pathways model in the association of heterotrophic and autotrophic denitrification bacteria in the process of wastewater and sewage sludge purification was formed under condition of elementary sulfur presence. Energetic and synthesis reactions for an autotrophic denitrification were described.

Bio-filtration set-up system was formed for carrying out the process wastewater denitrification with using bio-sulfur and gaseous sulfur. The filtration method is used under anaerobic conditions along with immobilization on the sulfur carrier autotrophic denitrifying bacterial species such as Thiobacillus denitrificans and Thiomicrospira denitrificans. These species will oxidize various kinds of reduced sulfur to sulfate, in this case the nitrate is reduced and oxygen is released for its own metabolism of facultative thiobacteria. Thus, sulfur conversion leads to the reduction of nitrates to nitrites and, ultimately, the release of molecular nitrogen.

The implementation of wastewater treatment systems with autotrophic denitrification process use will provide an opportunity to expand the application scope of by-products such as of gaseous sulfur and bio-sulfur that currently minimal recycling in traditional industrial processing.

References

1. Yavorskoy, V. (2016). *Sulfure-gas production in Ukraine*. Lviv Polytechnic National University [in Russian].
2. Dmitriev, E. A., Kuznetsova, I. K., & Akimov, V. V. (2011). *Environmental aspects production sulfuric acid*. Moscow [in Russian].
3. Tsinberg, M. B., & Nenasheva M. N. (2013). Application of gas sulfur in the newest technologies. *Vestnik OGY*, Vol. 10, No. 159, 362–364.
4. Gavrilenko, A. B., Stepacheva, A. A., Molchanov V. P., & Sulman M. G. (2016). Complex denitrification of waste water. *Bulletin science and practice*, Vol. 10, 42–46 [in Russian].
5. Borovykh, E. P. (2011). Denitrification process in biological purification wastewater and calculation methods. *Water chemistry and ecology*, Vol. 11, 85–89 [in Russian].
6. EPA 832-F-07-014 (2007). *Wastewater Management Fact Sheet Denitrifying Filters*. Retrieved from: https://nepis.epa.gov.
7. Thomas, L. (2012). *White Paper Methanol Use in Wastewater Denitrification*. Methanol Institute, USA.
8. *Informatsionnyy byulleten' udaleniya azota*. Retrieved from https://www.ampc.com.au/uploads/cgblog/id338/6.

9. Lampe, D. G., & Zhang, T. C. (1996). *Evaluation of sulfur-based autotrophic denitrification*. Retrieved from https://www.osti.gov/biblio/422853.
10. Ammonium oxidation process and corpulent organic matter wastewater in anthropic anoxic conditions. Certificate of the authorship RU2010125001A (2011). Retrieved from https://patents.google.com/patent/RU2492148C2.
11. Plyatsuk, L. D., & Chernysh, Y. Y. (2016). The removal of hydrogen sulfide in the biodesulfurization system using granulated phosphogypsum. *Eurasian Chemico-Technological Journal*, Vol. 18, No. 1, 47–54.
12. *Biosulfur. Paqell – gas desulpherisation and sulphur recovery with THIOPAQ*. Retrieved from http://www.paqell.com/thiopaq/biosulfur.
13. *Technical sulfur*. Retrieved from http://mnpz.by/products/sera-tekhnicheckaya.
14. Qian, J., Jiang, F., Chui, H. K., Loosdrecht, C. M., & Chen, G. H. (2013). Industrial flue gas desulfurization waste may offer an opportunity to facilitate SANI® application for significant sludge minimization in freshwater wastewater treatment. *Water Science & Technology*, Vol. 67(12), 2822–2826, doi: 10.2166/wst.2013.187.
15. Wu, D., Ekama, G. A., Chui, H. K., et al. (2016) Large-scale demonstration of the sulfate reduction autotrophic denitrification nitrification integrated (SANI®) process in saline sewage treatment. *Water Res.*, Vol. 100, 496–507, doi: 10.1016/j.watres.2016.05.052.
16. *Denitrification in the recycling systems theory and practice* (2016). Retrieved from http://aquavitro.org/2016/01/30/denitrifikaciya-v-recirkulyacionnyx-sistemax-teoriya- i-praktika.
17. Liu, F., Huang, G., & Fallowfield, H. (2014). *Study on heterotrophic-autotrophic denitrification permeable reactive barriers (HAD PRBs) for in situ groundwater remediation*. Springer. Retrieved from http://www.springer.com/978-3-642-38153-9.

Використання сульфуру в біологічних системах біологічної дентріфікації стічних вод

Пляцук Л. Д.[1], Черниш Є. Ю.[1*], Аблєєва І. Ю.[1], Козій І. С.[1], Балінтова М.[2], Матяш Я. О.[1]

[1] Сумський державний університет, вул. Римського-Корсакова, 2, м. Суми, 40007, Україна;
[2] Технічний університет м. Кошице, вул. Летна, 1, м. Кошице, 040 01, Словаччина

Анотація. У статті основна увага приділяється вивченню можливості використання мінеральних носіїв з сірки (біо-сірки / елементарної сірки) в системах анаеробного очищення стічних вод в умовах автотрофної денітрифікації. Теоретичні аспекти роботи засновані на біохімічної формалізації процесів очищення з використанням системно-синергетичного підходу для опису закономірностей автотрофних денітрифікуючих мікроорганізмів на основі принципів автокаталізу природних систем. Спеціальне програмне забезпечення використовувалося для визначення необхідних екологічних і трофічних груп мікроорганізмів та для реалізації схем трофічних взаємодій в асоціаціях мікроорганізмів-денітрифікаторів. Таксономічна класифікація призначена на основі бази даних KEGG (Кіотська енциклопедія генів і геномів). Була розроблена система біофільтрації для проведення денітрифікації модельних стічних вод з використанням біо-сірки і газової сірки. Метод фільтрації використовується в анаеробних умовах з іммобілізацією на носії з сірки аутотрофний денітрифікуючих бактеріальних видів Thiobacillus denitrificans і Thiomicrospira denitrificans. Трансформації сірки цими мікроорганізмами призводить до відновлення нітратів до нітритів і до вивільнення молекулярного азоту. Механізми конверсії сірки в природних екосистемах дозволяють зробити висновок про доцільність використання її як сорбційного сірковмісного мінерального носія в системах очищення стічних вод з конверсією в органічну форму (з карбонатом мікробних клітин). Модель шляхів взаємодії в асоціації гетеротрофних і автотрофних денітрифікуючих бактерій у процесі очищення стічних вод і мулових осадів була сформована за умови присутності елементарної сірки. Описано енергетичні реакції і реакції синтезу для автотрофної денітрифікації. Впровадження систем очистки стічних вод з використанням процесу автотрофної денітрифікації дасть змогу розширити сферу застосування ряду побічних продуктів, таких як газоподібна сірка та біо-сірки, які в даний час мінімальні для традиційної промислової переробки.

Ключові слова: денітрифікація, біо-сірка, газова сірка, стічні води, мінеральні носії.

JOURNAL OF ENGINEERING SCIENCES
ЖУРНАЛ ІНЖЕНЕРНИХ НАУК
ЖУРНАЛ ИНЖЕНЕРНЫХ НАУК

Web site: http://jes.sumdu.edu.ua

DOI: 10.21272/jes.2018.5(1).h3 Volume 5, Issue 1 (2018)

UDC 658.567

Research of the Energy Characteristics of Municipal Solid Waste in Cherkassy

Sigal O.[1], Boulanger Q.[2], Vorobiov L.[1], Pavliuk N.[1], Serhiienko R.[1]

[1] Institute of Engineering Thermophysics of NAS of Ukraine, 2a, Zhelyabova St., Kyiv, 03057, Kyiv;
[2] JSC "BETEN International", 79 la Bruyere Av., Vitry-Sur-Seine, 94 400, France

Article info:
Paper received: February 18, 2018
The final version of the paper received: March 22, 2018
Paper accepted online: March 25, 2018

***Corresponding Author's Address:**
liv298@ukr.net

Abstract. The waste management system of Ukraine, is being reformed to bring it in line with European standards for the use of the material and energy potential of waste. Selection of the optimal system should be based on the statistical representativeness of the results of a detailed analysis of the morphology of the municipal waste of each locality in accordance with the socio-economic profile of individual zones of the city and the seasons of the year, as well as the energy and environmental characteristics of the waste. But there are no standards for determining of energy characteristics of municipal solid waste in the country. This paper shows results of characteristics research of municipal solid waste in Cherkassy city carried out in accordance with the new approaches. A methodology for determining the humidity, net calorific value and ash content of municipal solid waste is developed. The results of experimental studies of humidity, calorific value and ash content for 8 components of waste: paper, cardboard, composite materials, textiles, hygiene products, plastic, other combustible materials, wood shavings are presented. Humidity is also determined in organic residues and in fine fractions. The results of the research are used to develop an integrated waste management and recycling system in Cherkassy.

Keywords: morphological composition, secondary energy resource, municipal solid waste, methodology, calorific value, moisture, ash content.

1 Introduction

The increase in the amount of waste is a concern for many countries in the world. Accumulation of municipal solid waste (MSW) threatens to become a global problem for Ukraine. For many years the country has been working on a simplified system of solid waste management, when almost all waste was mixed in a general not weatherproof container and was taken for disposal in landfills.

In the context of the global trend to reduce the consumption of fossil fuels and replacing them with renewable and alternative sources of energy legislation of the civilized countries of the world is directed at the use of material and energy potential of MSW (more than 20 % of the municipal solid waste of these countries is used for the production of electric and thermal energy) [1]. This approach is enshrined in the Framework Directive No 2008/98/EU of 19.11.2008 "On waste and repealing certain Directives", also known as the Waste Framework Directive or WFD [2], etc.

European principles of waste management laid the basis for a National waste management strategy (NWMS) in Ukraine till 2030, approved by the Cabinet of Ministers of Ukraine [3]. Within two years after the approval of the NWMS, regional waste management plans should be developed. Selection of the waste management system should be based on the analysis of MSW morphology of and energy characteristics of its components.

For the implementation of the principles of NWMS Cherkassy city Council supported by the Ministry of Finance of France, invited the French company "BETEN INGENIERIE" to develop Ukraine's first integrated project for the disposal, processing, valorization (increasing the cost by selecting components for reuse) and efficient secondary recycling of solid waste in Ukraine. The purpose of the project is to optimize and substantiate the processes of municipal solid waste management, reduce the amount and area of landfills in the city of Cherkasy and the surrounding area, and build waste composting and sorting plant.

The company "BETEN INGENIERIE" has analyzed the morphology of MSW to study their exact annual composition in accordance with the demographic and socio-economic profile of individual areas of the Cherkassy city (population, trade establishments, industrial

facilities), in accordance with the accepted European methodology.

Analysis of the energy characteristics of MSW components in Cherkassy city, which can be used for energy valorization, and nutrient content in the waste that is subject to composting, was performed by the Institute of Technical Thermophysics of the National Academy of Sciences of Ukraine on request and with the financing of "BETEN INGENIERIE".

2 Literature Review

The main energy characteristics that determine the expediency of using MSW as a secondary energy resource are humidity, net calorific value (NCV) and ash content.

The research of these characteristics is carried out by experts from many countries of the world. Analysis of publications carried out by the authors [4], showed significant difference in the classification of the morphology of solid waste and in calorific value of components in different countries and Ukraine (Table 1). According to the Commission's Decision on the European List of Waste [5], the classification of MSW components includes 40 items, while in Ukraine, according to the Order Ministry of Regional Development, Construction and Housing and Communal Services of Ukraine of Ukraine, only 11 ones [6], which complicates the study of component characteristics.

Table 1 shows that the use of MSW as a secondary energy source can replace the corresponding amount of fossil fuels, which is extremely relevant for Ukraine [7].

Table 1 – Generalized morphology and net calorific value of MSW components in the leading countries of the world, Ukraine and CIS countries

The type of MSW component	Net calorific value of solid waste, MJ/kg			
	EU, WB	Ukraine (data up to 2014)	Russian Federation	Kazakhstan
Organic materials (Food waste)	1.9–4.1	3.1–3.8	3.4–6.2	3.3
Paper and cardboard	6.5–16.0	7.5–11.5	9.5–15.0	9.9
Plastic	20.1–35.0	24.4	24.4–28.0	24.4
Textiles	11.8–19.0	12.1–15.0	14.0–19.1	15.7
Leather and rubber	N/A	20.9–25.2	23.0–33.5	25.8
Wood	13.6	13.4–14.5	14.0–15.0	14.5
Small remains	2.6–3.5	3.1	4.6–8.7	4.6
Other	32.0	N/A	18.1	N/A

This work is aimed at the adaptation of the MODECOM methodology for the determination of the morphological composition of MSW with taking Ukrainian conditions into account; development of recommendations for methodological approaches to the determination of energy characteristics of MSW components in Ukraine: humidity, NCV and ash content, as well as conducting experimental studies of the energy characteristics of Cherkassy city.

3 Research Methodology

3.1 Methodology of determination of morphological composition

The MODECOM methodology is developed by the French Agency for Environmental Management and Energy Management (ADEME) and fully complies with European standards aimed at ensuring the statistical representativeness of the research results. In particular, samples are collected in different areas of the city in accordance with the demographic and socio-economic profile of individual zones. In addition, samples are taken from both housing stock and commercial, administrative and industrial facilities. Typically, samples are taken from (1) the private sector, (2) the sector of multiapartment buildings, (3) the trade and administrative sector, (4) the industrial zone.

The morphological composition of MSW was determined by the following indicators:

– granulometry;

– type of material;

– potential to avoid landfill.

Morphological study complied the requirements of European regulations - on sampling waste (standard EN 14899) and on the collection of samples of solid waste in containers (norm X30-413).

In Cherkassy, 13 samples weighing around 600 kg were selected in each of the two worst seasons of the year (due to the high humidity of the solid waste): December-January and August-September, which ensured high accuracy of the results.

For sorting by category, each sample was mixed, then sorting was done according to the size of the waste (more than 100 mm, from 20 to 100 mm, up to 20 mm), the type of material (13 categories: organic, paper, cardboard, composite materials, textiles, sanitary textiles, plastics, combustible materials, glass, metals, non-combustible materials, hazardous household waste, fine fraction (up to 20 mm), and subspecies of material (more than 30 subcategories). Further systematic weighing of samples of waste was carried out.

3.2 Methodology of determination of MSW energy characteristics

At present, Ukraine has no standards for the study of humidity, NCV and ash content for MSW, but standards exist for defining these characteristics for solid organic fuels [8–11]. At the same time, international standards and harmonized standards exist in some CIS countries [12–15]. These standards have some differences in methods of preparation of samples, measurement and processing of their results. Most studies have been carried out in accordance with Ukrainian standards, but, taking into account the peculiar properties of MSW, certain operations have been conducted with taking into account requirements of international standards.

The main difference between solid waste and conventional solid organic fuels, in terms of experimental determination of energy properties, is its significant heterogeneity, both in composition and in humidity.

In the study of fuels, as a rule, an analytical sample of 1 g is prepared, shredding it to the size of the particle of 0.1–0.2 mm and homogenizing.

Analysis of the energy characteristics of MSW components in Cherkasy city was conducted for 11 separate components, exceeding the classification according to the Order of the MHCP of Ukraine [6]. All materials that were not included in the inert and reprocessed waste were analyzed. The preparation of experimental samples showed a significant heterogeneity of the components of the MSW even within one component, which, due to the small weight and the need for thorough homogenization of the sample significantly complicated the study of characteristics and resulted in a significant dispersion of results and increase uncertainty of measurements. This is confirmed by previous authors' studies [4].

The analytical sample is kept in the laboratory room until the air-dry state is reached, and then at least two parallel measurements of the moisture, ash content and NCV of the analytical sample were carried out. The difference in measurement results in parallel measurements should not exceed the limits specified with the normative documents. The moisture for each component was measured at the delivery state for the entire sample volume, then the components were shredded, homogenized, dried and brought to air-dry state, the humidity and ash content in the analytical state were measured for the entire volume of the prepared specimens.

In the NCV study of heterogeneous samples, a spread of measurement results was observed that exceeded the permissible difference between the two measurements, so at least five experiments were performed and the result was defined as arithmetic mean. For a qualitative study of the energy characteristics of MSW, it is appropriate for Ukraine to introduce a more detailed European classification.

3.3 Method of determination of moisture content

For each of the components provided, the determination of relative humidity is made for two states - delivery and analytical. The method consists in weighing the sample in the initial state, drying the sample at a given temperature to a constant mass and weighing the sample in a dry state. Drying of most samples is carried out at temperature (105 ± 2) °C, but for components with low melting temperature, for example, polyethylene or Styrofoam, drying is carried out at a temperature (70 ± 2) °C. Relative humidity was determined by the ratio of the total change in mass of the sample to the initial mass.

3.4 Method of determination of ash content

The ash content of samples were determined by the slow ashing in accordance with the requirements of GOST 11022-95 (ISO 1171-97) [9]. A crucible or a boat with the sample is weighed and placed in muffle, heated to 500°C for 60 minutes and held at this temperature for 60 minutes, then the temperature was raised to (815±10)°C for 60 minutes and maintained at this kept for 2 hours. Different duration of exposure is recommended for different types of traditional fuels, usually from 30 minutes to 2 hours, for a MSW test the maximum duration of 2 hours were selected. After exposure crucible or boat is taken out of the oven, cooled for 5 minutes on a ceramic or metal support and then in a closed desiccator to room temperature and weighed. The ash content of the analytical sample was calculated as a percentage that represents the ration between weights of the remnants after ashing and the initial mass of sample.

3.5 Method of determination of net calorific value

The methodology generally complies with the standard methods for solid fuels GOST 147-95 (ISO 1928-76) [10] and DSTU ISO 1928 [11].

Measurements were carried out in an automated bomb calorimeter of the heat flow (Kalve type) [16]. The device is anhydrous, does not require water weighing and a determination of its temperature rise, as required by traditional water calorimeters. After completion of measurements, the device outputs the energy Q_T (J) allocated in the bomb.

Net calorific value of combustion of an analytical sample in a bomb is Q_b^a calculated by the formula, kJ/kg:

$$Q_b^a = \frac{Q_T - q_{\text{wr}} \cdot (m_1 - m_2) - q_{pap} \cdot m_4}{m_3}, \qquad (1)$$

where Q_T is the total heat emitted during the combustion of the sample according to the readings of the device; q_{wr} = 2 510 kJ/kg, q_{pap} = 15 627 kJ/kg – specific calorific value of inflammable wire and paper package; m_1, m_2 – initial and remaining mass of the wire; m_3 – mass of sample; m_4 – mass of the paper package.

Gross calorific value of an analytical sample, taking into account corrections for the creation and dissolution of acids, was calculated according to [10, 11] by the formula, kJ/kg:

$$Q_s^a = Q_b^a - \left(94 \cdot S^a + \alpha \cdot Q_b^a\right), \qquad (2)$$

where 94 – coefficient, taking into account the heat of formation of sulfuric acid from sulfur dioxide and dissolution of sulfuric acid in water by 1 % sulfur, passed at combustion of fuel in sulfuric acid, kJ/kg; S^a – mass fraction of sulfur in the analytical sample of fuel, %; $\alpha \cdot Q_b^a$ – an amendment that takes into account the heat of formation and dissolution in water of nitric acid, the value of which is determined by calibrating the calorimeter $\alpha \cdot Q_b^a$ = 29 kJ/kg.

The higher heat of combustion for dry fuel at constant volume Q_s^d and fuel in the delivery condition was calculated according to the formulas, kJ/kg:

$$Q_s^d = Q_s^a \frac{100}{100 - W^a}; \quad Q_s^r = Q_s^a \frac{100 - W^r}{100 - W^a}. \tag{3}$$

In determining of the net calorific value according to the standards [10, 11], generally use the notion of NCV at constant volume, which is traditionally calculated by the formulas, kJ/kg:

– for working condition:

$$Q_i^r = Q_s^r - 24{,}42\left(W^r + 8{,}94H^r\right); \tag{4}$$

– for dry condition:

$$Q_i^d = Q_s^d - 24{,}42 \cdot 8{,}94H^d = Q_s^d - 218{,}3H^d. \tag{5}$$

The Annexes to these standards also provide formulas for calculating the calorific value at constant volumes, which are harmonized with the current international standards, and have different calculation factors, kJ/kg:

– for working condition:

$$Q_{i,V}^r = \left(Q_{s,V}^d - 206H^d\right)\frac{100 - W_t^r}{100} - W_t^r; \tag{6}$$

– for dry condition:

$$Q_{i,V}^d = Q_{s,V}^d - 206H^d. \tag{7}$$

In the latest standards [12–15], on the contrary, the concept of calorific value at constant pressure is the main one and the following formulas are given, kJ/kg:

– for working condition:

$$Q_{i,p}^W = [Q_{s,V}^d - 212{,}2H^d - 0{,}8(O^d + N^d)]\times \times\left(1 - 0{,}01W\right) - 24{,}43W; \tag{8}$$

– for dry condition:

$$Q_{i,p}^d = Q_{s,V}^d - 212{,}2H^d - 0{,}8\left(O^d + N^d\right) \tag{9}$$

The analysis of the above formulas shows that the difference in the results of the calculations by the various given methods is rather small, but for the verification of this fact, parallel calculations for the dry fuel state according to formulas (5), (7), (9) have been performed and the relative (in percentages) the difference between the largest and the smallest values (Table 2).

For arbitrary working humidity W^r and ash content A^r, hydrogen and sulfur content is calculated according to the formulas [17], %:

$$\mathrm{H^r} = \mathrm{H^{daf}} \times \frac{100 - W^r - A^r}{100}; \quad \mathrm{S^r} = \mathrm{S^{daf}} \times \frac{100 - W^r - A^r}{100}. \tag{10}$$

In the above formulas, *A* is ash content; *W* – humidity; *H*, *N*, *O*, *S* – relative content (as a percentage) of hydrogen, nitrogen, oxygen, sulfur, respectively; upper indexes of the designation of the state: *d* - dry, daf – dry, ash free, *r* – working (deliveries); lower indices: *s* – gross heat; *i* – net heat; *p* – under constant pressure; *V* – for constant volume.

4 Results

Calculations of NCV were done for the three conditions of components: analytical Q_i^a, delivery Q_i^r, dry Q_i^d. The results of calculations are presented in Table 2. The table also shows the values of NCV at constant volume $Q_{i,V}^d$ and at constant pressure $Q_{i,p}^d$, calculated from formulas (7) and (9), and the highest relative (in percent) difference between values for dry state.

According to the calculations, it was found that the difference between the values of the heat of combustion for the dry state, calculated according to different methods, does not exceed 0.54 %, and the absolute difference is less than 0.12 MJ/kg, that does not exceed the value of the permissible difference of the results in the measurements . Thus, for technical calculations, the use of each of the values is permissible, and then the value Q_i^d calculated by formula (5) is given.

Influence of humidity of components on the heat of their combustion is shown in Fig. 1.

The data in Fig. 1 clearly demonstrate the negative effects of moisture on the energy characteristic of solid waste.

The following parameters were studied:

– calorific value and the content of heavy metals in waste;

– the content of nutrients in the waste that is subject to composting;

– the content of heavy metals in MSW that is to be buried.

The main results of determining the humidity, calorific value and ash content of MSW components in Cherkassy city is given in Table 3.

Table 2 – Results of NCV determination for MSW components by different methods

Generic component name	H^{daf}, %	Q_i^a, MJ/kg	Q_i^r, MJ/kg	Q_i^d, MJ/kg	$Q_{i,V}^d$, MJ/kg	$Q_{i,p}^d$, MJ/kg	max δQ_i^d, %
Paper	6.2	13,236	9.335	14.334	14.410	14.372	0.53
Cardboard	6.2	13.221	8.407	14.195	14.271	14.232	0.54
Composite materials	7.2	27.639	20.450	28.542	28.631	28.586	0.31
Textiles	6.8	15.784	10.481	16.789	16.873	16.830	0.50
Hygiene products	6.8	25.944	2.617	27.314	27.398	27.356	0.31
Plastic	9.3	38.020	33.164	38.355	38.469	38.412	0.30
Other flammable materials	7.2	17.872	16.166	18.186	18.274	18.230	0.49
Wood parcel (Green waste)	6.1	16.721	15.952	18.166	18.241	18.203	0.41

Table 3 – The main results of determining the humidity, ash content, calorific value of MSW components in Cherkassy city

Generic component name	Delivery condition (working condition)				Dry condition, W = 0 %		
	Humidity Wr, %	Ash content Ar, %	GCV Q_s^r	NCV Q_i^r	Ash content Ad, %	GCV Q_s^d	NCV Q_i^d
			MJ/kg	MJ/kg		MJ/kg	MJ/kg
Paper	30.2	7.8	10.95	9.33	11.2	15.69	14.33
Cardboard	35.1	8.3	10.09	8.41	12.8	15.55	14.19
Composite materials	26.4	6.2	22.17	20.45	8.5	30.11	28.54
Textiles	33.3	1.3	12.18	10.48	2.0	18.27	16.79
Sanitary textiles	83.2	1.9	4.83	2.62	11.3	28.80	27.31
Plastic	13.0	4.1	35.13	33.16	4.7	40.39	38.35
Other flammable materials	10.2	10.7	17.74	16.17	11.9	19.76	18.19
Wood parcel (Green waste)	11.1	2.5	17.34	15.95	2.8	19.50	18.17
Organic Remnants	74.9	–	–	–	–	–	–
Small fraction of MSW	47.6	–	–	–	–	–	–

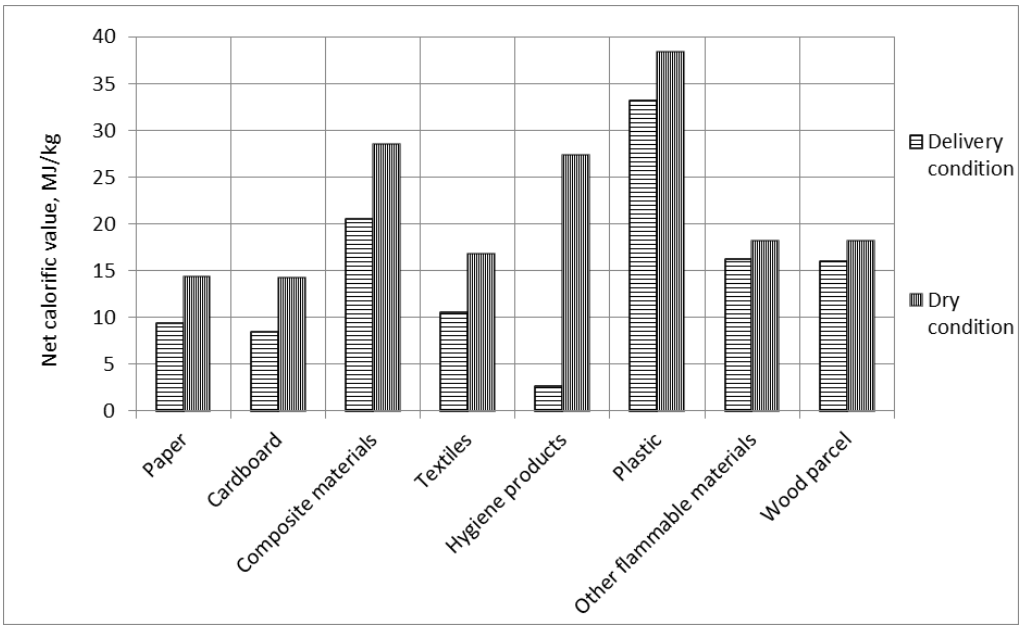

Figure 1 – Influence of humidity on the NCV of MSW components

The results of the research indicate significant differences in the studied characteristics in different components of the waste. The highest content of moisture was attributed to organic residues and hygiene products – 74.9–83.2 %, the smallest – to other combustible materials, wood particles and plastic – 10.2–13.0 %. Hygiene products had the lowest calorific value – 2.62 MJ/kg, the highest – plastic – 33 MJ/kg.

The results of the experimental study of GCV and calculations of the NCV of MSW components in the dry state show a significant increase in calorific value compared to moist components in the delivery state. The calorific value of hygiene products has increased by almost 10 times. The calorific value of the cardboard has increased by 69 %, textiles – by 60 %, paper – by 54 %, composite materials – by 40 %. The calorific value of components with less hygroscopicity has increased significantly less: calorie plastic increased by 16 %, other combustible materials – by 12 %, wood particles – by 14 %.

The results of ash content studies of MSW components in the delivery state showed values ranging from 1.3 % (textiles) to 10.7 % (other combustible materials). The ash content of MSW components in the dry state ranged from 2.0 % (textiles) to 12.8 % (cardboard).

The values of ash content were somewhat higher than that inherent in pure materials, which is probably due to the contamination of the studied components with soil particles.

5 Conclusions

The above described method and process of sorting and weighing of detailed subcategories allows:

– to precisely determine the potential of waste valorization, because today not all types of plastic are valorized with the same way;

– to design, measure, accept and approve the feasibility study for the processing of municipal waste: composting, methanization (biological decomposition with the release of biogas), sorting or use for energy production.

The studies showed significant heterogeneity of MSW components even within the same component that led to substantial variability in results and increase the uncertainty of measurement due to small weight and need for careful homogenization the sample, which experimentally investigated. That significantly complicated the definition of characteristics. This indicates the necessity of adopting in Ukraine of European methods of detailed morphology of solid waste.

The implementation of the NWMS requires the approval of standards for determining the energy performance of municipal solid waste. In the framework of the recommendations on methodological approaches to the definition of moisture content, calorific value and ash content of MSW. Approval of these recommendations was carried out in the study of the energy characteristics of MSW components in Cherkassy city.

The calorific value of MSW depends on the morphological composition and humidity of the components. In the samples tested in the state of supply humidity ranged from 10.2 to 74.9 % with ash content from 1.3 to 10.7 %. Drying of components increases their calorific value from 1.1 to 10.4 times.

It is expedient to optimize the waste collection process in order to efficiently use the energy potential of solid waste. According to European practice, solid waste is collected in closed containers, which are located underground or under sheds, in order to prevent action the atmospheric precipitation on MSW. If possible, such practice should be introduced in Cherkassy city.

The results of the research are used to develop a “Plan to prevent waste generation” and an integrated waste recycling and utilization system in the city of Cherkassy. According to NWMS, such a plan will be mandatory for each city up to 2020.

6 Acknowledgements

The main results of the scientific research were carried out with the support of the French company “BETEN INGENIERIE”.

References

1. What a Waste. A Global Review of Solid Waste Management. *World Bank*, 2012. Retrieved from https://siteresources.worldbank.org/INTURBANDEVELOPMENT/Resources/336387-1334852610766/What_a_Waste2012_Final.pdf.
2. Directive 2008/98/EU of the European Parliament and of the Council of 19 November 2008 on waste and repealing certain Directives. Retrieved from: http://eur-lex.europa.eu/legal-content/EN/TXT/PDF/?uri=CELEX:32008L0098&from=EN.
3. Resolution of the Cabinet of Ministers of Ukraine “On approval of the National Waste Management Strategy until 2030” (No. 820 from November 8, 2017). Retrieved from: http://zakon2.rada.gov.ua/laws/show/820-2017-%D1%80 [in Ukrainian].
4. Sigal, O. I., Krikun, S. S., Pavliuk, N. Yu., Satin, I. V., Plashikhin, S. V., Kirzhner, D. A., Semeniuk, M. V., & Kamenkov, G. B. (2017). A research on the amount of heat produced during combustion of mixed municiapl solid waste in Kiev city. *Industrial heat engineering*, Vol. 39, No. 3, 78–84 [in Ukrainian].
5. 2000/532/EU: Commission Decision of 3 May 2000 replacing Decision 94/3/EU establishinga list of wastes pursuant to Article 1(a) of Council Directive 75/442/EU on waste and Council Decision 94/904/EU establishinga list of hazardous waste pursuant to Article 1(4) of Council Directive 91/689/EU on hazardous waste. Retrieved from: http://eur-lex.europa.eu/LexUriServ/LexUriServ.do?uri=CONSLEG:2000D0532:20020101:EN:PDF.

6. Order of the Ministry of Housing and Communal Services dated February 16, 2010 No. 39 "On Approval of Methodological Recommendations for the Determination of the Morphological Composition of Solid Waste". Retrieved from: http://document.ua/pro-zatverdzhennja-metodichnih-rekomendacii-z-viznachennja-m-doc17422.html [in Ukrainian].
7. Pavliuk, N. Yu., & Sigal, O. I. (2015). Approaches to the problem of municipal solid waste in the world and in Ukraine. *Industrial heat engineering*, Vol. 37, No. 3, 74–81 [in Ukrainian].
8. GOST 27314-91. *Solid mineral fuel. Determination of moisture*. Interstate Standard. Retrieved from: http://docs.cntd.ru/document/1200024258 [in Russian].
9. GOST 11022-95 (ISO 1171-97). *Solid mineral fuels. Methods for determination of ash*. Interstate Standard. Retrieved from: http://docs.cntd.ru/document/gost-11022-95 [in Russian].
10. GOST 147-95 (ISO 1928-76). *Solid mineral fuel. Determination of the highest combustion heat and calculation of the lowest combustion heat*. Interstate Standard. Retrieved from: http://docs.cntd.ru/document/1200024029 [in Russian].
11. DSTU ISO 1928:2006 *Solid mineral fuels. Determination of gross calorific value by the bomb calorimetric method, and calculation of net calorific value*. Retrieved from: http://document.ua/paliva-tverdi-mineralni_-viznachennja-naivishoyi-teploti-zgonor15093.html [in Ukrainian].
12. ISO 1928:2009. *Solid mineral fuels. Determination of gross calorific value by the bomb calorimetric method and calculation of net calorific value*. Retrieved from: https://www.iso.org/standard/41592.html.
13. GOST 147:2013 (ISO 1928:2009, MOD). *Determination of gross calorific value and calculation of net calorific value*. Interstate Standard. Retrieved from: http://docs.cntd.ru/document/1200107606 [in Russian].
14. GOST 33108-2014 (EN 15400:2011 MOD). *Solid recovered fuel. Determination of calorific value*. Interstate Standard. Retrieved from: http://docs.cntd.ru/document/1200120566 [in Russian].
15. EN 15400:2011. *Solid recovered fuels. Determination of calorific value*. – Retrieved from: https://shop.bsigroup.com/ProductDetail/?pid=000000000030205126.
16. Vorobiov, L. I., Dekusha, L. V., Nazarenko, O. A., & Grishchenko, T. G. (2017). The practical application of quasidifferetial calorimetry method in the device for combustion heat measurement. *Industrial heat engineering*, Vol. 39, No. 1, 71–75 [in Russian].
17. GOST 27313-95. *Solid mineral fuel. Symbols of analytical results and formulae for calculation of analyses to different bases*. Interstate Standard. Retrieved from http://docs.cntd.ru/document/1200024257 [in Russian].

Дослідження енергетичних характеристик твердих побутових відходів м. Черкаси

Сігал О. І.[1], Буланже К.[2], Воробйов Л. О.[1], Павлюк Н. Ю.[1], Сергієнко Р. В.[1]

[1] Інститут технічної теплофізики НАН України, вул. Желябова, 2а, м. Київ, 03057, Україна;
[2] АТ "БЕТЕН Інтернешнл", просп. ла Брюєр, 79, Вітрі-сюр-Сен, 94 400, Франція

Анотація. В Україні реформується система поводження з відходами для приведення її у відповідність до європейських стандартів використання матеріального та енергетичного потенціалу відходів. Вибір оптимальної системи має ґрунтуватись на статистичній репрезентативності результатів детального аналізу морфології муніципальних відходів кожного населеного пункту відповідно до соціально-економічного профілю окремих зон міста та сезонів року, а також їх енергетичних та екологічних характеристик. Але в країні відсутні стандарти з визначення основних енергетичних характеристик твердих побутових відходів.Відповідно до нових підходів проведено дослідження твердих побутових відходів м. Черкаси. Розроблені рекомендації щодо методологічних підходів до визначення вологості, теплоти згоряння та зольності твердих побутових відходів. Наведені результати експериментальних досліджень вологості, теплоти згоряння та зольності 8 компонентів відходів: паперу, картону композитних матеріалів, текстилю, продуктів гігієни, пластику, інших горючих матеріалах, деревного стружку. Вологість визначена також в органічних рештках та у дрібній фракції. Результати дослідження використовуються для розробки комплексної системи переробки та утилізації відходів у м. Черкаси.

Ключові слова: морфологічний склад, вторинний енергоресурс, тверді побутові відходи, методика, теплота згоряння, вологість, зольність.

JOURNAL OF ENGINEERING SCIENCES
ЖУРНАЛ ІНЖЕНЕРНИХ НАУК
ЖУРНАЛ ИНЖЕНЕРНЫХ НАУК
Web site: http://jes.sumdu.edu.ua
DOI: 10.21272/jes.2018.5(1).h4 Volume 5, Issue 1 (2018)

UDC 504.06

Efficiency Analysis of Tracking and Stationary Solar Panel Modes Against Solar Radiation

Samaulah H.[1*], Basir Y.[1], Helmi M.[1], Faturrizky F.[1], Sugawara A.[2]

[1] Tridinanti University of Palembang, 30129 South Sumatera, Indonesia;
[2] Niigata University, 950-2181 Niigata, Japan

Article info:
Paper received: April 4, 2018
The final version of the paper received: May 24, 2018
Paper accepted online: May 27, 2018

[*]**Corresponding Author's Address:**
hsamaulah@gmail.com

Abstract. The utilization of solar energy sources is done by using photovoltaic (solar panels). The energy emitted by the sun is fluctuating. This change in radiation energy will also affect the output of solar panels. The relationship of change is what will be measured, observed and proven in this study. The observations are made using a gauge called the solar power meter, where this device can read the amount of solar radiation energy in the W/m^2 unit. While the output to be measured is the output power generated by the solar panel itself. Measurement in this study was done using two modes; i. e. stationary mode and tracking mode. The stationary mode is done by placing the solar panel face with slope and azimuth in a predetermined direction, while the tracking mode is to place the solar panel face exactly 90° to the sun. Evidently by placing the solar panels to keep the sun coming up, it can achieve efficiency up to 14.1 % compared to stationing solar panels stationed 75° to the north which can only achieve efficiency of 13.7 %.

Keywords: radiation energy, photovoltaic, efficiency, solar panel.

1 Introduction

Sun energy or better known as solar energy has now become one of the alternative energy sources for the generation or provision of electrical energy. The existence of science in the development of new and renewable resources is a solution in answering the problematic about the limited availability of fossil resources. Radiation from solar energy is absorbed through medium called solar panels and then converted into electrical energy [1–2].

Given the nature of the sun that is always changing every time, it can be ascertained that the electrical energy generated by a solar panel will also experience fluctuations. This needs to be observed and taken into account in order to establish the best tilt angle or even the best mounting mode of a solar panel in a particular location where solar panels can generate maximum electrical energy according to their highest wattage value.

This research attempt to discover to objectives; they are 1) proving the relationship of the angle of solar panels to the intensity of solar radiation that can be absorbed by solar panels; and 2) discover and prove the relation of the intensity of solar radiation absorbed by the solar panel with its output power. Therefore, this study focused on the magnitude of the intensity of solar radiation that can be absorbed by a solar panel and the power generated by solar panels positioned at a predetermined angle and time.

2 Literature Review

2.1 Sunlight

Solar energy supplies energy to the earth in the form of radiation. Solar energy system is exposed to different amounts of sunlight, which controls the amount of power generated by the solar energy conversion system. In other words, the system generates more power when it is exposed to greater amount of sunlight. Each year there are about $3.9 \cdot 10^{24}$ J ($1.08 \cdot 10^{18}$ kW·h). Throughout the year, the distance between the sun and the earth varies between $(1.47–1.52) \cdot 10^8$ km.Consequently, irradiance E° fluctuates between 1.325–1.412 W/m^2. The Earth's atmosphere retract and reduces the sun's radiation through the process of reflection, absorption (ozone, water vapor, oxygen and carbon dioxide) and scattering (air molecules, dust particles or pollution). For sunny weather during the day, the irradiance reaching the earth's surface are 1 W/m^2.

2.2 Solar panels

2.2.1 The structure of solar panels

Solar panels are generally used to harness solar energy [3–8]. Silicon solar panels get heated to a temperature of more than 70 °C when they are subjected to intense sunlight for a prolonged duration of time. At this high tem-

perature, these panels show low efficiency while converting sunlight into energy. As a result, the system performance is diminished and the power generation system encounters a one-third loss approximately [9–10]. Therefore, a solar energy system is exposed to different amounts of sunlight, which controls the amount of power generated by the solar energy conversion system. In other words, the system generates more power when it is exposed to greater amount of sunlight.

One piece of solar cells illuminated by the sun can only produce a dc voltage of 0.5–1.0 V, and short-circuit currents in the scale of mA/cm^2. Therefore, a solar module typically consists of 28–36 solar cells and the total produces a dc voltage of 12 V in standard irradiation conditions. This collection of solar modules is then arranged in a field called solar panels (Figure 1).

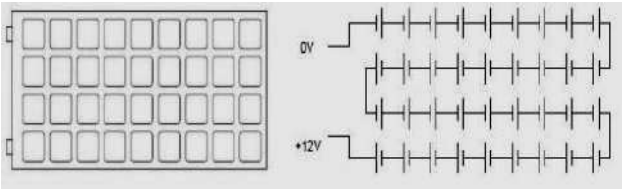

Figure 1 – The Solar Module (series)

2.2.2 How solar cells work

The photon is absorbed around depletion layer which is boundary between N-type silicon and P-type and an electron and a hole are separated. The electrons are attracted to the N-type silicon side, resulting in a potential voltage. It will increase electrical energy that can later be stored into a battery (Figures 2–3).

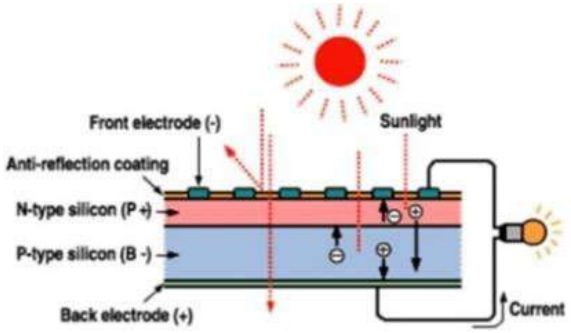

Figure 2 – How solar panels work

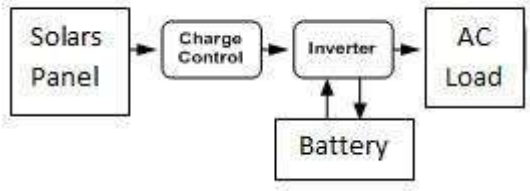

Figure 3 – Workflow of solar panels

The working process of receiving solar radiation by solar panels is to be converted into electrical energy.

2.2.3 Efficiency

The input power itself is the product of the intensity of solar radiation with the cross-sectional area of the solar panel.

$$P_{in} = E \cdot A, \quad (1)$$

where P_{in} – input power, W; E – intensity of solar radiation, W/m^2; A – cross section area, m^2 (Figure 4).

Several factors can reduce or even increase the efficiency of such solar panels, such as surface temperature of solar panels, power losses present in the connecting cable, and others [6]. However, ignoring these factors, efficiency can be calculated using the following equation:

$$P_{in} \cdot n = P_{out}, \quad (2)$$

where n – efficiency value; P_{out} – output power.

The effect of this solar intensity by assuming the temperature of the solar panel at a temperature of 25 °C. Practically, the surface temperature of solar panels will also fluctuate [2]. The solar cell will operate optimally if its surface temperature remains normal and stable at 25 °C. A rise in temperature higher than normal will weaken the voltage V_{oc} (Figure 5).

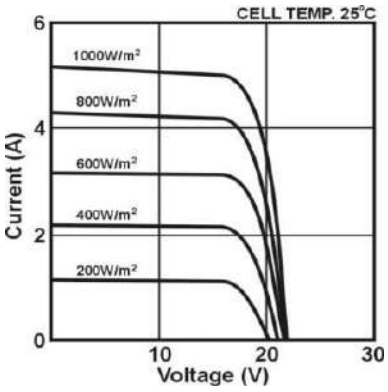

Figure 4 – The effect of intensity change

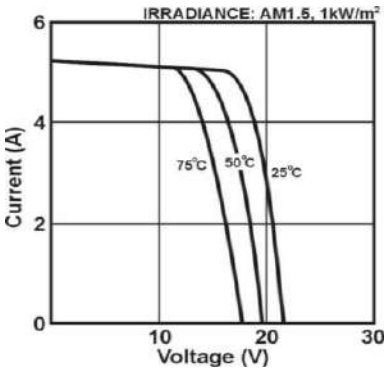

Figure 5 – The curve of solar cell surface temperature change effect

3 Research Methodology

3.1 Research workflows

The diagram of the research flow is presented in Figure 6.

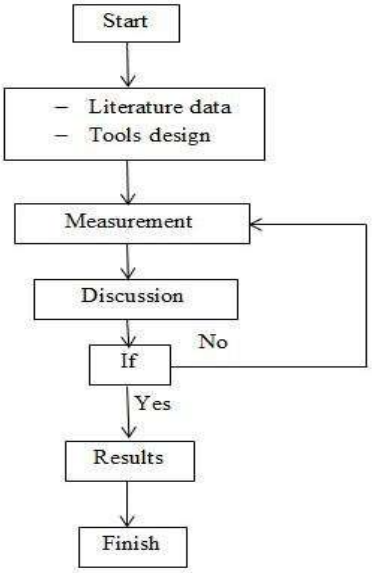

Figure 6 – The diagram of the research flow

3.2 Specification of solar module

The specification of Solar Cell 50WP (Figure 7) is presented in Table 1.

Table 1 – Specification of Solar Cell 50WP

Specification (Polycrystalline)	Information
Maximum power P_{max}	50 W
Maximum power voltage V_{mp}	16.5 V
Maximum power current, I_{mp}	3.34 A
Open circuit voltage, V_{oc}	21.1 V
Short circuit current, I_{sc}	4.23 A
Nominal operating cell temperature, *NOCT*	45 ± 2 °C
Maximum system voltage	1 000 V
Maximum series fuse	16 A
Total mass	6.5 kg
Dimensions	775×680×28 mm

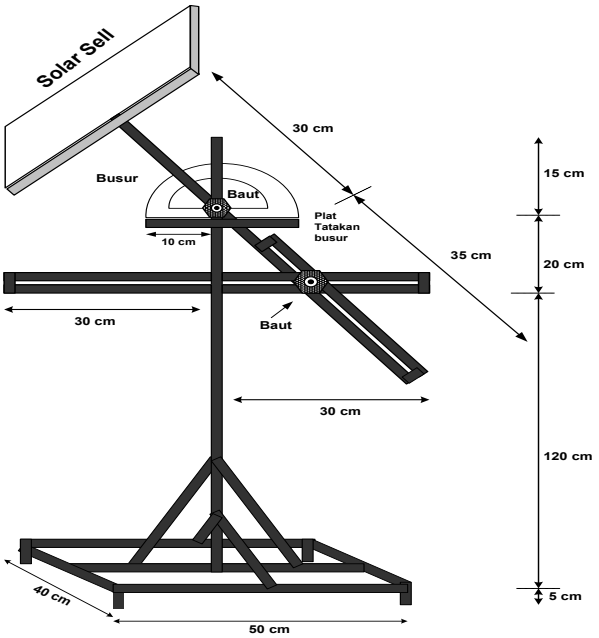

Figure 7 – Manual solar tracker

3.3 Position of solar panel

For stationary solar panels, this condition is set for each measurement time:

– putting solar panels in one fixed position;
– azimuth: 180° facing north;
– slope: 75°.

For solar tracking panels, its placement basically means always positioning solar panels by precisely following the direction of the sunlight. The adjustment of the tilt of the solar panel is adjusted at the following angles to adjust the direction of the sun on each hour:

– azimuth: 180° facing east;
– slope: from 30° to 150° with step 15°.

3.4 Time and location measurement

This measurement is done in rooftop of Magister Management Building of Tridinanti University of Palembang. Objects that need to be measured are the intensity of solar radiation absorbed by solar panels, as well as the current and output voltage of solar panels. For that the measuring tools that need to be used includes: Solar Power Meter and Multimeter (Figure 8).

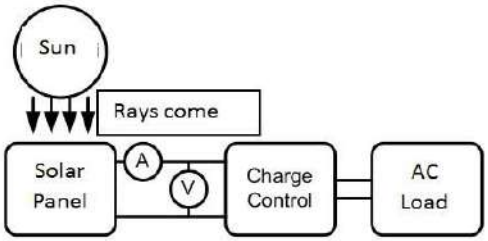

Figure 8 – The measurement circuit

4 Discussion and Analysis

4.1 The relationship of the angle to the radiation of the sun per day

The comparison of solar radiation intensity is presented in Table 2 and Figure 9, where E_2 – intensity of solar radiation captured by solar panel tracking; E_1 – intensity of solar radiation captured by stationary solar panels.

Table 2 – Comparison of solar radiation intensity

Time	Radiation, W/m^2		
	Stationary panel	Tracking panel	$\Delta E = E_2 - E_1$
08:00	246.64	326.46	79.82
09:00	294.72	362.47	67.75
10:00	424.12	464.40	40.28
11:00	398.87	431.90	33.03
12:00	394.01	454.21	60.2
13:00	336.36	399.47	63.11
14:00	329.27	439.75	110.48
15:00	259.51	355.46	95.95
16:00	177.43	320.87	143.44

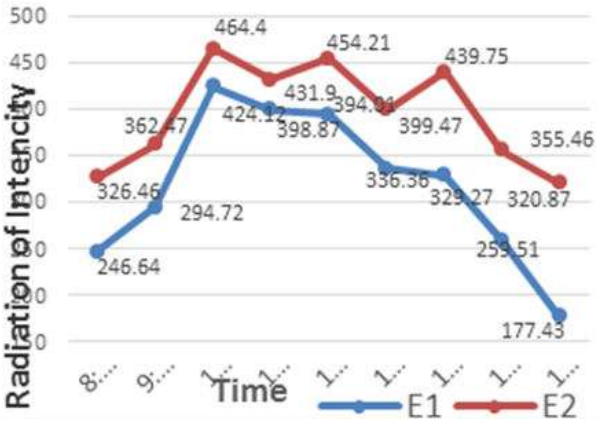

Figure 9 – The average radiation solar comparison curve per day

From the curve above we can see that solar panels with tracking mode can capture more solar radiation in a day. This is evidenced by the deviation value between the two that shows positive results.

The lowest increase is at 11:00, i. e. 33.03 W/m^2, or 8.3 %:

$$n = \frac{33.03}{397.95} \cdot 100\ \% = 8.3\ \%.$$

The highest average increase was at 16:00, i. e. 143.44 W/m^2 or 81 %:

$$n = \frac{143.44}{177.43} \cdot 100\ \% = 81\ \%.$$

A positive ΔP value indicates that the output power of the solar panel with tracking mode (perpendicular to the sun) is greater than the stationary solar panel. This is directly proportional to the intensity of solar radiation (Table 3, Figure 10). Where as the increased intensity of solar radiation that can be absorbed by a solar panel, it will also increase the output power.

Table 3 – Difference in output power of both solar panel modes

Time	Output power, W		
	P_1	P_2	$\Delta P = P_2 - P_1$
08:00	13.78	22.83	9.05
09:00	18.00	25.26	7.26
10:00	27.95	32.68	4.73
11:00	26.76	29.54	2.78
12:00	28.38	33.70	5.32
13:00	21.99	27.58	5.59
14:00	21.21	28.40	7.19
15:00	16.34	23.15	6.81
16:00	9.96	22.26	12.3

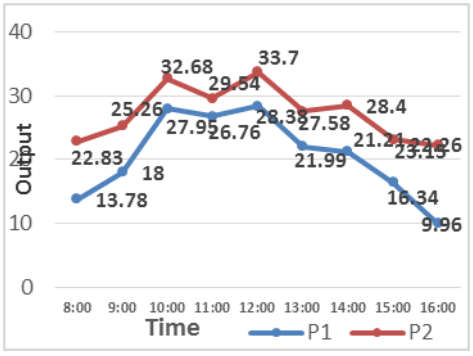

Figure 10 – Average power comparison curve

In Table 3, P_1 is the output power of the stationary solar panel; P_2 is the solar power output tracking.

The lowest power increase is at 11:00 o'clock at 2.78 W or 10 %.

$$n = \frac{2.78}{26.76} \cdot 100\ \% = 10.0\ \%.$$

4.2 Efficiency

Using the number equation (1) to determine the input power and equation (2) to determine its efficiency.

Table 4 – Efficiency of stationary solar panel output power

Time	Radiation, W/m^2	$P_{in} = E \cdot A$, W	P_{out}, W	$n = P_{out} / P_{in}$, %
08:00	246.64	129.98	13.78	10.60
09:00	294.72	155.32	18.00	11.59
10:00	424.12	223.51	27.95	12.50
11:00	398.87	210.20	26.76	12.73
12:00	394.01	207.64	28.38	13.67
13:00	336.36	177.26	21.99	12.41
14:00	329.27	173.53	21.21	12.22
15:00	259.51	136.76	16.34	11.95
16:00	177.43	93.51	9.96	10.65

Table 5 – Efficiency of solar panel tracking power output

Time	Radiation, W/m^2	$P_{in} = E \cdot A$, W	P_{out}, W	$n = P_{out} / P_{in}$, %
08:00	326.46	172.04	22.83	13.27
09:00	362.47	191.02	25.26	13.22
10:00	464.40	244.74	32.68	13.35
11:00	431.90	227.61	29.54	12.98
12:00	454.21	239.37	33.70	14.08
13:00	399.47	210.52	27.58	13.10
14:00	439.75	231.75	28.40	12.25
15:00	355.46	187.33	23.15	12.36
16:00	320.87	169.10	22.26	13.16

Referring to table above, we can see that solar panels are placed in a static state on the 180° slope facing north and azimuth 75°, has an efficiency value below its standard. The conditions that enter the efficient range only occur at 12:00 which is also the peak of sun exposure in west Indonesia in particular.

In the solar panel tracking, the state is relatively efficient except at an average of 14:00 and 15:00. This may happen because of various factors; including weather, surface temperature of solar panels and power losses [7]. However, the subject of our discussion is that there is an increase in the efficiency of its output when the solar panel is positioned perpendicular to the sun.

4.3 Average solar radiation intensity ratio of four solar panel modes in one full day

Comparing these four solar panel placement modes based on the average intensity of captured solar radiation and output power in a single day can be seen from the curves below (Figure 11), where E_1 – intensity of solar radiation captured by the northern stationary 70° solar panels; E_2 – intensity of solar radiation captured by the solar panel tracking north-south; E_3 – intensity of solar radiation captured by 70° stationary east solar panels; E_4 – intensity of solar radiation captured by solar panels tracking east-west.

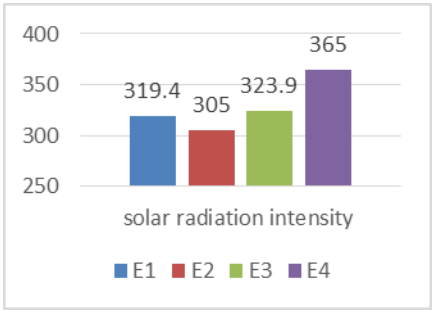

Figure 11 – Graph of solar radiation intensity comparison of the four-mode solar panels

The eastern-western tracking mode with 15° changes per hour is still much better than the eastern stationary 70° mode as has been the standard provision of solar panel installation in Indonesia. While comparing east stationary 70° solar panels with a 70° north stationer; 70° eastern stationary mode is still better at capturing solar radiation though not much different.

4.4 Comparison of average output power of all four solar panel modes in one full day

By calculating the output power obtained from the output voltage and current output of solar panel, the data as in Table 6, where p – output power of the northern stationary 70° solar panels; P_2 – solar power output tracking north-south; P_3 – output power of the eastern stationary 70° solar panels; P_4 – solar panel power output tracking east-west.

Table 6 – The average power of the solar panel outputs are all four modes

Time	Power output, W			
	P_1	P_2	P_3	P_4
07:00	7.45	6.77	8.96	4.90
08:00	14.62	23.19	21.26	18.62
09:00	29.55	27.09	34.23	37.05
10:00	32.17	33.22	36.42	37.37
11:00	38.95	39.58	40.81	42.19
12:00	40.15	40.89	40.09	43.14
13:00	25.95	28.80	26.88	31.00
14:00	33.37	33.11	29.01	36.89
15:00	12.33	12.36	10.11	14.59
16:00	12.71	9.97	6.97	17.97
17:00	4.85	3.12	4.33	6.79
18:00	2.13	1.51	1.50	2.38
X	20.56	21.63	21.71	24.41

In this measurement, it concentrates on the ratio of the total average solar panel output power to all four solar panel modes.

This is shown the highest average output power in one full day can be generated by solar panels tracking east - west. This data proves that the installation of solar panels with this mode is the best compared to the other 3 modes.

Figure 12 – Graph of output power ratio of all four solar panel modes

5 Conclusion and recommendations

The results of the measurement and discussion can be summarized as follows:

– the angle of a solar panel is very influential on the intensity of solar radiation that can be absorbed by a solar panel, which by positioning the solar panel remains perpendicular to the sun, maximizing the absorption of sun radiation 8.3–81.0 % compared with positioning the solar panel in a stationary state;

– the intensity of sunlight is proportional to the output power of a solar panel, where the increase in power that can be achieved by setting the position of the solar panel perpendicular to the sun is 10–23 % compared to positioning the solar panel on a stationary state.

Based on the conclusions, it can be suggested:

– to maximize efficiency, solar panels are expected to be positioned perpendicular to the sun. This is possible by using automatic solar tracker;

– installation of solar panels should be located in high places that are not blocked by the shadow of the any objects or other buildings;

– in the case of measurement and testing, it should use more than one solar panel to adjust the number of modes to be measured to avoid errors caused by time delay in measurement.

References

1. Arbab, H., Jazi, B., & Rezagholizadeh, M. (2009). A computer tracking system of solar dish with two-axis degree freedoms based on picture processing of bar shadow. *Renew Energy,* 34, 1114–1118.
2. Arismunandar, W. (1995). *Teknologi rekayasa surya*. Jakarta, Vol. 1, pp. 17.
3. Ghosh, H. R., Bhowmik, N. C., & Hussain, M. (2010). Determining seasonal optimum tilt angles, solar radiations on variously oriented, single and double axis tracking surfaces at Dhaka. *Renew Energy*, 35, 1292–1297.
4. Hoesin, H. (2011). *Memahami radiasi matahari dari enam hal, menuju langit biru dan teknologi pemanfaatanya*. Accessed online at September 9th, 2017.
5. Yohana, E. (2010). *Pengaruh suhu permukaan photovoltaic module* 50 W *peak* terhadap daya keluaran yang dihasilkan menggunakan reflektor dengan variasi sudut reflektor 0°, 50°, 60°, 70°, 80°. Jurnal Universitas Diponegoro, Semarang, Universitas Diponegoro.
6. Raditya, G. (2015). *Faktor yang mempengaruhi kinerja solar panel*. Accessed online at August 30th, 2017.
7. Sidopekso, S., & Febtiwiyanti , A. E. (2010). *Studi peningkatan output modul surya dengan menggunakan reflektor*. Jurnal Universitas Negeri Jakarta. Jakarta: Universitas Negeri Jakarta.
8. Soeparman, S. (2015). *Teknologi tenaga surya*. Malang, Vol. 1.
9. Sudibyo, M. (2012). *Menimbang ulang penyatuan zona waktu Indonesia*. Accessed online.
10. Zahr, M., Friedrich, D., & Kloth, T.Y. (2010) Bionic photovoltaic panels bio-inspired by green leaves. *Journal of Bionic Engineering*, Vol. 7, pp. 284–293.

Аналіз ефективності відстежувальних і стаціонарних режимів сонячної панелі проти сонячної радіації

Самаула Х.[1], Базір Й.[1], Гелмі М.[1], Фаттурізки Ф.[1], Сугавара А.[2]

[1] Палібангбанський університет м. Тридінанті, 30129, м. Тридінанті, Індонезія;
[2] Університет Ніїгата, 950-2181, м. Ніїгата, Японія

Анотація. Використання джерел сонячної енергії здійснюється із використанням фотоелектричних, сонячних панелей. Енергія, випромінювана сонцем, коливається. Ця зміна енергії випромінювання також впливає на випуск сонячних панелей. Спостерігаються зміни вимірюваних відношень, що доведено у цьому дослідженні. Спостереження проводяться за допомогою вимірювального приладу – лічильника сонячної енергії, здатного фіксувати інтенсивність енергії сонячного випромінювання, Вт/м^2. Хоча вихідний сигнал, що вимірюється, тобто вихідна потужність, вироблена як панель сонячних батарей. Вимірювання в цьому дослідженні здійснювалось за допомогою двох режимів: стаціонарного і режиму відстеження. Стаціонарний режим реалізується розміщенням сонячної панелі з нахилом та азимутом у заздалегідь визначеному напрямку, у той час як режим стеження – розміщенням сонячної панелі на 90° до сонця. Певним способом розмістивши сонячні батареї, вони можуть досягти ефективності до 14.1 % порівняно зі стаціонарними сонячними панелями, розташованими під кутом 75° до півночі з досягненням ефективності 13.7%.

Ключові слова: енергія випромінювання, фотоелектрична енергія, ефективність, сонячна панель.

JOURNAL OF ENGINEERING SCIENCES
ЖУРНАЛ ІНЖЕНЕРНИХ НАУК
ЖУРНАЛ ИНЖЕНЕРНЫХ НАУК
Web site: http://jes.sumdu.edu.ua
Volume 5, Issue 1 (2018)

Copyright Agreement

We, the Authors of the Manuscript publishing in the Journal of Engineering Sciences, in the case of acceptance for publication, transfer to Founders and Editorial Board the underlined rights:

– publishing this article in English and distribution of the printed version;

– English translation of the article (for articles in Ukrainian or Russian) and distribution the hard copy of the translation;

– distribution of the electronic version of the article, as well as electronic version of English translation (for articles in Ukrainian or Russian) through any electronic means (by hosted on the official web-site of the Journal, in electronic databases, repositories, etc.).

We reserve the rights without the consent with the Editorial Board or Founders:

– to use the article materials in whole or partly for educational purposes;

– to use the article materials in whole or partly to write own dissertations;

– to use the article materials for thesis preparing, conference materials, as well as for presentations;

– to post electronic copies (including the final electronic version downloaded from the official web-site of the Jounal):

– on the personal web-sources of the all co-authors (web-sites, web-pages, blogs, etc.);

– on the web-sources of authors working organizations (including electronic institutional repository);

– on the International Scientometric Databases (CrossRef, DOAJ, Index Copernicus Indexing, etc.);

– on non-commercial Open Access sources (e.g. arXiv.org).

In all cases, the presence of citations to the article or hyper-link to the electronic copy of on the official web-site of the journal is obligatory.

By this agreement we also certify that the submitted manuscript:

– does not violate the copyrights of other persons or organizations;

– has not been published previously in other publishing houses and submitted for publication in other Journals.

JOURNAL OF ENGINEERING SCIENCES
ЖУРНАЛ ІНЖЕНЕРНИХ НАУК
ЖУРНАЛ ИНЖЕНЕРНЫХ НАУК
Web site: http://jes.sumdu.edu.ua
Volume 5, Issue 1 (2018)

Dear Authors of the Journal of Engineering Sciences!

The Editorial Board of the Journal of Engineering Sciences pays special attention to the structure of the articles according to the "Enhancement of requirements to specialized editions registered in the databases of Ukrainian State Commission for academic degrees" (minutes No. 7-05/1 from January 15, 2003). Only original articles by the authorship of up to 5 authors are accepted for the publication according the **Template** with the following elements:

– general statement of the problem and its relation with the important scientific or practical problems;
– analysis of the recent investigations and publications in the same research field;
– statement of the significance of the general problem that were not solved before;
– statement of the purpose of the research article;
– description of the initial data of the research with the justification of the achieved scientific results;
– conclusions and ways for further development of the research.

All the articles are reviewed by the independent double-blind procedure.

All the authors should sent via e-mail jes@sumdu.edu.ua the electronic version of the following materials:

– article **in English** according to the **Template**;
– information about authors and their affiliation with the related address.

ATTENTION!

If one of the mentioned components is not sent or there are many stylistic, orthographic and grammatical errors, the article will not be taken into consideration by the Editorial Board and will not be reviewed.

Minimum size of the materials:

1. Scientific – theoretical articles (up to 25 000 symbols, about 14 pages) that deal with the theoretical research and descriptions of physical laws concerning the investigated phenomena; theoretical generalizations and fundamental principles proved by the experimental research data.
2. Scientific-practical articles (up to 10 000 symbols, about 6 pages) that deal with scientific experiments and real experience. They include the statement of the proposed methods for the experimental research or means for the observation of the studied phenomena. An essential part of these articles is the description of the achieved results and their explanation acquired in the process of immediate interaction with the object of investigations, its significance and practical implementations.
3. Scientific-methodological articles (up to 15 000 symbols, about 8 pages) that deal with the review of processes, methods, instruments for solving scientific and applied problems; the statement of the new methodology, results of which allow creating more precise methodology on the basis of up-to-date methodology for the implementation of discovered laws.

The Ministry of Education and Science of Ukraine

Міністерство освіти і науки України

Министерство образования и науки Украины

JOURNAL OF ENGINEERING SCIENCES

ЖУРНАЛ ІНЖЕНЕРНИХ НАУК

ЖУРНАЛ ИНЖЕНЕРНЫХ НАУК

Scientific Journal

Науковий журнал

Научный журнал

Відповідальний за випуск
Д. В. Криворучко
Комп'ютерне складання та верстання:
І. В. Павленко
Коректори:
Н. З. Клочко, С. М. Симоненко

Responsible for release:
D. V. Kryvoruchko
Computer design and typesetting
I. V. Pavlenko
Correctors:
N. Z. Klochko, S. M. Symonenko

Підписано до друку 25.06.2018. Формат 60x84/8.
Папір офс. Друк офс.
Ум. друк. арк. 14,43. Обл.-вид. арк. 17,23.
Наклад 100 пр. Замовлення №
Сумський державний університет, вул. Римського-Корсакова, 2, 40007, м. Суми, Україна
Свідоцтво про внесення суб'єкта видавничої справи до Державного реєстру
ДК № 3062 від 17.12.2007.

Надруковано у друкарні СумДУ,
вул. Римського-Корсакова, 2, 40007, м. Суми, Україна

Editorial Board: 2 Rymskogo-Korsakova St., 40007 Sumy, Ukraine
Contact Phones: +38 (0542) 331024; +38 (099) 3845740
E-mail: jes@sumdu.edu.ua
Web-site: http://jes.sumdu.edu.ua

State registration certificate of the print mass-media No. 20499-10299 ПР.